Preparation of Nanosusponanoemulsion and Nanosuspomicroemulsion Novel Combination Formulations Suitable for Personalised Medicine

Luangwitchajaroen, Yuvared

Awarding institution:
King's College London

Preparation of Nanosusponanoemulsion and Nanosuspomicroemulsion: Novel Combination Formulations Suitable for Personalised Medicine

Yuvared Luangwitchajaroen

A thesis submitted in partial fulfillment of the requirements

for the degree of Doctor of Philosophy

in the

Faculty of Life Sciences & Medicine

April 2017

King's College London

Abstract

A wide variety of formulations have been explored in attempt to improve the apparent aqueous solubility of poorly-water soluble drugs such as oil-in-water nanoemulsions (NE), oil-in-water microemulsions (ME) and drug nanoparticles (NPs). There would be advantage gained if two poorly-water soluble drugs could be combined in a single formulation, particularly with respect to the ability to personalise a patient's medicine. In this study therefore, two novel combination formulations, which we have termed a "nanosusponanoemulsion (NSNE)" and a "nanosuspomicroemulsion (NSME)", consisting of either NE or ME containing a low dose drug and NP comprised of a high dose drug, respectively have been studied. The particular aim of this study is to prove the principal that, by the rational design of NSNE and NSME, it is possible to prepare combination formulations suitable for the delivery of two poorly-water soluble drugs for use in personalised medicine.

Studies involved the preparation and physico-chemical characterization of NSNE and NSME prepared from the mixing of NP, prepared by wet bead milling and stabilised by the anionic surfactant, sodium dodecyl sulphate (SDS), and either NE stabilised by the nonionic surfactant, Brij 97, and containing the triglyceride oil, glyceryl trioctanoate (TON) or a ME stabilised by SDS and containing either ethyl butyrate (EB) or ethyl caprylate (EC). Testosterone propionate (TP) was used as the low-dose model drug and was solubilised in the NE and ME, whilst griseofulvin (GF) was the high-dose model drug used to prepare the NPs. A range of physico-chemical techniques were used to characterize the individual systems, namely the NP, NE and ME, as well the NSNE and the NSME and included UV spectroscopy, photon correlation spectroscopy (PCS) as well as small angle neutron scattering (SANS) which was used to individually monitor the *in situ* stability of the individual components of the NSNE and NSME.

Significantly in the combined formulations, some of the GF from the NPs was solubilised in the NE and the ME. In addition, while the solubility of TP in the NE remained constant in the presence of the SDS-stabilised GF-NPs, the amount of TP in the ME decreased upon contact with the GF-NP, suggesting that the GF displaced some of the TP molecules in the ME. PCS studies showed that the particle size of GF-NP, when in the form of a NSNE, i.e. in contact with the NE initially increased in size but

thereafter remained relatively stable whilst the particle size of GF-NP in the form of a NSME remained unchanged. On the other hand, the SANS studies indicated that the TP-containing NE with a low amount of TON were stable for at least 24 hours contact with the GF-NP when in the form of a NSNE. These results suggest that the NSNE is more suitable than the NSME for the administration of two poorly water-soluble drugs in a single formulation for use in personalised medicine.

Acknowledgements

First and foremost, my sincere gratitude goes to my supervisor Professor Jayne Lawrence for her invaluable guidance, support and encouragement throughout all works in this thesis. This thesis would not have been possible without her guidance and patience.

Many thanks to the Rutherford Appleton Laboratory (RAL) for giving neutron beam time for this project. I am grateful to Dr. Ann Terry of RAL for offering her great help without hesitation on neutron data modeling and instrumentation. I would also like to express my gratitude to Dr. David Barlow for his valuable time and comments on neutron data analysis.

I wish to thank Dr. Hisham Al-Obaidi for his help in the lab during my first year. I would also like to thank all my friends and members of the Pharmaceutical Biophysics Group who are always friendly, supportive and helpful, especially Orathai Louthai, Lili Cui and Yussif Saaka.

The last but not least, my deepest gratitude goes to my family; Yongyutt, Malee, Yavared, Yongyot and Kanokwan, for their unlimited love, support and encouragement.

Table of Contents

Table of Contents

List of Figures

List of Tables

Abbreviations and Symbols

Å	Angstrom
a	major semi-axis
A	surface area
Aerosol-OT	di-2-ethylhexyl sulfosuccinate
b	minor semi-axis
BCS	Biopharmaceutics Classification System
b_i	coherent neutron scattering length of nucleus i
B_{inc}	incoherent background scattering
Brij 97	polyoxyethylene (10) oleyl ether
B24T3/10	a 10 times diluted NE (24 w/w% Brij 97 and 3 w/w% TON)
B24T3/10-TP	a 10 times diluted NE (24 w/w% Brij 97 and 3 w/w% TON containing saturated amount of TP)
B24T5/10	a 10 times diluted NE (24 w/w% Brij 97 and 5 w/w% TON)
B24T5/10-TP	a 10 times diluted NE (24 w/w% Brij 97 and 5 w/w% TON containing saturated amount of TP)
C	concentration
cmc	critical micelle concentration
CP	cloud point
d	molecular length scale
d	particle diameter
D	bulk density
D	translational diffusion coefficient
d(H)	hydrodynamic diameter
DDAO	N,N-dimethyldodecylamine-N-oxide

DDAPS	3-N,N-dimethyldodecylammoniopropanesulfonate
d-EB	deuterated ethyl butyrate
d-EC	deuterated ethyl caprylate
DTAB	dodecyltrimethylammonium bromide
d-TON	deuterated glyceryl trioctanoate
e	electronic charge
EB	ethyl butyrate
EC	ethyl caprylate
F(Q)	single particle form factor
GF	griseofulvin
GF-NPs	griseofulvin nanoparticles
GF-NS	griseofulvin nanosuspension
G_I	interfacial free energy
h	Hamaker constant
H	distance between centres of particles
H'	distance between surfaces of two spheres
HLB	hydrophilic-lipophilic balance
H-P S(Q)	Hayter-Penfold structure factor
HPMC	hydroxypropylmethyl cellulose
I	ionic strength
I(Q)	intensity of the scattered radiation
IND	indomethacin
IND-NPs	indomethacin nanoparticles
k_B	Boltzmann's constant
k_H	Huggins coefficient
k_i	incident wave vector

k_K	Kraemer coefficient
k_s	scattered wave vector
m	mass
ME	microemulsion
mol vol	molecular volume
MW	molecular weight
n	neutron refractive index
N_A	Avogadro's constant
N_{agg}	aggregation number
NE	nanoemulsion
no.	number
n_p	average number density of droplet
NS	nanosuspension
NSME	nanosuspomicroemulsion
NSNE	nanosusponanoemulsion
NSB24T3/10	nanosusponanoemulsion consists of B24T3/10 and GF-NPs
NSB24T3/10-TP	nanosusponanoemulsion consists of B24T3/10-TP and GF-NPs
NSB24T5/10	nanosusponanoemulsion consists of B24T5/10 and GF-NPs
NSB24T5/10-TP	nanosusponanoemulsion consists of B24T5/10-TP and GF-NPs
NSS20B14/5	nanosuspomicroemulsion consists of S20B14/5 and GF-NPs
NSS20B14/5-TP	nanosuspomicroemulsion consists of S20B14/5-TP and GF-NPs
NSS20C08/5	nanosuspomicroemulsion consists of S20C08/5 and GF-NPs
NSS20C08/5-TP	nanosuspomicroemulsion consists of S20C08/5-TP and GF-NPs
o/w	oil-in-water
P(Q)	form factor
PCS	photon correlation spectroscopy

PIT	phase inversion temperature
PVDF	polyvinylidene fluoride
PVP	polyvinylpyrrolidone
Q	scattering vector
R	radius of spherical particles
Rc	radius of core
R_{core}	core radius
R_{H-P}	radius of Hayter-Penfold structure factor
Rs	radius of shell
S(Q)	interparticle structure factor
SAA	surfactant
SANS	small angle neutron scattering
SAXS	small angle X-ray scattering
SBO	soybean oil
SDS	sodium dodecyl sulphate
SLD	scattering length densities
SSE	sum of squared errors
S20B14/5	a 5 times diluted ME (20 w/w% SDS and 14 w/w% EB)
S20B14/5-TP	a 5 times diluted ME (20 w/w% SDS and 14 w/w% EB containing a saturated amount of TP)
S20C08/5	a 5 times diluted ME (20 w/w% SDS and 8 w/w% EC)
S20C08/5-TP	a 5 times diluted ME (20 w/w% SDS and 8 w/w% EC containing a saturated amount of TP)
T	temperature
TBN	tribuytrin
TLN	trilaurin
TON	glyceryl trioctanoate

TP	testosterone propionate
TPN	tripalmitin
U_0	depth of the potential
UPW	ultrapure water
UV	ultraviolet-visible spectroscopy
v	shape factor
V	scattering volume
V_A	force of attraction
Vc	volume of core
Vcore	volume of core
V_D	primary minimum
V_M	primary maximum
V_R	electrical repulsion force
V_S	secondary minimum
Vs	steric stabilisation
Vs	volume of shell
Vshell	volume of shell
Vshell(dry)/Vcore	ratio of volume fraction of the dry head group and core
V_T	total potential energy
w	distance from the centre of the reference particle
w/o	water-in-oil
W_1	solvation expressed as g solvent/g solute
X	axial ratio
x	core of axial ratio
YTZ	yttrium zirconia
Z	aggregate charge

Abbreviations and symbols

γ	interfacial tension
δ	shell thickness
ΔG	changing in free energy
ε	permittivity
ε	dielectric constant
η	liquid viscosity
η_{rel}	relative viscosity
η_{sp}	specific viscosity
θ	scattering angle
λ	wavelength
ρ	density
ρ_0	density of solvent
ρ_c	scattering length density of core
ρ_s	scattering length density of shell
ρ_{SLD}	scattering length density
$\rho_{solvent}$	scattering length density of solvent
$\tilde{\upsilon}$	partial specific volume
$\tilde{\upsilon}_1^0$	partial specific volume of the solvent
Φ	volume fraction
ψ_0	surface potential
$[\eta]$	Intrinsic viscosity

Chapter 1 Introduction

1. Background

A large number of extremely poorly-water soluble compounds have been developed as potential therapeutic agents in the pharmaceutical industry. Indeed, up to 70% of new drug candidates have been reported to show poor aqueous solubility (Kawabata et al., 2011). One of the most important problems of oral administration arising from the poor water solubility of a drug is that insufficient drug is dissolved in the fluid of gastrointestinal tract to ensure its adequate uptake through the epithelial cells of the small intestine. One of the main challenges, therefore, facing researchers developing new drug formulations (or medicines) is the preparation of delivery systems containing poorly-water soluble drugs suitable for administration to patients. Another complication is whether the patient is in the fed or fasted state as this can affect the bioavailability and therefore the therapeutic response of the drug (Date et al., 2004; Merisko-Liversidge et al., 2003).

Two factors greatly influence a drug's bioavailability, namely its solubility and its membrane permeability. These two factors that formulation techniques aim to improve (Leuner et al., 2000). However, the requirement for an innovative formulation to increase the apparent solubility of a poorly-water soluble is one of the most challenging aspects of drug development (Keck et al., 2006; Leuner et al., 2000; Serajuddin, 1999; Vasconcelos et al., 2007; Wang et al., 2013). Based on the knowledge of a drug's solubility and permeability, the biopharmaceutics classification system or BCS divides drug molecules into four different classes as shown in Figure 1.1 (Lipinski et al., 2001; Rautio et al., 2008). Most poorly-water soluble drugs fall into BCS class II and IV. One technique to improve the bioavailability of a poorly-water soluble drug is to improve the rate-limiting step of absorption by increasing the dissolution rate of the drug (El-Badry et al., 2009; Jia, 2005; Khadka et al., 2014; Pouton, 2006).
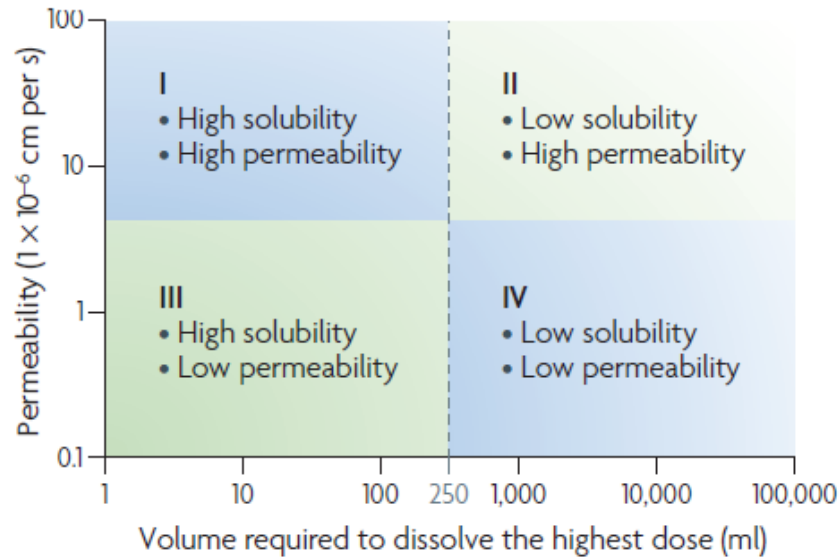
Figure 1.1 Classification of drugs into four different groups using the Biopharmaceutics Classification System or BCS (Rautio et al., 2008).

In order to enhance the dissolution rate of a poorly water-soluble drug, several strategies/formulations have been employed. Over the last few decades, a range of strategies including increasing the surface area of powdered drug, changing the drug's crystalline form and designing novel nanocarriers for its controlled release, have been used to try and improve the dissolution rate and bioavailability of a poorly water-soluble drug. A very promising way to improve a drug's bioavailability is by the use of improved formulations, such as nanoemulsions, microemulsions and solid dispersion technologies. Numerous reviews support the hypothesis that such preparations can improve the solubility, dissolution kinetics and bioavailability of hydrophobic drugs (Chen et al., 2011; Ghosh et al., 2006; Mueller et al., 1994; Shafiq et al., 2007). Even though such approaches have been successfully used commercially to enhance the dissolution rate of low dose, poorly water-soluble drugs, many current research projects are focusing on the development of enabling nanoformulation technologies for the delivery of high dose drugs, for example, the production of nanosized of drug particles. Research illustrates that drug nanoparticles can be used to increase the drug dissolution rate by reducing particle size and therefore increasing surface area (Date et al., 2004; Hu et al., 2004; Merisko-Liversidge et al., 2008). In addition to increasing drug dissolution, drug nanoparticles have been proven to improve the drug bioavailability and enhance

the drug exposure in formulations intended for both oral and parenteral delivery (Merisko-Liversidge et al., 2008; Wang et al., 2013).

In parallel, combination drug therapies have become increasingly popular as a means to improve the treatment for the patients with a range of chronic diseases including AIDS, TB, diabetes and also cardiovascular diseases where the polypill (which contains 4 drugs - losartan, amlodipine, hydrochlorothiazide and simvastatin) is gaining much interest. Combination therapy is a term used for the administration of multiple medications or therapies to fight the same condition. There are many advantages of using combination formulations comprising two, or indeed more, drugs for combination therapy. For instance, combination formulations are considered to improve patient compliance, simplify disease management, reduce cost as well personalise the medication. For example, Kim et al. (2013) developed a fixed dose combination formulation comprising of 3 drugs, namely losartan, amlodipine and hydrochlorothiazide for prophylaxis or treatment of cardiovascular disease. The formulation demonstrated both a higher rate of dissolution and greater stability than the conventional formulations, thus showing the combination formulation to be at least biologically equivalent or possibly even superior to the conventional dosage forms of the same medicines. Furthermore, William et al. (1984) demonstrated advantages from a combination formulation comprising of triamterene and hydrochlorothiazide intended to treat patients with mild to moderate hypertension, which resulted in the maintenance of normal levels of serum electrolyte, while the levels of uric acid and creatinine were unchanged when compared to the conventional formulation. Indeed one combination therapy recently approved in the US by the FDA is the combination of paclitaxel and gemcitabine for the treatment of metastatic adenocarcinoma of the pancreas, paclitaxel acts as a microtubule inhibitor, while gemcitabine replaces segments of cell DNA to force apoptosis. Leyden et al. (2001) showed that a combination formulation comprising of 1% clindamycin and 5% benzoyl peroxide gel produced both a more rapid and greater reduction in the extent of *Propionibacterium acne* when compared to the traditional formulation of clindamycin alone. As demonstrated here, the use of combination drug therapies is opening the possibility of tailoring a dose to a patient individual need i.e. personalised medicine.

The goal of personalised medicine is to achieve the right drug in the right does for the right person at the right time in order to avoid the drug adverse reactions, eliminate invalid therapy, improve treatment efficiency, and thereby achieve optimal health outcomes. Although personalised medicine is not a new concept, doctors and pharmacists have been aiming to administer the right drugs to the right patients for many years, it has only recently attracted wide spread attention as our understanding of human genetics and its influence in disease, not only in cancer but also other chronic diseases such as HIV, TB and diabetes, has greatly improved. For example, it is now increasingly common to develop new drugs to treat specific sub-populations of patients based on their genetic make-up. One area, however, that has received, by comparison, very little attention to date is the personalisation of the medicine in respect to its dose. Indeed, as described above there is a strong case to prepare medicines that contain a combination of drugs, in this way it would be possible to reduce production costs, simplify disease management and improve patient compliance, amongst other things.

In this study, two related novel combination drug delivery systems, namely a "nanosusponanoemulsion (NSNE)" and a "nanosuspomicroemulsion (NSME)" consisting of a nanosuspension of drug mixed with either a drug-containing oil-in-water nanoemulsion or an oil-in-water microemulsion, respectively, have been prepared. The aim of these formulations is to combine a high dose, poorly-water soluble drug in the form of a nanosuspension with a low dose, poorly-water soluble drug contained in either an oil-in-water nanoemulsion or microemulsion in a single formulation.

The preparation of a drug nanoparticle, means that most of the nanoparticle is drug, unlike the situation of a drug-containing nanoemulsion and microemulsion, where only a small portion of the particle is drug. For this reason drug nanoparticles are ideal for the administration of high-dose drugs, while nanoemulsions and microemulsions are only suitable delivery vehicles for low dose drugs. Griseofulvin (class II BCS) is an antibiotic, fungistatic drug administrated orally for the treatment of dermatophyte and ringworm infections. The usual adult dose of micronized griseofulvin for the treatment of tinea corporis, tinea crusis or tinea capitis is 500 mg /day, while a 1 g/day is required for tinea pedis and tinea unguium treatment. Because of griseofulvin's poor water-solubility coupled with the high dose required for treatment using griseofulvin, means that it is an ideal model drug for the production of nanoparticles in the present study.

While the low dose (30-50 mg/mL) required for the poorly-water soluble, steroidal drug, testosterone propionate, makes it an ideal candidate for loading into either the nanoemulsions or the microemulsions in the novel combination formulation.

1.2 Nanoemulsions and microemulsions

1.2.1 Definition

Over the last decade or so, nanoemulsions and microemulsions have become more popular in the food and pharmaceutical industries because of their many perceived advantages, including being able to protect and increase the bioavailability of lipophilic substances encapsulated within them (Narang et al., 2007). Unfortunately, there is much confusion around the terms microemulsion and nanoemulsion, mainly because of the prefixes used to describe them. The term of "micro-" means 10^{-6}, whilst the term of "nano-" means 10^{-9}, which would infer that a microemulsion contains on average 1000x larger particles than a nanoemulsion, when in reality the particles in a microemulsion are in fact smaller than those in a nanoemulsion. The reason for this confusion is that the phase microemulsion was used before the size of the particles they contained was determined and had become well-established before the term nanoemulsion was introduced. In this context it is interesting to note that the first microemulsions were prepared by diluting an emulsion, hence the prefix "micro-". As a consequence in the present thesis, nanoemulsions and microemulsions will be defined in terms of size and structure of the particles they contain, their preparation and stability in order to understand the differences and similarities of these systems.

In terms of size, recent literature has stated that the upper particle size of a nanoemulsion droplets could be as large as 500 nm (Anton et al., 2008), although upper limits of 200 nm (Huang et al., 2010) and 100 nm (Rao et al., 2012) have all been quoted. Recently McClements (2012) has argued that an upper limit of 100 nm would lead to a number of potential benefits of nanoemulsions including improved stability, high optical clarity and the increased bioavailability of any encapsulated lipophilic compounds. Although there is some variability in the size range quoted for nanoemulsions, a particle size range of 20-200 nm is most typically seen, in contrast to the widely quoted size range of 5-100 nm for microemulsions. Normally, the physical

appearance of a microemulsion is clear, whilst that of nanoemulsions can range from clear through translucent. In this context it is worth noting that the appearance of colloidal system is generally translucent or transparent when the dispersed particle size is less than 30 nm (Wooster et al., 2008).

1.2.2 Structure

Nanoemulsions and microemulsions are typically composed of oil, water, surfactant and possibly a co-surfactant. Figure 1.2 shows schematic diagrams of the three of the most common types of microemulsions, namely droplets of oil-in-water (O/W), bicontinuous phases and droplets of water-in-oil (W/O), which type of microemulsion is formed depends on concentration of the various components, and the nature and arrangement of the molecules present. In contrast, nanoemulsions form only O/W and W/O droplets, they do not form bicontinuous phases. Both O/W nanoemulsions and microemulsions possess a disperse phase of oil which is separated from the bulk polar aqueous phase from an interfacial monolayer of surfactant molecules in which the hydrophobic portion is in contact with the disperse oil phase and the hydrophilic head groups of the surfactants is bathed by the continuous aqueous phase. W/O nanoemulsions and microemulsions similarly contain an interfacial surfactant monolayer but of reversed configuration such that the surfactant head groups are directed towards the centre of the droplets where disperse aqueous phase resides, while the hydrophobic or hydrocarbon chains of the surfactant are expressed on the exterior in contact with the non-polar phase.
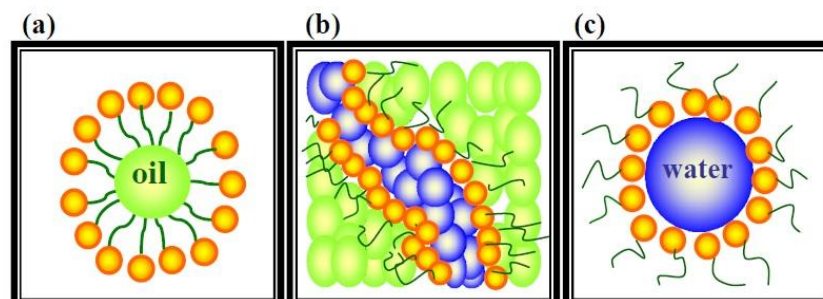
Figure 1.2 Schematic represents three common types of microemulsion structures: (a) oil-in-water and, (b) bicontinuous and (c) water-in-oil type.

In this study, we are concerned only with a system suitable for encapsulating hydrophobic drug in a continuous aqueous phase so O/W nanoemulsions and microemulsions, consisting of oil surrounded with surfactant molecules dispersed in an aqueous medium, were examined due to their ability to solubilise poorly water-soluble drug in a core of their droplets and thereby increase apparent aqueous drug solubility. Figure 1.3 shows schematic diagram of microemulsions and nanoemulsions composed of oil, water and surfactant.
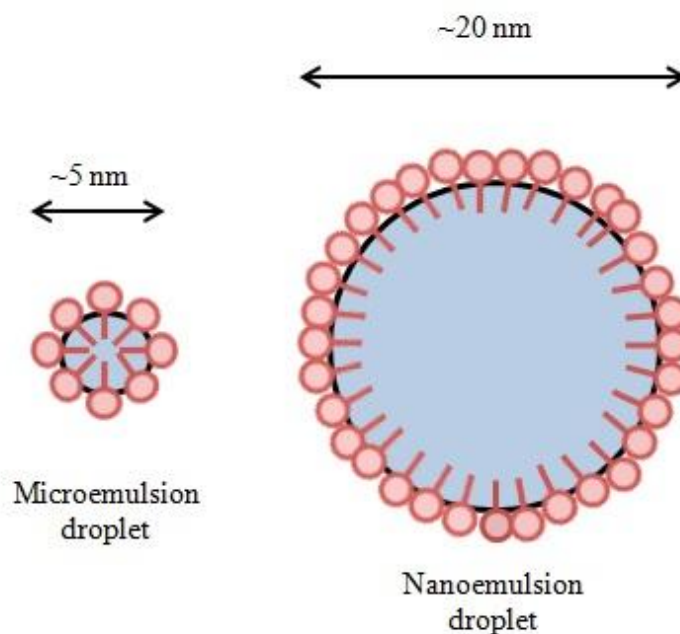
Figure 1.3 Schematic diagram of nanoemulsion and microemulsion composed of oil, water and surfactant showing approximate dimensions.

1.2.3 Formation of nanoemulsions and microemulsions

The major distinction between nanoemulsions and microemulsions is their thermodynamic stabilities: nanoemulsions are thermodynamically unstable while microemulsions are thermodynamically stable. Figure 1.4 shows the differences in the free energy of nanoemulsion and microemulsion systems compared with their phase separated state (bulk oil and water phases). Nanoemulsions have a higher free energy than the phase separated state, while microemulsions have a lower free energy.
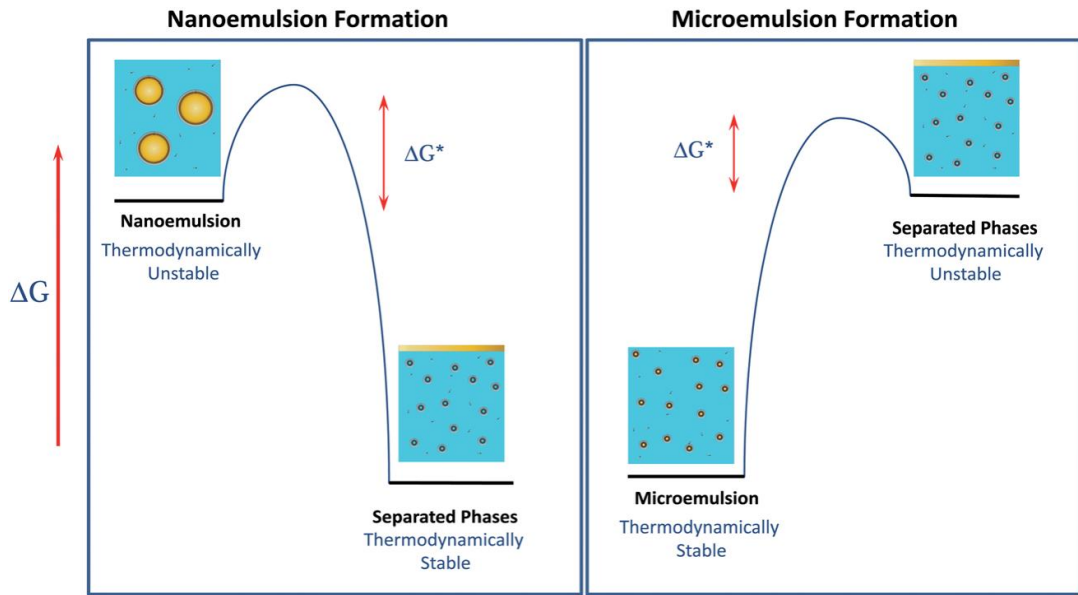
Figure 1.4 Schematic diagrams of the free energy of microemulsion and nanoemulsion systems compared to their phase separated state (McClements, 2012).

A simple mathematical model of thermodynamic stability can be used to explain this difference by calculating the free energy of formation of a nanoemulsion and microemulsion from their individual components. To a first approximation, the free energy of formation of a colloidal dispersion from the individual phases depends on the interfacial free energy (ΔG_I) and the configuration entropy ($-T\Delta S_{config}$) :

$$\Delta G_{formation} = \Delta G_I - T\Delta S_{config}$$

where the interfacial free energy (ΔG_I) is equal to the increase in the contact area between the oil and the aqueous phases (ΔA) multiplied by the interfacial tension (γ) at the oil-water interface at constant temperature, pressure and interfacial chemical potential:

$$\Delta G_I = \gamma \Delta A$$

In addition, the interfacial free energy term is usually positive as increasing the contact area and the interfacial tension is positive. As a consequence, this interfacial free energy term always opposes nanoemulsion and microemulsion formation.

The configuration entropy ($-T\Delta S_{config}$) is dependent upon the number of ways in which the oil phase can be arranged within the system. The configuration energy is always

negative because the number of possible arrangements of the oil phase in an emulsified state is much greater than in a non-emulsified state, and therefore the configuration energy always favours the formation of a colloidal (emulsified) dispersion.

Initially, the interfacial tension of the system depends on the curvature of the surfactant monolayer. Nanoemulsions are formed when the interfacial tension at the oil-water boundary in the emulsified system is similar to the interfacial tension at a planar oil-water interface. However, upon decreasing particle size, the interfacial free energy becomes increasingly less negative/more positive (i.e. unfavorable to the formation of a colloidal dispersion) due to an increasing contact area, while the configuration free energy becomes more negative (i.e. favorable to the formation of a colloidal dispersion) as the oil droplets increase the number of different ways in which the oil can be organized. Overall, the total free energy change becomes increasingly positive because the interfacial free energy term dominates over the configuration entropy term.

Microemulsions contain a larger number of smaller droplets than a nanoemulsion. The formation of the large number of smaller droplets leads to an increase in the contact area, resulting in an unfavourable energy change. In this case, however, the interfacial free energy contribution is complicated and depends upon the size of the droplets, in that the interfacial free energy increases as droplet size decreases, although when the droplet size approaches the radius of the optimum curvature of the surfactant monolayer this leads to creation of ultralow interfacial tensions, resulting in a reduction in the interfacial free energy that opposes the formation of a colloidal dispersion. As a consequence therefore, the overall free energy of formation is negative as a result of a large significant, favourable change in entropy.

1.2.4 Preparation of nanoemulsions and microemulsions

In terms of preparation, nanoemulsions always require the input of external energy to convert the separated oil and water phases into a (thermodynamically unstable) colloidal dispersion. Nanoemulsions are usually prepared by the input of external energy, the power of which depends upon the physico-chemical mechanism of the droplet disruption. Generally, high-energy emulsification procedures, such as high-pressure homogenizers (Schultz et al., 2004), sonicators and ultrasound generators (Gaikwad et

al., 2008; Kentish et al., 2008) are required to produce a nanoemulsion. Alternatively, nanoemulsions can be prepared by low energy methods such as phase inversion temperature (PIT), phase inversion composition and self-emulsifying methods (Izquierdo et al., 2005; Maestro et al., 2008). In these cases, smaller nanoemulsion droplets are formed when the system undergoes a phase inversion in response to a change in either composition and/or temperature (Mason et al., 2006). Indeed PIT is one of method widely used low energy methods to produce nanoemulsions (Forgiarini et al., 2001a; Forgiarini et al., 2001b; Izquierdo et al., 2002).

Oil-in-water nanoemulsions, of very small and uniform droplet size, stabilised by nonionic surfactants are typically prepared by the PIT method (Izquierdo et al., 2004; Rao et al., 2010). This approach is based on changes in the molecular geometry/hydrophobicity of nonionic surfactants with temperature (Shinoda et al., 1964). Nanoemulsions are frequently prepared by heating a mixture of oil, water and surfactant to the PIT, where the hydrophilic and lipophilic properties of the mixed emulsifier are balanced (Forster et al., 1990), after which the mixture is rapidly cooled (Morales et al., 2003; Rao et al., 2010).

In contrast, microemulsions can be formed spontaneously by simply mixing oil, water and surfactant without any external energy because they are thermodynamically stable systems. However, in practise, external energy, such as stirring or heating, is often added in order to overcome any kinetic energy barriers to microemulsion formation. Consequently, it is often difficult to distinguish between nanoemulsions and microemulsion based purely on their method of preparation.

In the present study, nanoemulsions will be prepared using phase inversion temperature (PIT) method, which results in the formation of an optically transparent colloidal dispersion when a mixture of oil, water and surfactant is heated up just above the phase inversion temperature of the system and then cooled to ambient with continuous and vigorous stirring. In contrast, microemulsions will be prepared by mixing oil, water and surfactant with the aid of a stirrer at room temperature.

1.2.5 Stability

Emulsions will normally breakdown over by a number of different physico-chemical mechanisms which includes separation (creaming and sedimentation), flocculation, coalescence (Capek, 2004; Solans et al., 2005; Tadros et al., 2004) and Ostwald ripening. Which of these breakdown processes occurs depends upon the composition of the system, such as the nature of the oil and surfactant, solvent (continuous phase), the concentration of oil and surfactant, pH, ionic strength and environmental conditions, such as temperature and pressure. Figure 1.5 schematically illustrates the range of breakdown processes in emulsions.
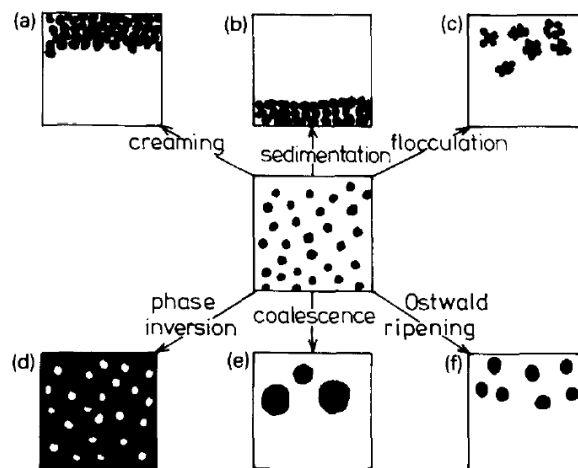
Figure 1.5 Schematic diagram of breakdown processes (Tadros, 1990).

Even though nanoemulsions are stable against flocculation and coalescence (Deminiere et al., 1998), the particle size of the nanoemulsions tend to grow as a function of time by Ostwald ripening (Capek, 2004; Kabalnov, 2001; Tadros et al., 2004; Taylor, 1998). The process of Ostwald ripening in an O/W nanoemulsion is one of the main problems of nanoemulsions. This results from the difference in solubility between the small and large droplets (Izquierdo et al., 2004; Tadros, 1990). When the oil phase has some solubility in continuous, dispersion medium, the smaller nanoemulsion droplets possess a higher local oil solubility than the larger droplets due to the difference in Laplace pressure of the droplets (Tadros, 1990).

Furthermore, microemulsions may become unstable if chemical changes occur in the components during storage, or alternatively the environmental conditions are altered. For instance, microemulsions can breakdown if they are diluted or alternatively temperature changes (McClements, 2012; Rao et al., 2011). As a consequence, it is important to understand the effect of composition and environmental conditions on the phase behaviour of the oil, surfactant and water systems in order to develop the successful microemulsion system.

1.2.6 Application of nanoemulsions and microemulsions in drug delivery

Even though nanoemulsions and microemulsions can be formed in different ways, the advantages of their use as a carrier vehicle for drugs are the same. Indeed, nanoemulsions and microemulsions have attracted much interest over recent years as drug delivery vehicles because their many beneficial properties including their transparency, their ease of preparation, an ability to be sterilized by filtration and their ability to improve the apparent aqueous solubility of a wide range of drug molecules, especially poorly-water soluble drugs. Table 1.1 lists the commercially available nanoemulsion and microemulsion formulations. The most convenient, easiest and cost effective way to administer a drug is via the oral route, which as a consequence dominates the drug delivery market. However, the oral delivery of poorly water soluble drugs poses some serious problems, such as poor drug stability and a limited ability of the drug to permeate the gastrointestinal membrane. Both nanoemulsions and microemulsions have been proposed to enhance the oral bioavailability of a range of drugs due to a variety of reasons including the protection against degradation in the gastrointestinal tract they provide a drug, the prolongation of the drug transit time, and their ability to target to specific sites in the gastrointestinal tract to utilise specific absorption pathways (Thiagarajan, 2011). Besides their use as oral drug delivery systems, there are many reports of nanoemulsions and microemulsions being exploited for a whole range of delivery routes, such as, intranasal (Mistry et al., 2009), transdermal (Ktistis et al., 1998; Trotta, 1999; Valenta et al., 2004), pulmonary (Bivas-Benita et al., 2004), ophthalmic (Kapoor et al., 2008), and parenteral (Araújo et al., 2011) delivery. However, despite these reports, most of the research on nanoemulsions and microemulsions (including water-in-oil and oil-in-water types) as drug delivery

systems has focused on their use as oral drug delivery systems to improve the bioavailability of drugs.

Table 1.1 Commercial nanoemulsion and microemulsion formulations

Drug	Brand	Company	Indication
Nanoemulsion formulations			
Propofol	Diprivan®	Astra Zeneca	Anesthetic
Dexamethasone	Limethason®	Mitsubishi Pharmaceuticals	Steroid
Flurbiprofen axetil	Ropion®	Mitsubishi Pharmaceuticals	Non-steroidal analgesic
Vitamin A,D,E, K	Vitalipid®	Fresenius Kabi	Parenteral nutrition
Microemulsion formulations			
Cyclosporine A	Sandimmune Neoral®	Norvartis Pharmaceuticals	Immunosuppressant
Ritonavir	Norvir®	AbbVie, Inc.	HIV/AIDS
Tipranavir	Aptivus®	Boehringer-Ingelheim	HIV/AIDS

1.3 Nanoparticle production

Nanoparticles are defined as particles in the size range 10 to 1,000 nm (Mohanraj et al., 2006). Generally reducing the particle size to the nano-sized range increases the surface area from which the drug can dissolve, which in turn leads to an improvement in drug dissolution rate and therefore most likely an increased bioavailability of the drug. The dissolution rate achieved from drug nanoparticles is much higher than that obtained using conventional size reduction techniques such as micronisation. As a consequence, nanoparticles have been explored as a means to improve the apparent aqueous solubility of a range of hydrophobic drugs (Khadka et al., 2014; Merisko-Liversidge et al., 2008; Yarnell, 2012). Moreover, research has found that using nanoparticles to deliver drug

can reduce the need for the use of solvents, such as Cremophor® EL (polyethoxylated caster oil), in the formulation.

Basically, drug nanoparticles can be prepared from one of two processes, either a 'top down' process in which large particles are broken down into smaller particles or a 'bottom up' process whereby the precipitation or crystallization of materials is carefully controlled to obtain the desired particle size. The two main 'top down' methodologies are media (or wet bead) milling and high pressure homogenization while the two main 'bottom-up' approaches are precipitation or crystallization.

1.3.1 Media milling

Making nanoparticles by media (or wet bead) milling normally consists of mixing drug, water and stabiliser and milling the resultant crude suspension with milling media - generally yttrium zirconia, spherical glass, ceramic or plastic (highly cross linked polystyrene resin) beads. The diameter of the beads is usually in the size range 0.4-3.0 mm. The process of making nanoparticles by wet bead milling starts with loading the crude aqueous suspension of drug and stabiliser together with the milling beads into the mill. Next the crude suspension is agitated at a very high shear rate in the milling chamber as shown in Figure 1.6. As a result of this agitation, the drug particle size is reduced by the presence of the beads to the nanometer size range. The advantages of this technique are minimal batch-to-batch variation, the avoidance of using organic solvents, the narrow particle size range, the ease of preparation and the ease of scale-up to industrial production levels. A number of crystalline drug nanoparticles, produced by wet bead milling, have been launched on the market including Rapamune®, Emend® and Megace®.
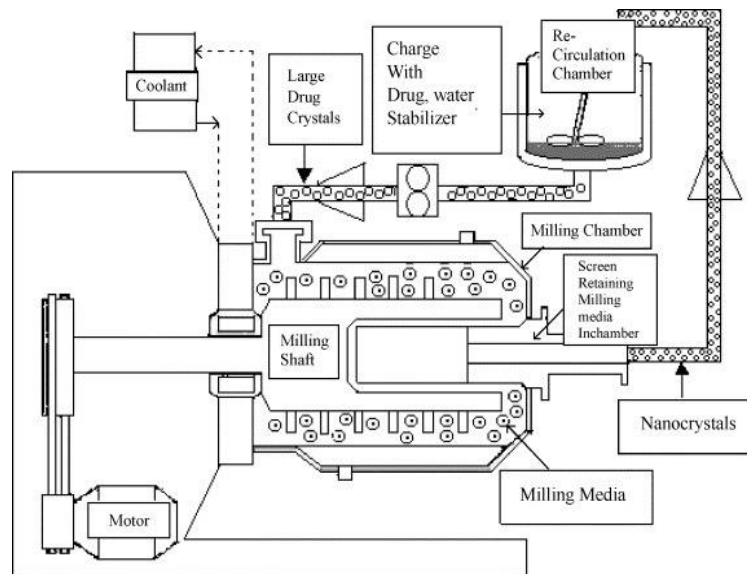
Figure 1.6 The media milling scheme (Merisko-Liversidge et al., 2003).

1.3.2 High pressure homogenization

Müller et al. (1999) developed homogenization methodology to produce nanometer particles. This methodology is now patented to SkyePharma using Dissocubes® as the name trade. Triglide® is an example of a drug produced by this technique. To produce nanoparticles by this methodology, typically, the drug is suspended in a stabiliser solution such as surfactant solution, which is then forced through a narrow gap at a high pressure of approximately between 15,000-30,000 psi resulting in a high velocity. Whilst maintaining the energy in the system, the static pressure of the system decreases dramatically below the vapour pressure of water leading to the suspension starting to boil. As a consequence the pressure of the system rapidly increases to ambient and consequently gas bubbles are imploded at the normal air pressure after the suspension exits from homogenization gap as shown in Figure 1.7. Therefore, reduction of particles can occur by the combination of this implosion force with the high shear forces experienced in the homogenization gap and the impact of particles. The resultant particle size can be controlled by the temperature, the power density of the homogenizer and the number of homogenization cycles used. The advantages of this technique are that it is easy to scale up, there is minimal batch-to-batch variation, the resultant particles are of a narrow size range and contain a low level of contaminates. One

drawback of this technique usually is the frequent clogging of the gap with highly concentrated drug formulations.
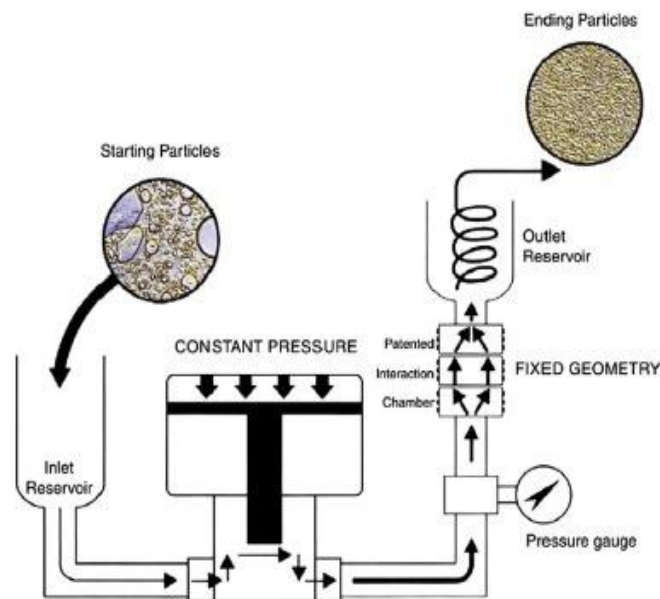
Figure 1.7 High-pressure homogenization processing scheme (Ghadimi et al., 2011)

1.3.3 Precipitation

Practically, this technique is performed by dissolving drug in a solvent and then adding a miscible, anti-solvent to precipitate the drug out of solution. In addition, surfactants may be added to either the solvent or anti-solvent to improve the stability of these nanoparticles. Nevertheless, this technique has some limitations. Firstly, the selection of the optimal precipitation conditions for nanoparticle production requires a high nucleation rate and a low growth rate to ensure that crystal growth controls the size and size distribution of the nanoparticles. One problem with this technique concerns safety and arises from the use of non-aqueous solvents as well as the possibility of residual solvent contamination.

Comparison of these three techniques of nanoparticles production led to the use in the present study, of wet bead milling for drug nanoparticle production. This particular technique was selected because of its many advantages, including the ease of nanoparticle production with no need to undertake prior pre-micronisation.

1.4 Nanoparticle stabilisation

The formation of nanoparticles from larger drug particles can be broken down into three stages: (1) wetting of the powder, (2) breaking up of aggregates and agglomerates and the reduction of particles to the colloid size of 1 nm to 1 μm and (3) stabilisation of the colloidal dispersion (Goodwin, 2006). Note that it is essential that an adequate amount of stabiliser is able to coat the nanoparticles as soon as they are produced by fracture of the larger particles, otherwise the benefits of the increased drug surface area will be lost (Merisko-Liversidge et al., 2003).

The strong forces of particle-particle attraction that increase as particle size decreases, arise from the high surface area to volume ratio and the resultant high surface energy. In order to reduce this high surface energy, the system responds by reducing its surface area, either by precipitation or agglomeration of the particles, as a result of the presence of strong, long-range attractive, van der Waals forces between particles. It is consequently essential, if the reduction in particle size is to be maintained, to provide a long range repulsion to overcome the tendency of the system to aggregate. It is necessary therefore to add a suitable stabiliser to provide these repulsive forces at the surface of the nanoparticles. The stabiliser can act to counterbalance the van der Waal's forces of attraction between colloidal particles by providing either repulsive electrostatic and/or steric forces.

1.4.1 Electrostatic stabilisation

The use of ionic surfactant and/or polymers, for instance, sodium dodecyl sulphate, dodecyl trimethyl ammonium bromide and hypromellose acetate succinate, in a nanoparticle system can act to introduce an electrostatic charge on the particle surface to stabilise particles (Han et al., 2012; Kuo et al., 2004; Lee et al., 2011). Figure 1.8 shows schematic diagram of the electrical double layer that is seen when a negatively charged particle is immersed in a polar medium. As can be seen, the negative surface charge of solid particles attracts ions of the opposite charge, here positively charged ions, from the surrounding aqueous medium at the Stern layer. However as the number of 'adsorbed' positively charged counter ions is insufficient to neutralise the negatively charged particle, a diffuse 'electrical double layer' is formed comprising of both positively and

negatively charged co-ions but with an excess of positively charged counter ions to neutralise the surface charge of the particle surface. Beyond the edge of the diffuse double layer, in the bulk of solution, there are equal number of positively charged counter ions and negatively charged co-ions. Note that charged surfactants and polymers can easily adsorb to surfaces of opposite charge in aqueous medium.
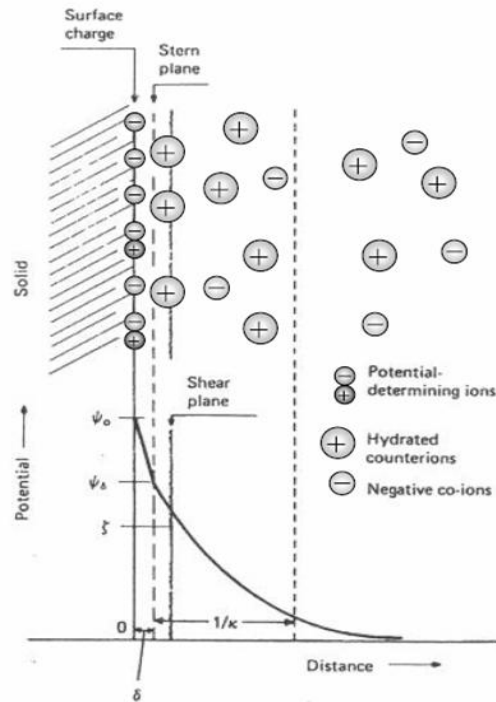
Figure 1.8 Schematic diagram of the electrical double layer formed when a negatively charged surface is immersed in a polar medium (Florence and Attwood, 1998)

The theory of electrical stabilisation of colloids is referred to the Derjaguin, Landau, Verwey, and Overbeek (DLVO) theory of colloid stability. According to the DLVO theory, the total potential energy (V_T) acting on a colloidal particle is the summation of van der Waal's forces of attraction (V_A) and the electrical repulsive forces (V_R).

$$V_T = V_A + V_R$$

1.4.1.1 Attractive forces

Hamaker was the first to quantify the total effect of van der Waals forces on a collection of colloidal particles, assuming that the total attractive energy varied with the sixth

power of the distance between two particles. The equation describes the forces of attraction (V_A) between two spheres of equal radius (R) at the distance between their centres (H):

$$V_A = -\frac{h}{6}\left(\frac{2R^2}{H^2 - 4R^2} + \frac{2R^2}{H^2} + \frac{H^2 - 4R^2}{H^2}\right)$$

where h is the Hamaker constant which depends on the properties of the particles and the dispersion medium. When the distance between the surfaces of the two spheres (H') is small, and the particles are large relative to the distance of separation, the equation reduces to:

$$V_A = \frac{-hR}{12H'}$$

The van der Waals forces of attraction are high when the distance between particles is small, but drops off rapidly when the distance between particles increases.

1.4.1.2 Electrical repulsive forces

The repulsive forces between particles are increased by the osmotic effect which produces an increase in the number of charged species on the overlap region of the diffuse electrical double layer. These repulsive forces increase as a function of the distance between particles as shown:

$$V_R = 2\pi\varepsilon R\psi_0^2 exp[-kH]$$

where ε is the permittivity of the polar liquid, R is the radius of the spherical particles, ψ_0 is zeta potential, and H is the distance between particles. The surface potential of a particle be determined using electrophoretic measurements.

1.4.1.3 Total potential energy

The full DLVO theory is expressed as the variation in total potential energy (V_T) as a function of the distance between particles, as shown in Figure 1.9.
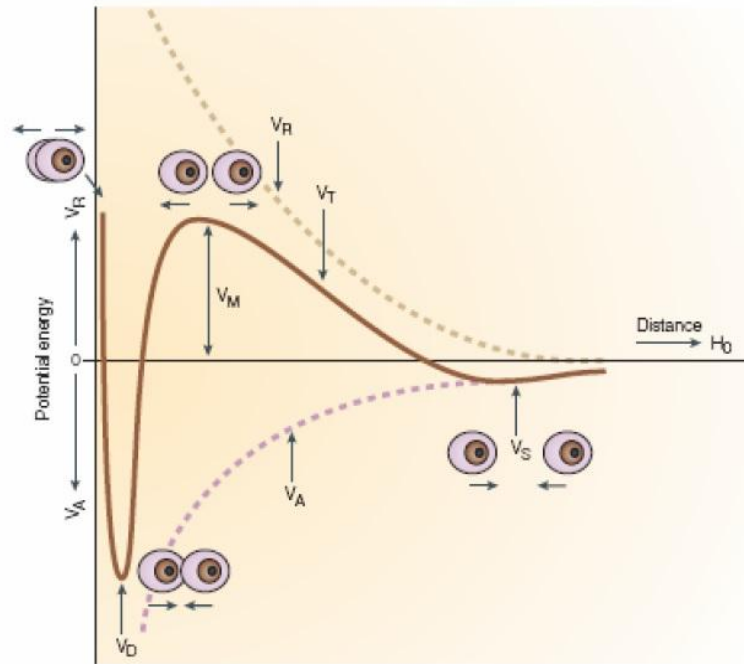
Figure 1.9 The total potential energy curve (V_T) between two particles is the summation of the van der Waal's forces of attraction (V_A) and electrical repulsive forces (V_R) as a function of the distance between particles (H). Taken from Rabinow (2004).

According to the DLVO theory, as two particles approach, if the particles possess enough energy to overcome the energy barrier or primary maximum (V_M), the attractive forces arise rapidly and dominate the total potential energy leading to irreversible aggregation of particles at the primary minimum (V_D). It is therefore essential that the nanoparticles in dispersion do not reach the primary minimum. If two particles do approach each other this closely then the formation of either coalescence or recrystallisation may occur. In contrast, at the secondary minimum (V_S), particles are held in a weak and reversible flocculation which can be easily reversed and the particles re-dispersed with the additional energy, such as shaking. Stabilisers, such as surfactants and polymers, can be used to provide sufficient repulsive forces between particles to ensure that they never reach the primary minimum, thereby positively impacting on the stability of the system.

1.4.2 Steric stabilisation

Nowadays, the term steric stabilisation has been widely used to describe the stabilising action of macromolecules particularly nonionic surfactants and/or polymers. Steric stabilisation generally occurs due to the absorbed surfactant and polymer layers on the dispersed particles. Steric stabilisation of particles can be achieved by a range of nonionic surfactants and/or polymers, for instance, Tween®, Brij®, hydroxylpropylmethylcellulose (HPMC) and polyvinylpyrrolidone (PVP). Figure 1.10 shows schematic of steric stabilisation of colloidal particles is achieved by attaching macromolecules to the surfaces of the colloidal particles.
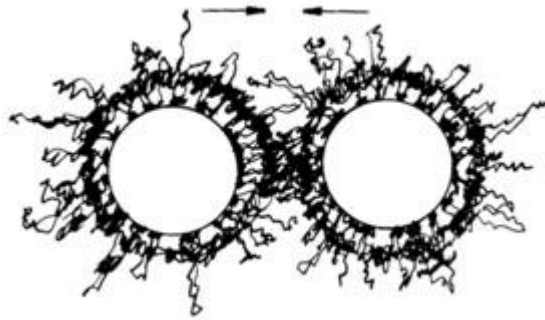
Figure 1.10 Schematic of steric stabilisation (Shi, 2002).

Modifications to the DLVO theory have been proposed to account for steric stabilisation (Vs) from adsorbed macromolecules:

$$V_T = V_A + V_R + V_S$$

Figure 1.11 illustrates the effect of V_S on the total potential energy curve showing that repulsive forces dominate between two particles at most interparticle distances and that, significantly, the primary minimum observed using electrostatic stabilisation alone is absent.
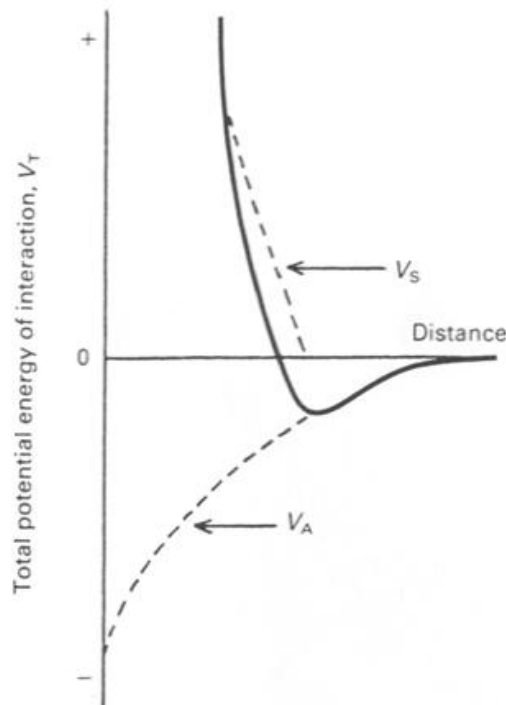
Figure 1.11 Total potential energy curve (solid line) for sterically stabilised particles showing the effect of the steric stabilisation term (V_S).

In non-aqueous dispersions, the adsorption of stabilisers onto the surface of particles results in a physical barrier to aggregation by either entropic or osmotic constraints. Firstly, in order for aggregation of two particles coated with nonionic polymers or surfactants to occur, the hydrophilic chains of the stabilisers have to be compressed which is entropically unstable and results in a repulsive force between the particles. Secondly, an osmotically-induced influx of solvent molecules into the region where the adsorbed surfactant and polymer layers overlap drives the particles apart. In both cases van der Waal's forces are overcome. Stabilisation by these two effects is commonly encountered in non-aqueous dispersions. However in aqueous dispersions, enthalpic stabilisation predominates especially for the stabilisers possessing polyoxyethylene chains. For example, when two hydrated polymer molecules approach each other, some of the water of hydration is released, which consequently possess a greater degree of freedom than when it was associated with the polyoxyethylene chains. In order to release water molecules from the polymer chain, there must be an energetically unfavourable, positive enthalpic change.

Steric stabilisation of colloidal particles has several benefits over electrostatic stabilisation which includes a relative insensitivity to the presence of electrolytes, equal efficacy in both aqueous and non-aqueous dispersion media, equal efficacy at both high and low solids content, and a reversibility of flocculation (Shi, 2002).

1.4.3 Electrosteric stabilisation

Electrosteric stabilisation is the combined use of nonionic surfactants/polymers and ionic surfactants or charged polymers such as a polyelectrolyte. As two particles approach each other, the combined adsorbed polymer/charged layer causes electrosteric repulsions between particles (Runkana et al., 2006) thereby overcoming the attractive van der Waals interactions (Lim et al., 2009; Seebergh et al., 1994; Yeap et al., 2012). Even though there is not much literature studying the effects of electrosteric stabilisation, there is increasing interest in the mechanism of this type of stabilisation.

1.4.4 Application of nanosuspensions in drug delivery

Drug nanoparticles have been widely used explored for use in a range of drug delivery technologies, including oral, injectable, inhalable, and buccal applications (Basa et al., 2008; Cooper, 2010; Van Eerdenbrugh et al., 2008). Table 1.2 gives examples of nanosuspension formulations on the market.

Table 1.2 Nanosuspension formulations in the market (Gao et al., 2013; Junyaprasert et al., 2015; Rabinow, 2004)

Drug	Indication	Company	Route
Paclitaxel	Anticancer	American Pharmaceutical Partners	Intravenous
Silolimus	Immunosuppressant	Wyeth	Oral
Aprrpitant	Anti-emetic	Merck	Oral
Cytokine inhibitor	Crohn's disease	Cytokine PharmaSciences	Oral
Busulfan	Anticancer	Supergen	Intrathecal
Budesonide	Asthma	Sheffield Pharmaceuticals	Pulmonary
Silver	Eczema, atopic dermatitis	Self-developed	Topical
Paliperidone palmitate	Anti-depressant	Johnson & Johnson	Injection
Finofibrate	Hypercholesterolemia	Abbott	Oral

The oral route is the preferred route for drug administration due to its convenience, good patient compliance and low production costs. Drug nanoparticles can increase the drug dissolution rate as well as exhibiting improved adhesion to the intestinal mucosa which allows better contact of the delivery system with the intestinal cells and results in a greater concentration gradient of the drug across the gastrointestinal tract into blood which leads to an increase in intestinal drug absorption (Arunkumar et al., 2009; Chen et al., 2005; Yadollahi et al., 2015).

For parenteral administration, advantages of this administration by this route include avoidance of first-pass metabolism, reliable dosing and higher bioavailability. However, drug particles for this route of administration need to be smaller than 5 μm in order to prevent the blockage of capillaries (Arunkumar et al., 2009). Nanosuspensions therefore improve therapeutic efficiency and reduce the cost of therapy through improved dosing efficiency and the need for smaller injection volumes (Lou et al., 2009).

Nanosuspensions as ocular drug delivery systems offer several advantages. For example, the surface of the nanoparticles can be modified by using polymers appropriate for the desired effect (Nagarwal et al., 2009). Drug loss is reduced because

of the natural adhesiveness of drug nanoparticles (Das et al., 2011), while the enhanced drug dissolution rate results in an increase in the extent of absorption (Kassem et al., 2007).

Pulmonary nanosuspensions can not only solve the problem of poor drug solubility in pulmonary secretions as well as the lack of selectivity through direct delivery to the target pulmonary cells (Jacobs et al., 2002) but can also improve drug diffusion and dissolution rate, resulting in an increased bioavailability and the prevention of undesirable drug deposition in the mouth and pharynx (Yadollahi et al., 2015).

It is clear that the advantages of nanoparticles can result in a significant increase in the drug dissolution rate and therefore an enhancement of the drug's bioavailability (Chingunpituk, 2011; Rabinow, 2004).

1.5 Classification of surfactants

Normally, surfactants are classified into four types dependent upon the charged nature of their polar head group. Firstly, surfactants with a negatively charged head group are referred to as anionic, while a positively charged surfactant head group means that the surfactant is described as being cationic. Surfactants with uncharged head groups are termed nonionic surfactants. The last type of surfactant are the zwitterionic surfactants which consist of a head group that has both a negatively and positively charge. Table 1.3 gives examples of each surfactant type.

Table 1.3 Examples of surfactants in each class. (Lindhardt C, 2005)

Type of surfactant	Example
Nonionic	polysorbates (i.e. Tween 20, Tween 80), ethoxylated 4-(1,1,3,3-tetramethylbutyl)phenol (Triton X-100), alkyl-polyethylene glycol ether (i.e. polyoxyethylene (23) lauryl ether (Brij 35), polyoxyethylene (10) oleyl ether (Brij 97))
Anionic	sodium dodecyl sulphate, sodium cholate hydrate,phosphatidyl inositol, deoxycholic acid, sodium salt, sodium propionate, potassium sorbate
Cationic	benzalkonium chloride, dodecyl trimethyl ammonium bromide, cetyl pyrimidinium bromide, cetyl trimethyl ammonium bromide
Zwitterionic	lecithins, cephalins

Anionic surfactants contribute the largest group of available surfactants and include fatty acid salts, sulfates, ether sulfates and phosphate esters. As a rule, anionic surfactants are generally sensitive to salt, particularly to divalent or multivalent cations, and to pH. A consequence of this sensitivity, there is the possibly of controlling the release of drug from a delivery system as it passes down the gastrointestinal tract, experiencing changes in pH.

Cationic surfactants frequently contain an amine head groups and are frequently used as antibacterial agents. Because of the nature of their head group charge, the properties of these surfactants, in particular their surface activity and self-assembly, are strongly influenced by the presence of salt and by solution pH. One important benefit of this type of surfactant is their use in topical drug delivery and in oral hygiene products. Nevertheless, cationic surfactants usually are irritant and sometimes toxic, leading to their limited use in drug delivery.

Surfactants with uncharged or nonionic head groups (known as nonionic surfactants) often contain an oligo(ethylene oxide) head group, and with the exception of phospholipids, are the most widely used type of surfactant in drug delivery. The nonionic nature of this head group makes these surfactants relatively insensitive to salt

and changes in pH. In contrast, however, they are more sensitive to changes in temperature. As a consequence, nonionic surfactants as a group are less irritation than charged surfactants. Furthermore, for the same hydrocarbon chain length, the critical micelle concentration (cmc, i.e. the concentration at which the surfactants start to form micelles) of nonionic surfactants is much lower than the cmc of a charged surfactant making this group of surfactants more appropriate for the purposes of drug delivery.

With the exception of phospholipids, zwitterionic surfactants are less commonly encountered than cationic, anionic and nonionic surfactants. The head group of zwitterionic surfactants frequently consists of a positively charged quaternary amine group and either a negatively charged sulphonate or carboxylate group. Because of the nature of the zwitterionic head group, this class of surfactant can either be positively charged (at low pH), negatively charged (at high pH) or effectively neutral (at intermediate pH). Due to their low irritation ability, surfactants in this class are widely used in personal care products.

1.6 Physico-chemical characterization of nanoemulsion, microemulsion and nanosuspension systems

1.6.1 Phase behaviour

A study of the phase behaviour of nanoemulsions and microemulsions can help the understanding of both the theoretical and experimental results obtained. Generally, plotting the phase behaviour of nanoemulsions and microemulsions containing oil, water and surfactant using a ternary phase diagram is very common. In a ternary phase diagram, each of the apices represents 100% of the particular component. Figure 1.12 illustrates the range of possible phase structures that can be formed upon mixing oil, water and surfactant, including micelles, nanoemulsions, microemulsions and bilayers. The microstructures formed can be divided into two main groups. Firstly, the size-limited or 'discrete' self-assemblies, which might be characterized as spherical structures such as micelles and nanodroplets. The second group is the infinite or 'unlimited' self-assemblies, which exhibit aggregation over macroscopic length scales in one, two or even three dimensions. As a consequence such structures are referred to as liquid crystalline structures. Examples of one, two or three dimensional, liquid

crystalline, structures include the hexagonal phase, the lamellar phase, and the cubic phase and bicontinuous structures. A micelle can be formed in one of two orientations, namely normal and reverse, similarly nanoemulsions and microemulsions can also be in normal and reverse orientation, namely as oil-in-water nanoemulsions and microemulsions and water-in-oil nanoemulsions and microemulsions.
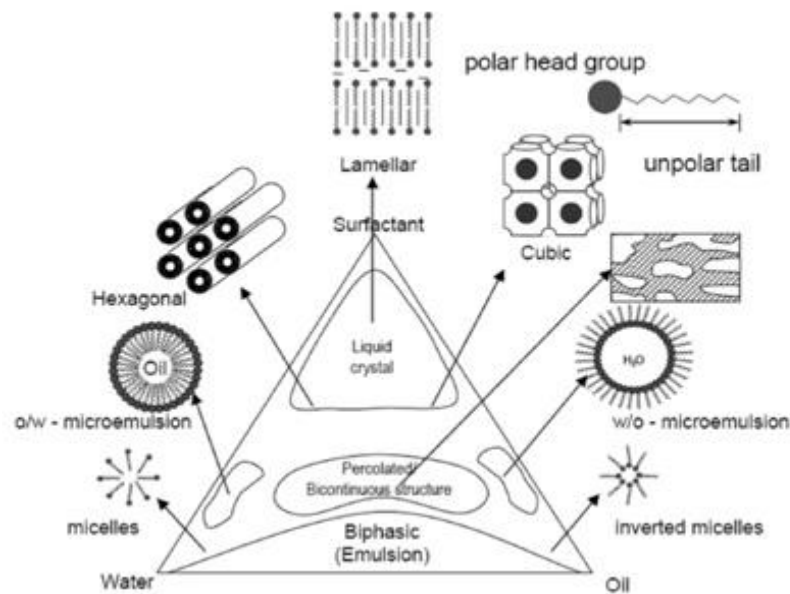
Figure 1.12 Schematic diagram representing the hypothetical phase behaviour of a ternary mixture of water, oil and surfactant. Modified from Moulik and Paul (1998).

1.6.2 Phase inversion temperature (PIT)

In addition to the PIT method being using for preparation of nanoemulsions, a PIT experiment can be used to explain the way in which oils of different molecular volume/weight are solubilised into either the microemulsion and nanoemulsion droplets (Wasutrasawat, 2011). Most of nonionic surfactants, particularly those containing a polyoxyethylene head group, form aqueous micellar solutions which exhibit a PIT upon heating (Corti et al., 1984). An oil-in-water microemulsion and nanoemulsion is formed a low temperatures but transforms into a water-in-oil microemulsion and nanoemulsion at higher temperatures (transitional phase inversion) (Engels et al., 1995; Engelskirchen et al., 2007; Morales et al., 2003). During cooling, a nanoemulsion crosses a point of

zero spontaneous curvature and minimal surface tension, promoting the formation of dispersed oil droplets in aqueous phase due to the surfactant is preferentially soluble in the water (Fernandez et al., 2004; Izquierdo et al., 2004).

When the colloidal system containing a polyoxyethylene surfactant is heated up to the PIT, the clear solution becomes cloudy and *vice versa* as the solution temperature is increased. This clouding is due to the interactions between the polyoxyethylene-containing surfactant monomers in the aggregate changing from repulsive to attractive as higher temperatures as a consequence of the dehydration of the polyoxyethylene chains. These changes lead to a decrease in the effective area of the surfactant head group and a change in aggregate shape upon increased temperature to more elongated, bicontinuous or even an inverted W/O structure. When the PIT of a nanoemulsion decreases in comparison to the corresponding parent micelle, it is suggestive of the shape of nanoemulsion aggregates becoming more asymmetric. In contrast, an increase in the PIT as a function of increasing oil content is indicative of the oil forming a core in the centre of the nanoemulsion droplet which, as a consequence, becomes more spherical in shape(Aveyard et al., 1986; Malcolmson et al., 1998). Note, that if there is no increase in the PIT as a function of increasing oil content, this is suggestive that the oil chains intimately mix with the hydrophobic surfactant chains, rather than forming a core in the centre of the nanoemulsion droplet (Wasutrasawat, 2011).

1.6.3 Viscosity

Viscosity has been used widely as a technique for the analysis and/or characterization of a range of colloidal systems including synthetic polymers (Debye et al., 1948), biological macromolecules (López Martínez et al., 2003), nanoparticles (García de la Torre et al., 2007; Pamies et al., 2008), wormlike macromolecules and micelles (Bohdanecky, 1983; Masuelli, 2013), nanoemulsions (Kumar et al., 2009) and microemulsions (Hsieh, 2010).

The viscometric behaviour of surfactants in solution is frequently studied to enable the physico-chemical characterization of their aggregation forms. In particular, the technique provides information about a number of fundamental properties of the colloidal systems in solution, including their interaction with the solvent and the

conformation of flexible (linear and nonlinear) chains and rigid particles of arbitrary shape (Ozeki et al., 1980; Pamies et al., 2008; Panmai et al., 1999; Penott-Chang et al., 2007). Significantly for the present project, viscometry is used extensively to investigate the hydration and/or shape of nanoemulsion and microemulsion droplets in order to provide the complementary information for analysing small angle neutron scattering data. In this respect, Einstein's viscosity equation relates the relative viscosity (η_{rel}) of dilute dispersions of spherical non-deformable, non-interacting particles, such as a dilute micelle solution, to the volume fraction ($\emptyset$) they occupy in the system (Florence et al., 1999).

$$\eta_{rel} = 1 + 2.5\emptyset$$

The equation is valid in situations when $\emptyset$ is less than 0.05.

However, if the particles are asymmetric, Einstein equation can be modified to:

$$\eta_{rel} = 1 + v\emptyset$$

where v is a shape factor related to the axial ratio (a/b) of the particle, defined as an oblate or prolate ellipsoid.

In order to determine the intrinsic viscosity [η] of the surfactant aggregates, both the Huggins and Kraemer equations can be used. Extrapolation to zero surfactant concentration of the linear relationship obtained from the function of reduced viscosity and inherent viscosity against concentration, namely the Huggins and Kraemer equations, respectively yields the intrinsic viscosity (Pamies et al., 2008). An extrapolated value of [η] of 2.5 is indicative of unhydrated, symmetrical particles - a value of greater than this indicates that the particles are solvated and/or asymmetrical. Usually, the Huggins and Kraemer equations are used to illustrate the dilute solution properties of surfactant aggregates in solvents (Aveyard et al., 1989; Bergenholtz et al., 1995; Devi et al., 2003; Ortega et al., 2007).

The 'reduced' Huggins viscosity is defined as:

$$\frac{\eta_{sp}}{C} = [\eta] + k_H[\eta]^2 c$$

where η_{sp} is specific viscosity, C is a given concentration, η_{sp}/C is the reduced viscosity and k_H is the Huggins coefficient.

The Huggins equation is frequently used in combination with the Kraemer equation to obtain a second estimate of intrinsic viscosity:

$$\frac{\ln \eta_{rel}}{C} = [\eta] - k_K [\eta]^2 c$$

where η_{rel} is the relative viscosity and k_K is the Kraemer coefficient.

Furthermore, if a particle is hydrated, it will be associated with a larger volume fraction than its unhydrated counterpart. The Oncley equation defines volume fraction as $[\tilde{\upsilon} + W_1 \tilde{\upsilon}_1^0]$ (Elworthy et al., 1965), so that the equation becomes as:

$$[\eta] = v[\tilde{\upsilon} + W_1 \tilde{\upsilon}_1^0]$$

where $\tilde{\upsilon}$ is a partial specific volume of the particles, W_1 is a solvation expressed as g solvent/g solute, and $\tilde{\upsilon}_1^0$ is a specific volume of the solvent.

The above equation allows the calculation of the level of hydration, $W_1 \cdot v = 2.5$ (for spherical particles). As expressed in the above equation, there are two contributions to the intrinsic viscosity, namely shape and size or volume. Consequently, the value of $[\eta]$ can be used to estimate the shape of the aggregates in solution, assuming that is if hydration is known.

1.6.4 Zeta potential

Figure 1.13 shows a particle surface in aqueous solution, predominantly covered with negative charges. Frequently, the zeta potential is the parameter used to represent the charge of the particle and is widely used in product stability studies and surface adsorption research (Delgado et al., 2007; Xu, 2008) even though it in fact corresponds to a potential at an unknown distance from the particle surface (Goodwin, 2006).
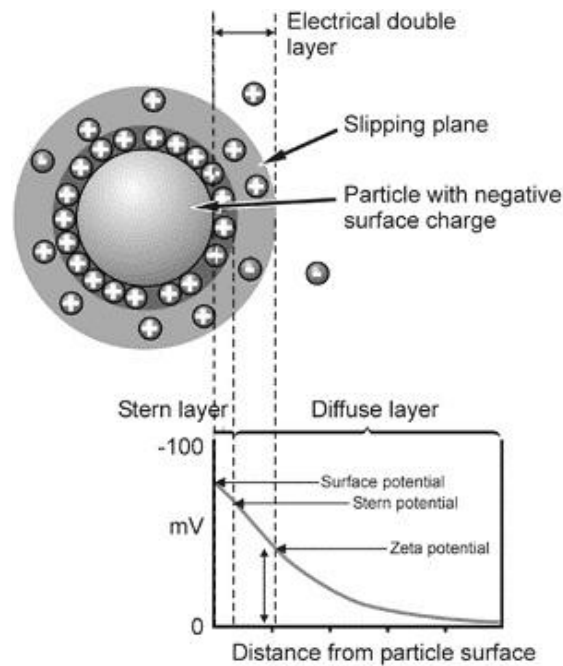
Figure 1.13 Schematic of the electrical double layer at the surface of solution-phase nanoparticles. Modified from Freire (2011).

As is well known, in an aqueous solution, charged nanoparticles possess a layer of oppositely charged ions which are strongly associated with their surface, referred to as the Stern layer. A second, more diffuse outer layer contains an excess of ions of the opposite charge to that of the nanoparticle. Together, these two layers are called the electrical double layer. As the nanoparticle moves in solution due to Brownian diffusion or some externally applied forces, a distinction is created between ions in the diffuse layer that move with the nanoparticle and ions that remain with the bulk, continuous phase. The electrostatic potential at this "slipping plane" boundary, which is related to the surface charge of the nanoparticle is determined when measuring the zeta potential of the nanoparticle. The zeta potential is determined by applying an external electric field to the solution and measuring the resultant electrophoretic mobility of the nanoparticles (Clogston et al., 2011). Note that it is the electrophoretic mobility of the nanoparticles that is actually measured, rather than the zeta potential *per se*, in much the same way as the diffusion coefficient is measured when determining the particle size of a particle using photon correlation spectroscopy. Müller et al. (2001) found that if the zeta potential of nanoparticles is ± 30 mV then that nanoparticle is likely to be stable.

1.6.5 Photon correlation spectroscopy

Photon correlation spectroscopy (PCS) or dynamic light scattering is used to measure particle size. The random motion of colloidal particles in solution is called "Brownian" motion and is a result of the movement of the solvent molecules surrounding them. The motion of the colloidal particles in solution is inversely proportional to its particle size with small particles moving faster and further than large particles in the same time period. The velocity of the Brownian motion of the particles is defined as the translational diffusion coefficient (D), which can be related to particle size by the Stokes Einstein equation.

$$d(H) = \frac{k_B T}{3\pi\eta D}$$

where $d(H)$ is the hydrodynamic diameter, D is the translational diffusion coefficient, k_B is the Boltzmann's constant, T is the absolute temperature in degrees Kelvin and η is the liquid viscosity.

PCS measures an 'equivalent particle diameter' which is known as the apparent hydrodynamic diameter of the particles dispersed in solution, by mathematically analyzing the variation in the intensity of light scattering over time as determined using an autocorrelator.

PCS is widely used for particle sizing since it is a rapid measurement technique and requires only a small amount of sample. In addition, it is possible to measure particle size in a wide variety of suspending liquids. There are, however, a few drawbacks to this technique. First, this technique does not provide the information about the shape of particles, while a small amount of dust can make the measurements and their subsequent interpretation difficult (Tscharnuter, 2006). This drawback can be addressed by the use of filtered water to prepare the samples.

1.6.6 Small angle neutron scattering

One of the most important techniques used to determine the structure of a particle on the nanometer scale is neutron scattering. Small angle neutron scattering (SANS) is a

diffraction technique that exploits the wave particle duality of a neutron and its unique nuclear properties to provide information on particle morphology including the size and shape of a molecule, such as a surfactant, and its assemblies, such as a micelle (Bergström et al., 1999; King, 1999). Despite this, the technique has a number of disadvantages, not the least being the fact that it is slow and expensive as the experiment takes several days and must be performed at large international facilities. Overall however, SANS is probably the best technique to measure the internal structure and shape of small, colloidal particles.

There are two ways to produce neutrons. Firstly, neutrons are produced by the fission of a heavy atom such as uranium-235 in a nuclear reactor, i.e. a "continuous" or "steady state" source. The second way to produce neutrons is using a "pulsed" or "spallation" neutron source, where particle accelerators and synchrotrons are used to generate intense, high-energy, proton beams which are directed at a target composed of heavy nuclei to produce a beam of neutrons (King, 1999). After producing a beam of neutron, the beam is moderated to decrease its velocity and to produce neutrons of the required wavelength for the experiment. An example of a pulsed neutron source is the Rutherford-Appleton Laboratory, Didcot, UK, which was used in the present study.

The most fundamental difference between neutron and other scattering techniques such as light scattering and X-ray scattering is that neutrons are scattered by the nucleus itself whereas light and X-ray are scattered by the electrons around atomic nuclei. Significantly, neutrons are scattered differently by different isotopes of the same element due to the fact that an isotopes neutron scattering ability is determined by its scattering length. For instance, H_2O and D_2O contain different isotopes of hydrogen which exhibit significantly different scattering lengths such that the scattering length densities of the two molecules are -0.56 x 10^{-6} and 6.39 x 10^{-6} Å^{-2}, respectively. As a result of this property, various part of a structure can be specifically highlighted by selectively protonated or deuterated chemical to be "invisible" to neutron by contrast matching.

As with any scattering techniques, an image of the characteristic distances and interactions within the sample can be constructed from the ensemble of all the correlations production from the wave scattered by the sample at a given angle. Static light scattering and small angle X-ray scattering (SAXS) notionally provide the same

information for the sample as small angle neutron scattering. However, in contrast to light and X-ray scattering which occur due to interactions of the light and X-ray beams with the electron cloud around the atom, and are therefore dependent upon atomic number, the scattering of neutrons occurs due to interaction of the neutron beam with the nuclei and is not dependent upon atomic number, varying in intensity with atomic number of the atom.

Although, light scattering, and particularly PCS, is used widely to determine the particle size of a colloidal sample, there are limitations when the samples are turbid or are highly concentrated (Brown et al., 1975; Goodwin, 2006) or contain more than one population of particles. Furthermore, due to the wavelength of light, the scattering vector, Q, is less than 0.002 Å^{-1}, a fact which limits light scattering to larger aggregates and which means that light scattering cannot use for determination for determining the shape of small micellar aggregates. While X-ray scattering does not suffer these particular limitations, it does suffer from the drawback that the X-ray beam may cause irreversible sample damage, especially for biological samples such as proteins and lipids but also for molecules such as surfactants (Martis et al., 2011; Stanley et al., 2014).

In contrast, neutron scattering possess many advantages over light and X-ray scattering, such as the fact that neutrons do not possess a charge and can therefore penetrate into a sample without damaging it, and that it is possible, by altering the scattering length of the sample, to specifically "highlight" (by contrast matching) part of the system of particular interest. As a consequence of these, and other advantages, small angle neutron scattering (SANS) was used in the present study to determine the size and morphology of the nanoemulsion and microemulsion droplets in a presence of nanoparticles over time.

1.6.6.1 Theory of small-angle neutron scattering

The scattering vector

Once in contact with a sample, neutrons can undergo a series of events, including absorption by the sample, multiple, coherent/incoherent scattering by the sample, or even transmission through the sample. In SANS, only the coherent elastic interaction

between the neutron beam and the sample is considered. Figure 1.14 shows the coherent scattering of neutrons by a sample. The momentum transfer or wave vector transfer is known as the scattering vector or Q which is described by the relationship between the incident, namely k_i, and the scattered, namely k_s, wave vectors (Figure 1.14).
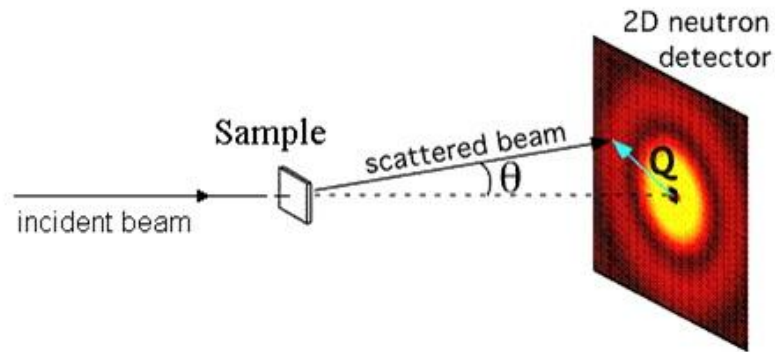
Figure 1.14 Scattering of neutrons by a sample (NIST, 2015).

The magnitude of scattering vector (Q) can be written as:

$$Q \; = \; |Q| = |k_s - k_i| = \frac{4\pi n \; sin\left(\frac{\theta}{2}\right)}{\lambda}$$

when n is "neutron" refractive index, θ is the scattering angle and λ is the incident neutron wavelength. In practise, n is found to be slightly less than unity. Neutrons of the right wavelength are totally externally reflected from an interface so that n can be approximated to ~ 1. Normally, Q has dimensions of (length)$^{-1}$ and is quoted either as nm^{-1} (SI units) or, more typically as Å^{-1}.

By substituting the equation above into Bragg's law of diffraction:

$$\lambda = 2d \; sin\left(\frac{\theta}{2}\right)$$

it is possible to obtain the very simple expression:

$$d = \frac{2\pi}{Q}$$

where the molecular length scale (*d)* is obtained over a particular Q range.

This equation allows the ready determination of the molecular length scale (*d*) in a sample from the position of any diffraction peak in Q space (King, 1999)

1.6.6.2 Scattering length density and contrast matching

One of the important factors when determining particle size and morphology using light scattering technique is the difference in the speed of travel of light in the solute and solvent, namely the difference in refractive index. Exactly the same principle applies in X-ray scattering, although the difference here is known as the difference in electron density, while in neutron scattering, the equivalent difference is the neutron scattering length density.

The scattering length density, ρ_{SLD} of a molecule with *i* atoms may be readily calculated from the simple expression:

$$\rho_{SLD} = \sum_i b_i \frac{DN_A}{MW}$$

where *D* is the bulk density of the molecule, b_i is the coherent neutron scattering length of nucleus *i*, N_A is Avogadro's constant and *MW* is molecular weight. The scattering length density normally has dimensions of (length)$^{-2}$ and is expressed in units of 10^{10} cm^{-2} or 10^{-6} Å^{-2}.

Contrast matching is a powerful tool, only useful in neutron scattering studies, to study multicomponent samples. In any experiment, the contrast term is described as the square of the difference between the scattering length density (or "neutron" refractive index) of the part of sample of interest, and the surrounding medium. At the contrast match point, i.e the point in where the difference in scattering length densities is zero, there is no neutron scattering observed from the part of the sample of interest, which has effectively become "invisible" to neutrons. For example, Smarsly et al. (2001) studied the mechanism of nitrogen sorption into porous silica by contrast matching the silica and the condensed nitrogen to each other in order to establish the number of "empty" (nitrogen free) pores.

In neutron scattering studies the difference in scattering (both in terms of phase and intensity) between a proton and a deuterium is widely exploited in contrast match studies. For example, using a mixture of D_2O (scattering length density, 6.39 x 10^{-6} $Å^{-2}$) and H_2O (scattering length density, 0.56 x 10^{-6} $Å^{-2}$) it is often possible to match the scattering length density of the medium to the scattering region of interest and thereby making it "invisible" as is illustrated in Figure 1.15.
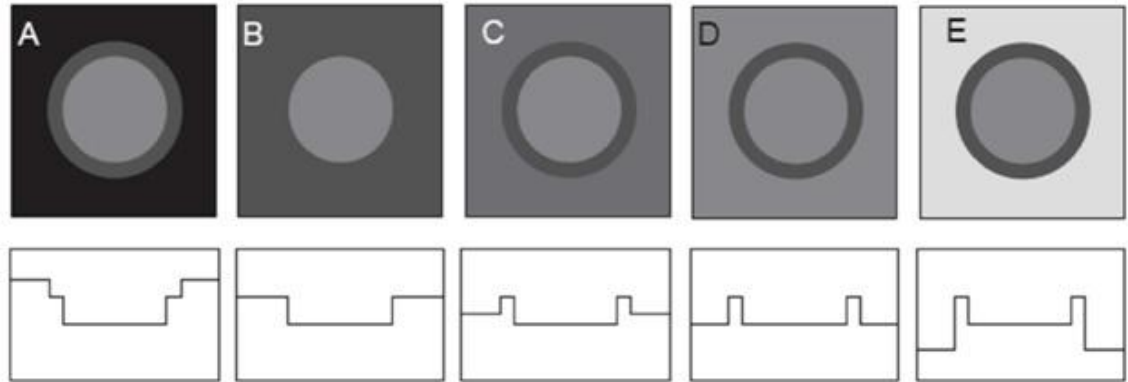
Figure 1.15 Schematic representation of a contrast variation experiment using different D_2O/H_2O mixtures to study core shell nanoparticles. The second row of figures schematically show the scattering length density profile across the core shell structure (Rübe et al., 2005)

1.6.6.3 SANS data interpretations

The absolute SANS intensity of scattering is outlined below;

$$\frac{d\Sigma}{d\Omega}(Q) = n_p P(Q) S(Q)$$

where $d\Sigma/d\Omega$ is the differential scattering cross section, n_p is the average number density of droplet in scattering volume (V). The term $P(Q)$ is well known as a form or shape factor, which is a dimensionless function which describes how $d\Sigma/d\Omega$ is modulated by interference effects between radiation scattered by different parts of the same scattering centres (King, 1999). As a consequence, this term depends on both the size and shape of the scattering centre in an absence of interference effects. $S(Q)$ or the structure factor represents the effect of interference due to neighbouring scatterers and depends on their relative positions.

1.6.6.4 Models of form factors $P(Q)$

A core-shell model is widely used to describe the scattering obtained from micelles or microemulsions/nanoemulsions, where the core is considered to consist of the surfactant tails of the surfactant (or in the case of a microemulsion/nanoemulsion, oil) while the shell is composed of the surfactant head groups (or in the case of a microemulsion/nanoemulsion, surfactant). Pedersen (1997) found that micelles or microemulsions could be well fitted by assuming one of two shapes, namely a sphere or an ellipsoid. The form factor is weighted by the relative volumes of the core and shell of the droplets as well as their scattering length densities.

The form factor for a core shell model of spherical particle is:

$$F(Q) = \frac{4}{3}\pi R_c^3 (\rho_c - \rho_s)\frac{3j_i(qR_c)}{qR_c} + \frac{4}{3}\pi R_s^3(\rho_s - \rho_{solvent})\frac{3j_i(qR_s)}{qR_s}$$

where $j_i(x) = (\sin x - x\cos x)/x^2$, and when V_c and V_s are the volumes of core and shell, R_c and R_s are the radius of core and shell, ρ_c, ρ_s and $\rho_{solvent}$ are the scattering length densities of core, shell and solvent. $F(Q)$ is integrated during the fitting procedure using a Schultz distribution function to account for sample polydispersity.

For ellipsoidal droplets, the corresponding form factor is written as:

$$\langle f(Q)^2 \rangle_0 = \int_0^{\pi/2}\left(V_c(\rho_c - \rho_s)F_1\left(qR_c\sqrt{sin^2\theta + \varepsilon_c^2 cos^2\theta}\right) + \right.$$
$$\left.(V_c + V_s)(\rho_s - \rho_0)F_1 \times \left(qR_s\sqrt{sin^2\theta + \varepsilon_s^2 cos^2\theta}\right)^2\right)^2 \sin\theta d\theta$$

where Vc and Vs are the volumes of core and shell, ρ_c, ρ_s and ρ_0 are the scattering length densities of core, shell, and alkane, Rc and Rs are the semi-axes of core and shell, and ε_c and ε_s are the axial ratios of core and shell.

1.6.6.5 Models for structure factor $S(Q)$

The structure factor, $S(Q)$, describes how $(d\sum/d\Omega)$ is modulated by interference effects between neutrons scattered by different scattering bodies (King, 1999). As a

consequence, it depends on the degree of local order in the sample, which increases with the concentration of scattering bodies in the system.

Many previous studies have found that a hard-sphere model can satisfactorily describe the structure factor for many nanoemulsion and microemulsion systems (Arleth et al., 2001; Preu et al., 1999), particularly when a nonionic surfactant is used to prepare/stabilise the system (Nagao et al., 2005). As a consequence, therefore, the structure factor derived by using the Percus-Yevick approximation was used in the present study for analysis of the nanoemulsions stabilised by nonionic surfactant.

The equation is used as following (Ashcroft et al., 1966):

$$S(q) = \frac{1}{1 - nc(qR_s)},$$

$$c(qR_s) = -4\pi R_s^3 \int_0^1 ds\, s^2 \frac{\sin sqR_s}{sqR_s} (\alpha + \beta_s + \gamma_s{}^2)$$

where $c(qR_s)$ is the direct correlation function and

$\alpha = (1 + 2\eta)^2 / (1 - \eta)^4$,

$\beta = -\dfrac{6\eta(1 + \eta/2)^2}{(1 - \eta)^4}$,

$\gamma = (1/2)\eta(1 + 2\eta)^2 / (1 - \eta)^4$

η is a packing-density parameter and it is related to the concentration of spheres (φ) as follows:

$$\eta = (\pi/6)\varphi R_s^3$$

As stated above, the hard-sphere model derived by Percus and Yevick is most suitable for fitting the SANS data of nanoemulsions stabilised by nonionic surfactant. However, in the case of microemulsions stabilised by an anionic surfactant, such as SDS, the Hayter-Penfold model is more appropriate and has been widely used to successfully describe charge interactions in such systems (Hayter et al., 1983):

$$U(w) = d \cdot U_0 \exp[-k(w - d)]/w$$

where U_0 is the depth of the potential, *1/k* the decay constant of this potential, *d* is particle diameter and *w* is the distance from the centre of the reference particle. In the equivalent hard-sphere model, the repulsive potential is considered to be infinite when the inter-particle distance is smaller than the effective hard-sphere diameter and zero when the inter-particle distance is larger than the effective hard-sphere diameter.

1.6.6.6 SANS fitting and analyzing

For micelles and nanoemulsions stabilised by the nonionic surfactant, Brij 97, the best fit model for the SANS data was a monodisperese oblate ellipsoid (Wasutrasawat, 2011). This form factor is described by:

$$P(Q) = \int_0^1 |F(Q,\mu)|^2 \, d\mu$$

$$F(Q,\mu) = \frac{3(\sin x - x \cos x)}{x^3}$$

$$x = Q[a^2\mu^2 + b^2(1-\mu^2)]^{1/2}$$

where μ is the cosine of the angle between the scattering vector Q and the asymmetry axis of the ellipsoid, with major and minor axis a and b, respectively.

As the interparticle structure factor, *S(Q),* for dilute nanoemulsions, stabilised by nonionic surfactants, is typically the result of very weak attractive interactions, the Percus Yevick approximation for hard spheres is most commonly used (MarzAn et al., 1993).

In contrast to the SANS data obtained for the Brij 97-stabilised systems, the SANS data obtained for micelles and microemulsions prepared using the anionic surfactant, SDS, have been reported to be most successfully fitted using the core-shell monodisperse prolate ellipsoid model (Caponetti et al., 2004; Griffiths et al., 2005; Hsieh, 2010). For the SDS-stabilised micelles when the core-shell particle model is used, it is assumed that the core is comprised of the hydrocarbon chains of surfactant, while the shell is made up of the surfactant head groups, the associated counter-ions and some solvent

molecules (Berr et al., 1986; Berr et al., 1989; Thurn et al., 2002; Yang et al., 2000; Zemb et al., 1985). While in case of SDS-stabilised microemulsions, it is assumed that the core is composed of all oil molecules together with the surfactant tails and shell is comprised of the surfactant head groups with any associated counter-ions and the water of hydration (Hsieh, 2010). In order to account for the strong intermicellar interactions present in the SANS data obtained for SDS containing systems, it is necessary to use a different interparticle structure factor, *S(Q)*, than was used for the Brij 97 stabilised systems, the S(Q) in a Haytor-Penfold model was used instead (Hsieh, 2010).

The intensity of the scattered radiation, I(Q) as a function of the wave-vector, Q, is given by:

$$I(Q) = n_m[S(Q)\langle F(Q)\rangle^2 + \langle|F(Q)|^2\rangle - F(Q)^2]B_{inc}$$

where *F(Q)* is the single particle form factor which depends on the size and shape of the particle, *S(Q)* is the interparticle structure factor, B_{inc} is a constant term representing the incoherent scattering background, and n_m is the number of micelles per unit volume.

Hayter and Penfold (1983) showed that the term $[S(Q) \langle F(Q)\rangle^2 + \langle|F(Q)|^2\rangle - F(Q)^2]$ was calculated from the decoupling approximation for determining the morphology of the scattering species, where:

$$F(Q) = V_1(\rho_1 - \rho_2)F_0(QR_1) + V_2(\rho_2 - \rho_{solvent})F_0(QR_2)$$

subscript 1 shows the scattering from hydrocarbon core while subscript 2 represents the scattering from the polar shell.

In the present study, an elliptical core-shell model was used for the anionic microemulsions. Here both F(Q) and F(Q)^2 require numerical integration over a scattering angle θ between Q and the axis of the ellipsoid to account for the random distribution of orientations of the ellipse. The first term represents the scattering from the core (subscript 1) of radius R_i and axial ratio *X*, and the second, the polar shell (subscript 2):

$$V_i = \frac{4}{3}\pi X R_i^3$$

$$\text{and } F_0(QR_i) = \frac{3j_i(QR_i)}{QR_i}$$

where j_i is the first-order spherical Bessel function of the first kind.

The *S(Q)* in Hayter-Penfold model is described by four parameters, namely, a hard sphere volume fraction, $\varnothing_{hard\ sphere}$, a hard sphere particle radius, $R_{hard\ sphere}$, the micellar charge, *Z*, and the inverse Debye screening length, k^{-1}.

The hard sphere volume fraction is given by:

$$\varnothing_{hard\ sphere} = \frac{4\pi N_{Avocadro}(S_t - S_f)a^3}{3N_{agg}}$$

where S_t and S_f correspond to the total and monomeric concentration of surfactant and *a* is the equivalent spherical outer radius of an ellipse, $R = X^{1/3}(R_{core} + \delta)$ when δ is defined as the shell thickness.

The intermicellar interaction is modelled through a dimensionless screened Coulombic potential, given by:

$$u(r) = 2Ru_0 exp\,[-K(r-2R)]/r$$

$$r > 2R$$

where *K* is the Debye–Huckel inverse screening length, calculated by:

$$K = [8\pi N_A e^2 I/10^3 \varepsilon k_B T]^{1/2}$$

and u_0, the contact potential, given by:

$$u_0 = Z^2 e^2/(8\pi \varepsilon \varepsilon_0 R(1+KR)^2)$$

where N_A is Avogadro number, *e* is the electronic charge, ε is the dielectric constant of the medium, k_B is the Boltzmann's constant, *T* is the temperature of the sample, ε_0 is the permittivity of free space, *I* is the ionic strength of the solution, and *Z* is the micellar charge.

The model used in this study for analyzing the morphology of the microemulsions stabilised by the anionic surfactant, SDS, was adopted from the model used to analyze

the SDS micelle, namely that of a charged elliptical core-shell particle. In this study, the hypothesis is assumed that core is consisted of the hydrocarbon chains of the surfactant and all oil molecules and shell is composed of the surfactant head groups along with any associated counter-ions and the water of hydration.

The V_{core} and V_{shell} of the microemulsions can be derived from the following equations:

$$V_{core} = \frac{4}{3}\pi R_{core}^2 (R_{core}X)$$

where x is the inner axial ratio.

$$V_{shell} = V_{total} - V_{core} = \frac{4}{3}\pi X[(R_{core} + \delta)^3 - R_{core}^3]$$

or

$$V_{shell} = N_{agg}V_{head} + \emptyset_{H_2O}V_{shell}$$

In summary, in the present study, the SANS data obtained for the Brij 97-stabilised nanoemulsions were fitted using a core-shell monodisperse oblate model for the form factor together with the Percus and Yevick approximation for the structure factor, while the microemulsions stabilised by anionic surfactant SDS were fitted using a core-shell monodisperse prolate ellipsoid together with the Hayter-Penfold structure factor.

1.7 Aims of the current project

The aim of this study was the formulation of two novel combination formulations, termed a nanosusponanoemulsion (NSNE) and a nanosuspomicroemulsion (NSME), which are composed of either an oil-in-water nanoemulsion or an oil-in-water microemulsion, each containing the model hydrophobic drug, testosterone propionate, and a nanosuspension of griseofulvin nanoparticles. It is intended that such formulations might be of use in personalised medicine. In order to understand the novel combination formulations, the present study was divided into two main sections. The first being the preparation and characterisation of the oil-in-water nanoemulsions, oil-in-water microemulsions and nanosuspensions used to prepare the novel combination formulations and the second being the characterization of the NSNEs and the NSMEs.

Firstly, the formation and physico-chemical properties of oil-in-water nanoemulsions and oil-in-water microemulsions were investigated in determine whether it is possible to obtain as high loading delivery of poorly-water soluble drug, here testosterone propionate. For the nanoemulsions, nonionic surfactant namely polyoxyethylene-10-oleyl ether (Brij 97) was chosen to stabilise nanoemulsions containing the oil, glyceryl trioctanoate (TON). In addition, sodium dodecyl sulphate (SDS) is selected to stabilise microemulsions containing either ethyl butyrate or ethyl capylate. Note that preliminary studies showed that it was not possible to prepare SDS stabilised microemulsions containing TON. Griseofulvin nanoparticles have been prepared using wet bead milling to determine the amount of the anionic surfactant, SDS to produce the correct size nanoparticle, taking account of particle size and zeta potential. Last but not least, the novelty of the present study is the formation of a combination formulation, termed either a NSNE or a NSME, comprising a combination of either an oil-in-water nanoemulsion or an oil-in-water microemulsion containing the model hydrophobic drug testosterone propionate and a nanosuspension of griseofulvin nanoparticles, respectively.

In this study, the physico-chemical properties of nanoemulsions, microemulsions and nanoparticles when in a form of the NSNE and NSME, as well as the component systems have been determined using variety of techniques, including phase behaviour, the phase inversion temperature, viscosity, zeta potential, UV spectroscopy, photon correlation spectroscopy and small angle neutron scattering.
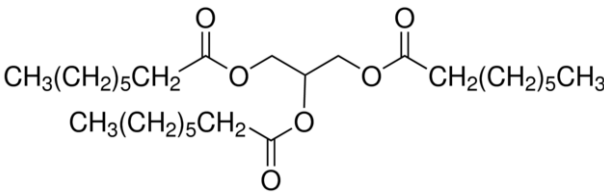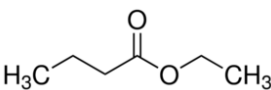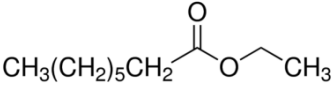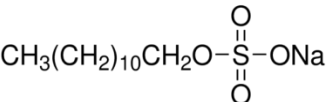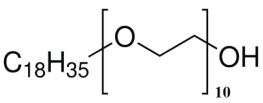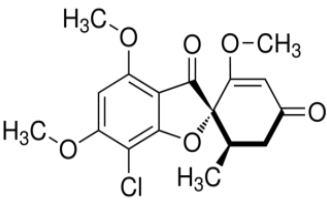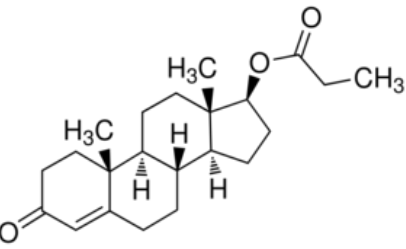
Chapter 2 Experimental

2.1 Materials

All chemicals were commercially available, were of the highest grade available and were used as received without any further purification. Griseofulvin (GF) (97% purity) was purchased from Alfa Aesar® (Geel, Belgium) while testosterone propionate (TP) was obtained from Sigma Chemical Co. Ltd. (Dorset, UK). Sodium dodecyl sulphate (SDS) and polyoxyethylene-10-oleyl ether (Brij 97, $C_{18:1}E_{10}$, PEO-10) were supplied by the Sigma Chemical Co. Ltd. (Dorset, UK). Glyceryl trioctanoate (TON) was purchased from Fluka Chemicals (St. Gallen, Switzerland) while ethyl butyrate (EB) and ethyl caprylate (EC) were obtained from Sigma Chemical Co. Ltd. (Dorset, UK). Deuterated oil, glyceryl trioctanoate (d15, 98.9 atom% D), was purchased from QMX Laboratories (Essex, UK). Yttrium zirconia (YTZ) beads of size 0.44 mm (0.35-0.5 mm range), with minimal contamination levels acceptable for pharmaceuticals (Ruddy et al., 1998), were obtained from GlaxoSmithKline (Harlow, UK). Isopropanol was supplied by Fisher Chemical (Leics, UK). D_2O (99.9 atom% D) was obtained from Aldrich Chemical Company (Dorset, UK). Ultrapure water (UPW) supplied by a well-seasoned, all glass still (D4000 Distinction, Sterling, UK) was used throughout. The chemical structure of oils, surfactants and drugs used are shown in Table 2.1.

Table 2.1 Chemical structure of oils, surfactants and drugs

Chemical name	Chemical structure
glyceryl trioctanoate	
ethyl butyrate	
ethyl caprylate	
sodium dodecyl sulphate	$CH_3(CH_2)_{10}CH_2O-\overset{O}{\underset{O}{S}}-ONa$
Brij 97	$C_{18}H_{35}\left[O\diagup\diagdown OH\right]_{10}$
griseofulvin	
testosterone propionate	

2.2 Methodology

2.2.1 Development of oil-in-water nanoemulsions and microemulsions

The oil-in-water (o/w) nanoemulsions studied contained the triglyceride, TON, and were stabilised by the nonionic surfactant, Brij 97. All nanoemulsions were prepared individually in 2 g aliquots by weighing out the required amount of oil, surfactant and water directly into a vial. After the addition of a small magnetic stirrer bar, the mixture was heated at 70-75 °C for 15 minutes, after which time it was removed from the heat and continually and vigorously stirred for 15 minutes (i.e. until cool).

The o/w microemulsions stabilised by the anionic surfactant SDS and containing either of the ethyl ester oils, EB or EC, were prepared without the use of heat. As with the nanoemulsions, all microemulsions were prepared individually in 2 g aliquots by weighing out the required amount of oil, surfactant and water directly into a vial. After the addition of a magnetic stirrer bar, the mixture was stirred continuously for 30 minutes at ambient temperature. The stirring of the microemulsions was purely to speed up formation.

2.2.2 Phase behaviour

In order to characterize the range of compositions over which the nanoemulsions and microemulsions form, partial ternary phase diagrams were constructed by preparing a large number of individual samples of oil, surfactant and water, according to the methodology outlined in section 2.2.1. Typically, the surfactant concentration used was in the range 5 and 40 w/w%. The resulting phase behaviour of the samples at constant temperature and pressure were plotted on a partial ternary phase diagram. Each apex of the partial ternary phase diagram represents a w/w% of one component, while any point along on an axis represents a binary mixture of water and oil, oil and surfactant, or surfactant and water, while any point within the a partial phase diagram represents a mixture of the three components. Each sample was observed visually, immediately after preparation, after 1 week and after 1 month. In all cases, care was taken to avoid evaporation of the sample, particularly those containing the volatile ethyl ester oils. Nanoemulsions and microemulsions were defined in the present study as clear, fluid,

non-birefringent samples that were stable for 4 weeks. The main difference between a nanoemulsion and a microemulsion being the requirement for the in-put of energy, typically heat, during the preparation of a nanoemulsion. Previous studies have indicated that if a nanoemulsion or a microemulsion was stable at 1 month, then it would exhibit a long term stability for periods in excess of one year (Malcolmson, 1993). Gels were classified by as clear, non-birefringent systems, the meniscus of which did not change after tilting the sample through an angle of 180°.

After determining the phase behaviour of the Brij 97-stabilised nanoemulsions and the SDS-stabilised microemulsions, a range of nanoemulsion and microemulsion formulations were selected for further study as a component of a novel combination delivery system. As part of the intention of developing the novel drug delivery system was to increase the apparent aqueous solubility of a poorly-water soluble drug, nanoemulsions and microemulsions containing the highest amount of oil were selected for further study as it was hoped that these systems would be able to exhibit the greatest increase in the apparent solubility of any water insoluble drug they incorporate. Although selecting nanoemulsions and microemulsions for further study, other properties such as their viscosity were also considered.

In the current study, two nanoemulsions stabilised by 24 w/w% of Brij 97 and containing either 3 or 5 w/w% of TON, denoted as B24T3 and B24T5, were selected for further investigation. In addition, two microemulsions stabilised by 20 w/w% SDS and containing either 14 w/w% of EB or 8 w/w% of EC and denoted as S20B14 and S20C08, respectively were chosen for study. The nanoemulsion, B24T3, and the microemulsions, S20B14 and S20C08, were selected as they were within the region of nanoemulsion and microemulsion existence, respectively while B24T5 was selected as it was just on the upper boundary of the area of nanoemulsion existence. In the novel delivery system, the B24T3 and B24T5 nanoemulsions were denoted as stock systems and diluted 10 times prior to use, while the microemulsions, S20B14 and S20C08, also denoted as stock were diluted 5 times prior to their use. It was found necessary to prepare stock solutions as it was not possible to prepare directly the nanoemulsions and microemulsions containing a low amount of surfactant and oil. For instance, Malcolmson (1993) found that a microemulsion could not be directly prepared at a composition of 4 w/w% of Brij 96 and 0.5 w/w% of soybean oil, although the same

composition could be achieved by the dilution of a microemulsion composed of 24 w/w% Brij 96 and 3 w/w% soybean oil. Furthermore, in a previous study on Brij 97-stabilised-nanoemulsions containing oils of varying molecular volume (namely EB, EC, ethyl oleate, tributyrin, Miglyol 812 and soybean oil) there was no evidence of a change in aggregate shape or size upon dilution of the sample to similarly low surfactant and oil concentrations as used in the present study (Warisnoicharoen et al., 2000). In contrast, the dilution of microemulsions stabilised by an ionic surfactant, such as bis-2-ethylhexylsulfosuccinate (Aerosol-OT) and SDS, would be expected to undergo shapes change upon dilution (Eastoe et al., 1992), which may lead to slightly different properties such as solubilisation ability. The concentrations of the diluted nanoemulsions and microemulsions were found to be suitable for study by SANS as they were sufficiently dilute to avoid the presence of strong interparticle interactions (Hsieh, 2010; Wasutrasawat, 2011). Wasutrasawat (2011) found that, using SANS, interparticulate interactions were only observed in Brij 97 micelles at a concentration of 12 and 24 w/w% surfactant - no peaks indicative of interparticulate interactions were seen at lower Brij 97 concentrations of 1.2-4.8 w/w%. While, Hsieh (2010) found that SDS micelles at a concentration of 3 w/v% showed the existence of a peak in the SANS data is common behaviour for ionic surfactant solutions.

Table 2.2 lists the compositions of the stock and diluted nanoemulsions and microemulsions used in the present study, together with the codes by which these stock solutions were referred to. Note that when a stock solution had been diluted 10 or 5 times, a /10 or /5 was added to the end of the code to denote this fact - for example "B24T3/10" means that the stock B24T3 (which contains 24 w/w% Brij 97 and 3 w/w% TON) had been diluted 10 times while "S20B14/5" denotes that the stock S20B14 (which contains 20 w/w% SDS and 14 w/w% EB) had been diluted 5 times. Testosterone propionate (TP) saturated nanoemulsions and microemulsions were prepared by adding an excess of TP to the diluted nanoemulsions and microemulsions which were then left to rotate on a wheel, generally for 24 hours, following which time any excess TP was removed by passing the drug-saturated sample through a 0.22 µm (cellulose acetate) millipore filter. When a sample was saturated with drug in this manner, a -TP was added to the end of the code such that B24T3/10-TP means a 10 times diluted stock nanoemulsion which contained 24 w/w% Brij 97 and 3 w/w% TON that is saturated with TP.

Table 2.2 Compositions and codes of the stock and diluted nanoemulsions and microemulsions used in the study, with or without a saturation amount of TP

Sample	Code	Nature and amount of surfactant added (w/w%)		Nature and amount of oil added (w/w%)			Amount of aqueous phase added (w/w%)
		Brij 97	SDS	TON	EB	EC	Water
Stock nanoemulsions	B24T3	24	-	3	-	-	73
	B24T5	24	-	5	-	-	71
Stock microemulsions	S20B14	-	20	-	14	-	66
	S20C08	-	20	-	-	8	72
Diluted nanoemulsions	B24T3/10	2.4	-	0.3	-	-	94.6
	B24T5/10	2.4	-	0.5	-	-	97.1
Diluted microemulsions	S20B14/5	-	4	-	2.8	-	93.2
	S20C08/5	-	4	-	-	1.6	94.6
TP saturated nanoemulsions	B24T3/10-TP	2.4	-	0.3	-	-	94.6
	B24T5/10-TP	2.4	-	0.5	-	-	97.1
TP saturated microemulsions	S20B14/5-TP	-	4	-	2.8	-	93.2
	S20C08/5-TP	-	4	-	-	1.6	94.6

2.2.3 Nanoemulsions stability

The stability of the nanoemulsions, B24T3/10, B24T5/10, B24T3/10-TP and B24T5/10-TP, was assessed visually and by determining the apparent hydrodynamic size of the nanoemulsion droplets by photon correlation spectroscopy (PCS) immediately after preparation, and 24, 48 and 72 hours, and 1, 2 and 3 weeks, and 1 and 2 months after preparation. Each nanoemulsion was prepared and examined in triplicate. Note that because of the high charge and the very small particle size of microemulsions stabilised by SDS, it was not possible to measure their size in the present PCS study. The PCS

study, and therefore the apparent hydrodynamic size (i.e. effective diameter) and polydispersity index of the nanoemulsions, was performed using a Brookhaven ZetaPlus particle sizer v2.29 (Brookhaven instruments, UK), fitted with a He-Ne laser operating at 677 nm, using a measurement angle of 90° and operating at an experimental temperature of 25 ± 0.1°C. Unless otherwise stated, the analysis of the PCS data used a viscosity of 0.89 cP and a refractive index of 1.33 for the water, continuous phase. A clear, 4-sided, 10 mm path length disposable polystyrene cuvette was used for the PCS measurements. Each of the triplicate nanoemulsions prepared was measured for 30 seconds and was the average of ten repetitions. As a consequence, the results were recorded as the average of the hydrodynamic apparent size $\pm$ the standard deviation as well as the average of the polydispersity index $\pm$ the standard deviation.

2.2.4 Determination of cloud point and phase inversion temperature

The cloud point (CP) or phase inversion temperature (PIT) is defined as the temperature, in which the micellar or nanoemulsion solutions changing from clear to turbid. Generally, the micelle CP and the PIT of each of the nanoemulsions is measured by detecting the increase in turbidity (either via by UV spectroscopy or by visual assessment) as a function of temperature. The appearance of turbidity is due to the growth in the size of the micelles with temperature. In this present study, the CP and the PIT of the micelles and Brij 97-stabilised nanoemulsions, respectively were determined by visual assessment. The Brij 97 micellar solutions and nanoemulsions were examined by both heating and cooling the samples at a rate of ~ 1°C min^{-1} with stirring throughout and determining the temperature at which the samples become cloudy and clear, respectively. The temperatures at which cloudiness appears and the clearing occurs should be less than 1°C different. The CP and PIT thus reported are the mean of 3 separate determinations of the clouding and clear temperatures. Note that the micellar and SDS-stabilised microemulsions solutions could not be determined as ionic surfactants such as SDS do not grow as a function of temperature, indeed the size of ionic micelles tends to slightly reduce when the temperature is increased.

2.2.5 Viscosity

An Ubbelohde (dilution, or suspension capillary) viscometer was used to determine the intrinsic viscosity of the micelles, nanoemulsions and microemulsions. Prior to use, the Ubbelohde viscometer was cleaned by first soaking in concentrated detergent solution, repeatedly rinsing with distilled water, washing in acetone and finally drying under a stream of nitrogen. 10 mL of the most concentrated micellar, nanoemulsion or microemulsion sample to be measured (with or without TP) was then placed into the Ubbelohde viscometer along with a small magnetic stirrer to ensure adequate mixing of the sample. The Ubbelohde viscometer and its contents were then immersed in a precision water bath (CT 1650, Schott-Geräte, Hofheim, Germany) at a temperature of $25 \pm 0.01^{\circ}C$ for 30 min equilibration prior to the measurement of viscosity. The speed of magnetic stirrer was altered so it was not fast enough to result in the formation of bubbles in the sample to be measured. Once the sample contained in the Ubbelohde viscometer had equilibrated, its flow time was automatically measured three times using the attached Viscosity Measurement Unit AVS 350 (Schott-Geräte, Hofheim, Germany). A difference in flow time of ± 0.02 s for the three measurements was considered to be of sufficient accuracy for the present study. The sample in the viscometer was then automatically diluted with distilled water 4 times using a programmable ViscoDoser AVS 20 Piston Burette and the viscosity of the resulting samples determined. Viscosity results were analyzed to determine both the reduced viscosity and inherent viscosity as a function of concentration, which was plotted to obtain via linear regression the Huggins and Kraemer extrapolations, respectively (Devi et al., 2003). The average of the reduced viscosity and inherent viscosity from the Huggins and Kraemer extrapolations at a zero surfactant concentration was determined to the intrinsic viscosity of the sample (η).

2.2.6 Density

The density of individually prepared micellar, nanoemulsions and microemulsions (including B24T3/10, B24T5/10, S20B14/5 and S20C08/5 in the presence and absence of TP) samples (according to section 2.2.2) was determined. Sample was transferred into a previously calibrated pycnometer of 10 mL volume such that the pycnometer was

full with sample when no stopper was fitted. The pycnometer was then stored at a constant temperature of 25 ± 0.01°C and once equilibrated, the pycnometer was stoppered (reducing evaporation and contamination) and the mass of the sample contained in the pycnometer determined using a calibrated Sartorius analytical balance with a precision of ± 0.00001 g. The volume of the pycnometers was previously calibrated by determining the weight of water they contained and converting this to volume using the density of pure water.

$$d = \frac{m}{v}$$

where m is mass and v is volume of the sample. The unit of density is g/mL. The density of all samples was measured in triplicate using three different density bottles (i.e. n = 9).

2.2.7 Preparation nanosuspension

Nanosuspensions of griseofulvin nanoparticles (GF-NPs) were prepared by wet bead milling griseofulvin using a Retsch MM 400 mixer mill (Glen Creston Ltd, Stanmore UK), Figure 2.1. Solutions of stabiliser, namely 0.25, 0.5, 1, 1.5, 2 and 10 w/w% SDS, were prepared by weighing the required amount of surfactant and water and mixing using a magnetic stirrer. A crude GF suspension or slurry was then prepared by mixing 40 g of the stabiliser solution with 10 g of GF and stirring for 30 minutes prior to milling. In this study, the crude suspension contained 20 w/w% GF to increase possibility of the yttrium zirconia (YTZ) beads impacting with the drug particles during the milling process thereby aiding the production of the GF-NPs (Tirop, 2012).

Figure 2.1 Retsch MM400 Mixer Mill

To prepare GF-NPs, the crude GF suspension was milled for a total of 6 hours by mixing 10 mL of YTZ beads (0.44 mm diameter) with 10 mL of the crude GF suspension in a milling jar of 25 cm^3 capacity (Nylube, Nylecast,UK). The milling was performed at a shaking frequency of 25 Hz. Every hour the milling was stopped for 10 minutes in order to avoid over heating of the motor on the Retsch Mixer Mill. At this time a small amount of sample was taken from the milled suspension to assess its particle size. After 6 hours milling, the YTZ beads were separated from the GF nanosuspension (GF-NS) using a 60 mesh sieve, the GF-NS centrifuged at 13000 rpm for 90 minutes using a Biofuge Pico (Heraeus, Germany) and the supernatant removed and replaced with the same amount of fresh deionized water to maintain the same concentration of particles. In this way, the excess SDS was removed from the suspension in an attempt to reduce/prevent Ostwald ripening. The recovered YTZ beads were cleaned with copious amounts of water, rinsed with methanol, oven dried and reused. Before and after centrifugation to remove the excess SDS, the particle size of the various GF-NPs preparations was measured by PCS in order to determine which formulation(s) should be used for further study.

2.2.8 Particle size measurement of the GF-NP

The particle size (apparent hydrodynamic size and polydispersity index) of the GF-NP was performed using a Brookhaven ZetaPlus particle sizer v2.29 (Brookhaven

instruments, UK), fitted with a He-Ne laser operating at 677 nm, using a measurement angle of 90° and operating at an experimental temperature of 25 ± 0.1°C. Analysis of the PCS data used a viscosity of 0.89 cP and a refractive index of 1.33 for the water, continuous phase. A clear, 4-sided, 10 mm path length disposable polystyrene cuvette was used for the PCS measurements. The methodology was adapted from that of Tirop (2012), namely 2-3 drops of GF-NS were diluted with water to give a final GF concentration of 0.02 w/w% of GF to give a sensible count rate. In order to measure particle size of the GF-NPs stabilised by varying amounts of SDS, namely 0.25, 0.5, 1, 1.5, 2 and 10 w/w% SDS, the samples were prepared triplicate. Each of the triplicate GF-NP samples were measured for 30 seconds and was the average of ten repetitions. As a consequence, the results were recorded as the average of the hydrodynamic apparent size ± the standard deviation as well as the average of the polydispersity index ± the standard deviation.

2.2.9 Zeta potential measurement of the GF-NP

The zeta potential of the GF-NPs was determined using a Zetasizer Nano ZS (Malvern instruments, UK). The GF-NPs to be measured were placed in a disposable folded capillary cell with gold electrodes at 25 ± 0.1°C and, after 120 seconds equilibration, the zeta potential of the sample measured for 30 seconds with ten repetitions. Note that the zeta potential of all samples was measured at the same concentration as their particle size. The zeta potential was expressed as the average of zeta potential ± the standard deviation (n = 9).

2.2.10 Preparation of nanosusponanoemulsions and nanosuspomicroemulsions

The novel nanosusponanoemulsions (NSNEs) and nanosuspomicroemulsions (NSMEs) delivery systems were prepared by simply mixing 0.24 ml of GF-NPs (as prepared) and 0.76 ml of either diluted nanoemulsions or microemulsions. This amount and concentration of nanosuspension (NS) was selected because, according to Goodwin (2006) and Tirop (2012), a final 3.5% volume fraction of GF-NPs was sufficient to avoid, or at least reduce, multiple scattering due to particle–particle interactions in a

scattering experiment. Similarly, the amount and concentration of nanoemulsions or microemulsions was enough to measure the sample using a scattering technique as well as avoid interparticulate interactions between the samples.

Both freshly prepared GF-NPs (stabilised by 1.5 w/w% SDS) and either freshly prepared nanoemulsions or microemulsions were used to formulate the NSNEs or NSMEs, respectively. NSNEs and NSMEs were both prepared in 1.5 mL microfuge tubes, which were tightly closed and covered with aluminum foil to prevent the occurrence of any photoreaction. Table 2.3 shows the compositions and the codes of the NSNEs and NSMEs prepared in the absence and presence of TP. The letters NS added to the front of any code denote the fact that these systems are NSNEs or NSMEs - for instance the code NSB24T3/10-TP denotes a mixture of GF-NS and a 10 times diluted stock nanoemulsion (prepared form a stock of 24 w/w% Brij 97 and 3 w/w% TON) and containing a saturated amount of TP.

Table 2.3 Compositions and the codes of the nanosusponanoemulsions and nanosuspomicroemulsions used in the study

Nanosusponanoemulsions (NSNEs) and Nanosuspomicroemulsions (NSMEs)	Code	Nanosuspension (0.24 mL)	Nanoemulsion or Microemulsion (0.76 mL)
NSNEs no TP	NSB24T3/10	GF-NS	B24T3/10
	NSB24T5/10	GF-NS	B24T5/10
NSMEs no TP	NSS20B14/5	GF-NS	S20B14/5
	NSS20C08/5	GF-NS	S20C08/5
NSNEs with TP	NSB24T3/10-TP	GF-NS	B24T3/10-TP
	NSB24T5/10-TP	GF-NS	B24T5/10-TP
NSMEs with TP	NSS20B14/5-TP	GF-NS	S20B14/5-TP
	NSS20C08/5-TP	GF-NS	S20C08/5-TP

2.2.11 Drug solubilisation

In order to determine the solubility/solubilisation of TP in the various systems under study, a calibration curve of TP was prepared by first making a stock solution containing an accurately known quantity of TP (approximately 40 mg) in 20 mL isopropanol. This stock solution was then serially diluted by taking 50, 100, 150, 200, 250 and 300 µl aliquots and made to volume (20 mL) with isopropanol. Similarly in order to determine the solubility of GF in the various systems, a calibration curve for GF was prepared from a stock solution containing an accurately known quantity of GF (approximately 10 mg) in 100 mL isopropanol was prepared. This stock solution was then serially diluted by taking 40, 80, 120, 160, 200, 240 and 280 µL aliquots and made to volume (20 mL) with isopropanol. Dilutions of both TP and GF stock solutions were carried out in triplicate. Isopropanol was used as blank. The UV spectra of each dilution of TP and GF was determined between 200 – 400 nm using 1 cm path length cells after correction for the absorbance of the isopropanol blank. The maximum absorption wavelengths of TP and GF were 240 and 292 nm, respectively. A UV/Vis spectrophotometer LAMBDA 2 (Perkin-Elmer, USA) was used throughout the study. Exemplar calibration curves obtained for both TP and GF are shown in the Appendix A.

2.2.11.1 Solubility of testosterone propionate and griseofulvin in micelles

In order to determine the amount of either TP or GF solubilised in the Brij 97 and SDS micelles, excess TP or GF was added to 1 mL of a micellar solution (either Brij 97 concentration of 0.2, 0.6, 1.2, 1.8 and 2.4 w/w% or SDS concentration of 1, 2, 3, 4 and 5 w/w% of SDS) contained in a microfuge tube (1.5 mL volume), which was then tightly closed and covered in aluminum foil ,to avoid the occurrence of any photodegradation reaction, and mixed on a rotating wheel. After mixing for 6, 24, 48, 72 and 96 hours, the samples were removed from the wheel and centrifuged for 30 minutes at a speed of 13000 rpm using a Biofuge Pico (Heraeus, Germany), after which the supernatant was removed and filtered through a 25 mm PVDF filter of 0.22 µm pore size. An aliquot of the filtered sample was diluted with isopropanol before measuring its absorbance using UV/Vis spectroscopy at the wavelength of 240 nm and 292 nm (i.e. the wavelength of maximum absorbance determined for TP and GF, respectively). A 'blank' comprising

of the corresponding micellar solutions without drug was treated in the same way. The results were shown as the average ± the standard deviation.

2.2.11.2 Solubility of griseofulvin nanoparticles in water

The solubility of GF-NPs in water was determined by mixing 0.24 mL of the GF-NS stabilised by 0.25, 0.5, 1, 1.5, 2 and 10 w/w% of SDS and 0.76 mL of water in a tightly closed microfuge tube (1.5 mL volume), which was covered in aluminum foil to avoid the occurrence of any photodegradation reaction and mixed on a rotating wheel. After mixing for 6, 24, 48, 72 and 96 hours, the samples were removed from the wheel and centrifuged for 30 minutes at a speed of 13000 rpm using a Biofuge Pico (Heraeus, Germany), after which the supernatant was removed and filtered through a 25 mm PVDF filter of 0.22 μm pore size. An aliquot of the filtered sample was diluted with isopropanol before measuring its absorbance using UV/Vis spectroscopy at the wavelength of 292 nm (i.e. the wavelength of maximum absorbance determined for GF). The results were shown as the average ± the standard deviation.

2.2.11.3 Solubility of both testosterone propionate and griseofulvin in either the nanoemulsions or the microemulsions

The solubility of TP in the Brij 97-stabilised nanoemulsions and SDS-stabilised microemulsions was determined by adding excess TP (~ 25 mg) in a microfuge tube (1.5 mL volume) containing 1 mL of B24T3/10, B24T5/10, S20B14/5 and S20C08/5. The microfuge tube was tightly closed, covered in aluminum foil, to avoid the occurrence of any photodegradation, and mixed on a rotating wheel. After mixing for 24 hours, the samples were filtered through a 0.22 μm pore size, 25 mm diameter PVDF filter. An aliquot of the filtrate was then diluted with isopropanol prior to measuring its absorbance using UV/Vis spectroscopy at the wavelength of maximum absorbance at 240 nm for TP.

Similarly, the solubility of TP in Brij 97-stabilised-nanoemulsions and SDS-stabilised microemulsions containing exactly the same amount of oil and surfactant as in the final

NSNE or NSME preparation was determined by mixing 0.76 mL of either B24T3/10-TP, B24T5/10-TP, S20B14/5-TP or S20C08/5-TP with 0.24 mL of deionized water in 1.5 mL microfuge tubes. A 'blank' comprising of the corresponding either nanoemulsions or microemulsions without drug was treated in the same way. These TP-containing samples were then mixed on a rotating wheel for 24, 48, 72 and 96 hours, after which time the samples were centrifuged at 30 minutes at a speed of 13000 rpm using a Biofuge Pico (Heraeus, Germany). The supernatant from each centrifuged sample was filtered using a 0.22 μm pore size 25 mm diameter of PVDF filter. A known aliquot of each filtrate was diluted with isopropanol prior to measuring its absorbance using UV/Vis spectroscopy at 240 nm (i.e. the wavelength of maximum absorbance for TP). The results were shown as the average ± the standard deviation.

Furthermore, in order to determine the solubility of TP in either the nanoemulsions or microemulsions in the presence of a saturation amount of GF, the solubility of TP in these samples was determined by adding an excess of GF in a microfuge tube (1.5 mL volume) containing 0.76 mL of either B24T3/10-TP, B24T5/10-TP, S20B14/5-TP or S20C08/5-TP and 0.24 mL of deionized water, tightly closing the microfuge tube, covering with aluminium foil, to avoid any photodegradation of the sample, and mixing the resulting sample on a rotating wheel. After 6, 24, 48, 72 and 96 hours, samples were removed from the wheel and centrifuged for 30 minutes at a speed of 13000 rpm using a Biofuge Pico (Heraeus, Germany), after which time the samples were removed from the wheel and filtered through a 0.22 μm pore size, 25 mm diameter PVDF filter. An aliquot of each supernatant was diluted with isopropanol before measuring its absorbance using UV/Vis spectroscopy at the wavelength of 240 nm (i.e. the wavelength of maximum absorbance determined for TP).

In order to determine the solubility of GF in either the nanoemulsions or microemulsions in the absence or the presence of a saturation amount of TP, the solubility of GF in these samples was determined by adding the excess GF in a microfuge tube (1.5 mL volume) containing 0.76 mL of either B24T3/10, B24T5/10, S20B14/5, S20C08/5, B24T3/10-TP, B24T5/10-TP, S20B14/5-TP or S20C08/5-TP and 0.24 mL of deionized water, tightly closing the microfuge tube, covering with aluminium foil and mixing the resulting sample on a rotating wheel. After 6, 24, 48, 72 and 96 hours the samples were removed from the wheel and centrifuged for 30 minutes

at a speed of 13000 rpm using a Biofuge Pico (Heraeus, Germany), after which time the samples were removed from the wheel and filtered through a 0.22 µm pore size, 25 mm diameter PVDF filter. An aliquot of each supernatant was diluted with isopropanol before measuring its absorbance using UV/Vis spectroscopy at the wavelength of 292 nm (i.e. the wavelength of maximum absorbance determined for GF).

2.2.11.4 Solubility of testosterone propionate and griseofulvin in the nanoemulsion of nanosusponanoemulsions and the microemulsion of nanosuspomicroemulsions.

NSNEs or NSMEs, with and without added TP, were prepared as described in Table 2.3 were placed in 1.5 mL volume microfuge tubes, which were then tightly sealed and covered with aluminum foil to protect from light. The foil covered sample-containing microfuge tubes were then rotated on a wheel for 0.5, 1, 1.5, 2, 2.5, 3, 6, 8, 24, 48, 72 and 96 hours, after which time the samples were centrifuged for 30 minutes at a speed of 13000 rpm using a Biofuge Pico (Heraeus, Germany) and then the resulting supernatant passed through 0.22 µm pore size filters using a 25 mm diameter PVDF filter. In order to determine the solubility of TP and GF in the nanoemulsion of NSNEs and the microemulsion of NSMEs containing TP, a known aliquot of each supernatant was diluted with isopropanol prior to measuring its absorbance using UV/Vis spectrometry at 240 and 292 nm, the wavelength maximums or TP and GF, respectively.

2.2.12 Particle size of the griseofulvin nanoparticles and nanoemulsions in the form of a nanosusponanoemulsion and nanosuspomicroemulsion by photon correlation spectroscopy

PCS was performed to determine the particle size of the GF-NPs when in the form of a NSNE and NSME in an absence and presence of a saturation amount of TP. The methodology used was that described in section 2.2.8. Firstly, the NSNEs and NSMEs, with and without TP, were prepared in microfuge tubes, compositions as listed in Table 2.3. The resulting samples (prepared in triplicate) were mixed on a rotating wheel for 4, 8, 12, 24, 48, 72 and 96 hours. In addition, the size of the GF-NPs measured

immediately after their mixing with either nanoemulsions or microemulsions was denoted as a time of less than 5 minutes. At each time interval, 2-3 drops of sample were diluted with water to give a griseofulvin concentration of approximately 0.02% wt - a concentration range optimised for particle size measurement. A clear, 4-sided, 10 mm path length disposable polystyrene cuvette was used for measuring the GF NPs size which was measured for 30 seconds and was the average of ten repetitions. The particle size of three individual GF-NP samples was measured and as a consequence, the results are shown as the average of the apparent hydrodynamic size ± the standard deviation. During these measurements it was assumed that, because of the much larger volume of the GF-NPs, it was not possible to 'see' and therefore measure the size of the much smaller volume nanoemulsion droplets and therefore the size recorded is a good estimate of the size of the GF-NPs.

In addition, the NSNE and NSME samples were centrifuged at 13000 rpm for 30 minutes using a Biofuge Pico (Heraeus, Germany) in order to separate the GF-NPs from the nanoemulsions or microemulsions. After centrifugation, the supernatant was composed of either the nanoemulsion or the microemulsion (diluted with some of the aqueous phase of the NS) while the pellet contained the sedimented GF-NPs. The particle size of the sedimented GF-NPs and the nanoemulsions (note that it was not possible to measure the SDS-stabilised microemulsions using light scattering) was monitored after their removal from the NSNE and NSME immediately (< 5 minutes) and after 4, 8, 12, 24, 48, 72 and 96 hours of contact. Prior to measurement by PCS, the pellet of the GF-NPs was re-suspended with the same volume of ultrapure water as the volume of the nanoemulsions or microemulsions, while the nanoemulsions supernatant was filtered through 0.22 µm pore size filters of 25 mm diameter and PVDF composition prior to measuring their particle size. A clear, 4-sided, 10 mm path length disposable polystyrene cuvette was used for measuring the sample's particle size which was measured for 30 seconds and was the average of ten repetitions. The particle size of three individual samples was measured and as a consequence, the results are shown as the average of the apparent hydrodynamic size ± the standard deviation. Note that because the particle size of SDS-stabilised microemulsions was too small and too highly charged to be determined using PCS, small angle neutron scattering (SANS) was used instead to characterize the microemulsions.

2.2.13 Small angle neutron scattering

SANS was performed using both the SANS2D and LoQ beams line at the ISIS pulsed neutron source (Rutherford Appleton Laboratory, Didcot, Oxford). Neutrons of wavelengths from 2 to 14 Å used for SANS2D were separated by time-of-flight and recorded on a 96.5 cm^2, two-dimensional detector positioned at 4 m from the sample. This instrumental set up produced a scatting vector in the range from 0.0045 to 0.8 Å^{-1}. Neutrons of wavelengths between 2.2 and 10 Å using LoQ were separated by time-of-flight and recorded on a 64 cm^2, two-dimensional detector positioned at 4.1 m from the sample. This instrumental set up gave a scattering vector in a range 0.008 and 0.22 Å^{-1}.

In the present study, all samples were measured at 25 ± 0.1°C by using 12 mm diameter neutron beam. The scattering and the transmissions of the samples were measured separately on LoQ while they were simultaneously recorded on SANS2D. For LoQ, the scattering of both the sample and solvent was usually accumulated for 20 μA, while the transmission measurements were accumulated for 10 μA. On the other hand, for SANS2D, the scattering and the transmission of the sample and the solvent were simultaneously measured and accumulated for 20 μA. In both cases, an empty cell was used as direct beam.

It is obvious that both the NSNE and NSME contain two populations of the particles. Because of the much smaller size and therefore volume of the nanoemulsions and microemulsions, it is not possible to measure their size using PCS these particles *in situ* in a NSNE or NSME, respectively. An important advantage of using SANS to examine the two populations of particles present in the novel combination system is that is possible to selectively make one of the populations of particles 'invisible' to the neutrons by matching the scattering length density of these particles to that of the solvent. This solvent is called the 'contrast match solvent'. Furthermore, SANS has an additional advantage over PCS in that it can provide information on the size, shape and internal structure of the particles. As a consequence of this selective highlighting, SANS can be used, not only to determine the morphology of the particles, including their size and the shape (i.e. nanoemulsions or microemulsions in the presence of GF-NPs and vice versa), but also to monitor *in situ* the stability of the various nanoemulsions, microemulsions and GF-NPs over time.

In order to study the nanoemulsions or microemulsions when in the form of a NSNE or the GF-NPs when in the form of a NSNE or NSME, the experiments were effectively divided into two sets. In one set of experiments, the GF-NPs were 'contrast matched' to the solvent to 'see' the nanoemulsions or microemulsions, while in the other set of experiments, the nanoemulsions or microemulsions were contrast matched to the solvent to make the GF-NPs 'visible'. Shown in Table 2.4 is the set of compositions were made containing different volume ratios of D_2O and H_2O in order to make the GF-NPs 'invisible', while a second set of compositions prepared using a mixture of D_2O and H_2O to make the nanoemulsions and microemulsions 'invisible'.

Table 2.4 Sets of compositions containing different volume ratios of D_2O and H_2O to make either the GF-NPs or nanoemulsions and microemulsions 'invisible'.

Composition (v/v%) of D_2O and H_2O to make the GF-NPs 'invisible'	Composition (v/v%) of D_2O and H_2O to make the nanoemulsions and microemulsions 'invisible'
30 : 70	0 : 100
35 : 65	5 : 95
40 : 60	10 : 90
45 : 55	15 : 85
50 : 50	20 : 80
55 : 45	25 : 75

2.2.13.1 Determination of contrast match solvents

In order to characterize the nanoemulsion or microemulsion drops, it was necessary to establish the composition of the solvent that was necessary to contrast match the GF-NPs and make them 'invisible'. Tirop (2012) established that the mixture of D_2O and H_2O required for contrast matching the GF-NPs (at a volume fraction of 3.5%) comprised of 43.25 v/v% D_2O/H_2O. To confirm this, the contrast match point was experimentally determined in the present study using GF-NPs prepared in a range of D_2O and H_2O mixtures (namely as 30:70, 35:65, 40:60, 45:55, 50:50 and 55:45) at a volume fraction of 3.5% GF-NPs, prepared by mixing 0.24 mL of the GF-NPs (as

prepared) with 0.76 mL of the various D_2O/H_2O mixtures. The neutron scattering intensity of these GF-NPs was plotted as a function of the composition of the D_2O/H_2O mixture and the solvent composition at which the minimum scattering intensity was obtained was selected as the contrast match solvent and used to prepare NSNEs or NSMEs in which the GF-NPs are 'invisible'. Encouragingly the experimentally determined composition of the D_2O and H_2O mixture agreed with the value reported by Tirop (2012).

In order to study the GF-NPs in situ in a form of the NSNEs and NSMEs, another contrast match solvent was required to make the nanoemulsions and microemulsions invisible. The theoretical contrast match solvent was determined by calculating the scattering length density (SLD) of the nanoemulsions and microemulsions. Fortuitously, the SLD of the various nanoemulsions and microemulsions were very similar. Therefore B24T3/10 was selected as the nanoemulsion with which to determine the composition of the contrast match solvent experimentally. To do this B24T3/10 was prepared in a range of D_2O and H_2O mixtures (namely as 0:100, 5:95, 10:90, 15:85, 20:80 and 25:75) by mixing 0.24 mL of the various D_2O/H_2O mixtures with 0.76 mL of B24T3/10. The neutron scattering intensity of these B24T3/10 was plotted as a function of the composition of the D_2O/H_2O mixture and the solvent composition at which the minimum scattering intensity was obtained was selected as the contrast match solvent and used to prepare NSNEs or NSMEs in which the nanoemulsions and microemulsions are 'invisible'. Encouragingly the experimentally determined composition of the D_2O and H_2O mixture was similar to that theoretically calculated.

2.2.13.2 Preparation of samples for small angle neutron scattering

In order to prepare GF-NPs-contrast matched NSNEs and NSMEs, GF-NPs stabilised with 1.5 w/w% SDS were prepared as described in section 2.2.7 using H_2O as solvent. After milling the GF-NPs for 6 hours, the GF-NPs were centrifuged at 13000 rpm for 90 minutes using a Biofuge Pico (Heraeus, Germany) and the H_2O solvent removed and replaced with an equivalent volume of the contrast match solvent. The centrifugation process was repeated twice more to ensure complete replacement of the H_2O with the contrast match solvent.

Before studying the nanoemulsions or microemulsions prepared using the NP contrast match solvent, the B24T3/10 nanoemulsion was studied using 3 contrasts, namely the drop, the core and shell contrasts, prepared using h-oil/h-surfactant/D_2O, d-oil/h-surfactant/H_2O and d-oil/h-surfactant/D_2O, respectively. After these initial experiments, nanoemulsions and microemulsions, namely B24T3/10, B24T5/10, S20B14/5, S20C08/5, B24T3/10-TP, B24T5/10-TP, S20B14/5-TP and S20C08/5-TP were individually prepared using the contrast match solvent in place of H_2O which was necessary to make the GF-NPs 'invisible'.

Due to the limited availability of deuterated materials, nanoemulsions could only be prepared using two contrasts, namely the drop and the core contrast while the microemulsions could only be prepared as the drop contrast. As described above the use of hydrogenated and deuterated materials can 'highlight' specific components in the nanoemulsions and microemulsions as shown in Figure 2.2. Note that when a sample is (partially) made from deuterated material, it was necessary to increase the weight of that component used over its protonated counterpart to ensure that the same volume of each component.
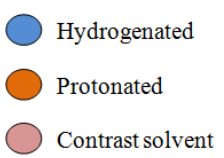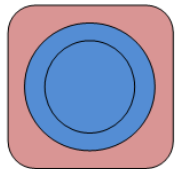
		Droplet	Core
Compositions			
Hydrogenated			
Protonated			
Contrast solvent			
Nanoemulsion	Surfactant	*h*-Brij 97	*h*-Brij 97
	Oil	*h*-TON	*d*-TON
	Solvent	the contrast solvent	the contrast solvent
Microemulsion	Surfactant	*h*-SDS	-
	Oil	*h*-EB or *h*-EC	-
	Solvent	the contrast solvent	-

Figure 2.2 Schematic representation of a SANS experiment on oil-in-water nanoemulsions and microemulsions exploiting contrast variation.

The SANS profiles of all samples, including the NSNEs and NSMEs (Table 2.5) studied, were measured in disc shape quartz cuvettes (Hellma) of 1 mm path length at times of 5 min, 4, 8, 12 and 24 h after their preparation. Note that although the measuring of the samples using SANS commenced at these time points after their preparation, each SANS measurement takes about 20 minutes and so the age of the sample was the time post plus 20 minutes. After their preparation 24 h, the NSNEs and NSMEs were centrifuged at 13000 rpm for 30 min using a Biofuge Pico (Heraeus, Germany) to separate the nanoemulsions or microemulsions from the GF-NPs. Both the nanoemulsions and microemulsions were re-measured as well as the re-suspended GF-NPs. In addition to measuring the NSNEs and NSMEs over time after their preparation, the GF-NPs, the nanoemulsions and the microemulsions that were used for the preparation of the NSNEs and the NSMEs were measured at the same concentrations as they were present in the NSNEs and NSMEs (Table 2.5). Note that determination of the GF-NPs *in situ* in a form of the NSNE composed of the GF-NPs and the nanoemulsions stabilised by Brij 97 containing high amount of TON were not studied because the PCS studies showed poor stability and also the limitation of beam time.

Furthermore, all the GF-NPs, nanoemulsions and microemulsions in an absence and presence of TP were freshly prepared prior to perform SANS study.

Table 2.5 Composition of the nanosusponanoemulsions and the nanosuspomicroemulsions

Composition of the NSNEs and NSMEs		Nanosuspension (0.24 mL)	Nanoemulsion or Microemulsion (0.76 mL)	Contrast solvent
Before mixing	Nanoemulsions	-	B24T3/10	0.24 mL
		-	B24T5/10	0.24 mL
	Microemulsions	-	S20B14/5	0.24 mL
		-	S20C08/5	0.24 mL
	GF-NPs	GF-NS	-	0.76 mL
NSNEs no TP	NSB24T3/10	GF-NS	B24T3/10	-
	NSB24T5/10	GF-NS	B24T5/10	-
NSMEs no TP	NSS20B14/5	GF-NS	S20B14/5	-
	NSS20C08/5	GF-NS	S20C08/5	-
NSNEs with TP	NSB24T3/10-TP	GF-NS	B24T3/10-TP	-
	NSB24T5/10-TP	GF-NS	B24T5/10-TP	-
NSMEs with TP	NSS20B14/5-TP	GF-NS	S20B14/5-TP	-
	NSS20C08/5-TP	GF-NS	S20C08/5-TP	-

2.2.13.3 Analysis of the SANS data for the nanoemulsions and microemulsions in the form of nanosusponanoemulsions or nanosuspomicroemulsions

The SANS data was reduced by the program, Mantid (Akeroyd et al., 2013). Firstly, a mask file is created to remove stray data points around the beam stop and at the outermost perimeter of the detector and also to remove any damaged pixels on the detector. Then the each set of scattering data was normalised using their own transmission data and then the normalised solvent scattering was subtracted from the sample scattering in order to leave only the scattering from the sample which was put on an absolute intensity scale.

All the SANS data were analyzed using the ''FISH'' program developed by Heenan (1989) at the Rutherford Appleton Laboratory. Before fitting the SANS data, the scattering length density (SLD) of each component, namely the surfactant, oil and solvent was determined (Table 2.6). In addition, the volume fractions of the core, consisted only of oil, and the shell, contained the whole surfactant molecule, of the nanoemulsions and microemulsions droplets were calculated using the amount of each component in the system. The value obtained for the hydration of the nano- and microemulsions determined from the viscosity and density measurements was explored for fitting the SANS data. However, in order to establish the best value of the solvation of the shell contained the whole surfactant molecule, before analysing the SANS data of the samples measured using the contrast match solvent, the SANS data for the 3 contrasts measured for B24T3/10 were fitted using FISH. In order to best fit to the SANS data, the results from the analysis must be physically reasonable and consistent. Note that each set of SANS data was individually fitted.

Preliminary analysis of the SANS data showed that the best model for fitting the nanoemulsions or microemulsions was a core-shell ellipsoid model in which the core of a nanoemulsion consists all oil molecules, while the shell consists of hydrated surfactant. In contrast the core of a microemulsion consists of oil together with surfactant tails while the shell consists of only hydrated head group of surfactant. As a consequence of these observations, the SANS data obtained for the Brij 97-stabilised nanoemulsions were analyzed using the core-shell ellipsoid model together with the Percus-Yevick, hard sphere, structure factor whilst the SANS data measured for the microemulsions stabilised by SDS were individually analyzed using an ellipsoidal core-shell model, together with Hayter-Penfold structure factor.

Table 2.6 Input parameters for the FISH program

Sample	Elemental composition	Density (g/cm^3)	Molecular weight (g/mol)	Molecular volume (Å^3)	SLD (Å^{-2}) x 10^{-6}
h-TON	$C_{27}H_{50}O_6$	0.90	470.65	868.68	0.31
d-TON	$C_{27}D_{44.5}H_{5.5}O_6$	0.95	521.05	868.68	5.45
h-Brij 97	$C_{38}H_{76}O_{11}$	1.03	708.94	1143.34	0.28
h-EB	$C_6H_{12}O_2$	0.88	116.1	232	0.284
d-EB	$C_6D_{12}O_2$	0.97	128.2	232	0.095
h-EC	$C_{10}H_{20}O_2$	0.87	172.3	340	5.670
d-EC	$C_{10}D_{20}O_2$	0.97	192.4	340	6.220
h-SDS	$CH_3(CH_2)_{11}SO_4Na$	1.01	288.37	421.5	0.337
solvent	D_2O	1.11	20.03	30	6.39
	H_2O	1.00	18.01	30	-0.56

Please note that, the SLD of solvent in this study was calculated from the ratio of SLD of D_2O and H_2O by volume.

2.2.13.4 Analysis of the SANS data for the griseofulvin nanoparticles in the form of nanosusponanoemulsions or nanosuspomicroemulsions

Reduction of the SANS data was performed by the program, Mantid (Akeroyd et al., 2013). To do this a mask file was first created in order to remove stray data points that are around the beam stop and any spurious points at the outermost perimeter of the detector, together with any damaged pixels on the detector. Subsequently, the scattering data from the solvent was normalised using the corresponding transmission data and then the normalised solvent scattering was subtracted from the sample scattering in order to leave only the scattering from the sample, which was then put on an absolute intensity scale. Before fitting the SANS data, the SLD of the griseofulvin and SDS-stabiliser calculated (Table 2.6). In addition, the volume fraction of the GF-NPs was calculated. The SANS data were analyzed using the ''FISH'' program developed by Richard Heenan (Rutherford Appleton Laboratory). In the present study, all SANS data

of the GF-NPs was analyzed using an ellipsoid model together with the Hayter-Penfold structure factor.

Chapter 3 Preparation of oil-in-water nanoemulsions, oil-in-water microemulsions and nanosuspensions

3.1 Preparation of nonionic surfactant stabilised nanoemulsions

3.1.1 Phase behaviour

In order to understand the phase behaviour of the oil-in-water nanoemulsion formulations, the area of nanoemulsion existence was determined by varying the concentration of the C8 triglyceride oil, TON, the nonionic surfactant, Brij 97 and water and plotting the results of the visibility studies, on a weight basis, on a triangular diagram (Figure 3.1a-b). Compositions that remained clear, one-phase and fluid for 1 month were described as (clear) nanoemulsions for the purposes of the study and are indicated by the green circles on Figure 3.1a. The red circles represent cloudy, one phase systems while the inverted blue triangles represent gels. The solid line delineates the upper limit of the nanoemulsion region.

Not surprisingly, because of the large molecular volume of TON, the maximum level of its incorporation into the clear nanoemulsions was only 4 w/w% at 30 w/w% of Brij 97. At higher oil concentrations, and/or at Brij 97 concentrations of less than 30 w/w%, cloudy, one-phase systems were formed while at higher Brij 97 concentrations, gels were formed (Figure 3.1a). These results are in agreement with those made by Wasutrasawat (2011) who reported a clear, nanoemulsion region of comparable extent (Figure 3.1b). In line with these observations, many researchers have suggested that the extent of the incorporation of oil into a nanoemulsion depends on its molecular weight and volume (Djekic et al., 2008; Malcolmson et al., 1995; Wasutrasawat, 2011). In this context, (Warisnoicharoen et al., 2000b) reported that the area of existence of oil-in-water nanoemulsions stabilised by Brij 97 and containing liquid triglycerides was largest with the largest molecular volume triglyceride, soybean oil (SBO) and smallest with the smallest chain triglyceride, tribuytrin (TBN) and intermediate with the medium chain triglyceride, Miglyol 812. However, the area of existence of oil-in-water

nanoemulsions stabilised by Brij 97 was smallest when prepared using the triglyceride, TON and largest when containing the intermediate sized triglyceride oils, tripalmitin (TPN) and trilaurin (TLN) (Wasutrasawat, 2011). It should be noted that TLN and TPN were both solid at room temperature. Even though TPN has a larger molecular weight and volume, it was TLN that exhibited the largest region of nanoemulsion existence (Wasutrasawat, 2011). As a consequence, in addition to oil molecular weight and/or volume, nanoemulsion formation appears to also depend on other factors such as oil and surfactant structure (Hsieh, 2010; Wooster et al., 2008).
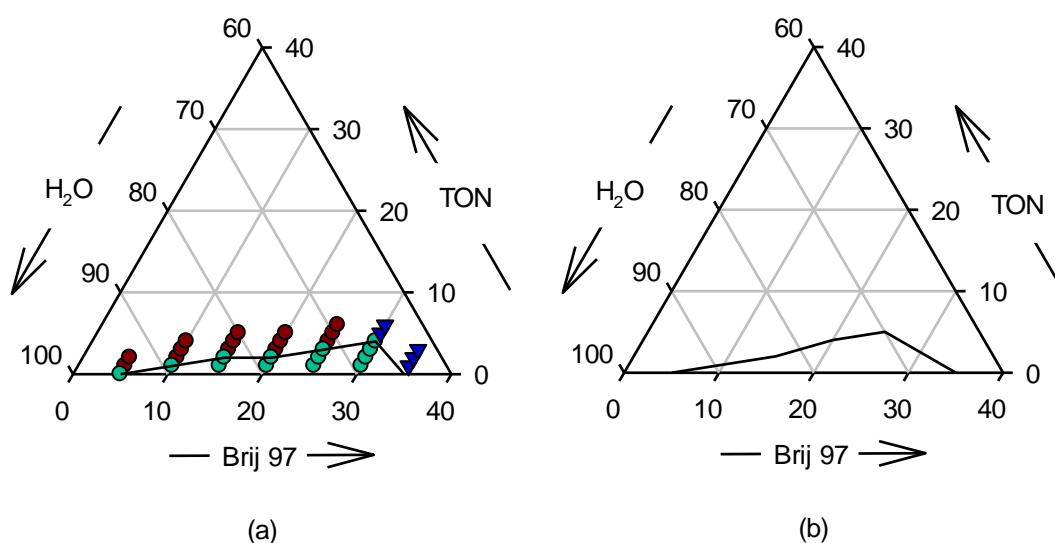
Figure 3.1 Partial phase diagram for the oil-in-water nanoemulsions stabilised by Brij 97 and containing the triglyceride oil, trioctanoate (TON) after 1 month storage at 25.0 ± 0.1 °C compared to the corresponding partial phase diagram of Wasutrasawat (2011). On the abscissa, the surfactant concentration (in w/w%) increases from left to right, while on the ordinate, the oil concentration (in w/w%) increases from bottom to top, and the water concentration (in w/w%) increases from top to bottom. The appearance of the samples was defined as clear (●), gel (●), cloudy (▼). The phase boundary was defined as a solid line.

3.1.2 Solubilisation of testosterone propionate

3.1.2.1 Solubility of testosterone propionate in Brij 97 micelles

The solubility of testosterone propionate (TP) in Brij 97 micelles was determined over time in order to determine both the kinetics and the equilibrium solubility of TP in the surfactant solutions (Figure 3.2). As can be seen, the equilibrium solubility of TP in the Brij 97 micelles was reached within 6 h as evidenced by the fact that the solubility

remained constant for least 96 h, as there was no significant difference ($p > 0.05$) in the solubility recorded over this period (longer time courses were not tested) and could therefore be averaged. In addition, the average TP solubility varied in a linear fashion over a wide range of surfactant concentrations (Figure 3.3), specifically the solubility of TP in the Brij 97 micelles ranged from 0.005 to 0.051 w/v% as the surfactant concentration varied from 0.2 to 2.4 w/w%. It is well established that the solubility of a poorly water soluble drug as a function of the concentration of surfactant is very low until the surfactant concentration reaches its critical micelle concentration (cmc) after which the solubility of the drug increases linearly with surfactant concentration (Carlota et al., 2005). As the cmc of Brij 97 in water at 25°C is low at 0.028 M or 0.002 w/w% (Warisnoicharoen, 1998), all the surfactant concentrations in the present study are well above the cmc of Brij 97 and as a consequence the solubilisation of TP varies in a linear trend with increasing surfactant concentration.
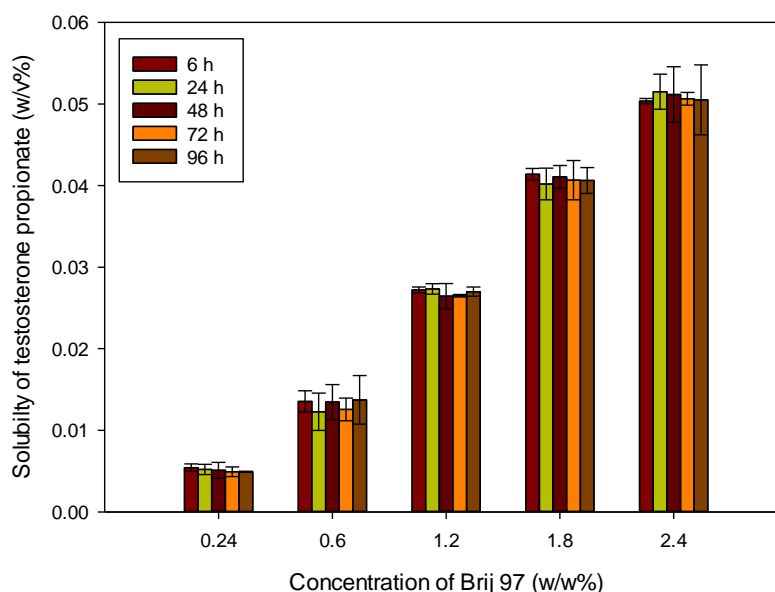
Figure 3.2 Solubility of testosterone propionate in Brij 97 micelles over time at 25.0 ± 0.1 ℃ (mean ± SD, n = 9).
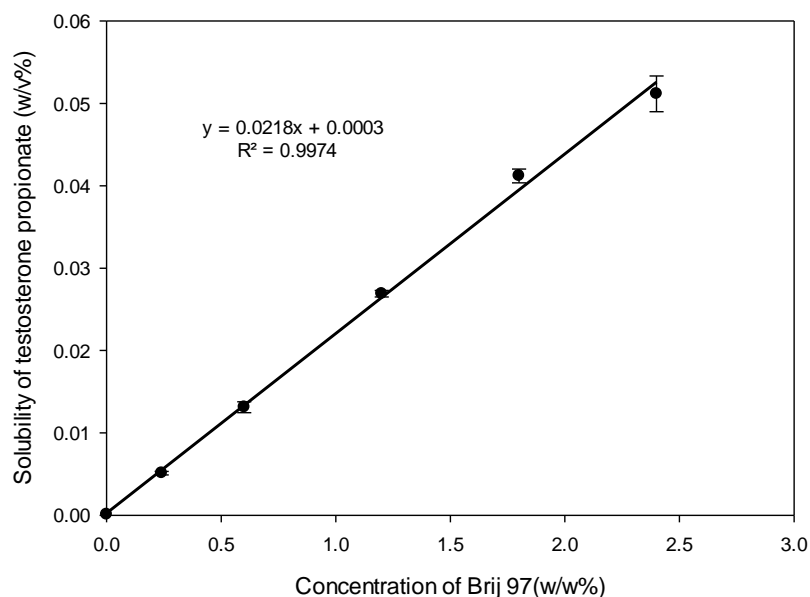
Figure 3.3 The average solubility of testosterone propionate of all time points (i.e. 6, 24, 48, 72 and 96 h) in Brij 97 micelles as a function of surfactant concentration at 25.0 ± 0.1 °C (mean $\pm$ SD, n = 5).

3.1.2.2 Solubility of testosterone propionate in Brij 97-stabilised nanoemulsions

In order to obtain the highest possible amount of the poorly-water soluble drug, TP, in an oil-in-water nanoemulsion, the nanoemulsions containing the highest amount of oil (namely 4 w/w% at 30 w/w% of Brij 97) were initially considered for use in the preparation of a NSNE, however this formulation was too viscous to prepare due to the high amount of surfactant present. As a consequence a clear, nanoemulsion containing 3 w/w% TON and stabilised by 24 w/w% Brij 97 was selected for study. In addition, a cloudy system, just outside the nanoemulsion phase boundary containing 5 w/w% TON and stabilised by 24 w/w% was also studied. The systems selected for examination in the present study were coded as B24T3 and B24T5, respectively. These systems were prepared as stocks which were generally diluted 10 times prior to use. It was necessary to use a stock as it was not possible to directly prepare the nanoemulsions at the low concentrations of surfactant (Figure 3.1) suitable for incorporation into the mixed nanoemulsion and nanosuspension formulations, and for study using techniques such as dynamic light scattering (PCS) and small angle neutron scattering (SANS). The diluted nanoemulsions containing 2.4 w/w% of Brij 97 and either 0.3 or 0.5 w/w% of TON were denoted B24T3/10 and B24T5/10, respectively.

Table 3.1 Solubility of testosterone propionate in Brij 97 micelle and nanoemulsions at 24 h and at $25.0 \pm 0.1\ ^{o}C$.

Sample	Concentration (w/v%) of testosterone propionate (mean ± SD, n = 9)
2.4 w/w% Brij 97 micelle	0.05 ± 0.00
B24T3/10	0.11 ± 0.01
B24T5/10	0.14 ± 0.01

An understanding of the affect of the presence of TP on the two TON-systems under examination was important. As shown in Table 3.1, the solubility of TP in 2.4 w/w% Brij 97 micelles, B24T3/10 and B24T5/10 at 24 h was approximately 0.05, 0.11 and 0.14 w/v%, respectively. It is clear that, at 24 h the solubility of TP in the nanoemulsions was at least twice the solubility of TP in Brij 97 micelles at the same surfactant concentration. Furthermore, the solubility of TP was greatest in the Brij 97-stabilised system that contained the most TON. These results suggest that the presence of TON had a positive effect on the level of incorporation of TP. In the absence of oil, i.e. in the case of surfactant micelles, it is expected that because TP is a hydrophobic drug, that it will most likely be solubilised in the interfacial region of the surfactant micelles. It is clear, however, that in the presence of TON, the drug is also soluble in the oil that forms the core of the nanoemulsion.

In addition, the solubility of TP in Brij 97-stabilised nanoemulsions that had been diluted 10 times with water (designated as B24T3/10 and B24T5/10) and then further diluted by taking 0.76 mL of nanoemulsion and making to 1.00 mL with water (as would be the case in the final combination formulation, which were denoted as B24T3/10/0.76 and B24T5/10/0.76) was determined (Table 3.2). Knowledge of the solubility of TP in these diluted nanoemulsions is important when understanding the behaviour of these nanoemulsions when in a presence of the GF-NPs. Significantly, the results show that solubility of TP was constant regardless of whether it was incubated with an excess of TP for periods of 24 to 96 h. Furthermore, it should be noted that the concentrations of surfactant and oil in the nanoemulsions in Table 3.2 were about 76% of those in Table 3.1 and significantly, as is clear from the results in Table 3.2 the level

of TP solubility in the diluted B24T3/10/0.76 and B24T5/10/0.76 nanoemulsions has decreased proportionally to be about 76% of those in Table 3.1, suggesting that TP solubility scales with surfactant and oil concentration.

Table 3.2 Solubility of testosterone propionate in diluted nanoemulsions over time at 25.0 ± 0.1 °C.

Sample	Concentration (w/v%) of testosterone propionate (mean ± SD, n = 9)			
	24 h	**48 h**	**72 h**	**96 h**
B24T3/10/0.76	0.08 ± 0.00	0.08 ± 0.00	0.07 ± 0.01	0.07 ± 0.01
B24T5/10/0.76	0.09 ± 0.01	0.09 ± 0.01	0.09 ± 0.01	0.09 ± 0.01

Interestingly, previous studies have reported that nanoemulsions could be prepared simply by adding a microemulsion into water and have noted that transparent nanoemulsions could be formed from a bicontinuous microemulsion (Morales et al., 2003; Solè et al., 2012; Tong et al., 2016; Wang et al., 2008). Once the Brij 97-stabilised nanoemulsion had been prepared in the present study, it was found possible to dilute the nanoemulsion to much lower Brij 97 concentrations than it was possible to prepare them at; this is an important result for the use of the nanoemulsions as delivery vehicles. According to Warisnoicharoen et al. (2000a), who measured the size of nanoemulsions stabilised by Brij 97 and containing either a small molecular volume oil such as ethyl butyrate, ethyl caprylate and tributyrin or a large molecular volume oil such as Miglyol 812, soybean oil and ethyl oleate using photon correlation spectroscopy and total intensity light scattering, there was no evidence of any change in nanoemulsion shape or size upon dilution.

The solubility of TP in these diluted nanoemulsions will be the starting point for comparing the solubility of TP in nanoemulsion in a presence of the GF-NPs.

3.1.3 Particle size of nanoemulsions in the presence and absence of testosterone propionate

In order to understand the effect of the amount oil and the presence or absence of TP on particle size, photon correlation spectroscopy (PCS) was used to measure the average hydrodynamic size and size distribution of the Brij 97-stabilised nanoemulsions.

Visual observation of the diluted Brij 97-stabilised nanoemulsions containing 0.3 w/w% of TON in an absence and presence of a saturation amount of TP showed that the nanoemulsions remained transparent for at least 2 months (longer time periods were not tested). In contrast, the diluted Brij 97-stabilised nanoemulsions containing 0.5 w/w% of TON, again in the absence and presence of a saturation amount of TP were transparent immediately after preparation, becoming bluish after 48 hours and cloudy by 72 hours and remaining cloudy for 2 months (longer time periods were not tested).

In this study, the droplet size of the Brij 97-stabilised formulations measured immediately after preparation by PCS was in the nanometre size range (Figure 3.4). In addition, the low polydispersibility values observed for the Brij 97-stabilised formulations suggest a high uniformity of droplet size. In terms of the nanoemulsion particle size, it can be seen that B24T3/10 nanoemulsions containing 0.3 w/w% of TON were about 2.5 nm smaller than the B24T5/10 nanoemulsions containing the higher amount of TON of 0.5 w/w%. As expected, the droplet size of the nanoemulsion increased with an increase in the amount of oil. Similar trends in droplet size have been previously seen in nanoemulsions prepared using polysorbate 20 as surfactant, ethanol as cosurfactant and a mixture of oleic acid and eucalyptus oil as oil, when the droplet size increased with an increase in oil concentration (Ali et al., 2014). In addition, it has been reported that the presence of a long chain oil in a nanoemulsion increases the volume of the core, decreasing the area of surfactant head group and increasing nanoemulsion droplet size, while the presence of short chain oils increase the area of the surfactant head group, favouring the formation of an oil-in-water droplet structure (Warisnoicharoen et al., 2000a).
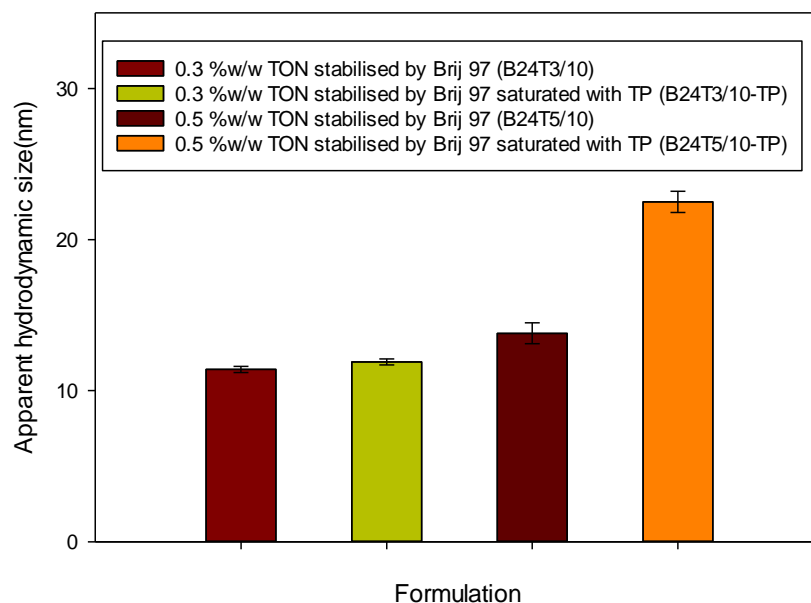
Figure 3.4 Apparent hydrodynamic size of nanoemulsions stabilised with 2.4 w/w% Brij 97 and containing 0.3 and 0.5 w/w% of trioctanoate (TON) in an absence and presence of a saturation amount of testosterone propionate immediately after preparation at 25.0 ± 0.1 $^{\circ}$C (mean $\pm$ SD, n = 9).

The presence of a saturation amount of TP on the droplet size of B24T3/10 nanoemulsions containing 0.3 w/w% of TON resulted in a very slightly greater size than in the equivalent nanoemulsions in the absence of drug, whilst the B24T5/10 nanoemulsions containing 0.5 w/w% of TON and saturated with TP were about 9 nm larger than their drug free counterparts (Figure 3.4).

In terms of nanoemulsion stability, the particle size of the B24T3/10 nanoemulsions containing 0.3 w/w% of TON, both in the absence and presence of a saturation amount of TP, slightly increased over the period of 2 months from 11.4 to 12.7 nm and 11.9 to 15.0 nm, respectively. Note that longer time courses were not studied. However, the droplet size of the nanoemulsions remained in the nanometre size range (Figure 3.5). In contrast, the particle size of the B24T5/10 nanoemulsions containing 0.5 w/w% of TON, in the absence and a presence of a saturation amount of TP, remained constant until 24 h and then thereafter increased in size up to 2 months (longer time courses not tested) reaching 146.4 and 150.7 nm, respectively (Figure 3.5). As a result, the nanoemulsions containing the higher amount of TON were less stable than those containing a lower amount of TON. In fact, nanoemulsions are possibly prone to the

growth of particle size over time by Ostwald ripening (Wooster et al., 2008). Wooster et al. (2008) found that the particle size of nanoemulsions stabilised by the mixture of surfactant composed of 5.6 w/w% of SDS and 16.6 w/w% of polyethylene glycol 6600 and containing 15 v/v% alkane, including dodecane, tetradecane, hexadecane and octadecane, was found to increase over time due to Ostwald ripening. In contrast, however, the small droplet size of the Brij 97 nanoemulsions makes them more resistant to physical destabilisation via gravitational separation, flocculation and/or coalescence because of their high Brownian motion and their highly efficient steric stabilisation (Capek, 2004; Tadros et al., 2004).
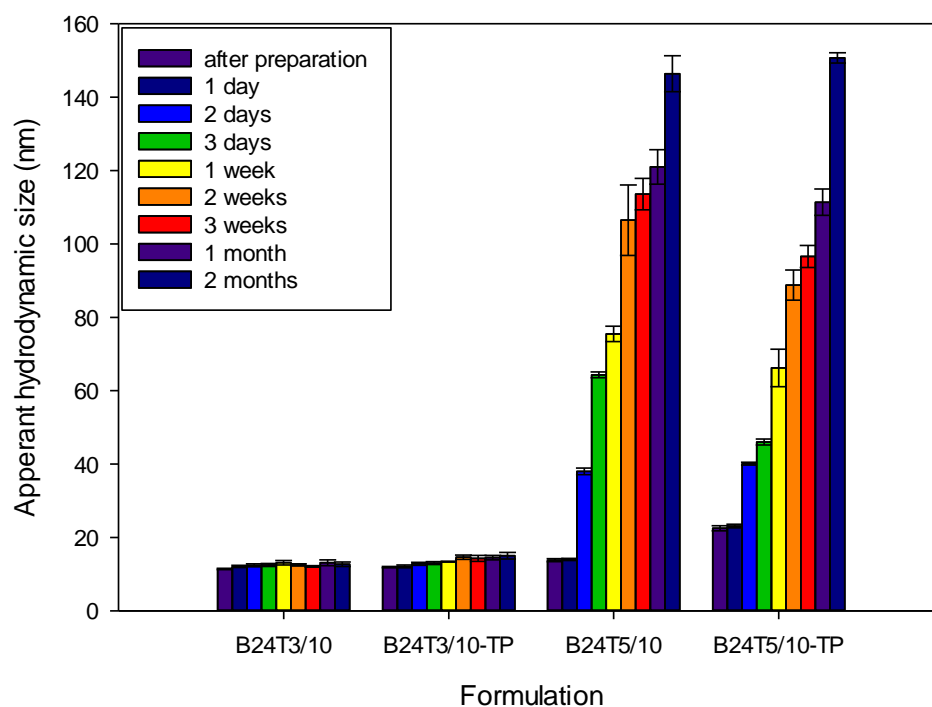
Figure 3.5 Apparent hydrodynamic size 25.0 ± 0.1 °C of the nanoemulsions stabilised by 2.4 w/w% Brij 97 and containing 0.3 and 0.5 w/w% of trioctanoate (TON) in an absence and presence of a saturation amount of testosterone propionate immediately after preparation (mean $\pm$ SD, n = 9).

In agreement with the visual observations, the PCS results showed that the particle size of nanoemulsions containing 0.3 w/w% of TON remained stable for 2 months. Conversely, the particle size of nanoemulsions containing 0.5 w/w% of TON significantly increased from 2 days to 2 months after preparation and were less stable

over time than their counterparts containing lower amounts of oil. In fact, it has been previously reported that nanoemulsions may lose their transparency over time due to an increase in droplet size (Tadros et al., 2004).

3.1.4 Cloud point and phase inversion temperature

The cloud point (CP) and phase inversion temperature (PIT) of micelles and nanoemulsions, respectively are sensitive to the structure and conformation of the surfactant aggregates. It is important to know the CP and PIT of the micelles and nanoemulsions to ensure that they are not close to the temperature range they will experience while being used as a drug delivery vehicle (Mathis et al., 1984). Figure 3.6 shows the CP of a 2.4 w/w% Brij 97 micellar solution and the PIT of the corresponding nanoemulsions containing 0.1-0.3 w/w% TON, in the presence and absence of a saturation amount of TP. In this study, regardless of the presence or absence of a saturation amount of TP, the CP of micelles and the PIT of nanoemulsions were all in the range 47 to 54 °C, well above the body temperature of 37 °C and the 'in-use' temperature of approximately 20-25 °C.
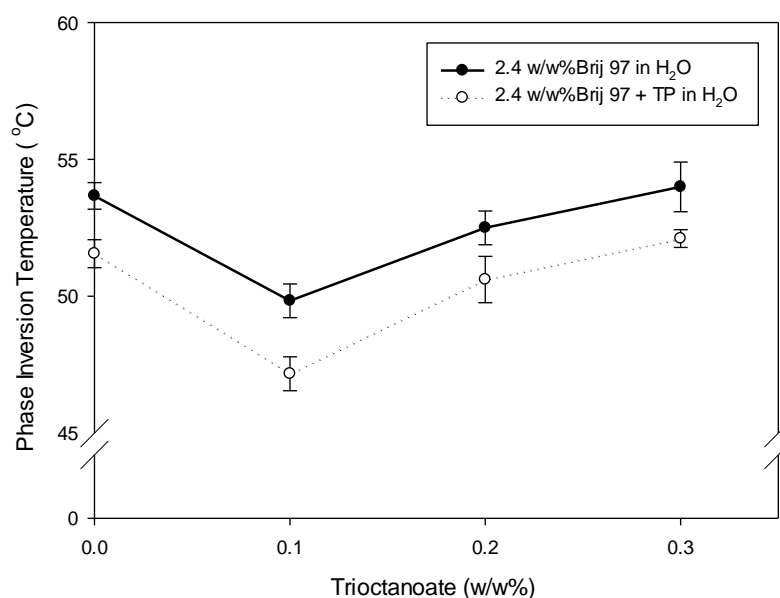
Figure 3.6 The cloud point and phase inversion temperature of 2.4 w/w% Brij 97 nanoemulsions as a function of trioctanoate (TON) concentration in the absence and presence of testosterone propionate (TP) (mean ± SD, n = 9).

The variation in the PIT of a nanoemulsion as a function of oil content is widely attributed to the variation in the location of the oil in the nanoemulsion droplet. For example increasing the oil content may result in the transformation of rod-like micelles (at low or no oil content) into globular aggregates upon increasing oil content and the formation of an oil core in microemulsions (Hoffmann et al., 1988). Indeed Malcolmson (1993) and Wasutrasawat (2011) reported that the shape of Brij 97 micelles were asymmetric, becoming more spherical upon increasing oil content and the consequent formation of a nanoemulsion. In addition, the PIT of a nanoemulsion can be affected by altering the chemical nature of the amphiphile, the addition of inorganic salts and both the nature and amount of oil (Aveyard et al., 1986).

In respect to the effect of the addition of oil on the structure of the surfactant aggregate, it is the relative molecular volume of oil that is important. Consequently, the definition of what is "small" or "large" molecular volume oil is related to the nature of the particular surfactant being studied. In general it is considered that the oil has a small molecular volume oil if its chain length is less than that of the hydrophobic chain length of the surfactant, whilst a large molecular volume oil has chain length similar to or longer than that of the surfactant hydrophobe (Chen et al., 1986).

As a rule, the presence of a large molecular volume oil tends to increase the PIT while the incorporation of a small molecular volume oil tends to result in a decrease in the PIT, although at high oil contents they may cause an increase in the PIT (Malcolmson et al., 1998). Large molecular volume oils tend to form a core in the centre of the surfactant aggregate/nanoemulsion resulting in one of two effects depending on the initial shape of the micelles. If the micelle was originally spherical, the addition of the oil may result in a change in both the effective head group area and the effective hydrophobic volume of the surfactant, if these changes balance each other then the degree of curvature of the aggregate will remain the same and therefore the resulting PIT will be similar to that of the corresponding micellar solution (Aveyard et al., 1986). If, in contrast, the micelles were initially asymmetric in shape, the addition of oil may encourage a change in nanoemulsion shape to spherical and a corresponding increase in the PIT of the nanoemulsions. Note however, that it is possible that the addition of low amounts of small molecular volume oil, may actually act in the same way as a cosurfactant, by increasing the effective volume of the surfactant hydrophobic chain and

also decreasing the effective area of hydrophilic head group of the surfactant, resulting in a lower curvature of the aggregates which become even more asymmetric, thereby lowering the PIT in much the same way.

The CP of the 2.4 w/w% Brij 97 micelles in an absence of TP was ~ 54 °C, which initially decreased to ~ 50 °C in the presence of 0.1 w/w% of TON, and then increased up to ~ 54 °C in the presence of 0.3 w/w% TON. The CP of the 2.4 w/w% Brij 97 micelles in the presence of a saturation amount of TP was ~ 52 °C (~ 2°C less than in the absence of TP), which then decreased to ~ 48 °C in the presence of 0.1 w/w% of TON, and subsequently increased to ~ 52 °C when 0.3 w/w% of TON was added. Regardless of the absence or presence of TP, the addition of a small amount of TON (i.e. 0.1 w/w%) to Brij 97 micelles resulted in a decrease in the PIT while the addition of a more TON (~ 0.3 w/w%) caused an increase in the PIT. Interestingly the PIT of nanoemulsions containing 0.3 w/w% TON was comparable to the CP of the equivalent Brij 97 micelles. As expected, the addition of the hydrophobic drug, TP to the Brij 97 micelles and Brij 97-stabilised nanoemulsions reduced the CP and PIT, respectively of these systems.

In this study, it appears that the presence of TON at low concentrations, acts in much the same way as cosurfactant by increasing the effective volume of the surfactant's hydrophobic chain and decreasing the effective area of its hydrophilic head group leading to the formation of more asymmetric drops and a lower PIT (Warisnoicharoen et al., 2000b). In contrast, the PIT of nanoemulsion increases with a further increase in the amount of oil as a consequence of the oil tending to go into the core of the droplet leading to a transformation of the asymmetric droplets to more symmetrical aggregates (Ko et al., 2003).

Based on these results, it would be anticipated that the 2.4 w/w% Brij 97 micelles and the nanoemulsions containing 0.1 w/w% TON were likely to be asymmetric, with the nanoemulsion droplets becoming more symmetric/less asymmetric upon the addition of further TON. In addition, as the PIT of nanoemulsions containing 0.3 w/w% of TON was the same as the CP obtained for the micelles, it is proposed that TON is, at least partially, solubilised in the interfacial surfactant region rather than being solubilised exclusively in the core. Encouragingly, the experimental results obtained in the present study are in good agreement with those of Wasutrasawat (2011).

Interestingly, Malcolmson et al. (1998) proposed that the hydrophobic drug, TP was likely to be solubilised in the interfacial region of a surfactant aggregate. As a consequence, it might be expected that any nanoemulsion containing TON would not exhibit an increase in the apparent aqueous solubility of TP solubility due to competition with TON for the site of solubilisation. However, as TP solubilisation in Brij 97-stabilised nanoemulsions in a presence of 0.3 and 0.5 w/w% TON was about twice and three times that obtained in Brij 97 micelles, it is most probable that TON is, at least partially, incorporated into the core of the nanoemulsion droplets. This result further supports the hypothesis that the asymmetric Brij 97 micelles become more spherical with the addition of TON and that the TON is both partially mixed with the surfactant tails as well as partially forming a core in the centre of the aggregate. This suggestion comes from combining the results of the PIT experiments (which indicated that TON penetrated into the surfactant layer but perhaps not deeply because the PIT did not changed much) with the solubilisation experiments (where the solubility of TP was significantly improved in the TON-containing nanoemulsion implying that the TON is located in the core of the nanoemulsion).

3.1.5 Effect of solvent on the properties of Brij 97-stabilised nanoemulsions

It is well established that differences in bond strength and bond length of hydrogen and deuterium may affect the resultant intermolecular interactions in systems prepared using H_2O with D_2O. For example Whiddon et al. (2001) found a large isotope effect on the critical points and phase boundaries when substituting H_2O with D_2O in an aqueous solution of alkylglucoside surfactant. The use of deuterium, as opposed to hydrogen, in this system caused the surfactant to 'appear' more hydrophobic due to the effect on the glucose head group of exchanging O-H for O-D, in particular the effect on its bond lengths and strengths. Despite these well-documented changes, however, when replacing H_2O with D_2O as a solvent in microemulsions stabilised by ionic and zwitterionic surfactants, there was no significant change in the solubilisation of drug in the microemulsions (Hsieh, 2010). Note that, in the present study. SANS measurements were performed at the solvent 'contrast match' point (see Chapter 4), which was a 43.25 v/v% mixture of D_2O in H_2O. As a consequence of the use of 43.25 v/v% D_2O/H_2O as solvent in the SANS experiments, it was important to study the physical properties of

the nanoemulsions (including phase behaviour, particle size, CP and PIT) in this solvent.

3.1.5.1 Effect of the presence of a mixture of D_2O and H_2O on phase behaviour of Brij 97-stabilised nanoemulsions

The ternary phase diagrams of TON in Brij 97-stabilised nanoemulsions in an aqueous solvent of 43.25 v/v% D_2O/H_2O and H_2O are shown in Figure 3.7a-b. As can be seen in Figure 3.7a, the maximum level of TON incorporation, which occurred at 30 w/w% of Brij 97, was 4 w/w%. Furthermore, at low to intermediate Brij 97 concentrations, cloudy nanoemulsions were formed at high TON and intermediate Brij 97 concentrations, while gels were observed at high TON concentrations and Brij 97 concentrations above 30 w/w%. Significantly for the present study, the area of nanoemulsion existence obtained for systems containing TON, Brij 97 and 43.25 v/v% D_2O/H_2O (Figure 3.7a) was the same as that obtained for the corresponding system using H_2O as solvent (Figure 3.7b).
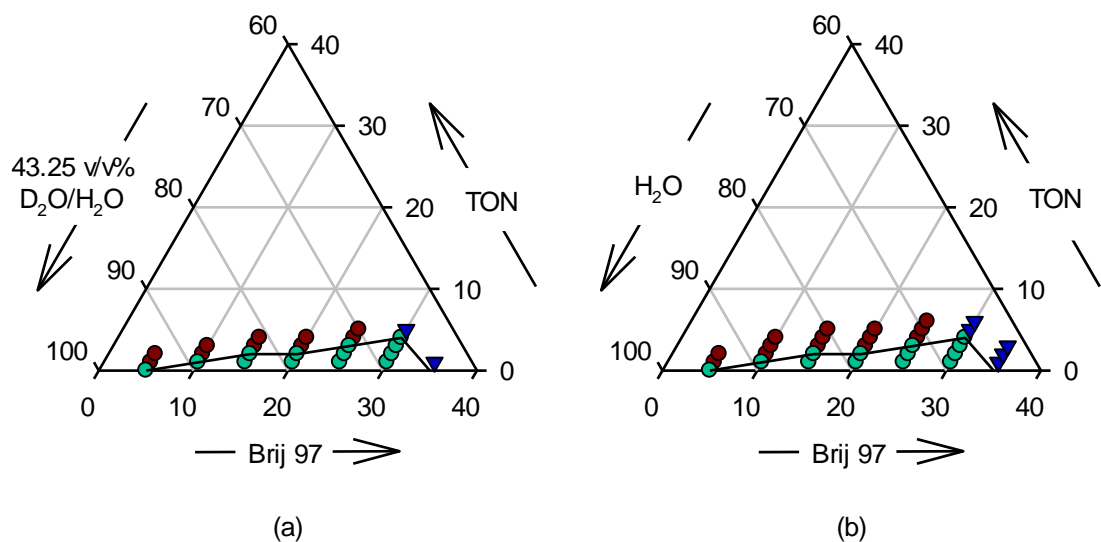
Figure 3.7 Partial phase diagrams for the oil-in-water (a; 43.25 v/v% D_2O/H_2O and b; H_2O) nanoemulsions stabilised by Brij 97 and containing the triglyceride oil, trioctanoate (TON) after 1 month storage at 25.0 ± 0.1 °C. On the abscissa, the surfactant concentration (in w/w%) increases from left to right, while on the ordinate, the oil concentration (in w/w%) increases from bottom to top, and the water concentration (in w/w%) increases from top to bottom. The appearance of the samples was defined as clear (●), gel (●), cloudy (▼). The phase boundary was defined as a solid line.

3.1.5.2 Effect of the presence of a mixture of D_2O and H_2O on nanoemulsion particle size at 25°C

Previous studies have reported that the use of D_2O as solvent in place of H_2O affects the size of the micelles formed by alkylglucosides surfactants (Ericsson et al., 2004; Whiddon et al., 2001). For example, Ericsson et al. (2005) reported that the particle size (as assessed by PCS) of the micelles formed by *n*-tetradecyl-*β*-d-maltoside when dissolved in D_2O were larger than those formed in H_2O.

In order to determine whether the use of the contrast match solvent, i.e. 43.25 v/v% D_2O/H_2O, had any effect on the particle size of nanoemulsion, PCS measurements were performed. Table 3.3 shows the apparent hydrodynamic size of nanoemulsions, in an absence and presence of a saturation amount of TP, when prepared in either 43.25 v/v% D_2O/H_2O or H_2O at 25 ºC. It is clear, however, from the results that there was no significant change in the particle size of the nanoemulsions when made in the two solvents immediately after their preparation as well as after 1, 2 and 3 days. Indeed, the same trend in the variation in the apparent hydrodynamic size of nanoemulsions prepared in both 43.25 v/v% D_2O/H_2O and H_2O was seen upon increasing the amount of oil (from 0.3 to 0.5 w/w% TON) and, whether or not a saturation amount of TP was present. Note that the apparent hydrodynamic size of nanoemulsions prepared in 43.25 v/v% D_2O/H_2O as a solvent as assessed by PCS was corrected for the appropriate continuous phase viscosity.

Table 3.3 Comparison of the apparent hydrodynamic size of nanoemulsions prepared in an absence and a presence of a saturation amount of testosterone propionate at 25.0 ± 0.1 ºC.

Sample		Apparent hydrodynamic size (nm) (mean $\pm$ SD, n = 9)	
		43.25 v/v% D_2O/H_2O	H_2O
B24T3/10	after preparation	11.1 ± 0.1	11.4 ± 0.2
	1 day	12.3 ± 0.2	12.1 ± 0.3
	2 days	12.3 ± 0.1	12.4 ± 0.4
	3 days	12.1 ± 0.1	12.5 ± 0.4
B24T3/10-TP	after preparation	12.3 ± 0.2	11.9 ± 0.2
	1 day	12.9 ± 0.4	12.1 ± 0.4
	2 days	13.1 ± 0.1	12.8 ± 0.4
	3 days	13.8 ± 0.3	13.0 ± 0.4
B24T5/10	after preparation	13.8 ± 0.2	13.8 ± 0.4
	1 day	14.2 ± 0.2	14.0 ± 0.3
	2 days	38.3 ± 0.2	38.0 ± 0.9
	3 days	64.3 ± 0.5	64.3 ± 0.8
B24T5/10-TP	after preparation	22.6 ± 0.2	22.5 ± 0.7
	1 day	23.3 ± 0.3	23.1 ± 0.5
	2 days	39.9 ± 0.4	40.1 ± 0.4
	3 days	46.8 ± 0.5	46.0 ± 0.8

3.1.5.3 Effect of the presence of a mixture of D_2O and H_2O on the cloud point and phase inversion temperature

Figure 3.8 shows that the phase inversion temperature of TON-containing Brij 97-stabilised nanoemulsions prepared in 43.25 v/v% D_2O/H_2O initially decreased slightly compared to the cloud point of Brij 97 micelles and then increased upon the addition of further oil, exactly the same trend as was seen in the Brij 97 micelles and Brij 97-stabilised nanoemulsion prepared in H_2O. There was however, a slight decrease in the CP of Brij 97 micelle and the PIT of nanoemulsions when prepared in 43.25 v/v% D_2O/H_2O as opposed to H_2O (Figure 3.9). Furthermore, it should be noted that, regardless of the precise composition of the aqueous solvent, the CP and PIT exhibited by the Brij 97 micelles and Brij 97-stabilised nanoemulsions are much higher than the experimental temperature of 25 °C used in the SANS study, and as a consequence this difference should not cause any problems in the performance and interpretation of the SANS experiment.
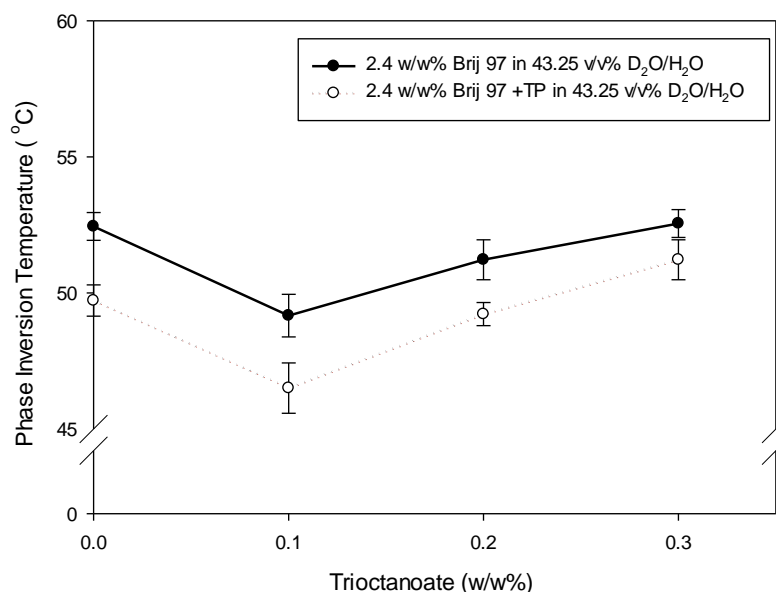
Figure 3.8 The cloud point and phase inversion temperature of 2.4 w/w% Brij 97-stabilised aggregates using 43.25 v/v% D_2O/H_2O as a function of trioctanoate (TON) content in the absence and presence of testosterone propionate (TP) (mean ± SD, n = 9).
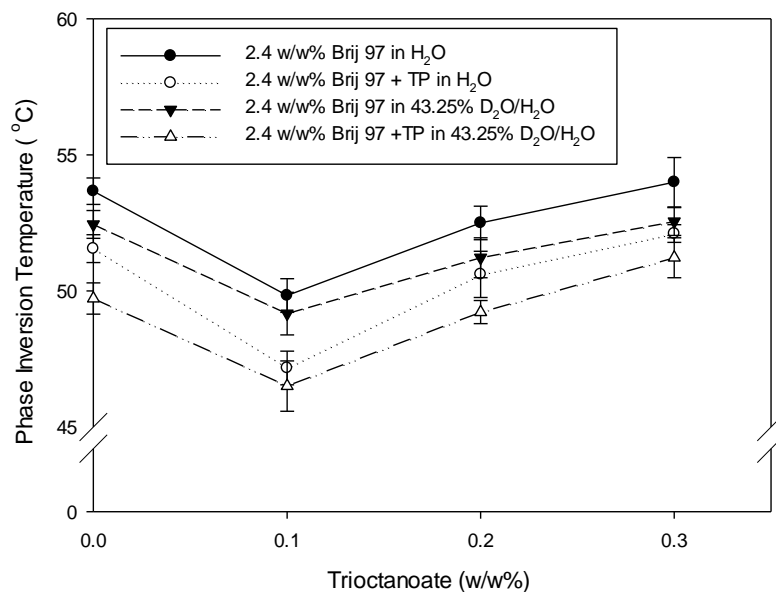
Figure 3.9 The cloud point and phase inversion temperature of 2.4 w/w% Brij 97-stabilised aggregates using either H_2O or 43.25 v/v% D_2O/H_2O as a function of trioctanoate (TON) content in the absence and presence of testosterone propionate (TP) (mean ± SD, n = 9).

In summary, B24T3/10 and B24T5/10 nanoemulsions can be prepared using 43.25 v/v% D_2O/H_2O as solvent without significantly affecting the physical properties of the nanoemulsions, in particular their phase behaviour, particle size, CP and PIT.

3.2 Preparation of ionic microemulsions

3.2.1 Phase behaviour

Figure 3.10a-b shows the partial phase diagrams of microemulsions prepared using water, sodium dodecyl sulphate (SDS) as surfactant and either ethyl butyrate (EB) or ethyl caprylate (EC) as oil. The oil-in-water microemulsions were defined as clear, fluid systems that were stable at room temperature for a period of at least 1 month. The solid line presents the upper boundary of the microemulsion region.

As can be seen from the partial phase diagrams of the SDS-stabilised microemulsions shown in Figure 3.10a, EB, the oil with the shorter alkyl chain length and smaller molecular volume, could be solubilised at a level of 18 w/w% at an SDS concentration of 20 w/w%, while in comparison, the larger molecular volume, longer alkyl chain

length oil, EC could be only solubilised up to a maximum of 9 w/w% at the same surfactant concentration. As shown in Figure 3.10b, Hsieh (2010) also determined the phase behaviour of microemulsions comprising water, SDS and either EB or EC and found that EB could be incorporated at levels up to 20% w/w at 25 w/w% of SDS, while EC could only be solubilised up to 8% w/w at 22 w/w% of SDS, results that are in good agreement with those obtained in the present study. Although noticeably, a small amount of either EB or EC could be incorporated at 30-35 w/w% of SDS, a result which Hsieh (2010) did not find and may probably reflects the purity of the two batches of SDS used as it is well known that SDS may degrade over time to produce dodecanol.

It is clear from the present study and those of others that the structure of oil impacts on the level of oil incorporated into the microemulsion. According to other researchers (Monduzzi et al., 1997; Warisnoicharoen, 1998), decreasing the alkyl chain length of the add oil (such as an alkane and the ethyl ester of an alkanoic acid) increases the amount of oil incorporated into microemulsions prepared using a nonionic surfactant. Warisnoicharoen et al. (2000b) also suggested that not only the molecular volume of the oil has an effect on the amount incorporated but that the structure of the oil could explain its preferred location within the microemulsion droplets. For example small molecular volume oils such as EB and EC can act in much the same way as a cosurfactant in that they can penetrate the hydrocarbon chain region of the interfacial surfactant layer. As a consequence, it might be expected that the smaller molecular volume oil, EB could be incorporated into the SDS microemulsions to a much greater extent that the slightly larger molecular volume oil, EC. In addition, because of its slightly longer hydrophobic chain length, EC is more likely to remain in the core of the microemulsion droplets rather than reside amongst the hydrophobic chain region of the interfacial surfactant monolayer.

(a)   (b)
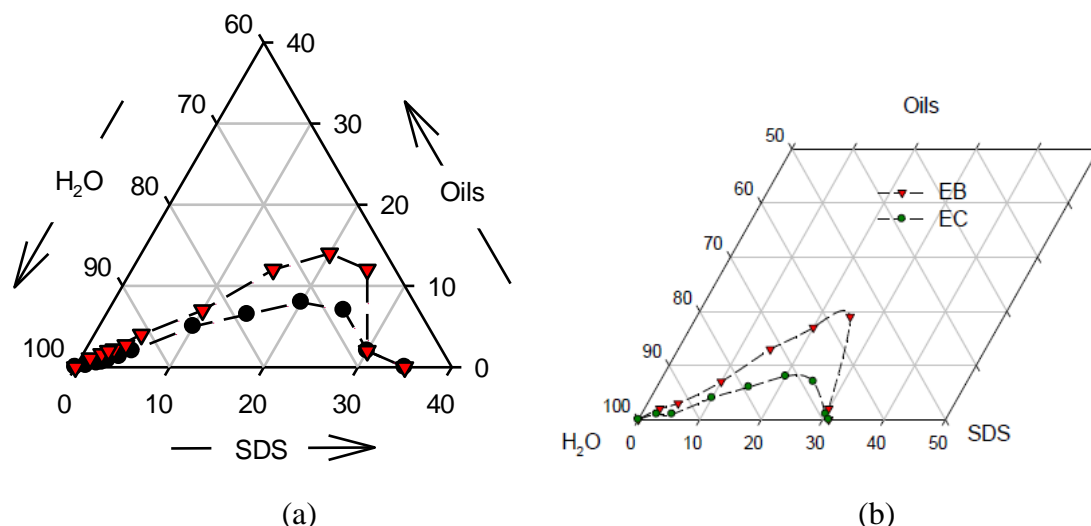
Figure 3.10 Partial phase diagrams for oil-in-water microemulsions stabilised by SDS and containing either ethyl butyrate (EB) (--▼--) or ethyl caprylate (EC) (--●--) in water at 25.0 ± 0.1 °C in this study comparing, on the right, that obtained by Hsieh (2010). On the abscissa, the surfactant concentration (in w/w%) increases from left to right, while on the ordinate, the oil concentration (in w/w%) increases from bottom to top, and the water concentration (in w/w%) increases from top to bottom.

3.2.2 Solubility of testosterone propionate

3.2.2.1 Solubility of testosterone propionate in oil

In the present study, TP was used as a model of a very poorly-water soluble, low dose drug: its solubility in water is recorded as 0.0009 w/w% (Malcolmson et al., 1998). Table 3.4 shows the solubility of TP in the oils, EB, EC and TON. The results show that the solubility of TP in EB, EC and TON at 24 h was, respectively approximately 19.9, 12.7 and 6.2 w/v% and that this solubility did not change over 3 days suggesting that the equilibrium solubility of TP in the oils was achieved within 24 h. The solubility of TP in EB was more than three times its solubility in TON, while the solubility of TP in EC was about twice the solubility of TP achieved in TON. The data obtained in the present study followed the pattern of TP oil solubility reported by Malcolmson et al. (1998) who found TP to be most soluble in the most polar oil.

Table 3.4 Solubility of testosterone propionate in oil over time at 25.0 ± 0.1 °C.

Oil	Concentration (w/v%) of testosterone propionate (mean ± SD, n = 9)		
	24 h	48 h	72 h
EB	19.92 ± 0.50	19.79 ± 0.33	20.04 ± 0.25
EC	12.73 ± 0.13	12.42 ± 0.11	12.68 ± 0.23
TON	6.18 ± 0.02	6.19 ± 0.02	6.18 ± 0.08

3.2.2.2 Solubility of TP in SDS micelles

The solubility of TP in SDS micelles was determined over a period of 4 days (Figure 3.11). As there was no significant difference ($p > 0.05$) in the solubility of TP in the SDS micelles over the 6 and 96 h tested (longer time courses were not tested) the solubility data was averaged. The results in Figure 3.12 show a linear relationship between the average TP solubility and surfactant concentration over a 5 fold increase in surfactant concentration - TP solubility increases from about 0.2 to 1.1 w/v% with an increase in SDS from 1 to 5 w/w%. In this context it should be noted that all the SDS concentrations in this study are well above their critical micelle concentration (cmc): the cmc of SDS in water at 25°C being 8 M or 0.24 w/w% (Luckey, 2014). Comparing the solubility of TP in micelles of SDS with micelles of Brij 97 shows that TP can be solubilised by SDS micelles to a much greater extent than in Brij 97 micelles. According to Hsieh (2010), the level of TP solubilised in micelles formed using C_{12} surfactants varied with the nature of the surfactant head group such that SDS exhibited a greater solubilising capacity than *N,N*-dimethyldodecyl-*N*-oxide which in turn was greater than dodecyltrimethylammonium bromide which was greater than dimethyldecylamminopropyl sulphate. This result was thought to be a consequence of the major site of drug solubilisation being the interface between the hydrocarbon core of the micelle and the hydrated head group region. Significantly, using molecular dynamic simulations, Allen et al. (2014) reported that, at equilibrium, the solubilised TP molecules are preferentially located among the polar head groups of the SDS molecules comprising the surfactant micelle.
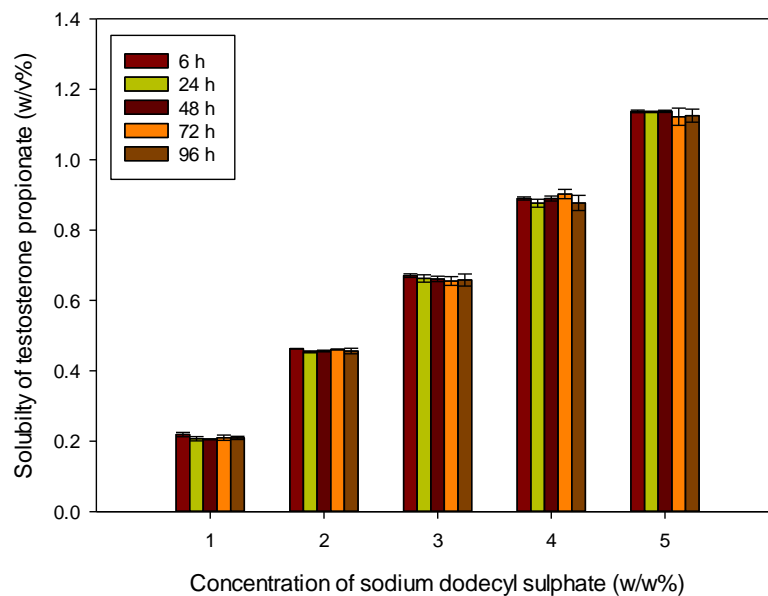
Figure 3.11 Solubility of testosterone propionate in sodium dodecyl sulphate micelles over time at 25.0 ± 0.1 °C (mean ± SD, n = 9).
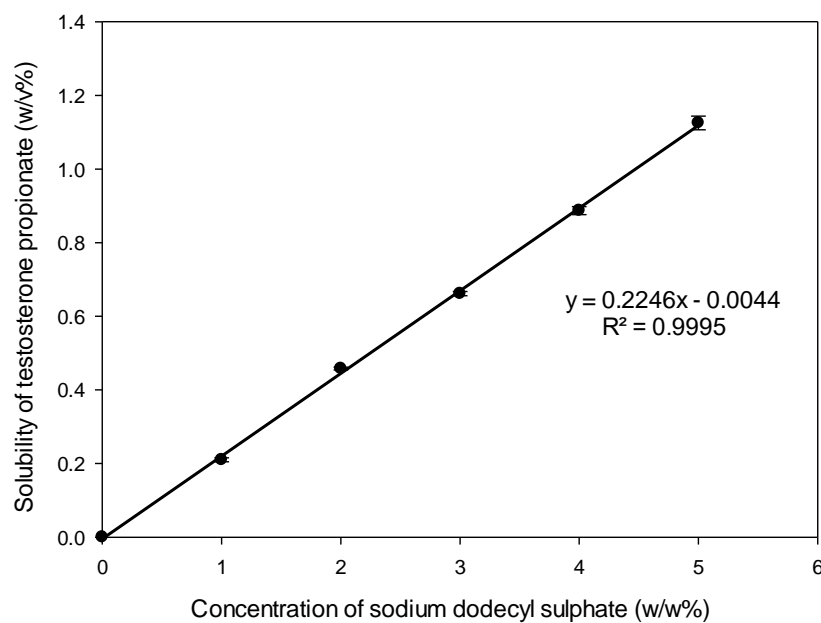
Figure 3.12 The average solubility of testosterone propionate of all time points (i.e. 6, 24, 48, 72 and 96 h) in sodium dodecyl sulphate micelles as a function of surfactant concentration at 25.0 ± 0.1 °C. (mean ± SD, n=5)

3.2.2.3 Solubility of testosterone propionate in sodium dodecyl sulphate-stabilised microemulsions

The SDS-stabilised microemulsions that contained the highest amount of oil (namely either 18 w/w% of EB or 9 w/w% of EC at 20 w/w% of SDS) were originally considered suitable for use in the preparation of the NSME, in order to load the highest amount of the poorly-water soluble drug, TP. Unfortunately these formulations were thought to be too viscous for NSME preparation due to the high concentration of oil they contain. Consequently two microemulsions stabilised by 20 w/w% SDS were selected for further study, one containing 14 w/w% of EB and the other one containing 8 w/w% of EC. The codes used to denote the selected microemulsions were S20B14 and S20C08, respectively. S20B14 and S20C08 were both chosen because they were within the clear oil-in-water microemulsion area. The S20B14 and S20C08 microemulsions were used as stocks and diluted 5 times prior to their use in subsequent studies. The codes of the diluted microemulsions were S20B14/5 and S20C08/5. The use of a stock solution to prepare these low surfactant concentrations microemulsions was necessary as it was not possible to directly prepare these microemulsions. The use of low SDS concentrations also has benefit when performing SANS as the interaction between particles is reduced to a minimum.

An understanding of the effect of the presence of TP in the various microemulsions was important for this study. As can be seen in Table 3.5, the solubility of TP in micelles prepared using 4 w/w% of SDS and microemulsions also prepared using 4 w/w% of SDS containing either 2.8 w/w% EB or 1.6 w/w% EC was 0.88, 0.66 and 0.93 w/v% respectively. The solubility of TP obtained in the SDS micelles was significantly greater than that observed in microemulsion containing 2.8 w/w% EB but significantly less than that recorded in microemulsion containing 1.6 w/w% EC at the same concentration of 4 w/w% of SDS. On the basis of the solubility of TP in the two ethyl ester oils, it was assumed that the microemulsions containing the oil with the greatest solubilising capacity for TP, i.e. EB, would demonstrate the greatest TP solubilisation. However as is clear from Table 3.5, this was not the case, as TP solubility was surprisingly greatest in the EC-containing microemulsions and least in the EB-containing microemulsions. Reassuringly a similar observation was also been made by Hsieh (2010) who reported that, despite TP's greater solubility in EB than EC, the

solubility of TP in microemulsions stabilised by zwitterionic surfactant, *N*-dodecyl-*N*,*N*-dimethyl-3-ammonio-1-propanesulfonate (DDAPS) was greatest in the EC-containing microemulsions rather than the EB-containing microemulsions. As the result of this observation, Hsieh (2010) proposed that expected increase in TP solubility in the presence of EB did not occur because the oil did not form a core in the centre of the microemulsion droplet, but rather was incorporated into the microemulsions in much the same way as a cosurfactant, being intercalated amongst the alkyl chain region of the surfactant monolayer and thereby not providing the additional locus of solubilisation for the drug.

Table 3.5 Solubility of testosterone propionate in sodium dodecyl sulphate micelles and sodium dodecyl sulphate -stabilised microemulsions at 25.0 ± 0.1 ℃.

Sample	Concentration (w/v%) of testosterone propionate (mean $\pm$ SD, n = 9)
4 w/w% SDS micelles	0.88 ± 0.01
S20B14/5	0.66 ± 0.01
S20C08/5	0.93 ± 0.01

The solubility of TP in SDS-stabilised microemulsions that had been diluted 5 times with water, (designated as S20B14/5 and S20C08/5) and then further diluted, 0.76 mL of 5 times diluted microemulsion to a final volume of 1.00 mL with water (as would be the case in the final combination formulation, which were denoted as S20B14/5/0.76 and S20C08/5/0.76) to help understand the behaviour of the diluted microemulsions when mixed with the GF-NPs. Significantly, the results showed that solubility of TP in the diluted microemulsions did not change over the 1 to 4 days time period they were measured (Table 3.6). In addition, in terms of concentration scaling, the concentrations of surfactant and oil of the microemulsions shown in Table 3.6 were 76% of those in Table 3.5, (i.e. the 5 times diluted microemulsions were further diluted after mixing 0.76 mL of the microemulsions with 0.24 mL water). As can be seen, it was clear that

the solubility of TP in the systems reported in Table 3.6 decreased proportionally to be about 76% of those in Table 3.5.

Table 3.6 Solubility of testosterone propionate in the diluted nanoemulsions over time at 25.0 ± 0.1 ℃.

Sample	Concentration (w/v%) of testosterone propionate (mean ± SD, n = 9)			
	24 h	48 h	72 h	96 h
S20B14/5/0.76	0.50 ± 0.02	0.51 ± 0.00	0.50 ± 0.02	0.49 ± 0.01
S20C08/5/0.76	0.71 ± 0.00	0.71 ± 0.00	0.71 ± 0.00	0.71 ± 0.00

Previous studies have reported that nanoemulsions could be prepared by adding a microemulsion into water and that a transparent nanoemulsion could be formed from the dilution of bicontinuous microemulsions (Morales et al., 2003; Solè et al., 2012; Tong et al., 2016; Wang et al., 2008). Interestingly, however once the SDS-stabilised microemulsions containing either 14 w/w% of EB or 8 w/w% of EC had been prepared, it was found to be possible to dilute the microemulsions using water to a much lower SDS concentration than it was possible to prepare them at. This was an important result for the use of these SDS-stabilised microemulsions as delivery vehicles.

When comparing the solubility of TP in nanoemulsions stabilised by Brij 97 and containing TON to the solubility of TP in SDS-stabilised microemulsions containing either EB or EC, it was clear that TP was most soluble in the EC-containing SDS microemulsions, followed by the EB containing ones, and finally the Brij 97-stabilised nanoemulsions containing TON, although it should be noted that the amount of surfactant and oil in the nanoemulsion and microemulsions were not the same.

This observation regarding the solubility of TP in the various nanoemulsions and microemulsions studied may be explained by the smaller molecular volume oils as EB and EC (which are the most polar oils and exhibit the greatest drug solubilising capacity) being more likely to penetrate into the hydrophobic chains of the interfacial surfactant region, while the larger molecular volume TON, in contrast, is more likely to

form in a core at the centre of the nanoemulsion droplets. Even in the case of SDS-stabilised microemulsions there were differences in the TP solubilising capacity, in that the microemulsions containing EB exhibited a lower smaller capacity for TP than those containing EC. This difference is considered to be a consequence of the way in which the two ethyl ester oils are incorporated into the microemulsions in that EB was considered to penetrate more deeply into the hydrophobic chains of the interfacial surfactant region than EC. Therefore, in order to confirm this hypothesis, a further study, such as SANS is needed to obtain detailed information on the morphology of nanoemulsion and microemulsion droplets.

3.2.3 Effect of solvent on the properties of sodium dodecyl sulphate-stabilised microemulsions

3.2.3.1 Effect of the presence of a mixture of D_2O and H_2O on the phase diagram of sodium dodecyl sulphate-stabilised microemulsions

When examining the microemulsion and nanosuspension combination product using SANS, it was necessary to use a mixture of D_2O/H_2O (43.25 v/v%) as solvent instead of H_2O, in order to make the griseofulvin nanoparticles 'invisible' to neutrons, thereby allowing the effect of the griseofulvin nanoparticles on the microemulsions to be determined. In order to understand whether the use of the 43.25 v/v% D_2O/H_2O solvent had any effect on the phase behaviour of the SDS microemulsions, microemulsions were prepared using 43.25 v/v% D_2O/H_2O as solvent. The partial phase diagram of SDS microemulsions prepared using this solvent are shown in Figure 3.13a, where it can be seen that the maximum level of EB was 18 w/w% and the maximum level of EC was 9 w/w%, both maxima occurring at 20 w/w% SDS. The formation of cloudy systems were observed at higher oil concentrations and low to medium SDS concentrations while the formation of gels were observed at high oil concentrations and SDS concentrations greater than 15-20 w/w%. The area of microemulsion existence for SDS microemulsions containing either EB or EC and prepared using 43.25 v/v% D_2O/H_2O (Figure 3.13a) was the same as when H_2O was used as solvent (Figure 3.13b), suggesting that the use of 43.25 v/v% D_2O/H_2O in place of H_2O had no significant effect on phase behaviour.
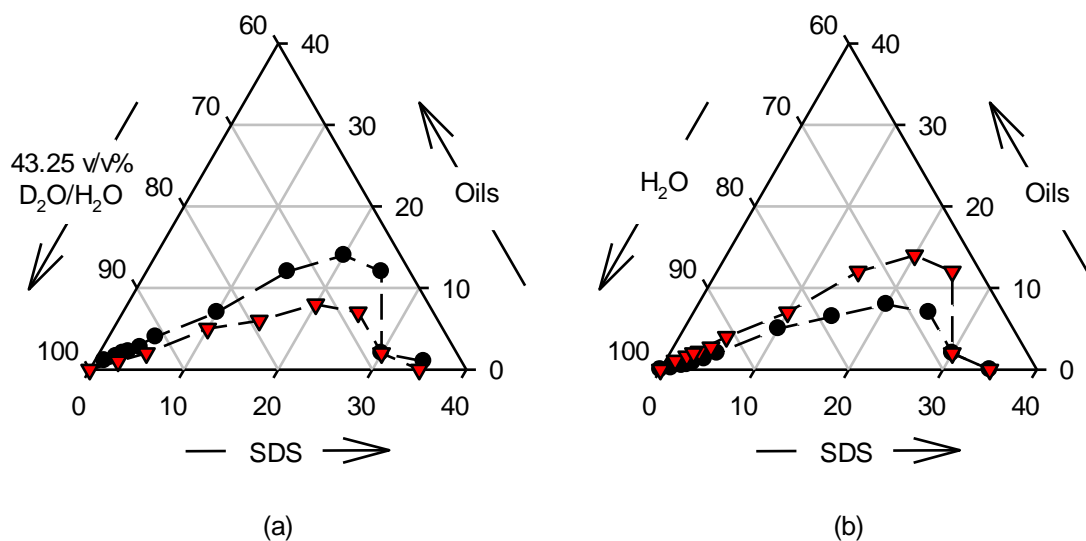
Figure 3.13 Partial phase diagrams for the oil-in-water microemulsions stabilised with SDS and containing either ethyl butyrate (EB) (-- ▼ --) or ethyl caprylate (EC) (--●--) and made in (a) 43.25 v/v% D_2O/H_2O and (b) H_2O at 25.0 ± 0.1 °C. On the abscissa, the surfactant concentration (in w/w%) increases from left to right, while on the ordinate, the oil concentration (in w/w%) increases from bottom to top, and the water concentration (in w/w%) increases from top to bottom.

In addition, microemulsions of composition S20B14 and S20C08 but diluted 5 times (i.e. S20B14/5 and S20C08/5) were also prepared using 43.25 v/v% D_2O/H_2O as solvent instead of H_2O and showed that the use of 43.25 v/v% D_2O/H_2O as solvent did not affect the physical properties on these diluted SDS-stabilised microemulsions. These preliminary studies confirm that it is possible to use 43.25 v/v% D_2O/H_2O as solvent when preparing SDS microemulsions for performing SANS experiments.

3.3 Preparation of nanosuspension

3.3.1 Formulation of griseofulvin nanoparticles by photon correlation spectroscopy studies

In order to make the desired NSNE and NSME it was necessary to prepare nanoparticles from the poorly-water soluble drug, griseofulvin (GF) using wet bead milling technique. A previous study by Goodwin (2006) confirmed that griseofulvin nanoparticles (GF-NPs) could be formed using SDS as stabiliser. Tirop (2012) also studied SDS-stabilised GF-NPs and confirmed that even though GF is a neutral drug, possessing no formally

charged groups, it can be only stabilised as nanoparticles using either anionic polymer or surfactant such as SDS. SDS which is a monoalkyl chain surfactant possesses a negatively charged sulphate head group. The hydrophilic-lipophilic balance (HLB) of SDS is 40, which means that it is very hydrophilic surfactant, indeed SDS dissolves rapidly in water to form micelles at a concentration of 2.365 g/L or 0.24 w/w% (Luckey, 2014).

When preparing GF-NPs, the variation in particle size is one factor that helps understand the stability of the system. In this study, dynamic light scattering was used to determine the particle size of the GF-NPs prepared using the wet bead milling technique. First of all, the variation in the particle size of the GF-NPs at hourly intervals during their production was determined in order to establish the milling time required for production of GF particles in a nano-size range for each concentration of SDS between 0.25 -10 w/w%. Figure 3.14 shows that the particle size of the GF-NPs stabilised by 0.25 -2 w/w% of SDS was below 500 nm after 4 hours milling and remained the same until, at least, 6 hours (longer time points not tested) while the particle size of the GF-NPs stabilised by 10 w/w% of SDS was below 500 nm after milling for 5 hours. As a consequence, a 6 h milling time was chosen for GF-NP production with every SDS concentration tested.
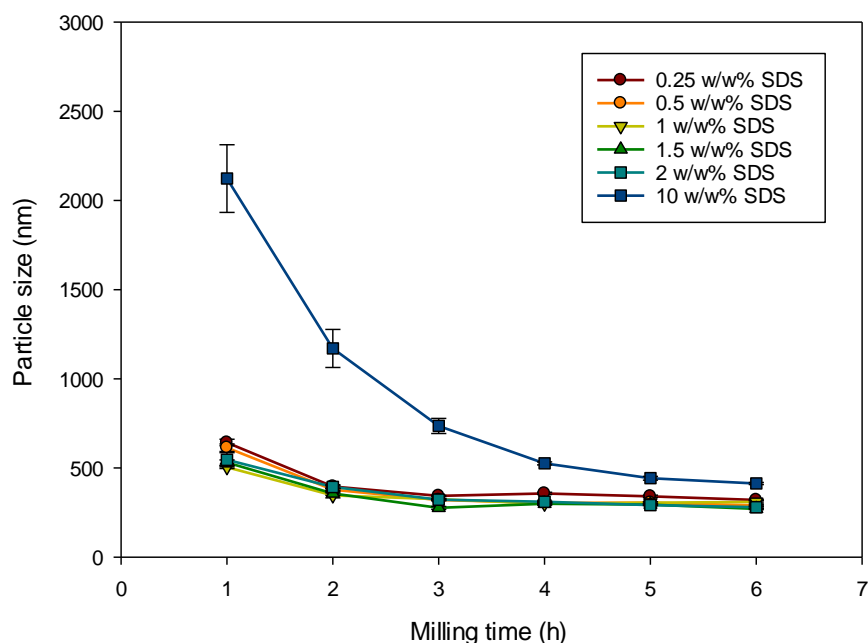
Figure 3.14 Particle size of griseofulvin nanoparticles with various concentration of sodium dodecyl sulphate (SDS) between 0.25 -10 w/w% over milling time at 25.0 ± 0.1 °C (mean ± SD, n = 9).

3.3.2 Effect of SDS concentration on the particle size and zeta potential of griseofulvin nanoparticles after milling

In order to understand the effect of SDS concentration on the production of GF-NPs, the particle size and zeta potential of the GF-NPs prepared using different concentrations of SDS were determined. Table 3.7 shows the particle size, polydispersity and zeta potential of GF-NPs prepared with various concentrations of SDS, i.e. between 0.25-10 w/w% SDS, after milling for 6 hours. The results show in Table 3.7 indicate that after milling for 6 hours, GF-NPs of particle size ~ 320 nm, could be produced using a SDS concentration of 0.25 w/w%. Increasing the SDS concentration in the range 0.5 to 1.5 w/w% resulted in a decrease of particle size from ~ 297 to 270 nm. Any further an increase of SDS concentration lead to an increase in the particle size of nanoparticle to ~ 422 nm, showing a decreased efficiency of milling at the higher surfactant concentrations, probably due to the need for higher specific energy consumption (Kwade, 1999). Tirop (2012) similarly investigated the preparation of GF-NPs using concentrations of SDS ranging from 0.1 to 10 w/w% and found that a SDS concentration of 1.5 w/w% produced the smallest GF-NPs, suggesting this was the optimum SDS concentration.

The stability of the nanosuspensions was assessed after they were centrifuged and the excess stabiliser removed and replaced with an equal volume of 'fresh' water. Significantly, after removal of excess surfactant all the GF-NPs remained in the nano-size range, especially those nanoparticles prepared using 1.5 w/w% SDS in which case the NPs exhibited a size of ~ 342 nm, despite the fact that the apparent hydrodynamic size of the NPs after centrifugation tended to increase slightly, as seen in Table 3.7. In addition, the polydispersity of the GF-NPs was unchanged remaining below 0.2, with the exception of the GF-NPs prepared using 10 w/w% SDS after centrifugation to remove the excess SDS. Tirop (2012) confirmed that the particle size of the GF-NPs stabilised by between 0.5 - 2 w/w% of SDS after milling for 6 hours remained the nano-size range after 1 year storage. Furthermore, the zeta potential of GF-NPs after milling 6 hours increased from -23.9 to -34.8 mV upon increasing SDS concentration from 0.25 - 10 w/w%. However, the zeta potential of GF-NPs stabilised by between 0.5 - 1.5 w/w% SDS after removing the excess SDS by centrifugation exhibited no significant change from the zeta potential of the GF-NPs before centrifugation. In addition, the zeta

potential of GF-NPs stabilised by 2 and 10 w/w% SDS changed from -30.0 to -27.7 mV and -34.8 to -27.1 mV, respectively. It is possible that the concentration of SDS at 2 and 10 w/w% was more than enough to coat on the GF-NPs while 0.25 w/w% of SDS was insufficient to produce GF-NPs. Furthermore, electrostatically-stabilised particles of zeta potential of +/- 30 mV are normally regarded as physically stability, while a value of +/- 20 mV is usually at 20 mV considered adequate for stabilisation (Jacobs et al., 2002; Müller et al., 2002). As a consequence, the GF-NPs stabilised by 1.5% w/w of SDS were considered physically stable enough for use as a novel delivery system.

Table 3.7 The apparent hydrodynamic size, polydispersity and zeta potential of griseofulvin nanoparticles prepared with varying concentrations of sodium dodecyl sulphate after 6 hours milling and after centrifugation to remove any excess sodium dodecyl sulphate at 25.0 ± 0.1 °C.

Sample	Particle size (mean ± SD, n = 9)	Polydispersity (mean ± SD, n = 9)	Zeta potential (mean ± SD, n = 9)
After milling 6 hours			
0.25 w/w% SDS	320.3 ± 8.3	0.122 ± 0.040	-23.9 ± 0.7
0.5 w/w% SDS	296.8 ± 6.8	0.081 ± 0.027	-27.2 ± 0.8
1 w/w% SDS	275.7 ± 3.7	0.085 ± 0.029	-28.0 ± 0.7
1.5 w/w% SDS	270.3 ± 3.8	0.142 ± 0.023	-29.2 ± 0.4
2 w/w% SDS	301.0 ± 4.1	0.055 ± 0.017	-30.0 ± 0.8
10 w/w% SDS	422.2 ± 9.0	0.165 ± 0.030	-34.8 ± 0.5
After centrifugation			
0.25 w/w% SDS	361.4 ± 13.3	0.169 ± 0.040	-23.5 ± 0.9
0.5 w/w% SDS	359.2 ± 4.6	0.151 ± 0.026	-26.7 ± 0.8
1 w/w% SDS	353.4 ± 7.0	0.162 ± 0.027	-27.5 ± 0.6
1.5 w/w% SDS	342.3 ± 6.8	0.079 ± 0.023	-28.5 ± 0.7
2 w/w% SDS	352.2 ± 8.7	0.125 ± 0.028	-27.7 ± 0.4
10 w/w% SDS	476.3 ± 46.9	0.281 ± 0.128	-27.1 ± 0.3

3.3.3 Solubility of GF nanoparticles

In order to determine the most suitable SDS concentration for GF-NP production, the solubility of griseofulvin in the supernatant obtained after centrifuging to remove the excess SDS was compared to the solubility of powdered GF in water. The solubility of GF in water was determined by adding powdered GF into water. It can be seen that the solubility of powdered GF reached its equilibrium value of 0.006 w/v% by 6 h (Figure 3.15). The aqueous solubility of GF in form of the GF-NPs was studied by measuring the solubility of GF in the supernatant after centrifugation by mixing 0.24 mL of the GF-NPs stabilised with various concentration of SDS with 0.76 mL of H_2O.

The solubility of GF in the supernatant after centrifugation of the GF-NP stabilised by 0.25 - 2 w/w% of SDS with water for 6 hours was similar to the solubility of powdered GF in water. This result suggests that most of the GF used to prepare the nanoparticles stabilised by 0.25-2 w/w% of SDS was in the form of NPs. In addition, these results suggest that there is no excess of SDS detected in the supernatant after removing by centrifugation because the solubility of GF in supernatant was similar to the solubility of GF in a form of powder in water, as shown in Figure 3.15.

This scenario did not happen with the GF-NPs stabilised by 10 w/w% of SDS as the solubility of GF in supernatant after mixing GF-NPs stabilised by 10 w/w% with water for 6 hours was more three times than the solubility of GF in a form of powder in water. It suggests that there were some free molecules of SDS left in a supernatant causing the formation of SDS micelles, leading to an increase in GF solubility. However, as can be seen in Figure 3.15, the solubility of GF in supernatant after centrifugation by mixing the GF-NPs stabilised by 0.5-1.5 w/w% with water did not significantly change from 6 to 96 h (p > 0.05) while in contrast, the solubility of GF in supernatant after centrifugation by mixing the GF-NPs stabilised by 0.25, 2 and 10 w/w% with water increased over the 96 h time period tested. Furthermore, it was clear that the stability of the GF-NPs stabilised by 0.25, 2 and 10 w/w% was not as high as the GF-NPs stabilised by 0.5-1.5 w/w%, which may be a consequence of the GF-NPs being prepared with too little or too much stabiliser. Furthermore, Ostwald ripening is known to occur in suspensions, including nanosuspensions, where the disperse phase has some degree of solubility in the continuous phase and is polydispersity systems, where the smaller particles dissolve and re-crystallize on the larger particles (Verma et al., 2011). Ostwald

ripening occur over time and frequently at increased temperature (Tirop, 2012). In the case of the GF-NPs stabilised with the low concentrations of SDS, it can be seen that the solubility of GF in supernatant after centrifuging increased from 6 h to 96 h compared to the solubility of powdered GF in water. Consequently, this increased solubility of GF may possibly be due to the presence of insufficient stabiliser leading to Ostwald ripening. Combining this information, with the physical stability of the GF-NPs stabilised with various concentrations of SDS shown in Table 3.7, it appears that the most suitable concentration of SDS for preparation of the GF-NPs was 1.5 w/w%, so all subsequent GF-NPs were prepared using 1.5 w/w% SDS.
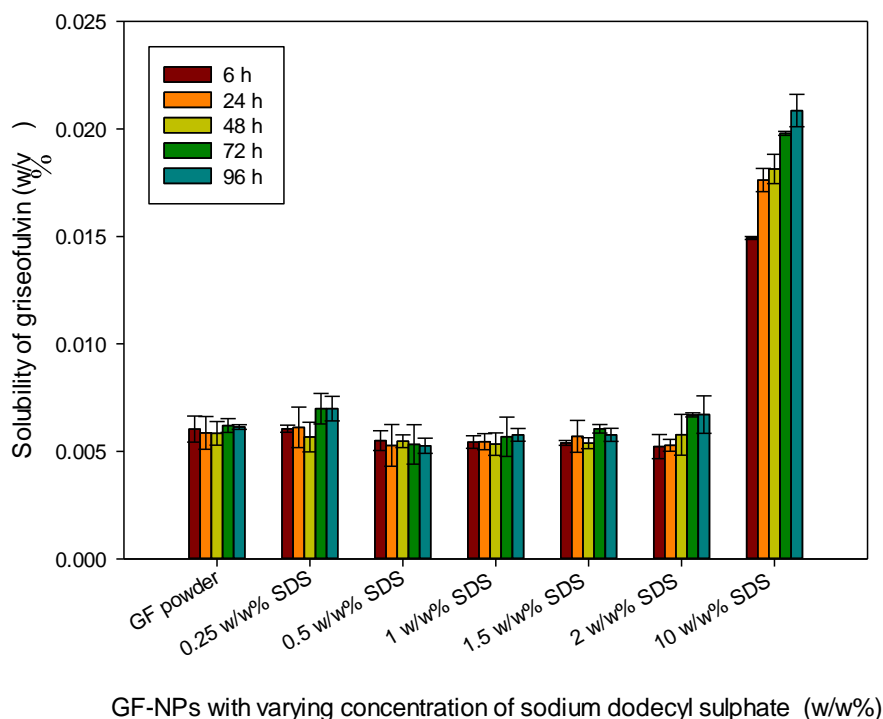
Figure 3.15 Aqueous solubility of griseofulvin in the form of powder and in supernatant after centrifugation of nanoparticles stabilised by 0.25 – 10 w/w% of SDS mixed with water over time at 25.0 ± 0.1 °C (mean ± SD, n = 9).

3.4 Chapter summary

Knowledge of the solubility of GF in supernatant after separation of the diluted-1.5 wt% SDS stabilised GF-NPs is a key to understanding the behaviour of the NSNEs and the NSMEs. For example, if GF solubility in the supernatant was seen to increase by mixing the 1.5 wt% SDS-stabilised GF-NPs after their mixing with the nanoemulsions or microemulsions, it might be concluded that the increased GF solubility was due to a presence of either the nanoemulsion or microemulsion.

Overall, it can be concluded that the solubility of hydrophobic drug, TP, can be increased by its incorporation into either a nanoemulsion or microemulsion, depending upon the molecular volume and structure of the incorporated oil. The nanoemulsions selected for further study were prepared from 24 w/w% of Brij 97 containing either 3 or 5 w/w% of TON. The microemulsions selected for further study contained 20 w/w% of SDS and either 14 w/w% of EB or 8 w/w% of EC. Furthermore, the optimum amount of SDS stabiliser to formulate the GF-NPs was determined to be 1.5 w/w%. All formulations were prepared freshly prior to their mixing in a NSNE and a NSME. It was found the possible to prepare the nanoemulsions and microemulsions using 43.25 v/v% D_2O/H_2O as solvent without significantly affecting the physical properties of the nanoemulsions and the microemulsions as indeed it was possible to replace the water the GF-NPs were prepared in with the contrast match solvent without any detrimental properties on the NPs.

Chapter 4 Preparation of nanosusponanoemulsions

4.1 Introduction

In this chapter, the preparation of novel nanosusponanoemulsions (NSNEs) is explored. While, in theory a NSNE can be readily prepared by mixing of a nanoemulsion and a nanosuspension, to our knowledge no worked has reported doing this. The main objective of this chapter, therefore, is to determine the possibility of combining a nanoemulsion and a nanosuspension into a NSNE. Here the nanoemulsions studied were the TP-containing B24T3/10-TP and B24T5/10-TP while the nanoparticles used were composed of GF and stabilised by SDS. In order to understand the behaviour of griseofulvin nanoparticles (GF-NPs) in the presence of a saturation amount of TP in the nanoemulsions determine the likely stability/instability of the NSNEs, the physico-chemical properties of NSNE over time were determined using a range of advanced analytical techniques including photon correlation spectroscopy (PCS) and small angle neutron scattering (SANS). It was also considered necessary to understand the likely solubilisation of the GF-NPs in the TP-saturated nanoemulsions to see if this would de-stabilise the systems of interest.

4.2 Solubility of griseofulvin

4.2.1 Solubility of griseofulvin in micelles

The solubility of GF in Brij 97 micelles was determined over time at 25 $^{\circ}$C to establish the solubility of GF in the surfactant solutions (Figure 4.1). The equilibrium solubility of GF in micelles was reached within 6 h and remained constant for at least up to 96 h (longer time courses were not tested). As there was no significant difference (p > 0.05) in the solubility of GF in the Brij 97 micelles over the 6 - 96 hours recorded the solubility data was averaged. Figure 4.2 shows the average solubility of GF in Brij 97 micelles. As can be seen the variation in GF solubility was linear over a wide range of

Brij 97 concentrations, with the solubility of GF in the Brij 97 micelles ranging from 0.01 to 0.04 w/v% as surfactant concentration increases from 0.2 to 2.4 w/w%. In all cases the concentration of Brij 97 is greater than its critical micelle concentration (cmc) thereby explaining the linear increase in GF solubility with surfactant concentration (Carlota et al., 2005).
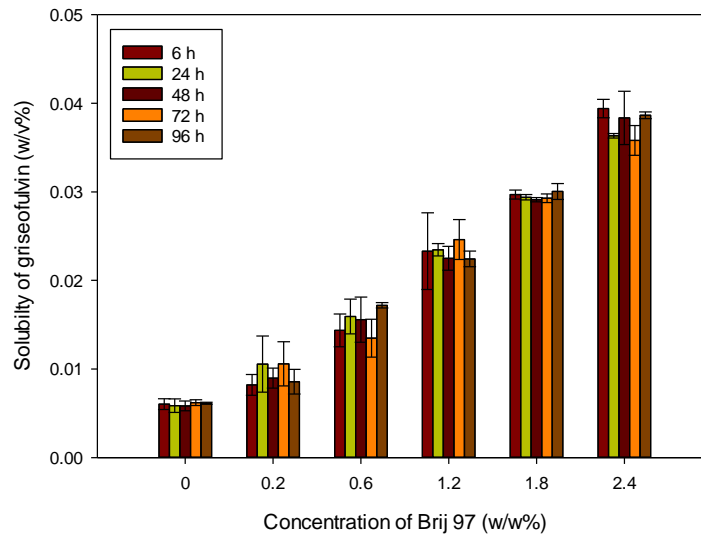
Figure 4.1 Griseofulvin solubilisation in varying concentrations of Brij 97 micelles over time at 25.0 ± 0.1 °C (mean $\pm$ SD, n = 9).
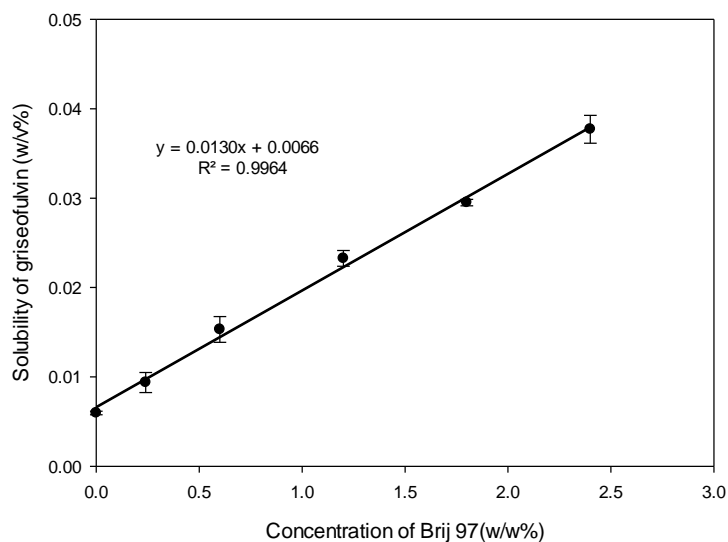
Figure 4.2 The average solubility of griseofulvin of all time points (i.e. 6, 24, 48, 72 and 96 h) in Brij 97 micelles as a function of surfactant concentration at 25.0 ± 0.1 °C (mean $\pm$ SD, n = 5).

4.2.2 Effect of griseofulvin on Brij 97-stabilised nanoemulsions incorporating testosterone propionate

In order to prepare a stable NSNE it is important to understand the behaviour of GF-NPs in the presence of TP-saturated Brij 97-nanoemulsions. In this part of the study, therefore, an excess of powdered GF was added to Brij 97-stabilised nanoemulsions, prepared in an absence and a presence of a saturation of TP. Note that the solubility of GF was investigated using the same concentration of nanoemulsions present in the NSNE, namely 0.24 ml of H_2O (the volume of GF-NPs used in the preparation of NSNE) and 0.76 mL of the ten-fold dilution of the stock nanoemulsion (i.e. B24T3/10 or B24T5/10). These further dilutions of B24T3/10 or B24T5/10 were denoted as B24T3/10/0.76 and B24T5/10/0.76. Table 4.1 shows the apparent aqueous solubility of powdered GF over time in diluted B24T3/10/0.76 or B24T5/10/0.76 nanoemulsions in both the absence and presence of a saturation amount of TP. As can be seen from Table 4.1, the solubility of powdered GF in B24T3/10/0.76 and B24T5/10/0.76 nanoemulsions was 0.04 and 0.05 w/v% at 6 h, regardless of the absence of TP. However, there was no significant effect ($p > 0.05$) on GF solubility of the oil content of the nanoemulsions at time points from 24 h to 96 h. The results showed that, with the exception of B24T5/10/0.76, there was no significant difference ($p > 0.05$) in the solubility of GF in the diluted nanoemulsions namely B24T3/10/0.76, B24T3/10-TP/0.76 and B24T5/10-TP/0.76 over the 6 h to 96 h tested. In the case of B24T5/10/0.76, there was a significant difference in GF solubility which decreased from 6 h to 24 h but thereafter remained constant up to 96 h (Table 4.1). It is worth commenting however that the decrease in GF solubility in the B24T5/10/0.76 nanoemulsions, although significant was not large. Comparing the solubility of powdered GF in the Brij 97 micelles (Figure 4.1) and nanoemulsions (Table 4.1) at the same concentration of Brij 97 (namely 1.8 w/v%), it is clear that GF was more soluble in the TON-containing nanoemulsions. In addition, Table 4.1 shows that the apparent aqueous solubility of GF in the diluted nanoemulsions was not affected by the presence of TP, at all time points measured (i.e. up to 96 h) ($p > 0.05$).

Table 4.1 Solubility of powdered griseofulvin in diluted Brij 97-stabilised nanoemulsions with and without a saturation amount of testosterone propionate at 25.0 ± 0.1 °C

Sample*	Concentration (w/v%) of griseofulvin (mean ± SD, n = 9)				
	6 h	**24 h**	**48 h**	**72 h**	**96 h**
B24T3/10/0.76	0.04 ± 0.00	0.04 ± 0.00	0.04 ± 0.00	0.04 ± 0.00	0.04 ± 0.00
B24T3/10-TP/0.76	0.04 ± 0.00	0.04 ± 0.00	0.04 ± 0.00	0.04 ± 0.00	0.04 ± 0.00
B24T5/10/0.76	0.05 ± 0.00	0.04 ± 0.00	0.04 ± 0.00	0.04 ± 0.00	0.04 ± 0.00
B24T5/10-TP/0.76	0.04 ± 0.00	0.04 ± 0.00	0.04 ± 0.01	0.04 ± 0.00	0.04 ± 0.00

*The solubility of griseofulvin was determined in supernatant after centrifugation of the NSNE, composed of 0.76 mL of nanoemulsion (namely B24T3/10, B24T3/10-TP, B24T5/10 and B24T5/10-TP) and 0.24 mL of H_2O, with and without a saturation amount of powdered griseofulvin (GF).

Table 4.2 shows the apparent aqueous solubility of TP in diluted nanoemulsions in an absence and a presence of a saturation amount of GF. Note that the compositions of the diluted nanoemulsions in Table 4.2 are the same as those in Table 4.1. In terms of the effect of a saturation amount of GF on the solubility of TP in the diluted nanoemulsions, it is clear that there is a difference in the results depending upon the amount of TON present. When the diluted nanoemulsions contain a low amount of TON, there was no significant difference in the level of TP solubility measured in the presence or absence of GF ($p > 0.05$). In contrast, in the high oil content nanoemulsions, there was a higher level of apparent TP solubility in the absence of GF than in its presence, at all time points measured (i.e. up to 96 h) with the exception of the first time point at 6 hours where the solubility was high in both the GF free and GF containing nanoemulsions.

Table 4.2 Solubility of testosterone propionate in nanoemulsions, with and without a saturation amount of griseofulvin at $25.0 \pm 0.1\ ^{\circ}\text{C}$.

Sample*	Concentration (w/v%) of testosterone propionate (mean ± SD, n = 9)				
	6 h	**24 h**	**48 h**	**72 h**	**96 h**
B24T3/10-TP/0.76 without GF	0.07 ± 0.00	0.08 ± 0.01	0.08 ± 0.00	0.06 ± 0.01	0.07 ± 0.01
B24T3/10-TP/0.76 with GF	0.08 ± 0.00	0.07 ± 0.00	0.08 ± 0.00	0.08 ± 0.00	0.08 ± 0.00
B24T5/10-TP/0.76 without GF	0.09 ± 0.01	0.09 ± 0.01	0.09 ± 0.01	0.08 ± 0.01	0.09 ± 0.01
B24T5/10-TP/0.76 with GF	0.09 ± 0.00	0.08 ± 0.00	0.08 ± 0.00	0.08 ± 0.00	0.07 ± 0.00

*The solubility of testosterone propionate (TP) was determined in the supernatant of the NSNE, composed of 0.76 mL of nanoemulsion (i.e. B24T3/10-TP or B24T5/10-TP) and 0.24 mL of H_2O, with and without a saturation amount of griseofulvin (GF).

Based on these results, it is highly likely that GF and TP are solubilised in the Brij 97-stabilised nanoemulsions containing a low amount of oil in different locations so that neither impinges on the solubility of the other. In comparison, the solubility of TP in nanoemulsions containing high amounts of TON in the presence of GF was lower than in the nanoemulsions without GF, suggesting that the presence of a saturation of TP might displace GF molecules in the surfactant aggregates.

4.3 Solubility of griseofulvin and testosterone propionate in the nanoemulsions contained in the nanosusponanoemulsions

It was possible to use bench top centrifugation to separate the Brij 97-stabilised nanoemulsions from the GF-NPs due to the differences in particle size and density of the two preparations. The supernatant contains the nanoemulsion while the lower layer contains the NPs. Note that the solubility of GF and TP was investigated in the nanoemulsion supernatant of the centrifuged NSNEs to remove the GF-NPs. (The

NSNE were composed of 0.24 ml of GF-NPs and 0.76 mL of a ten-fold diluted stock nanoemulsion (i.e. B24T3/10 or B24T5/10, with and without a saturation of TP).

Figure 4.3 shows the solubility of GF in the nanoemulsion supernatant, composed of either B24T3/10 or B24T5/10 in the presence or absence of TP, after mixing with GF-NPs for differing lengths of time. The nanoemulsions were separated from the GF-NPs using bench top centrifugation. The solubility of GF in the supernatant composed of B24T3/10 and B24T5/10 after separation of the GF-NPs was seen to increase to 0.022 w/v% within 30 minutes of mixing with the GF-NPs, where after it remained constant over the whole of the 96 h of the test (p > 0.05). Note that the solubility of GF in the nanoemulsions under these experimental conditions is about half that recorded for powdered GF in the nanoemulsions (Table 4.1).

In contrast with the data shown in Table 4.1, as can be seen from Figure 4.3, there was no significant effect (p > 0.05) on GF solubility of the oil content of the nanoemulsions, as the solubility of GF in the nanoemulsion supernatants, compare the results obtained for B24T3/10 and B24T5/10. However, it is consistent with the data in Table 4.1, there was no significant effect (p > 0.05) on GF solubilisation of the presence of a saturation amount of TP, compared B24T3/10 and B24T3/10-TP, and B24T5/10 and B24T5/10-TP.
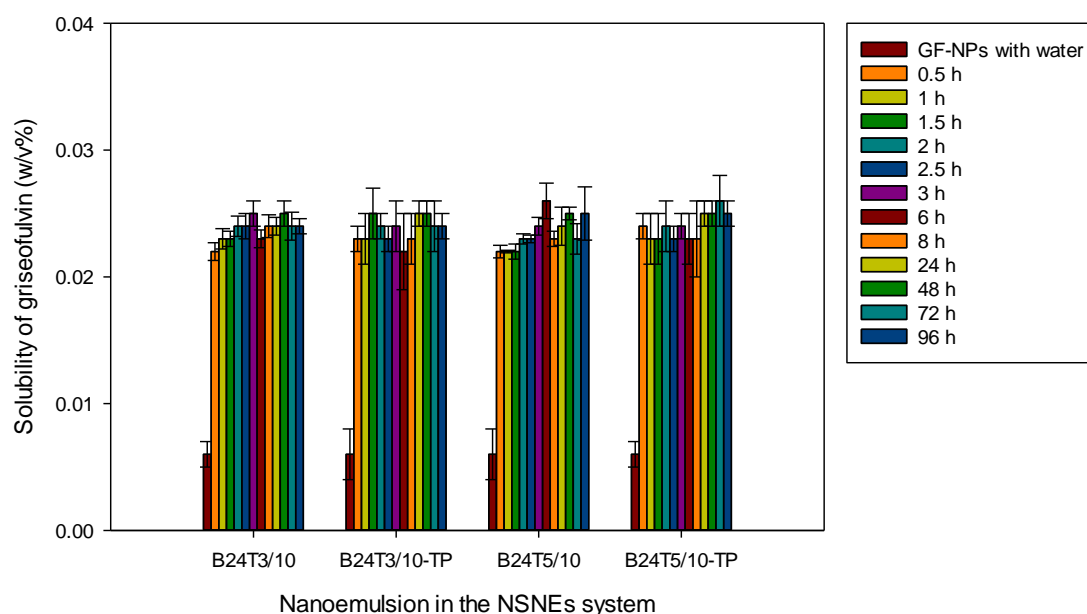
Figure 4.3 Solubility of griseofulvin in nanoemulsion supernatant in the form of NSNEs after separation from the GF-NPs for differing lengths of time at 25.0 ± 0.1 °C (mean ± SD, n = 9).

Figure 4.4 shows the solubility of TP in the supernatant of the B24T3/10 and B24T5/10 containing NSNEs after being mixing for differing lengths of time up to 4 days. The solubility of TP in the diluted nanoemulsions namely B24T3/10/0.76 and B24T5/10/0.76 before mixing with the GF-NPs was 0.08 and 0.09 w/v%, respectively (Table 4.2). As can be seen in Figure 4.4, the solubility of TP in supernatant of the B24T3/10 containing NSNEs remained constant throughout the whole 96 h of the test. In contrast, however, the solubility of TP in the supernatant of the B24T5/10 containing NSNEs almost halved over time of mixing with the GF-NPs, going from 0.09 to 0.05 w/v% over the 96 h of the test. This result may be a consequence of the instability of the parent B24T5 nanoemulsions and suggests that the presence of the GF-NPs may have increased the rate of nanoemulsion destabilisation.
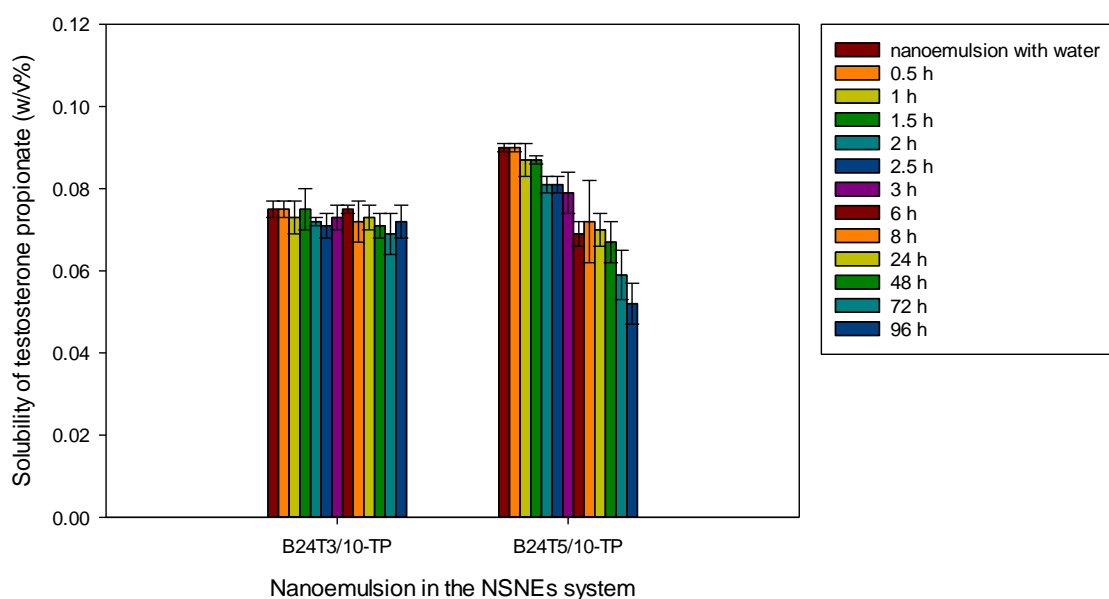
Figure 4.4 Solubility of testosterone propionate in nanoemulsion supernatant in the form of NSNEs after separation from the GF-NPs for differing lengths of time at 25.0 ± 0.1 °C (mean $\pm$ SD, n = 9).

In summary, the solubility of GF in the nanoemulsion supernatant of the centrifuged NSNE did not alter as a function of oil content or the presence of a saturation amount of TP. In contrast, while the solubility of TP in the supernatant of NSNE containing low amount of TON remained the same as in the starting diluted nanoemulsion, namely B24T3/10-TP/0.76, the solubility of TP in the supernatant of NSNE containing the

higher amount of TON, decreased over the 96 h contact time to about half the value of the original B24T5/10-TP/0.76 nanoemulsions. As a consequence, in nanoemulsions at low TON concentrations, it is highly likely that GF and TP are solubilised in different locations in the nanoemulsions, while the addition of more TON seems to perturb the solubilisation of TP and GF in the system enhancing its destabilisation.

4.4 Size characterization of the nanoemulsions and griseofulvin nanoparticles in the nanosusponanoemulsions

Visual observation of the NSNEs showed the clear separation of the nanoemulsions from the nanosuspension when left to stand undisturbed for periods of greater than an hour. However, the system was readily reformed after gently shaking the container in which the formulation was contained. It is possible that the separation of the NSNE preparation into its constituent parts is the result of the difference in the size distribution of the nanoemulsions and nanoparticles coupled with the difference in the density of the nanoemulsion and nanoparticles. This is in contrast to the physical instability reported for suspoemulsions (i.e. systems comprising of an emulsion and suspension) where small droplets were observed on the top of the system (Santos et al., 2013). As a result of the knowledge of the component formulations, the top layer of the NSNEs was deemed to be the nanoemulsion while the bottom layer was considered to be the GF-NPs. Investigating this phase separation using centrifugation to speed up the process revealed that there was no separation of oil on the top of nanoemulsion.

Figure 4.5 shows the particle size stability (measured as apparent hydrodynamic size) over time of GF-NPs in a form of a NSNE, along with, for comparative purposes, the corresponding particle size of the GF-NPs before mixing with the nanoemulsions. The results in Figure 4.5 show a large increase in the particle size of GF-NPs when in the form of a NSNE, regardless of the composition of the nanoemulsion with which they are mixed. Note that preliminary experiments indicated that it was not possible to prepare GF-NPs using Brij 97 as stabiliser.
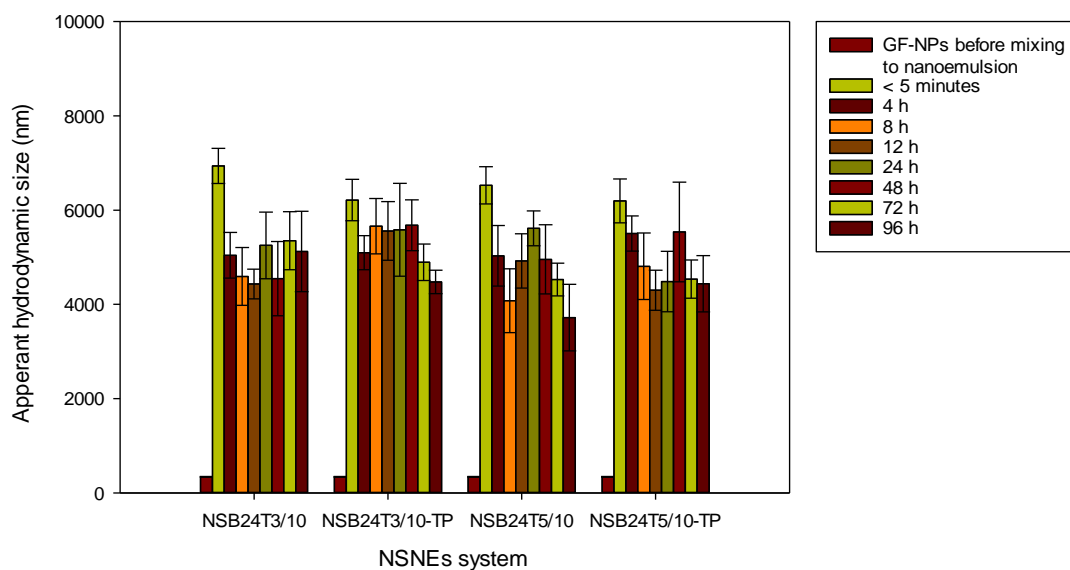
Figure 4.5 Particle size (as assessed by PCS) over time of griseofulvin nanoparticles (GF-NPs) when in a form of the NSNEs at 25.0 ± 0.1 °C (mean ± SD, n = 9).

These results suggest an interaction between Brij 97 and SDS resulting in either the desorption or thinning of the SDS layer of the electrostatically stabilised, GF nanoparticles and/or the incorporation of SDS molecules into the Brij 97 stabilised nanoemulsion droplets. Ruiz et al. (2000) reported that both chain-chain and head group-head group interactions may occur in a mixed micelle system. In this context it is interesting to note that in the case of the use of mixtures of ionic and nonionic surfactants to stabilise nanoparticles, nonionic surfactants which do not adsorb on their own may, in fact, co-adsorb in the presence of the other ionic surfactant. For example, it has been reported that the anionic surfactant, sodium p-octylbenzene sulfonate readily adsorbs on alumina, whilst the nonionic octaoxyethylene dedecyl ether does not. However, mixing the nonionic surfactant with the anionic sulfonate surfactant induced significant co-adsorption of the nonionic surfactant onto the alumina surface. This synergistic adsorption is attributed to the hydrophobic interaction between the anionic and the nonionic surfactants at the alumina-water interface as well as a reduction in the electrostatic repulsion between the anionic head groups mediated by the presence of nonionic surfactant (Somasundaran et al., 1992). In addition, the length of the hydrocarbon chain of the surfactant has been found to play an important role in the enhanced adsorption of mixtures of the anionic surfactant, SDS and the nonionic surfactant, polyoxyethylene alkyl ethers namely octaoxyethylene dedecyl ether on kaolin (Xu et al., 1991; Zhang et al., 2006). For example, the adsorption isotherm of

SDS was found to remain unchanged if the hydrocarbon chain length of the polyoxyethylene alkyl ethers was equal to or longer than that of the anionic surfactant, namely C12 (Zhang et al., 2006). Furthermore, the stronger chain-chain interactions observed between the C18:1 chain of Brij 97 and the C12 chain in SDS compared to the C12 chains of Brij 35 ($C_{12}EO_{23}$) and SDS, was attributed by Glenn et al. (2005) to the presence of dissimilar alkyl chain lengths in the former case. In addition to these hydrophobic chain interactions, there may be some sharing of some water molecules by different head groups and, as a consequence some of the water molecules may act as a 'bridge' between the different types of surfactant molecules (Glenn et al., 2005).

The NSNEs were expected to contain two populations of particles, namely nanoemulsion particles in the size range of ~ 10 - 25 nm, and GF-NPs of particle size ~ 350 nm. However, while it is possible to measure particle size *in situ* using PCS, it is difficult to confirm whether the particle size of the constituent particles, and in particular the nanoemulsions because of their very small particle size and volume, have changed. As a consequence, centrifugation was used to separate the nanoemulsion from GF-NPs and the particle size of the nanoemulsions and the re-suspended GF-NPs individually determined using PCS (Figures 4.6 and 4.7). Figure 4.6 shows the particle size of nanoemulsions (namely B24T3/10, B24T3/10-TP, B24T5/10 and B24T5/10-TP) before and after mixing with the GF-NPs for up to 96 h. The particle size of the nanoemulsions, namely B24T3/10, B24T3/10-TP, B24T5/10 and B24T5/10-TP, prior to mixing with the GF-NPs, were 11.4, 11.9, 13.8 and 22.5 nm, respectively. The particle size of 3 of the nanoemulsion types (namely B24T3/10, B24T3/10-TP, B24T5/10) indicated no change after mixing with GF-NPs for up to 96 h (longer time courses were not tested). Although in contrast, the particle size of the B24T5/10-TP nanoemulsions decreased significantly from 22.5 prior to mixing to 13.2 nm after minutes mixing with the GF-NPs, and thereafter fluctuated ~ 12 nm over the remaining 96 h. Infact, the only instability observed in nanoemulsions in contact with NSNE was observed in the nanoemulsions containing a high amount of TON and a saturation amount of TP.
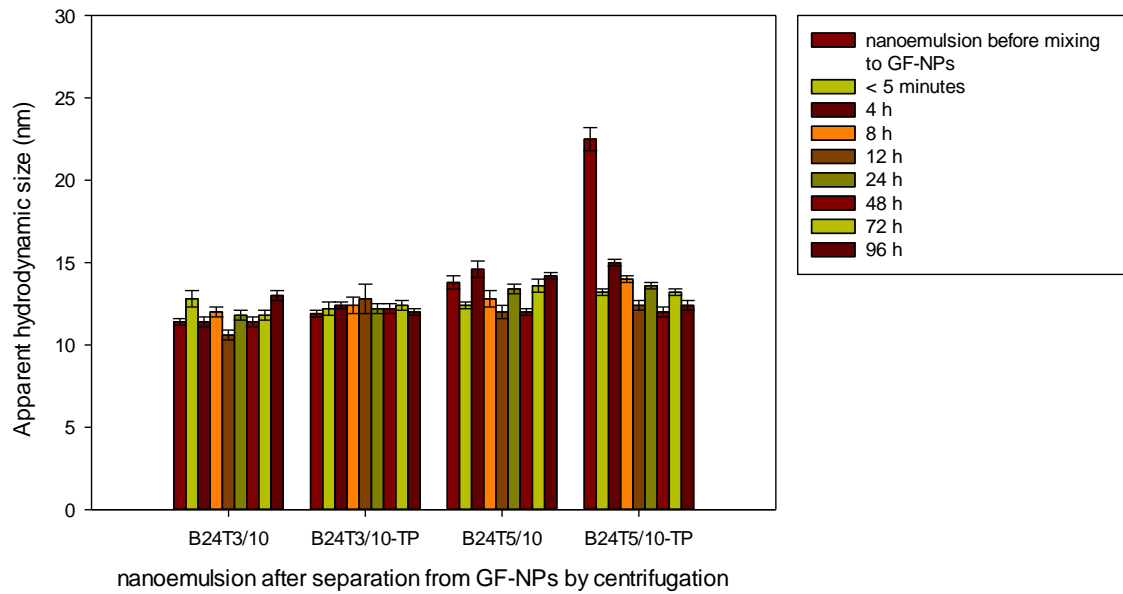
Figure 4.6 Particle size over time of the nanoemulsion after separation from the griseofulvin nanoparticles (GF-NPs) by centrifugation at 25.0 ± 0.1 °C (mean $\pm$ SD, n = 9).

Figure 4.7 shows particle size of the GF-NPs before and after mixing with nanoemulsions, namely B24T3/10, B24T3/10-TP, B24T5/10 and B24T5/10-TP, for up to 96 h. The particle size of GF-NPs before mixing with the various nanoemulsions was 342.3 nm. However, after mixing with the various nanoemulsions, their particle size increased to more than 2 microns.
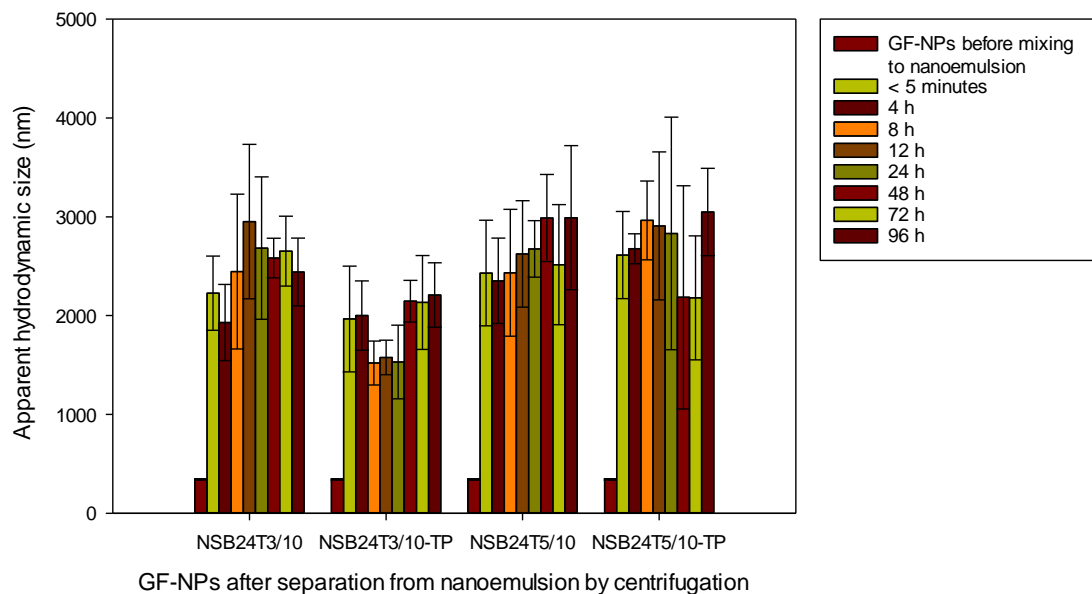
Figure 4.7 The particle size variation of griseofulvin nanoparticles (GF-NPs) after separation from the nanoemulsions at 25.0 ± 0.1 °C (mean $\pm$ SD, n = 9).

147

4.5 Determination of the hydration value of nanoemulsions

The intrinsic viscosity of a colloidal solution is a function of the size and shape of the particles present in the solution as well as any solute-solvent interactions present. Indeed the viscosity of a colloidal solution is very sensitive to any changes in the nature of the colloidal aggregates present. A value of the intrinsic viscosity of 2.5 mL/g, which was predicted by Einstein's equation, means the colloidal particles are spherical and un-solvated. Consequently, the intrinsic viscosity of a surfactant solution increases with an increase in surfactant concentration, due to either a change in the shape of the aggregates and/or an increase in the number of surfactant aggregates. For example, if there is an increase in the intrinsic viscosity of a colloidal solution and it was not due to a change in the shape of the aggregate, then the increase of intrinsic viscosity in likely to be a consequence of an increase in the number of aggregates present. Indeed Nagarajan et al. (1982) demonstrated that it is possible to understand a sphere-to-rod transition in micellar solutions by taking advantage of the use of viscometric techniques. The variation in the relative viscosity (η_{rel}) expressed as In η_{rel}/c, and specific viscosity (η_{sp}) expressed as η_{sp} /c, of Brij 97 micelles and nanoemulsions as a function of total surfactant concentration is shown in Figures 4.8 and 4.9, respectively.
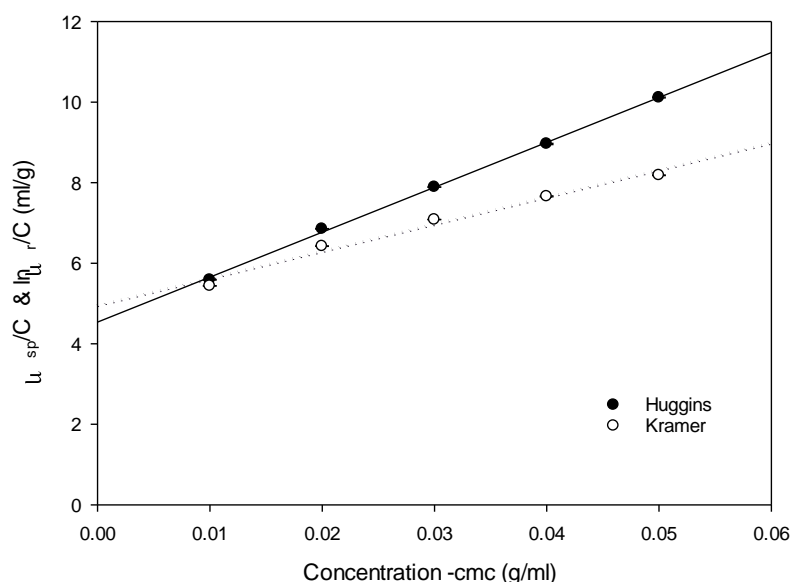
Figure 4.8 Variation in the intrinsic viscosity of Brij 97 micellar solutions as a function of concentration at 25.0 ± 0.1 °C (mean $\pm$ SD, n = 9).
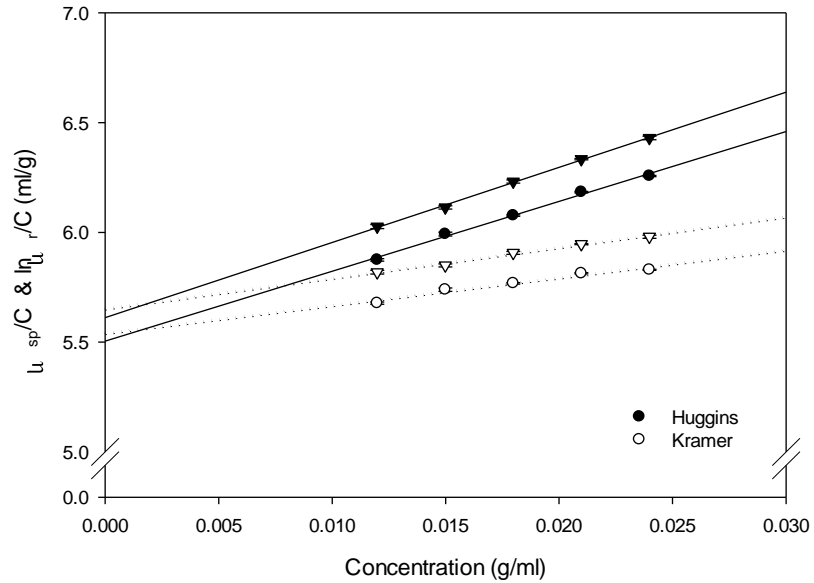
Figure 4.9 Variation in the intrinsic viscosity of Brij 97 nanoemulsions as a function of oil concentration at 25.0 ± 0.1 °C (●:B24T3/10, ▼:B24T5/10) (mean $\pm$ SD, n = 9).

The variation in the relative viscosity (η_{rel}) expressed as In η_{rel}/c, and specific viscosity (η_{sp}) expressed as η_{sp}/c, of B24T3/10 and B24T5/10 nanoemulsions in an absence and presence of a saturation amount of TP are presented in Figures 4.10 and 4.11, respectively. As can be seen that the variation results in both η_{rel} and η_{sp} of micellar solutions and nanoemulsions, the values of both η_{rel} and η_{sp} increased linearly with increasing of surfactant concentration, corrected by the cmc and the presence of a saturation amount of TP.
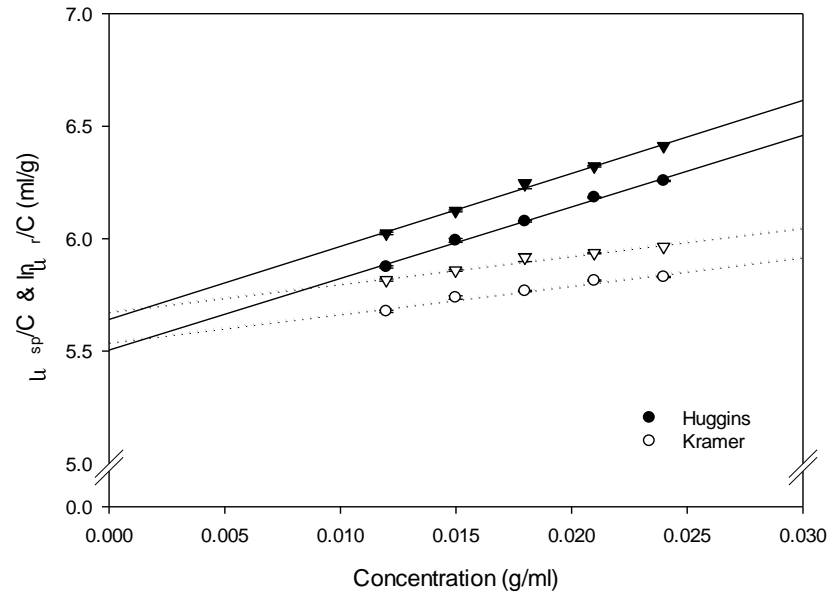
Figure 4.10 Variation of the intrinsic viscosity of Brij 97 nanoemulsions containing 0.3 w/w% of TON in an absence and presence of a saturation of TP at 25.0 ± 0.1 °C (●:B24T3/10, ▼:B24T3/10-TP) (mean ± SD, n = 9).
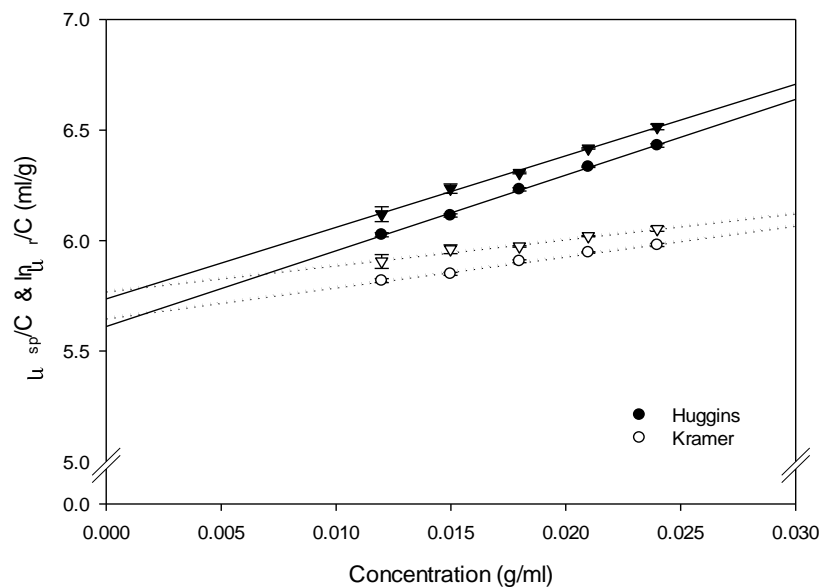
Figure 4.11 Variation of the intrinsic viscosity of Brij 97 nanoemulsions containing 0.5 w/w% of TON in an absence and presence of a saturation of TP at 25.0 ± 0.1 °C (●:B24T5/10, ▼:B24T5/10-TP) (mean ± SD, n = 9).

The intrinsic viscosity of Brij 97 micelles and nanoemulsions containing different amounts of TON, calculated from the average of the intercept of the Huggins and

Kraemers plots, is shown in Table 4.3. The effect of TON concentration and a presence of a saturation of TP on the intrinsic viscosity are shown in the extrapolation of the Huggins and Kraemers plots to zero surfactant concentration. As can be seen, the intrinsic viscosity increased with increasing oil content, suggesting that the presence of an increased amount of oil leads to an increased interaction with the surfactant molecules. Furthermore, the increased intrinsic viscosity obtained for the B24T3/10-TP and B24T5/10-TP nanoemulsions compared to the corresponding nanoemulsions, namely B24T3/10 and B24T5/10, suggests that either the shape of the aggregates have changed and/or an increase in the number of surfactant aggregates.

Table 4.3 The intrinsic viscosity of the Brij 97 micelles and Brij 97-stabilised nanoemulsions containing different amounts of TON with and without a saturated amount of TP at 25.0 ± 0.1 °C.

Sample	Intrinsic viscosity (ml/g) (mean ± SD, n = 9)
Brij 97 micelle	4.74 ± 0.29
B24T3/10	5.52 ± 0.02
B24T3/10-TP	5.64 ± 0.02
B24T5/10	5.63 ± 0.03
B24T5/10-TP	5.75 ± 0.02

In order to support the fitting of the SANS data, the viscosity measurements were performed on the Brij 97-stabilised systems in order to determine the hydration and a percent solvation of the surfactant shell. The partial specific volume of the micelles and nanoemulsions was calculated by equation:

$$\rho = \rho_0 + (1 - \tilde{\upsilon}\rho_0)C$$

where ρ and ρ_0 is the density of the solution and solvent at the concentration, C, and $\tilde{\upsilon}$ is the partial specific volume of the micelles and nanoemulsions. The density of the micelles, nanoemulsions and solvent are given in Appendix B.

The hydration value (W_1), expressed as the g of solvent/g of solute was calculated using the intrinsic viscosity (η) and the partial specific volume as shown in the following equation:

$$[\eta] = \nu[\tilde{\upsilon} + W_1\tilde{\upsilon}_1^0]$$

where ν is the shape factor and $\tilde{\upsilon}_1^0$ is the partial specific volume of the solvent. The shape factor can be determined from the conversion of the axial ratio value which was calculated by applying the Harding's ellipsoidal table (Table 4.4)

Table 4.4 Conversion of the shape factor (v) to the axial ratio (a/b) values for oblate ellipsoid of Revolution taken (Harding et al., 1995).

a/b	shape factor (v)
1	2.5000
1.1	2.5067
1.2	2.5244
1.3	2.5503
1.4	2.5826
1.5	2.6200
1.6	2.6613
1.7	2.7060
1.8	2.7533
1.9	2.8029
2	2.8544
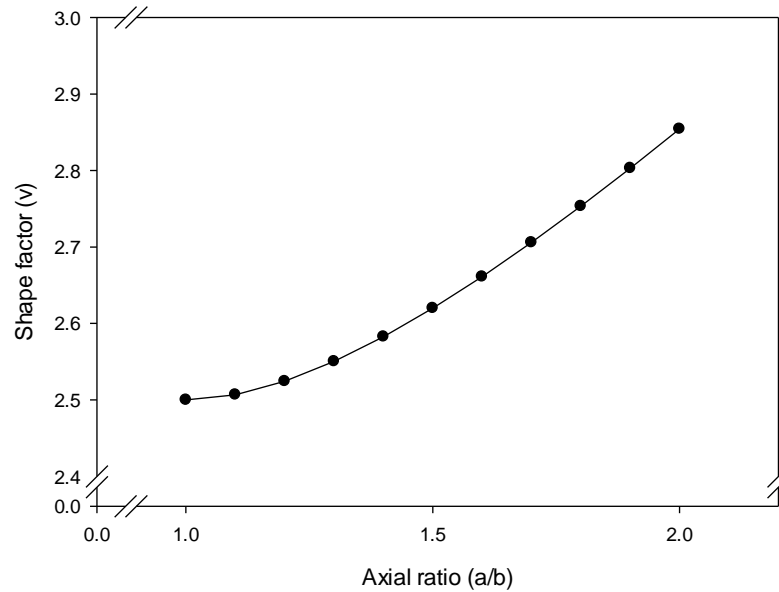
Figure 4.12 The variation in shape factor (*v*) as a function of the oblate ellipsoidal axial ratio fitted to a quadratic polynomial equation.

The percent solvent in the surfactant shell was used for fitting the SANS data and was calculated using the following equation:

$$\%solvent\ in\ shell = \frac{(no.molecule_{H_2O} \times mol\ vol_{H_2O})}{(no.molecule_{H_2O} \times mol\ vol_{H_2O}) + (mol\ vol_{\text{surfactant of 1 molecule}})} \times 100$$

where *mol vol* is the molecular volume, which has units of $\mathring{A}^3$. Note that the number of water molecules is calculated by the following equation:

$$no.molecule_{(H_2O)}\ per\ 1\ molecule\ of\ surfactant = \frac{\left(\frac{W_1}{MW_{H_2O}}\right)}{\left(\frac{1}{MW_{surfactant}}\right)}$$

where *MW* is the molecular weight (g·mol^{-1}).

It was also possible to determine the hydration of the aggregate from fitting the SANS using the droplet axial ratio obtained. In the SANS study, the shape determined for all the nanoemulsions droplets was that of oblate ellipsoids (discussed in the SANS section). During the initial fitting of the SANS data, it was established that the axial ratio of a whole drops of B24T3/10, B24T3/10-TP, B24T5/10 and B24T5/10-TP was approximately at 0.7. Table 4.5 gives the values for hydration and shell solvation for the various nanoemulsions calculated using the equations above is shown in Table 4.5. The

hydration value of the Brij 97 nanoemulsions obtained from the SANS measurements was in the range 1.2-1.3 mL/g, while the % solvent in the shell was 55-57 %. It was clear from Table 4.5 that the values for the hydration and percent of solvent in shell for the nanoemulsions containing the higher amount of TON was slightly greater than the corresponding values obtained for nanoemulsions containing the lower amount of TON, suggesting that the hydration value of the nanoemulsion increased with oil content. In addition, the values for hydration and percent of solvent in shell for nanoemulsions in the presence of the a saturation amount of TP was slightly higher than the values obtained for nanoemulsions in the absence of TP.

Table 4.5 Summary of the intrinsic viscosity and hydration value of the nanoemulsions containing different amounts of TON in the presence and absence at a saturation amount of testosterone propionate at 25.0 ± 0.1 ºC calculated by using the shape of the nanoemulsion obtained from SANS measurements.

Sample	intrinsic viscosity	partial specific volume	hydration	no molecule of water/Brij 97	%solvent in shell
B24T3/10	5.52	0.94	1.17	46.05	54.71
B24T3/10-TP	5.64	0.92	1.24	48.98	56.24
B24T5/10	5.63	0.92	1.22	48.16	55.82
B24T5/10-TP	5.75	0.92	1.27	50.05	56.77

4.6 Determination of aqueous solvent contrast match point for griseofulvin nanoparticles and nanoemulsions

The theoretical aqueous solvent contrast match point for GF was calculated from the scattering length density of GF to be 43.25:56.75 v/v% $D_2O:H_2O$. In order to confirm this, GF-NPs stabilised by 1.5 w/w% of SDS, were re-suspended in an aqueous solvent containing varying amounts D_2O ranging from 30 to 55 v/v%. The neutron scattering intensities of these samples were measured as a function of Q (Figure 4.13). The intensity of these samples at a Q value of 0 was then plotted as a function of % v/v D_2O in solvent (Figure 4.14). As can be seen the lowest scattering intensity was measured at a

concentration of 43.25 v/v% D_2O, confirming the theoretical calculation of the contrast match point of the GF-NPs.
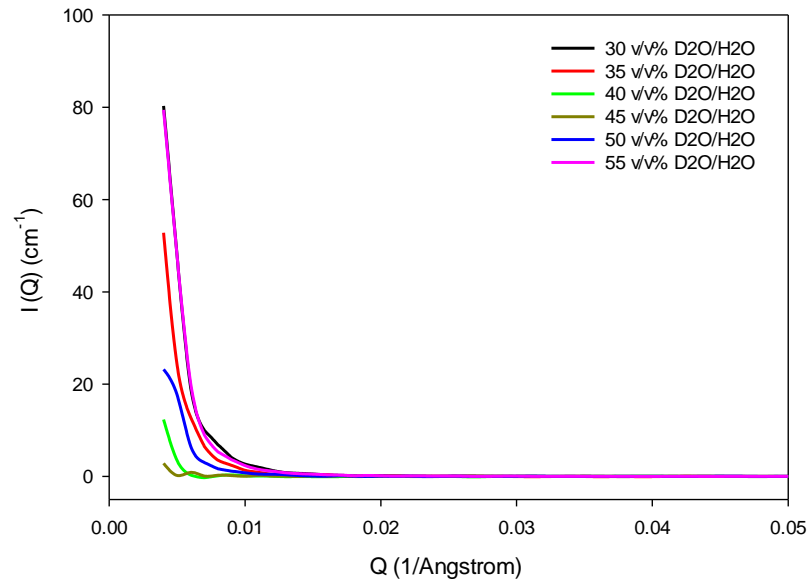
Figure 4.13 Variation in neutron scattering intensity as a function of Q for GF-NPs stabilised by 1.5 w/w% of SDS re-suspended in aqueous solvent of differing D_2O:H_2O composition. Measurements were performed on SANS2D at 25.0 ± 0.1 °C.
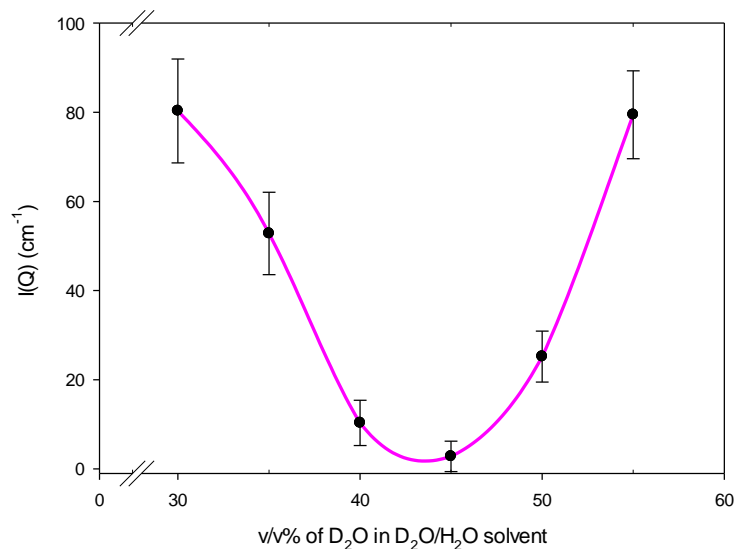
Figure 4.14 Variation in neutron scattering intensity at Q = 0 for GF-NPs stabilised by 1.5 w/w% of SDS re-suspended in aqueous solvent of differing D_2O:H_2O composition. Measurements were performed on SANS2D at 25.0 ± 0.1 °C.

In order to examine the GF-NPs *in situ* in the NSNEs, it is necessary to individually determine the contrast match solvent for Brij 97-stabilised nanoemulsions as well as the SDS-stabilised microemulsions. However, performing a SANS experiment takes several days and costs thousands of pounds per instrument day. Fortunately the theoretically calculated scattering length densities of the B24T3/10 and B24T5/10 nanoemulsions, S20B14/5 and S20C08/5 microemulsions were 0.29, 0.29, 0.30 and 0.24 $\times$ 10^{-6} Å^{-2} respectively, which are very close to each other and as a consequence, the B24T3/10 nanoemulsion was selected as an appropriate system with which to determine a suitable contrast match solvent to allow the study of GF-NPs *in situ* in the NSNEs. Therefore B24T3/10 nanoemulsions were prepared in a range of aqueous solvents of varying amount of D_2O in H_2O ranging from 0 and 25 v/v% and the variation in neutron scattering intensity measured as a function of Q (Figure 4.15). The B24T3/10 nanoemulsions re-suspended in 12 v/v% of D_2O in H_2O exhibited the lowest scattering intensity (Figure 4.16), suggesting that the nanoemulsions or microemulsions prepared in 12 v/v% of D_2O in H_2O would be invisible in a presence of GF-NPs prepared in the same solvent.
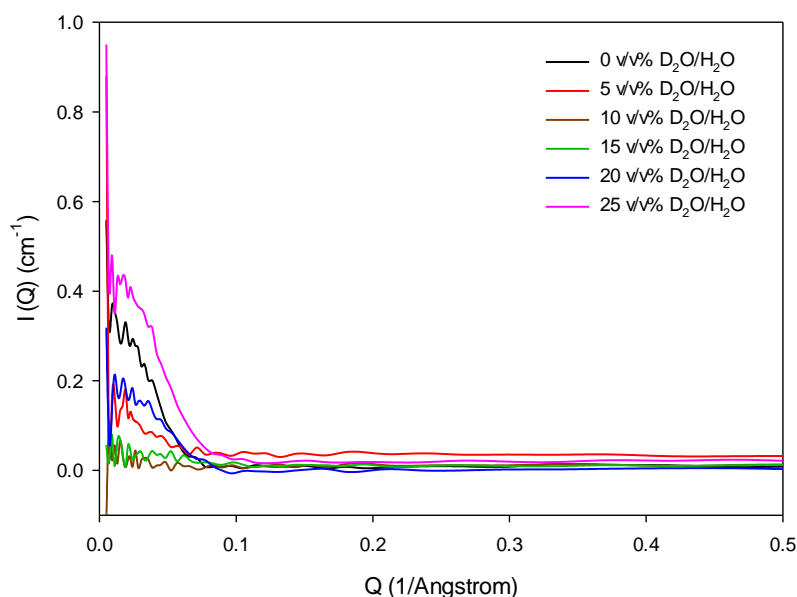
Figure 4.15 Variation in neutron scattering intensity as a function of Q for B24T3/10 nanoemulsion re-suspended in aqueous solvent of differing D_2O:H_2O composition. Measurements were performed on SANS2D at 25.0 ± 0.1 ºC.
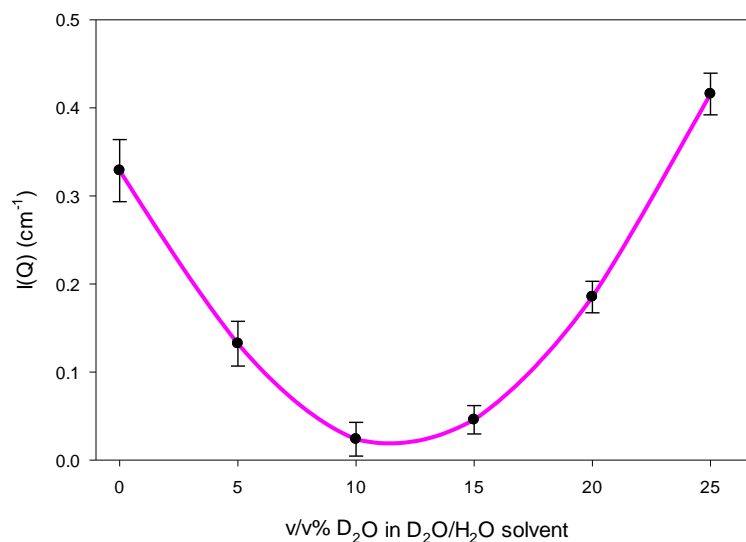
Figure 4.16 Variation in neutron scattering intensity at Q = 0 for B24T3/10 nanoemulsion in aqueous solvent of differing D_2O:H_2O composition. Measurements were performed on SANS2D at 25.0 ± 0.1 ºC.

In summary, in order to investigate the effect *in situ* in the NSNEs of GF-NPs on the nanoemulsions and microemulsions, the samples were prepared using a solvent of 43.25 v/v% of D_2O/H_2O, while in order to study the effect *in situ* in the NSNEs of the nanoemulsions and microemulsions on the GF-NPs, the samples were prepared in at 12 v/v% of D_2O/ H_2O.

4.7 Characterization of nanoemulsions and griseofulvin nanoparticles in nanosusponanoemulsions using small angle neutron scattering

4.7.1 Small angle neutron scattering studies of Brij 97 stabilised nanoemulsions using contrast match experiments

In order to find the best fit to the SANS data for the 3 contrasts, the adopted model in this study comprised of a core-shell ellipsoid with the core being composed only oil, a shell consisting of a whole surfactant molecule together with any water of hydration. The B24T3/10 nanoemulsion was selected over the B24T5/10 nanoemulsion for the SANS study to determine its size, shape and percent of solvent in shell as B24T5/10 was not a stable sample. In micellar solutions containing Brij 97 concentrations of 12 and 24 wt%, Wasutrasawat (2011) reported the presence of strong interparticle

interactions in the SANS data at a high Q value (0.06 Å^{-1}). In contrast, the SANS curves of Brij 97 micelles at lower surfactant concentrations of between 1.2 and 4.8 w/v% of Brij 97 exhibited no peak indicating the absence of strong interparticle interactions. As a consequence, in an attempt to avoid strong interparticle intereactions, the SANS measurements of the nanoemulsions were made using nanoemulsions comprising of 2.4 w/w% of Brij 97.

Originally the percent solvent in the shell of the Brij 97 nanoemulsions was assumed to be 55% from viscosity measurements. However, a previous study reported that the best fit to the SANS data of nanoemulsions containing 2.4 w/w% of Brij 97 and between 0.2 and 0.5 w/w% of TON were obtained using 20% percent of solvent in the shell (Wasutrasawat, 2011). As a consequence of these observations, the SANS datum obtained for the B24T3/10 nanoemulsions was fitted with varying a percent of solvent in shell from 20 to 55% in order to find out the most reasonable fit to the experimental data. Figures 4.17 and 4.18 show the SANS data from LoQ together with the best fits individually obtained using values of 20 and 55% for solvent in the shell for B24T3/10 nanoemulsions prepared using 3 contrasts, namely the core contrast (d-TON, h-Brij 97 and H_2O), the shell contrast (d-TON, h-Brij 97 and D_2O) and the drop contrast (h-TON, h-Brij 97 and D_2O). Table 4.6 gives the summary of the parameters used to obtain the best fits to the 3 neutron contrasts using a core-shell ellipsoid together (varying the percent of solvent in shell from 20-55%) with a hard sphere structure factor. It is reassuring that the 3 individually fitted data sets required very similar parameters. It was difficult to tell, however, which parameters gave the best fit by simple observation of the fitted data. Hence the sum of squared errors (SSE) was also used to assess the quality of the fits, in this study the lowest of SSE in the 3 contrasts studied, namely the core, shell and droplet contrasts were obtained using a value of 20 % of solvent in the shell.
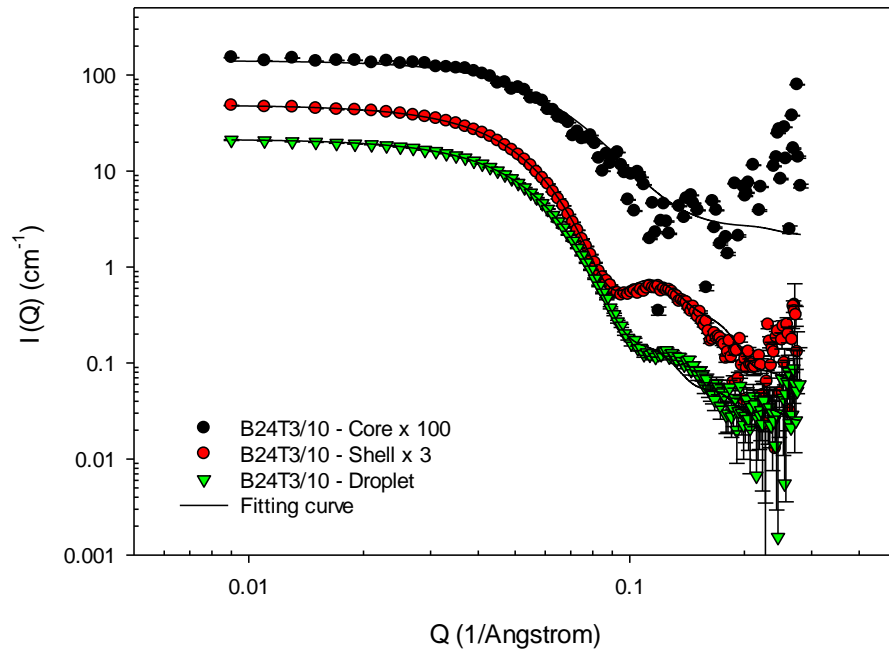
Figure 4.17 SANS data together with the individuals fit obtained for 3 contrasts, (namely the core (d-TON, h-Brij 97 and H_2O) the shell (d-TON, h-Brij 97 and D_2O), and the droplet (h-TON, h-Brij 97 and D_2O) of nanoemulsion containing 2.4 w/w% of Brij 97 and 0.3 w/w% of TON at 20 v/v% of solvent in shell. Measurements performed on LoQ at 25.0 ± 0.1 °C.
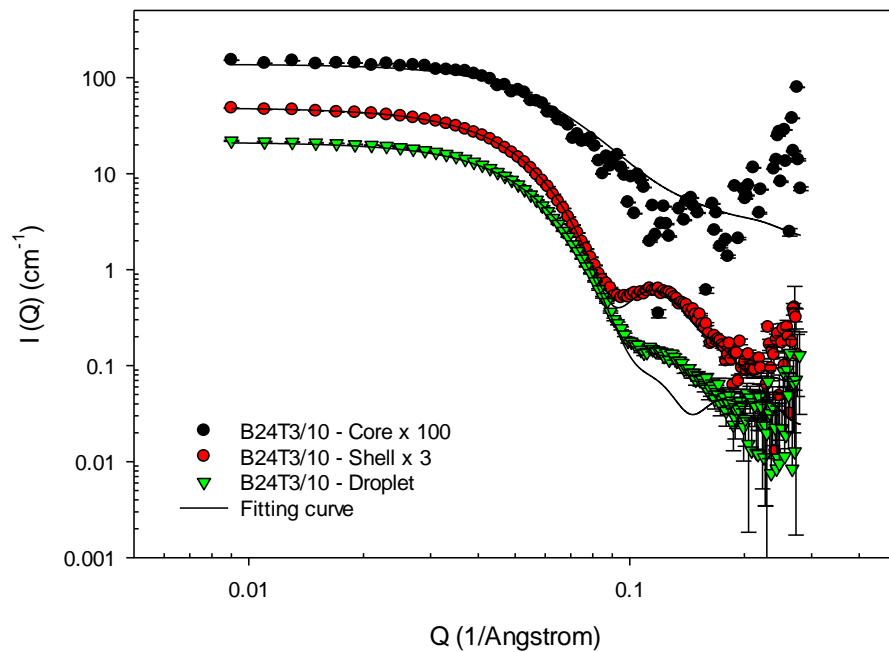
Figure 4.18 SANS data together with the individuals fit obtained for three contrasts, namely the core (d-TON, h-Brij 97 and H_2O) the shell (d-TON, h-Brij 97 and D_2O), and the droplet (h-TON, h-Brij 97 and D_2O), of nanoemulsion containing 2.4 w/w% of Brij 97 and 0.3 w/w% of TON at 55 v/v% of solvent in shell. Measurements performed on LoQ at 25.0 ± 0.1 °C.

Table 4.6 Summary of the individual fits for the core, shell and droplet contrasts of 2.4 w/w% Brij 97 nanoemulsions containing 0.3 w/w% of TON using a core-shell ellipsoid model together with a hard sphere structure factor $S(Q)$. The data was constrained using $V_{shell}(dry)/V_{core}$, with the percentage of solvent in shell from 20-55%.

A - Core contrast

solvent in shell	radius of core (Å)	core axial ratio (x)	shell thickness (Å)	sphere radius (Å)	minor radius (Å)	major radius (Å)	axial ratio (X)	N_{agg}	no oil in core	ratio of SAA: oil	no. H_2O /SAA
20%	31.1	0.4	23.6	55.2	34.6	54.7	0.6	273	51	0.19	10
25%	31.0	0.4	24.4	55.5	35.3	55.5	0.6	269	50	0.19	13
30%	30.6	0.4	25.0	55.8	35.7	55.6	0.6	258	48	0.19	16
35%	30.3	0.4	25.9	55.3	36.5	56.1	0.7	250	47	0.19	21
40%	29.8	0.4	26.5	55.4	36.9	56.4	0.7	237	44	0.19	25
45%	29.6	0.4	27.6	55.3	37.9	57.2	0.7	232	43	0.19	31
50%	28.6	0.4	28.0	56.3	37.9	56.6	0.7	208	39	0.19	38
55%	27.6	0.4	28.6	57.0	38.2	56.3	0.7	187	35	0.19	47

Note that the SSE of these samples increased from 200 to 300 after fitting with varying the percentage of solvent in shell between 20 and 55 %. Estimated uncertainly for the radius of the core, x and the sphere radius were ± 0.1, ± 0.1, ± 1.0, respectively.

B - Shell contrast

solvent in shell	radius of core (Å)	core axial ratio (x)	shell thickness (Å)	sphere radius (Å)	minor radius (Å)	major radius (Å)	axial ratio (X)	N_{agg}	no oil in core	ratio of SAA: oil	no. H_2O /SAA
20%	30.6	0.4	23.7	54.5	34.5	54.5	0.6	270	49	0.18	10
25%	30.4	0.4	24.2	54.6	34.7	54.6	0.6	258	47	0.18	13
30%	29.9	0.3	24.7	54.6	35.0	54.6	0.6	244	44	0.18	16
35%	29.3	0.3	25.2	54.6	35.3	54.5	0.7	229	42	0.18	21
40%	28.7	0.3	25.8	54.6	35.7	54.5	0.7	215	39	0.18	25
45%	28.1	0.3	26.4	54.5	36.0	54.5	0.7	200	36	0.18	31
50%	27.2	0.4	27.1	54.4	36.5	54.4	0.7	185	34	0.18	38
55%	26.3	0.4	27.9	54.0	37.2	54.2	0.7	169	31	0.18	47

Note that the SSE of these samples increased from 600 to 700 after fitting with varying the percentage of solvent in shell between 20 and 55 %. Estimated uncertainly for the radius of the core, x and the sphere radius were ± 0.1, ± 0.1, ± 1.0, respectively.

Table 4.6 Summary of the individual fits for the core, shell and droplet contrasts of 2.4 w/w% Brij 97 nanoemulsions containing 0.3 w/w% of TON using a core-shell ellipsoid model together with a hard sphere structure factor $S(Q)$. The data was constrained using $V_{shell}(dry)/V_{core}$, with the percentage of solvent in shell from 20-55%. (Continued)

C - Drop contrast

solvent in shell	radius of core (Å)	core axial ratio (x)	shell thickness (Å)	sphere radius (Å)	minor radius (Å)	major radius (Å)	axial ratio (X)	N_{agg}	no oil in core	ratio of SAA: oil	no. H_2O /SAA
20%	30.7	0.4	23.8	54.8	34.7	54.4	0.6	271	50	0.18	10
25%	30.0	0.4	24.2	54.4	35.0	54.3	0.7	257	47	0.18	13
30%	29.5	0.4	24.8	54.3	35.4	54.3	0.7	244	45	0.18	16
35%	29.2	0.4	25.3	54.5	35.6	54.5	0.7	231	42	0.18	21
40%	28.8	0.3	25.9	54.6	35.8	54.7	0.7	217	40	0.18	25
45%	28.2	0.3	26.5	54.7	36.2	54.7	0.7	203	37	0.18	31
50%	27.4	0.4	27.2	54.3	36.7	54.6	0.7	187	34	0.18	38
55%	26.4	0.4	28.0	54.7	37.4	54.4	0.7	172	31	0.18	47

Note that the SSE of these samples increased from 400 to 1800 after fitting with varying the percentage of solvent in shell between 20 and 55 %.
Note that each measurement took about 20 minutes. Consequently, the fitted parameters were obtained from the average of the scattering intensity of each sample over 20 minutes.
Note that estimated uncertainly for the radius of the core, x and the sphere radius were ± 0.1, ± 0.1, ± 1.0, respectively.

The surfactant aggregation number was obtained from the fitting of the SANS data by the dividing molecular volume of the surfactant shell after removal of the volume of water of hydration by molecular volume of one molecule of surfactant. Note that it was assumed that all the oil formed the core of the nanoemulsion. The aggregation number of the nanoemulsion decreased and a number of H_2O molecules per molecule of surfactant increased as the percent of solvation of the shell increased. The ratio of surfactant to oil molecules in the nanoemulsion was obtained by from the ratio of the mass of surfactant/surfactant molecular weight to mass of oil/oil molecular weight. For the B24T3/10 nanoemulsion, the experimental ratio of surfactant to oil molecules was 1:0.19, which means that 1 molecule surfactant solubilises 0.19 molecules of oil. After individual fitting the SANS data it was possible to calculate the ratio of surfactant to oil

molecules obtained from the SANS data as can be seen in Table 4.6, which, at a surfactant to oil ratio of 1:0.18 was reassuringly close to the experimental value.

Figures 4.17 and 4.18 show the experimentally obtained SANS profiles along with the individual fits to the core, shell and droplet contrasts of B24T3/10 nanoemulsions with 20 and 55 % solvent in shell, respectively. Significantly, however, the 3 SANS data sets (i.e. core, shell and droplet contrasts) were all fitted better when using the lower, 20 %, percent of solvent in shell (Figure 4.17) even though a value of 55 % of solvent in shell was obtained from the viscosity experiments. In addition, the data obtained from fitting the 3 contrasts using a 20 v/v% solvation value gave the closest value of the theoretical volume fraction (calculated from the composition of the nanoemulsions) to that of the total volume fraction calculated from the scale factor obtained from interpretation of the SANS data.

Based on these results it is possible to draw a schematic representation of the possible molecular architecture of a nanoemulsion droplet containing 2.4 w/w% of Brij 97 as surfactant and 0.3 w/w% of TON and containing 20% of solvent in shell (Figure 4.19).
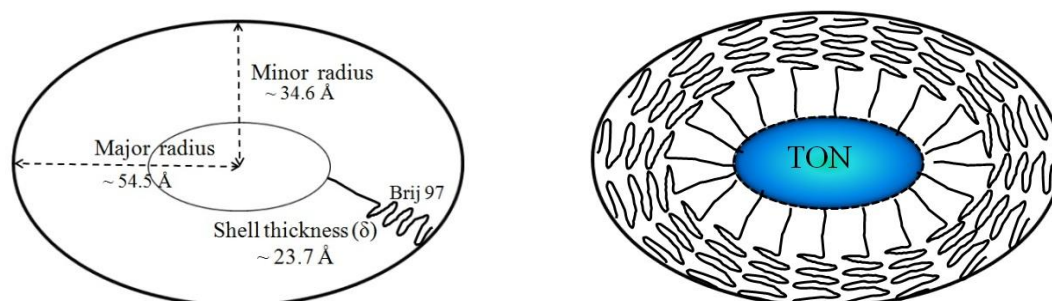
Figure 4.19 Schematic representation of the molecular architecture of nanoemulsion drop containing 2.4 w/w% of Brij 97 as surfactant and 0.3 w/w% of TON as oil.

Nanoemulsions in all subsequent SANS studies were prepared in a contrast match solvent of 43.25 v/v% D_2O/H_2O in order to study a potential of these nanoemulsions in a novel drug delivery system. Thus only drop and core contrasts of the Brij 97-stabilised nanoemulsions were examined. In all cases the solvation of the surfactant shell was assumed to be 20%.

4.7.2 Small angle neutron scattering of nanoemulsions prepared in 43.25 v/v% D_2O/H_2O

In this part of the study, samples of drop contrast were prepared using h-TON, h-Brij and 43.25 v/v% D_2O/H_2O. The summary of the parameters used to obtained the best fit to drop sets of neutron data, assuming a core-shell ellipsoid model and hard-sphere interactions (using the Percus-Yevick approximation) are shown in Tables 4.7 and 4.8. Tables 4.7 and 4.8 give the best fits to the drop contrasts of B24T3/10 and B24T5/10 nanoemulsions, both without and with a presence of a saturation amount of TP and assuming a 20 % level of solvent in shell, prior to exposure to GF-NPs.

The results indicate that prior to exposure to the GF-NPs the radius of nanoemulsion core, drop radius and the axial of core of the B24T3/10 nanoemulsion were ~ 28.9 Å, 52.5 Å and 0.4, while the equivalent dimensions of B24T5/10 nanoemulsion were ~ 36.8 Å, 59.2 Å and 0.5 respectively. As a consequence, the B24T5/10 nanoemulsion was slightly more spherical than the B24T3/10 nanoemulsion. This observation suggests that the nanoemulsion becomes slightly more spherical as the concentration of oil increases. In contrast, the shell thickness was approximately the same in both types nanoemulsions, implying that there was no change in the (lack of) penetration of TON into the surfactant interfacial layer as a function of oil concentration, over the range 0.3 and 0.5 w/w% of TON. This observation is in agreement with that reported by Wasutrasawat (2011), who found no different in the penetration of TON into the shell of 2.4 w/w% Brij 97-stabilised nanoemulsions containing TON concentrations in the range 0.1 - 0.5 w/w%. In addition, the increase in size of the nanoemulsions observed in the presence of an increasing concentration of TON agreed with the PCS data, where the size of nanoemulsion droplets increased with increasing oil content, even though the shape of nanoemulsion droplets could not be determined by PCS. Furthermore, the surfactant aggregation number of the B24T3/10 nanoemulsions increased from 252 to 357 with an increase in the amount of TON present from 0.3 to 0.5 w/w% Interestingly, there are clear differences in the surfactant aggregation numbers obtained with the two different amounts of oil present, even though the differences in size obtained with PCS were only slightly changed. This result is in agreement with the surfactant aggregation number of nanoemulsions prepared with Brij 97 and containing Miglyol 812, which increased from 155 to 238 as the surfactant-to-oil ratio increased from 1:0.1 to 1:0.3

(Warisnoicharoen et al., 2000). The increase in aggregation number seen upon increasing the oil concentration between 0.3 and 0.5 w/w%, in the present study, suggests that the oil was preferentially located into the core of the nanoemulsion droplet rather than in the interfacial surfactant monolayer.

When comparing the difference the results obtained for the nanoemulsions without and with a presence of saturation of TP (Tables 4.7 and 4.8), it was clear that the morphology of the nanoemulsion droplets were slightly affected by the presence of TP as the size (minor radius and major radius) of the drops was slightly larger in its presence. There is two probable ways in which the TP molecules might sit in the nanoemulsions, namely either in the core of the nanoemulsion drop and/or by being located in the surfactant shell. The results obtained in the present study suggest that the TP molecules could be incorporated both into the core and penetrated in the shell regions as both the radius of core and shell thickness were very slightly larger in its presence. In addition, the volume of a whole droplet can be calculated by $(4/3) \times \pi \times$ (Major radius) $\times$ (Minor radius)^2 for oblate ellipsoidal. In terms of the effect of the presence of TP on the surfactant aggregation number, this increased slightly in the presence of a saturation amount of TP. For example the surfactant aggregation number of B24T3/10 nanoemulsion increased slightly from 252 in the absence of TP to 267 in its presence, while the surfactant aggregation number of B24T5/10 nanoemulsion increased slightly from 357 to 376 upon the addition of TP.

Table 4.7 Summary of the individual fits for the drop contrast of 2.4 w/w% Brij 97 nanoemulsions containing 0.3 w/w% of TON without and with a presence of a saturation amount of testosterone propionate over time using a core-shell ellipsoid model and the hard sphere structure factor $S(Q)$, constrained $V_{shell}(dry)/V_{core}$, at 20 % of solvent in the shell.

Sample	radius of core (Å)	core axial ratio (x)	shell thickness (Å)	sphere radius (Å)	major radius (Å)	minor radius (Å)	axial ratio (X)	core volume (Å^3)	drop volume (Å^3)	N_{agg}	no. H_2O/SAA
B24T3/10											
t=0	28.9	0.4	23.4	52.5	35.0	52.3	0.7	40817	401542	252	10
t=4	29.0	0.4	23.4	52.9	35.1	52.3	0.7	40844	401800	253	10
t=8	29.0	0.4	23.4	52.6	35.0	52.3	0.7	40821	401578	252	10
t=12	29.0	0.4	23.4	52.5	35.0	52.4	0.7	40962	402960	253	10
t=24	29.1	0.4	23.5	52.4	35.2	52.6	0.7	41372	406997	256	10
B24T3/10-TP											
t=0	28.9	0.4	24.0	52.8	36.4	52.8	0.7	43242	425396	267	10
t=4	29.0	0.4	23.9	53.0	36.2	52.9	0.7	43151	424494	267	10
t=8	28.9	0.4	23.9	52.5	36.1	52.8	0.7	42779	420841	265	10
t=12	28.9	0.4	23.9	52.7	36.1	52.8	0.7	42798	421300	265	10
t=24	28.9	0.4	23.9	52.7	36.2	52.8	0.7	42947	422487	266	10

Note that each SANS measurement took about 20 minutes. Consequently, the fitted parameters were obtained from the average of each samples scattering intensity for over minutes. The SSE of these samples fluctuated approximately between 100 and 300. Estimated uncertainly for the radius of the core, x and the sphere radius were ± 0.1, ± 0.1, ± 1.0, respectively.

Table 4.8 Summary of the individual fits for the drop contrast of 2.4 w/w% Brij 97 nanoemulsions containing 0.5 w/w% of TON without and with a presence of a saturation amount of testosterone propionate over time using a core-shell ellipsoid model and the hard sphere structure factor *S(Q)*, constrained V_{shell}(dry)/V_{core}, at 20 % of solvent in the shell.

Sample	radius of core (Å)	core axial ratio (x)	shell thickness (Å)	sphere radius (Å)	major radius (Å)	minor radius (Å)	axial ratio (X)	core volume (Å³)	drop volume (Å³)	N_{agg}	no. H₂O/SAA
B24T5/10											
t=0	36.8	0.5	23.2	59.2	40.1	60.0	0.7	95756	605656	357	10
t=4	36.9	0.5	23.2	60.2	39.8	60.1	0.7	95254	602479	355	10
t=8	37.1	0.4	23.1	61.2	39.6	60.2	0.7	95049	601183	354	10
t=12	37.3	0.4	23.1	61.0	39.4	60.4	0.7	95136	601736	354	10
t=24	36.7	0.5	23.2	60.0	39.1	60.7	0.6	95370	603217	355	10
B24T5/10-TP											
t=0	37.3	0.5	23.8	60.0	40.5	61.4	0.7	100848	637861	376	10
t=4	37.3	0.5	23.8	61.1	40.3	61.5	0.7	100855	637908	376	10
t=8	37.2	0.5	23.7	61.3	40.4	61.4	0.7	101118	639572	377	10
t=12	37.2	0.5	23.7	60.0	40.2	61.4	0.7	100269	634204	374	10
t=24	37.2	0.5	23.8	60.9	40.4	61.5	0.7	101311	640795	377	10

Note that each SANS measurement took about 20 minutes. Consequently, the fitted parameters were obtained from the average of each samples scattering intensity for over minutes. The SSE of these samples fluctuated approximately between 100 and 300. Estimated uncertainly for the radius of the core, x and the sphere radius were ± 0.1, ± 0.1, ± 1.0, respectively.

Table 4.9 contains a comparison of the best fits obtained for the drop contrast of Brij 97-stabilised nanoemulsions, B24T3/10, prepared in D_2O and in 43.25 v/v% D_2O/H_2O. As can be seen, the parameters used to obtain the best fit, including the core radius, the core axial ratio and the shell thickness, were very slightly different in both solvents. Therefore it can be concluded that either the reduced difference in the scattering length densities in the 43.25 v/v% D_2O/H_2O solvent influenced the analysis and/or changing the solvent slightly affected the size and shape of the nanoemulsions. These slight differences were however not considered significant as the aim of the study is to confirm the stability and morphology of the nanoemulsion over time, both in the presence and absence of GF-NPs.

Table 4.9 Comparison of individual fitting of Brij 97-stabilised nanoemulsions, B24T3/10, prepared either in H_2O, D_2O or 43.25 v/v% D_2O/H_2O at 20% solvent in the shell.

Sample	radius of core (Å)	core axial ratio (x)	δ (Å)	sphere radius (Å)	major radius (Å)	minor radius (Å)	axial ratio (X)	N_{agg}	ratio of SAA:oil
B24T3/10 prepared in H_2O for core contrast and in D_2O for drop and shell contrasts									
Core	31.1	0.4	23.6	55.2	34.6	54.7	0.6	273	0.19
Shell	30.8	0.4	23.7	54.5	34.5	54.5	0.6	270	0.18
Drop	30.7	0.4	23.8	54.8	34.7	54.4	0.6	271	0.18
B24T3/10 prepared in 43.25 v/v% D_2O/H_2O									
Drop	28.9	0.4	23.4	52.5	35.0	52.3	0.7	252	0.19

Note that the SSE of these samples fluctuated approximately between 200 and 600. Estimated uncertainly for the radius of the core, x and the sphere radius were ± 0.1, ± 0.1, ± 1.0, respectively.

Figures 4.20-4.23 show the stability of the various Brij 97-stabilised nanoemulsions over the 24 hours of the experiment. As can be seen, all nanoemulsions were stable at least for 24 h (longer time courses not tested) as evidenced by the SANS profiles of the nanoemulsions which did not show any change in shape and size compared to that measured at t = 0, i.e. where the SANS of the nanoemulsions was measured within 30

minutes of their preparation. This observation is in good agreement with the PCS results, where the apparent droplet size of B24T3/10 and B24T5/10 nanoemulsions, measured immediately after preparation (in the presence or absence of a saturation amount of TP) was similar to those nanoemulsions at 24 h after preparation.
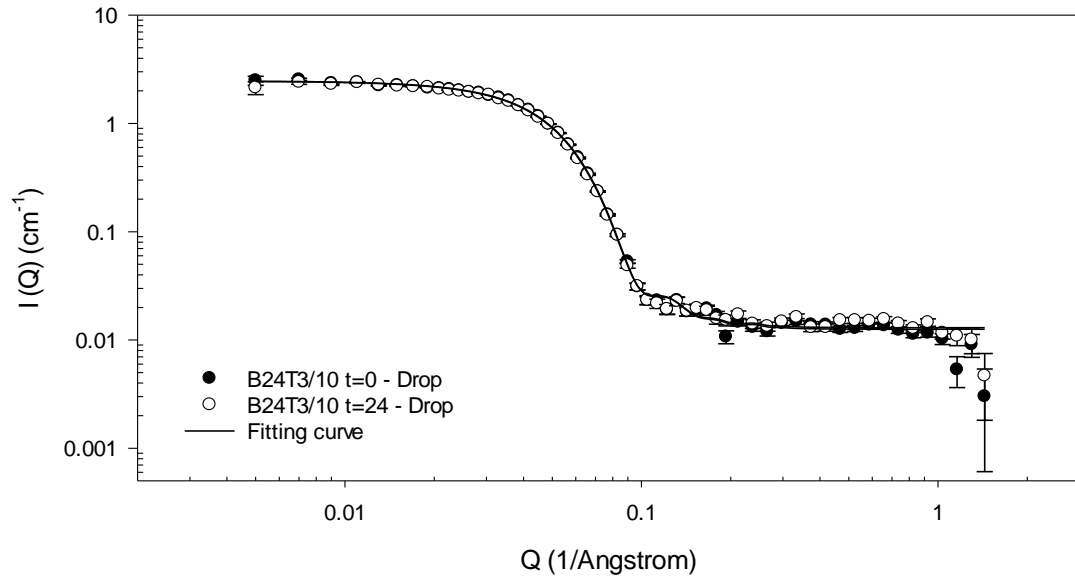
Figure 4.20 SANS data (drop contrast) and individual fits to nanoemulsions prepared using 2.4 w/w% of Brij 97 and 0.3 w/w% of TON at t = 0 and t = 24 hours after preparation. Measurements carried out on SANS2D at 25.0 ± 0.1 ℃.
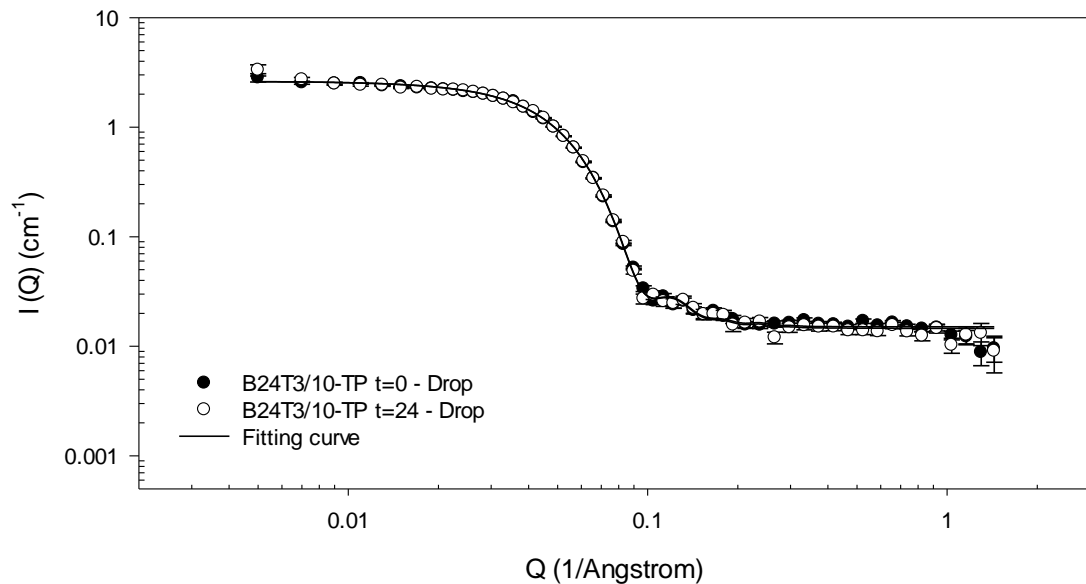
Figure 4.21 SANS data (drop contrast) and individual fits to nanoemulsions prepared using 2.4 w/w% of Brij 97 and 0.3 w/w% of TON in the presence of a saturation amount of testosterone propionate at t = 0 and t = 24 hours after preparation. Measurements carried out on SANS2D at 25.0 ± 0.1 ℃.
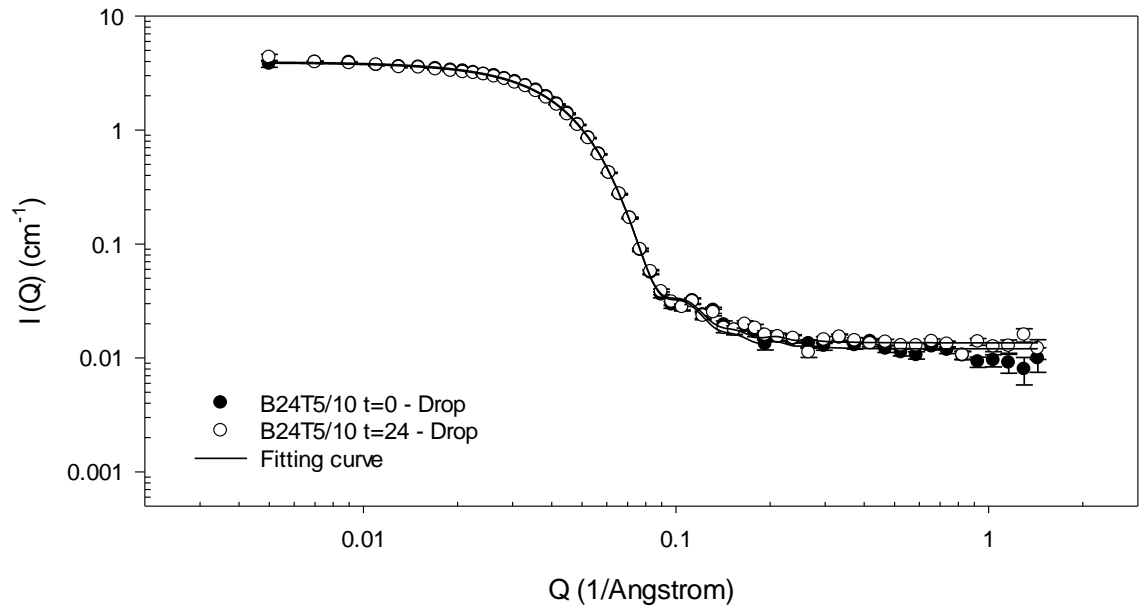
Figure 4.22 SANS data (drop contrast) and individual fits to nanoemulsions prepared using 2.4 w/w% of Brij 97 and 0.5 w/w% of TON at t = 0 and t = 24 hours after preparation. Measurements carried out on SANS2D at 25.0 ± 0.1 ℃.
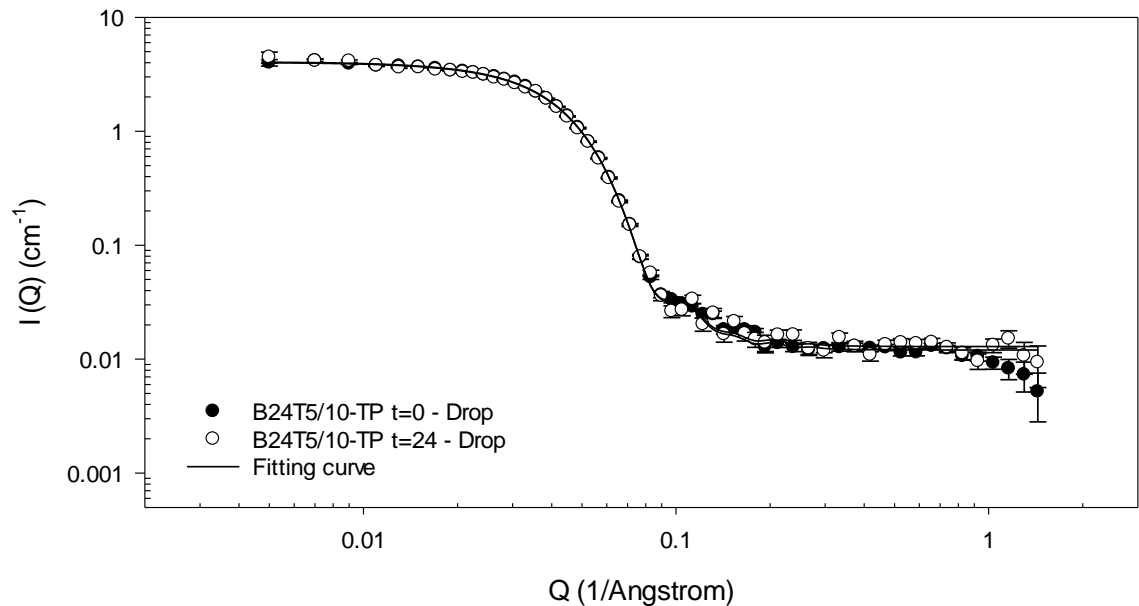
Figure 4.23 SANS data (drop contrast) and individual fits to nanoemulsions prepared using 2.4 w/w% of Brij 97 and 0.5 w/w% of TON in the presence of a saturation amount of testosterone propionate at t = 0 and t = 24 hours after preparation. Measurements carried out on SANS2D at 25.0 ± 0.1 ℃.

4.7.3 Small angle neutron scattering data of nanoemulsions in a nanosusponanoemulsion

SANS profiles, together with the best fits obtained for the drop (h-TON, h-Brij and 43.25 v/v% D_2O/H_2O) and core (d-TON, h-Brij and 43.25 v/v% D_2O/H_2O) contrasts of the nanoemulsions prior to their mixing with GF-NPs, after contact with GF-NPs for periods of up to 24 h, as well as after their separation from the GF-NPs after 24 h contact, were determined to assess the stability of nanoemulsions when in the NSNE (Tables 4.10 to 4.13). The parameters in Tables 4.10 to 4.13 were obtained using a core-shell ellipsoid model together with a hard sphere structure factor $S(Q)$, a constrained $V_{shell}(dry)/V_{core}$, and assuming 20% of solvent in the surfactant shell.

It should be noted that the parameters obtained from the SANS data using the core contrast as shown in Tables 4.10 to 4.13 are slightly different to those obtained when modelling the core contrast and shown in Tables 4.9. This difference might result from the SLD of *d*-TON being much closer in value to the SLD of contrast match solvent than the SLD of *d*-TON to the SLD of the H_2O so a consequence of the smaller difference in SLD is a reduction in the total scattering of the sample.

Table 4.10 Summary of the individual fits for drop and core contrasts of nanoemulsions prepared using 2.4 w/w% of Brij 97 and 0.3 w/w% of TON in an absence of a saturation amount of testosterone propionate prior to mixing with GF-NPs, after contact with GF-NPs for periods of up to 24 h as well as after separation of the nanoemulsions from the GF-NPs by centrifugation after 24 h contact.

Sample	radius of core (Å)	core axial ratio (x)	shell thickness (Å)	sphere radius (Å)	major radius (Å)	minor radius (Å)	axial ratio (X)
Drop contrast							
NE before mixing	29.3	0.4	23.6	52.9	35.4	52.9	0.7
NE at t=0	31.0	0.3	22.4	53.5	32.1	53.4	0.6
NE at t=4	30.9	0.3	22.2	53.0	31.7	53.1	0.6
NE at t=8	30.8	0.3	22.2	53.3	31.7	53.0	0.6
NE at t=12	30.6	0.3	22.3	52.8	32.1	52.9	0.6
NE at t=24	30.6	0.3	22.3	52.9	32.1	52.9	0.6
NE after separation	29.1	0.4	23.4	52.4	35.0	52.4	0.7
Core contrast							
NE before mixing	32.9	0.3	22.3	55.4	30.9	55.2	0.6
NE at t=0	33.9	0.2	21.9	55.8	29.9	55.8	0.5
NE at t=4	33.4	0.2	21.5	54.9	29.3	54.9	0.5
NE at t=8	33.1	0.2	21.5	54.4	29.4	54.5	0.5
NE at t=12	33.0	0.2	21.3	55.2	29.2	54.3	0.5
NE at t=24	32.9	0.2	21.3	54.1	29.1	54.1	0.5
NE after separation	32.0	0.3	22.3	52.9	30.9	54.3	0.6

Note that nanoemulsion (NE) at t = 0 was measured after mixing of the nanoemulsion and the GF-NPs for 5 minutes. In addition, each SANS measurement took 20 minutes. Consequently, the fitted parameters were obtained from the average scattering intensity of a sample over 20 minutes. The SSE of these samples fluctuated approximately between 100 and 200. Estimated uncertainly for the radius of the core, x and the sphere radius were ± 1.0, ± 0.1, ± 2.0, respectively.

Table 4.11 Summary of the individual fits for drop and core contrasts of nanoemulsions prepared using 2.4 w/w% of Brij 97 and 0.3 w/w% of TON in the presence of a saturation amount of testosterone propionate prior to mixing with GF-NPs, after contact with GF-NPs for periods of up to 24 h as well as after separation of the nanoemulsions from the GF-NPs by centrifugation after 24 h contact.

Sample	radius of core (Å)	core axial ratio (x)	shell thickness (Å)	sphere radius (Å)	major radius (Å)	minor radius (Å)	axial ratio (X)
Drop contrast							
NE before mixing	29.1	0.4	24.0	53.0	36.2	53.1	0.7
NE at t=0	31.3	0.3	22.8	54.0	32.8	54.1	0.6
NE at t=4	30.9	0.3	22.6	53.7	32.4	53.5	0.6
NE at t=8	30.9	0.3	22.6	53.4	32.4	53.5	0.6
NE at t=12	30.7	0.3	22.5	53.3	32.3	53.2	0.6
NE at t=24	31.1	0.3	22.4	53.1	32.0	53.4	0.6
NE after separation	28.4	0.4	23.1	51.6	34.8	51.5	0.7
Core contrast							
NE before mixing	33.1	0.3	22.8	56.5	31.7	55.9	0.6
NE at t=0	34.3	0.2	22.0	56.0	30.0	56.3	0.5
NE at t=4	33.2	0.2	21.4	54.6	29.2	54.6	0.5
NE at t=8	32.6	0.2	21.2	54.0	29.1	53.9	0.5
NE at t=12	33.0	0.2	21.2	54.3	29.0	54.2	0.5
NE at t=24	33.3	0.2	21.4	54.7	29.3	54.8	0.5
NE after separation	32.1	0.3	22.0	53.7	30.7	54.0	0.6

Note that nanoemulsion (NE) at t = 0 was measured after mixing of the nanoemulsion and the GF-NPs for 5 minutes. In addition, each SANS measurement took 20 minutes. Consequently, the fitted parameters were obtained from the average scattering intensity of a sample over 20 minutes. The SSE of these samples fluctuated approximately between 100 and 200. Estimated uncertainly for the radius of the core, x and the sphere radius were ± 1.0, ± 0.1, ± 2.0, respectively.

Table 4.12 Summary of the individual fits for drop and core contrasts of nanoemulsions prepared using 2.4 w/w% of Brij 97 and 0.5 w/w% of TON in an absence of a saturation amount of testosterone propionate prior to mixing with GF-NPs, after contact with GF-NPs for periods of up to 24 h as well as after separation of the nanoemulsions from the GF-NPs by centrifugation after 24 h contact.

Sample	radius of core (Å)	core axial ratio(x)	shell thickness (Å)	sphere radius (Å)	major radius (Å)	minor radius (Å)	axial ratio (X)
Drop contrast							
NE before mixing	36.8	0.4	21.9	58.8	36.5	58.7	0.6
NE at t=0	39.3	0.3	21.0	60.8	33.5	60.3	0.6
NE at t=4	37.7	0.3	20.1	57.7	32.1	57.8	0.6
NE at t=8	38.4	0.3	20.1	58.0	31.7	58.5	0.5
NE at t=12	38.4	0.3	20.2	58.0	32.0	58.6	0.6
NE at t=24	37.8	0.3	20.2	58.0	32.2	58.0	0.6
NE after separation	33.7	0.4	20.1	53.8	33.7	53.9	0.6
Core contrast							
NE before mixing	39.9	0.2	20.3	60.8	29.8	60.2	0.5
NE at t=0	40.8	0.2	20.0	60.7	29.0	60.8	0.5
NE at t=4	40.8	0.2	19.8	60.4	28.6	60.5	0.5
NE at t=8	41.7	0.2	19.6	61.4	28.2	61.4	0.5
NE at t=12	42.0	0.2	19.5	61.3	27.9	61.5	0.5
NE at t=24	40.8	0.2	19.3	60.2	27.7	60.1	0.5
NE after separation	34.9	0.2	17.7	52.2	26.1	52.6	0.5

Note that nanoemulsion (NE) at t = 0 was measured after mixing of the nanoemulsion and the GF-NPs for 5 minutes. In addition, each SANS measurement took 20 minutes. Consequently, the fitted parameters were obtained from the average scattering intensity of a sample over 20 minutes. The SSE of these samples fluctuated approximately between 100 and 400. Estimated uncertainly for the radius of the core, x and the sphere radius were ± 1.0, ± 0.1, ± 2.0, respectively.

Table 4.13 Summary of the individual fits for drop and core contrasts of nanoemulsions prepared using 2.4 w/w% of Brij 97 and 0.5 w/w% of TON in the presence of a saturation amount of testosterone propionate prior to mixing with GF-NPs, after contact with GF-NPs for periods of up to 24 h as well as after separation of the nanoemulsions from the GF-NPs by centrifugation after 24 h contact.

Sample	radius of core (Å)	core axial ratio (x)	shell thickness (Å)	sphere radius (Å)	major radius (Å)	minor radius (Å)	axial ratio (X)
Drop contrast							
NE before mixing	37.3	0.4	22.2	59.5	37.1	59.5	0.6
NE at t=0	39.2	0.3	21.0	60.3	33.4	60.2	0.6
NE at t=4	38.5	0.3	20.4	59.0	32.3	58.9	0.6
NE at t=8	39.6	0.3	20.8	59.0	32.9	60.4	0.5
NE at t=12	39.6	0.3	20.5	60.0	32.2	60.0	0.5
NE at t=24	38.3	0.3	20.2	59.0	31.9	58.4	0.6
NE after separation	34.7	0.4	20.7	55.6	34.6	55.3	0.6
Core contrast							
NE before mixing	40.5	0.2	20.4	60.9	30.0	61.0	0.5
NE at t=0	41.0	0.2	19.7	60.7	28.4	60.7	0.5
NE at t=4	42.1	0.2	20.1	62.1	29.0	62.2	0.5
NE at t=8	42.1	0.2	20.0	62.0	28.9	62.1	0.5
NE at t=12	41.6	0.2	19.4	60.9	27.8	61.0	0.5
NE at t=24	40.5	0.2	19.3	59.8	27.9	59.9	0.5
NE after separation	35.5	0.2	18.1	54.0	26.6	53.6	0.5

Note that nanoemulsion (NE) at t = 0 was measured after mixing of the nanoemulsion and the GF-NPs for 5 minutes. In addition, each SANS measurement took 20 minutes. Consequently, the fitted parameters were obtained from the average scattering intensity of a sample over 20 minutes. The SSE of these samples fluctuated approximately between 100 and 200. Estimated uncertainly for the radius of the core, x and the sphere radius were $\pm$ 1.0, $\pm$ 0.1, $\pm$ 2.0, respectively.

From Tables 4.10 to 4.13 it can be seen that the values of the fitted parameters obtained from the drop contrast were slightly different to those obtained from the core contrast. However, the different is only relatively small and the trends obtained for both contrasts are the same. It is interesting that, although the size of the nanoemulsions prepared using 2.4 w/w% of Brij 97 and 0.3 w/w% of TON in an absence and a presence of a saturation amount of testosterone propionate, measured in the presence of GF-NPs was slightly different than that measured prior to mixing, it is clear that the size and shape of the nanoemulsions before mixing with the GF-NPs and the nanoemulsion after separation from GF-NPs by centrifugation are, to all intents and purposes identical. Figures 4.24 and 4.25 show the SANS data obtained for the B24T3/10 nanoemulsions prior to mixing with the GF-NPs in the absence and presence of testosterone propionate and after separation by centrifugation after 24 hours contact with the nanoemulsions.
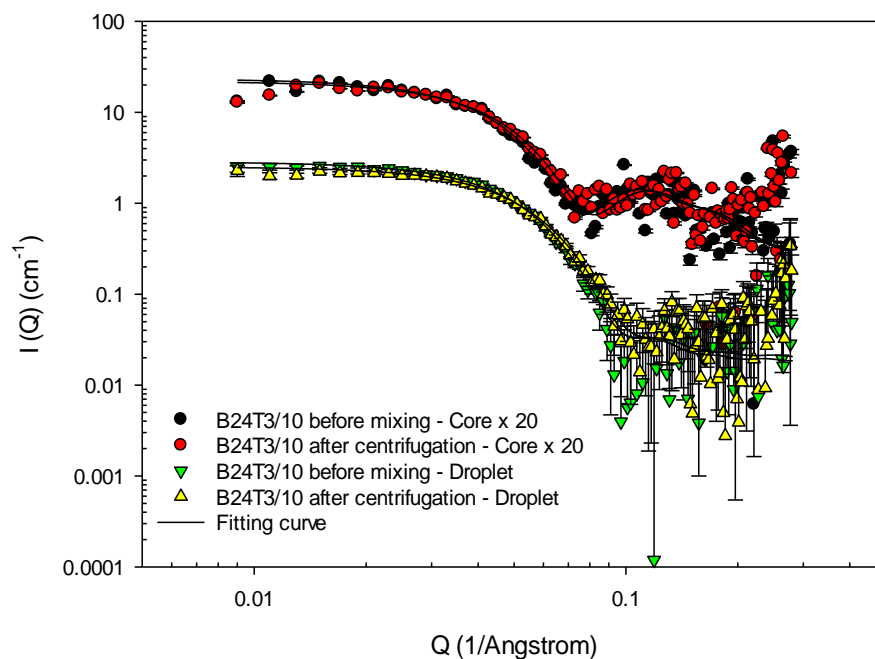
Figure 4.24 SANS data and best fits obtained for the core and drop contrasts of B24T3/10 nanoemulsions prior to mixing with GF-NPs and after separation from GF-NPs by centrifugation after 24 h contact. Fitted line obtained using the core-shell ellipsoid model with a hard sphere *S(Q)*. Measurements carried out on LoQ at 25.0 ± 0.1 ºC.
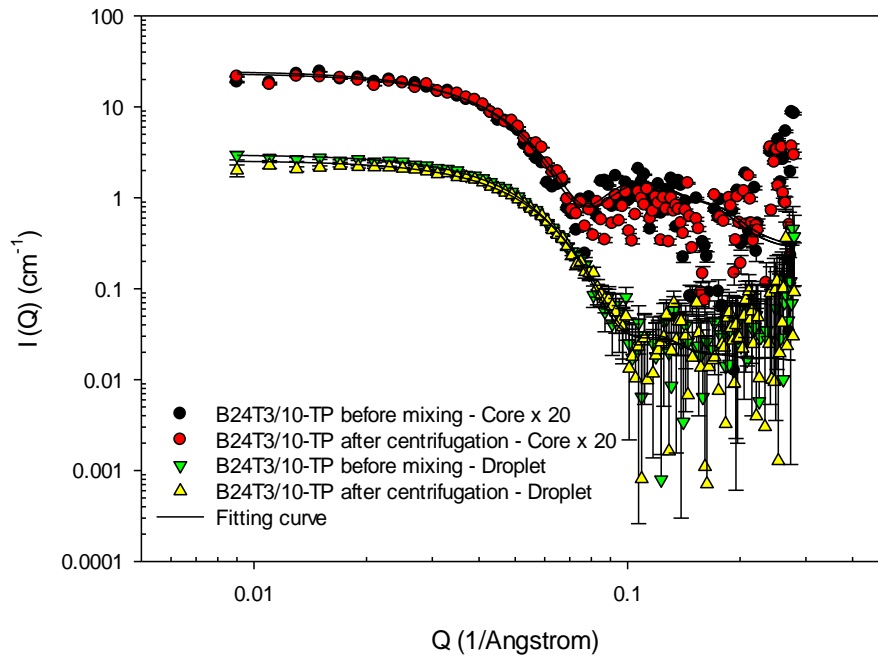
Figure 4.25 SANS data and best fits obtained for the core and drop contrasts of B24T3/10-TP nanoemulsions prior to mixing with GF-NPs and after separation from GF-NPs by centrifugation after 24 h contact. Fitted line obtained using the core-shell ellipsoid model with a hard sphere $S(Q)$. Measurements carried out on LoQ at 25.0 ± 0.1 ºC.

These SANS results were in good agreement with earlier PCS results, where the apparent drop size of the B24T3/10 and B24T3/10-TP nanoemulsions after their separation from the GF-NPs by centrifugation did not change from the size measured for those nanoemulsions prior to their exposure to the GF-NPs.

In contrast, the size and the shape of nanoemulsions prepared using 2.4 w/w% of Brij 97 and 0.5 w/w% of TON in an absence and a presence of a saturation amount of TP after separation from GF-NPs by centrifugation had slightly decreased in size compared to the size of the nanoemulsions prior to mixing with the GF-NPs (Figures 4.26 and 4.27). This observation may be due to the greater instability of the B24T5/10 nanoemulsions compared to the B24T3/10 nanoemulsions.
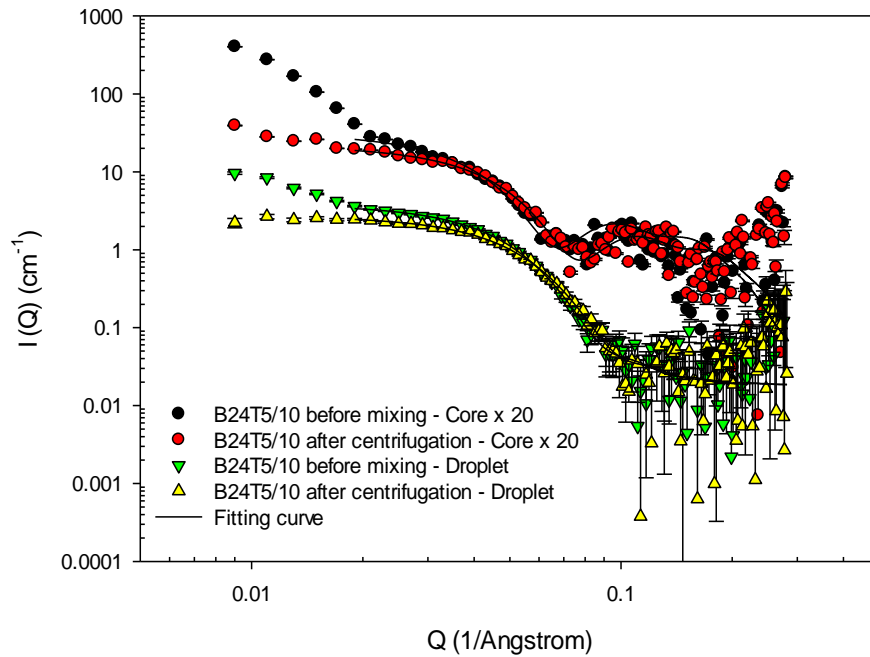
Figure 4.26 SANS data and best fits obtained for the core and drop contrasts of B24T5/10 nanoemulsions prior to mixing with GF-NPs and after separation from GF-NPs by centrifugation after 24 h contact. Fitted line obtained using the core-shell ellipsoid model with a hard sphere $S(Q)$. Measurements carried out on LoQ at 25.0 ± 0.1 °C.
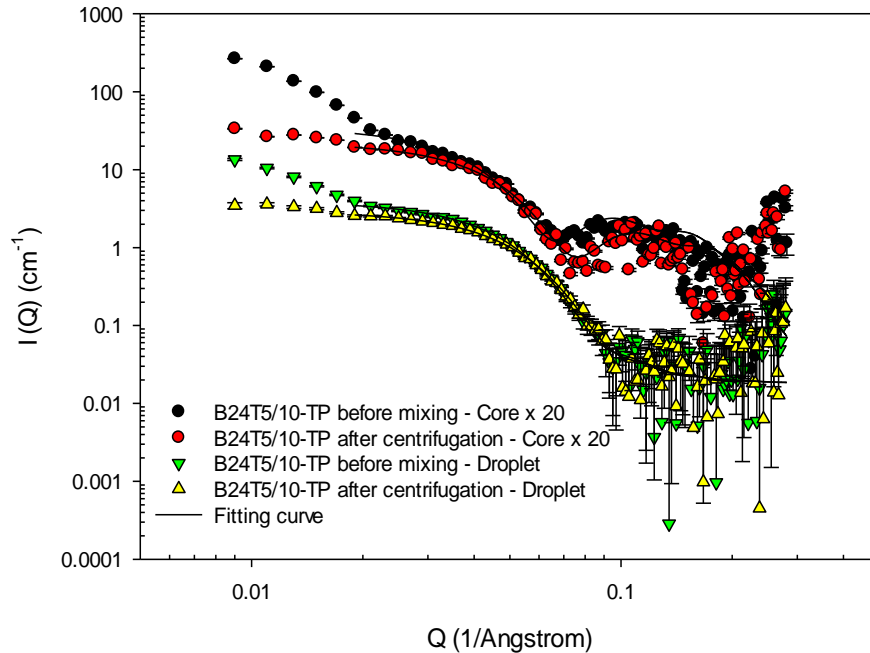
Figure 4.27 SANS data and best fits obtained for the core and drop contrasts of B24T5/10-TP nanoemulsions prior to mixing with GF-NPs and after separation from GF-NPs by centrifugation after 24 h contact. Fitted line obtained using the core-shell ellipsoid model with a hard sphere $S(Q)$. Measurements carried out on LoQ at 25.0 ± 0.1 °C.

Note that the SANS profiles obtained for B24T5/10 and B24T5/10-TP in this study (Figures 4.26 and 4.27) were slightly different from the study of those obtained for the nanoemulsion stability studies (Figures 4.22 and 4.23) as the scattering intensity recorded in Figures 4.26 and 4.27 was higher especially in the Q range 0.008 - 0.02 Å^{-1}. In this part of the study, B24T5/10 and B24T5/10-TP were prepared 2 days before commencing the SANS experiment. In good agreement with the stability recorded for the freshly prepared nanoemulsions shown in Figures 4.22 and 4.23, the particle size of the B24T5/10 and B24T5/10-TP nanoemulsions increased over time. Even though the B24T5/10 and B24T5/10-TP nanoemulsions studied here are not highly stable, the overall aim of this study was the understanding of the stability and morphology of nanoemulsions prior to and after contact with the GF-NPs when in the form of a NSNE. Therefore the data obtained for the B24T5/10 and B24T5/10-TP nanoemulsions will provide valuable information on nanoemulsion stability in a form of NSNEs over time.

In summary, nanoemulsions prepared using 2.4 w/w% of Brij 97 and containing 0.3 w/w% of TON, regardless of the presence of a saturation amount of TP and the GF-NPs stabilised by 1.5 w/w% of SDS, appear to exhibit sufficient stability (in terms of drug solubility and size and shape of the nanoemulsion droplets) to be able to deliver two drugs into the form of a novel combination formulation namely NSNE.

4.7.4 Small angle neutron scattering data of griseofulvin nanoparticles in a presence of nanoemulsion in a nanosusponanoemulsion

In this part of the study, contrast matching was used to make the Brij 97-stabilised nanoemulsions containing TON without and with a presence of a saturation amount of TP 'invisible' when in the form of a NSNE in order to determine the stability over time of the GF-NPs *in situ* and after the GF-NPs separation from the nanoemulsions after 24 h contact. Note that only nanoemulsions containing the lower amount of TON, without and with a presence of a saturation of TP namely as B24T3/10 and B24T3/10-TP, were studied as these nanoemulsions were the most stable as indicated by SANS and PCS in terms of drug solubilisation and morphology and also the limitation of beam time.

Figure 4.28 shows the SANS profiles obtained for GF-NPs prior to mixing with the B24T3/10 nanoemulsions, the GF-NPs when in the form of a NSNE over the 24 h

incubation time and also after their separation from the B24T3/10 nanoemulsion by centrifugation at 24 h contact. Figure 4.29 shows the SANS profiles obtained for the GF-NPs before mixing with the B24T3/10-TP nanoemulsions, GF-NPs in the form of NSNEs over the 24 h incubation time and also the GF-NPs after separation from B24T3/10-TP nanoemulsion by centrifugation at 24 h.
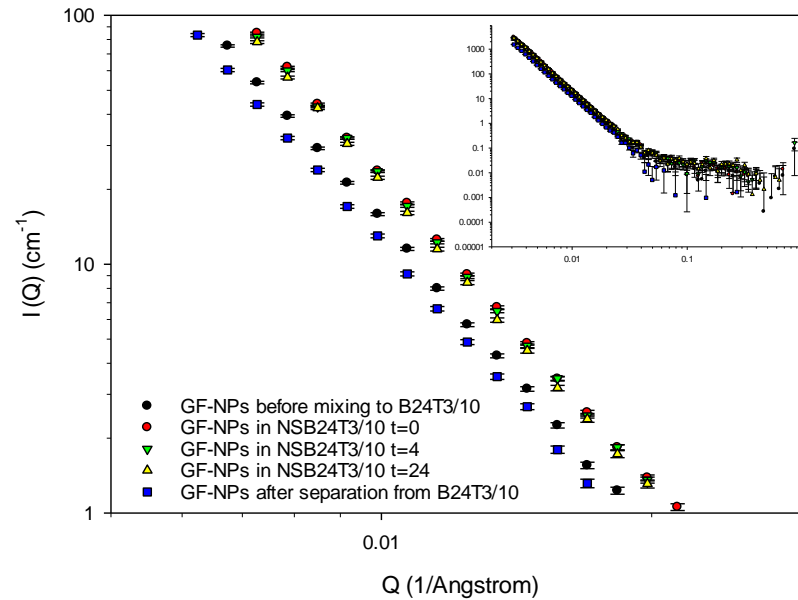
Figure 4.28 SANS profiles of GF-NPs before mixing with the B24T3/10 nanoemulsion, GF-NPs in a form of NSNEs over time and GF-NPs after separation from the B24T3/10 nanoemulsions by centrifugation at 24 h incubation time. Measurements carried out on SANS2D at 25.0 ± 0.1 ºC.
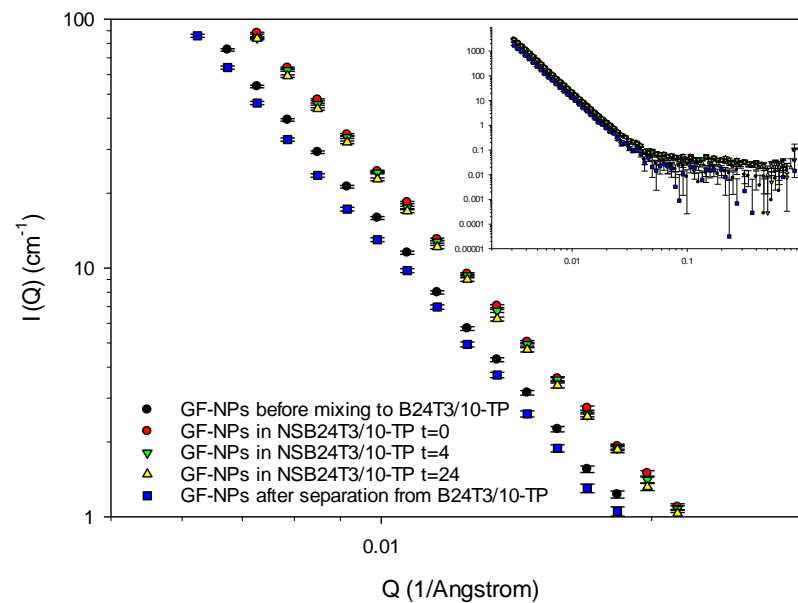
Figure 4.29 SANS profiles of GF-NPs before mixing with the B24T3/10-TP nanoemulsion, GF-NPs in a form of NSNEs over time and GF-NPs after separation from the B24T3/10-TP nanoemulsions by centrifugation at 24 h incubation time. Measurements carried out on SANS2D at 25.0 ± 0.1 ºC.

Firstly, the fitting of the SANS data obtained for the GF-NPs prior to mixing with the nanoemulsion was attempted using a solid ellipsoid model coupled with the Hayter-Penfold charged sphere factor to account for the charged nature of the SDS coating. However, it proved very difficult to reliably fit these samples due to the fact that it was possible to satisfactorily fit the SANS data using a wide range of values for the parameters such as the radius of core and core axial ratio. It was concluded, therefore, that it was most probable that the particle size of the GF-NPs was too large to be determined using SANS.

Interestingly, Figures 4.28 and 4.29 show that the slope of the SANS data for all the GF-NPs samples examined, i.e. the GF-NPs prior to mixing with the nanoemulsions, the GF-NPs when in the form of a NSNE and the GF-NPs after their separation from the nanoemulsions by centrifugation after 24 h incubation, were similar over the Q range 0.03 to 0.4 Å^{-1}, suggesting the particle size of the various GF-NPs did not change with the condition under which they were stored.

Furthermore, the slope of the SANS data of the GF-NPs after separation from the B24T3/10 and B24T3/10-TP nanoemulsions by centrifugation after 24 h incubation were slightly lower than SANS profiles of the GF-NPs before mixing with the nanoemulsions. As known, scattering intensity is influenced by the volume of the scattering particles, amongst other things. Based on this observation it was thought possible that the SANS data obtained for the GF-NPs after separation from the nanoemulsions had decreased in volume, resulting from the loss of some nanoparticles when re-suspending the GF-NPs after centrifugation before re-measuring samples. As a consequence the SANS data for the GF-NPs after separation from nanoemulsions were multiplied by a factor to see how much would have needed to be lost during the re-suspension process. It was found that the SANS data of the GF-NPs after separation from nanoemulsions including B24T3/10 and B24T3/10-TP by centrifugation at 24 h could be both multiplied by a factor of 1.2 to restore the data to the expected intensity (Figures 4.30 and 4.31) suggesting that about 20% of the GF-NPs had been lost during the process, possibly during the process of re-suspending the particles.
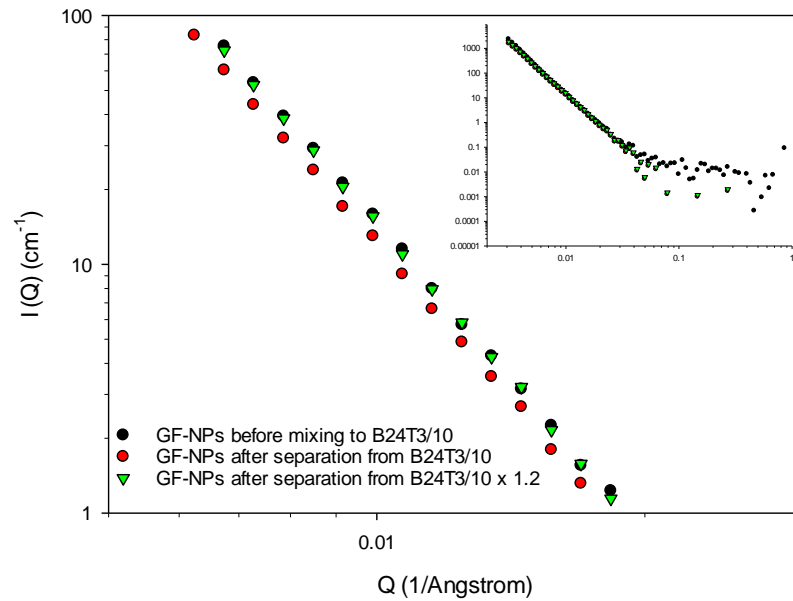
Figure 4.30 SANS profiles of GF-NPs before mixing with the B24T3/10 nanoemulsion, GF-NPs after separation from a B24T3/10 nanoemulsion and GF-NPs after separation from B24T3/10 nanoemulsion but multiplied by a factor of 1.2.
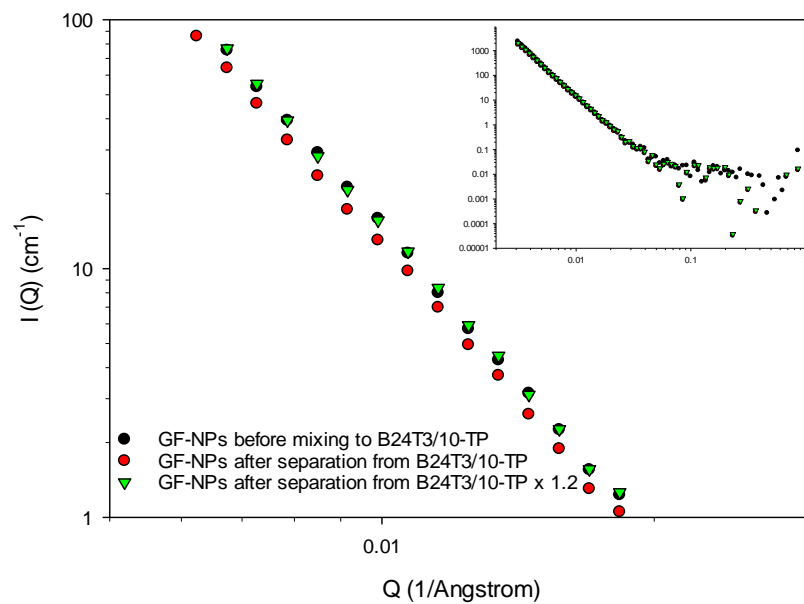
Figure 4.31 SANS profiles of GF-NPs before mixing with the B24T3/10-TP nanoemulsion, GF-NPs after separation from a B24T3/10 nanoemulsion and GF-NPs after separation from B24T3/10-TP nanoemulsion but multiplied by a factor of 1.2.

As a consequence, it may be concluded that the GF-NPs after separation from nanoemulsions containing low amount of TON by centrifugation was slightly difficult to re-disperse. However, this hypothesis could be tested if other advanced technique

such as scanning electron microscope was investigated in order to confirm the size and the shape of the GF-NPs after re-dispersing, unfortunately due to time constraints other techniques were not used.

Chapter 5 Preparation of nanosuspomicroemulsions

5.1 Introduction

In this chapter, the preparation of a novel delivery system is achieved by simply mixing a microemulsion and a nanosuspension. In this case 0.76 mL of a 5 times diluted microemulsion (either S20B14/5-TP or S20C08/5-TP) was mixed with 0.24 mL of GF nanosuspension. The main objective of this chapter is to determine whether it is possible to combine a microemulsion and a nanosuspension in one single formulation which has been termed a nanosuspomicroemulsion (or NSME). In the present study the microemulsions, which contained testosterone propionate (TP), were stabilised by the surfactant as SDS and contained either ethyl butyrate (EB) or ethyl capylate (EC) as oil while the nanoparticles were prepared from griseofulvin (GF). The physico-chemical properties of the SDS microemulsions and GF-NPs after mixing with each other were studied over time. For example, the individual and mutual solubility of GF and TP in the microemulsions comprising the NSMEs was determined by UV spectroscopy while the particle size and the shape of the microemulsions and nanoparticles were determined by small angle neutron scattering (SANS) and, where possible, photon correlation spectroscopy (PCS).

5.2 Solubility of griseofulvin

5.2.1 Solubility of griseofulvin in oil

In a present study, GF was used a model of a poorly-water soluble drug suitable for formulation as NPs. The aqueous solubility of GF has been determined as 0.006 w/v% from a previous experiment in section 3.3.3. Table 5.1 shows the solubility of GF in the oils namely as EB, EC, both used to prepare microemulsions and TON, used to prepare nanoemulsions, over a period of 3 days. The results in Table 5.1 show that the solubility of GF in EB, EC and TON at equilibrium was 0.40, 0.14 and 0.10 w/v%, respectively.

The equilibrium solubility was achieved within 24 h and thereafter remained constant over the 3 days of the study. The solubility of GF in EB was about four times its solubility in TON, while the solubility of GF in EC was almost twice the solubility of GF in TON. Furthermore, the solubility of GF followed the pattern of being most soluble in the most polar oil, namely EB, and least soluble in the least polar oil, TON. Comparing the solubility of GF and TP in the three oils, it is clear that the solubility of both GF and TP followed that the same trend, in that both were most soluble in EB and least soluble in TON. Even though there is a lack of general understanding in mechanism of drug solubilisation in oils, Malcolmson et al. (1998) reported that the solubility of poorly water-soluble drug, TP, in a wider range of followed the same trend in that the greatest solubility was observed in the most polar oil. As a consequence, it can be assumed that the oil polarity has an effect on the solubility of drug.

Table 5.1 Solubility of griseofulvin in oils over time at 25.0 ± 0.1 °C

Oil	Concentration (w/v%) of griseofulvin (mean ± SD, n = 9)		
	24 h	**48 h**	**72 h**
EB	0.40 ± 0.00	0.41 ± 0.00	0.41 ± 0.00
EC	0.14 ± 0.00	0.14 ± 0.00	0.14 ± 0.00
TON	0.10 ± 0.00	0.10 ± 0.00	0.10 ± 0.00

5.2.2 Solubility of griseofulvin in sodium dodecyl sulphate micelles

The solubility of GF in SDS micelles was determined over time to understand the relationship between GF solubility and surfactant concentration (Figure 5.1). The equilibrium solubility of GF in SDS micelles of all concentrations, was achieved by 6 h and remained constant at least up to 96 h (longer time courses were not tested). Note that there was no significant difference in the solubility of GF recorded in the various concentration SDS micelles at the times points tested, ranging from 6 to 96 h ($p > 0.05$). As a consequence the solubility data obtained at each SDS concentration was averaged over the whole of the time period tested. In addition, as can be seen from Figure 5.2, that the average solubility of GF in the SDS micelles varied in a linear manner with

increasing SDS concentration - the solubility of GF in SDS micelles of concentration ranging from 1 to 5 w/w% increased from ~ 0.1 to 0.5 w/v%. Generally, when the solubility of a poorly soluble drug is examined as a function of surfactant concentration, the solubility of the drug is usually very low until the surfactant concentration reaches its cmc (Carlota et al., 2005). The cmc of SDS in water at 25°C is 8 M or 0.24 w/w% (Luckey, 2014) so that all the surfactant concentrations used in this study were well above their cmc.
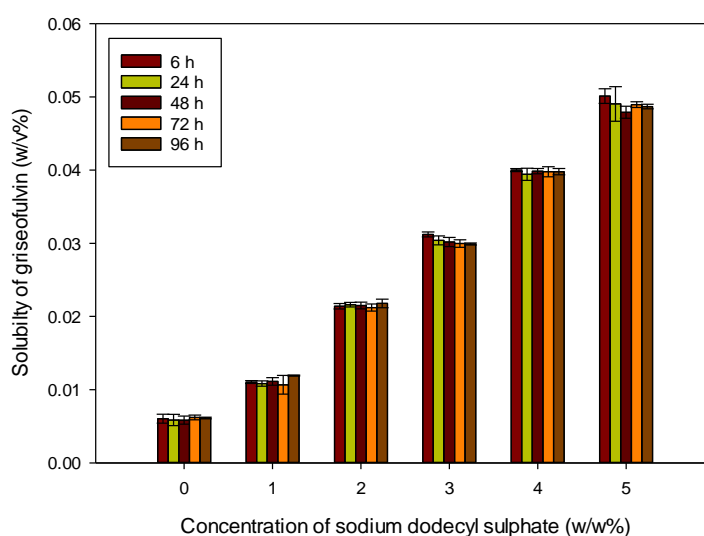
Figure 5.1 Solubility of griseofulvin in varying concentrations of sodium dodecyl sulphate micelles as a function of time at 25.0 ± 0.1 ℃ (mean $\pm$ SD, n =9).
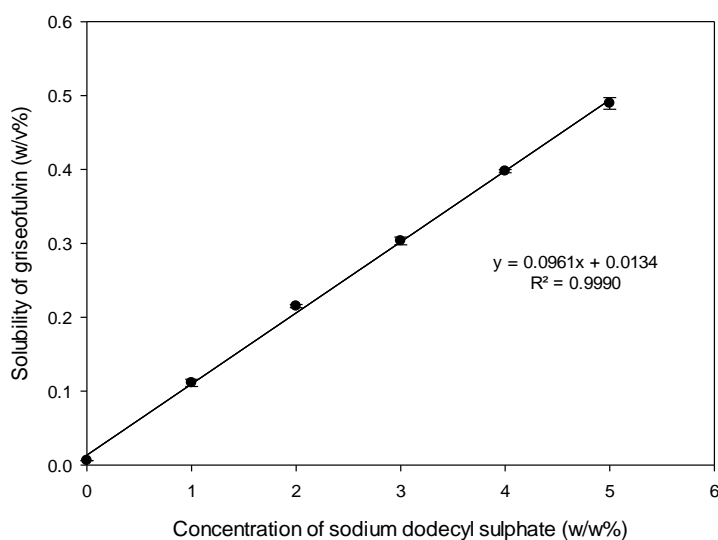
Figure 5.2 The average solubility of griseofulvin of all time points (i.e. 6, 24, 48, 72 and 96 h) in sodium dodecyl sulphate micelles as a function of surfactant concentration at 25.0 ± 0.1 °C. (mean $\pm$ SD, n = 5).

185

When comparing the solubility of GF in Brij 97 and SDS micelles, it can be seen that the solubility of GF in Brij 97 micelles of concentration 0.2 to 2.4 w/w% varied from 0.01 to 0.04 w/v%, whilst the solubility of GF in SDS micelles of concentrations ranging from 1 to 5 w/w% ranged from about 0.1 to 0.5 w/v%. From these results it is clear that GF is solubilised in SDS micelles to a much greater extent than in Brij 97 micelles. A similar trend in results is seen when the solubility of TP in Brij 97 and SDS micelles is examined, where the solubility of TP in Brij 97 is much less than its solubility in SDS micelles. It must be remembered however, that drug solubilisation in surfactant solution depends on a range of factors, including the chemical structure of the surfactant and the drug, the experimental temperature, pH, ionic strength and so on (Torchilin, 2001). Hsieh (2010) reported that the level of solubilisation of TP was significantly different in micelles prepared by SDS, *N,N*-dimethyldodecylamine-*N*-oxide (DDAO), dodecyltrimethylammonium bromide (DTAB) and 3-*N,N*-dimethyldodecyl ammoniopropanesulfonate (DDAPS), possibly be due to the major site of drug solubilisation being the interface between the hydrocarbon core of the micelle and the hydrated head group region. Similarly Krishna et al. (1989) found that the solubility of an anti-malarial drug, β–arteether in micelles formed by 1 w/v% of nonionic surfactants such as polyoxyethylene-9-octyl phenol and polyoxyethylene-20-cetyl ether was 0.39 and 0.43 mg/mL, respectively while the solubility of the drug in micelles formed by an equivalent amount of the ionic surfactants, SDS and tetradecyl trimethylammonium bromide, was 2.69 and 1.74 mg/mL, respectively. Krishna et al. (1989) suggested that these differences in β–arteether solubilisation where a consequence of whether it was incorporated into the micelle interior and/or it was adsorbed at the micelle-water interface.

5.2.3 Solubility of griseofulvin in sodium dodecyl sulphate-stabilised microemulsions

Firstly an understanding of the effect of the presence of GF on SDS-stabilised microemulsions is important to explain where the GF molecules could be solubilised within the microemulsions. An understanding of the behaviour of GF in the microemulsions when a saturation amount of TP was present was necessary prior to the mixing of the microemulsions with GF-NPs to produce the novel combination delivery

system. In this study, an excess of powdered GF was added to 0.76 ml of 5 times diluted SDS microemulsions in the absence and presence of a saturation amount of TP (i.e. S20B14/5, S20B14/5-TP, S20C08/5 and S20C08/5-TP) mixed with 0.24 ml of H_2O as would be the case in the final combination formulation (these 'double' diluted microemulsions were denoted as S20B14/5/0.76, S20B14/5-TP/0.76, S20C08/5/0.76 and S20C08/5-TP/0.76, respectively) to give the concentration of microemulsion present in the final NSME. After incubation of the powdered GF for the required time, the excess GF was removed via centrifugation and the amount of GF in the supernatant determined.

Table 5.2 shows the solubility of GF in SDS-stabilised microemulsions containing either EB or EC in the absence and the presence of a saturation amount of TP over time. The equilibrium solubility of GF in the SDS microemulsions containing EB and EC was reached by 6 h and thereafter maintained for at least up to 96 h (longer time courses were not tested). The solubility of GF in the SDS micelles of 3 w/w% at 24 h was 0.30 w/v% (Figure 5.1) whilst the solubility of GF in the diluted SDS microemulsions, S20B14/5/0.76 and S20C08/5/0.76, at the same SDS concentration was 0.172 and 0.236 w/v%, respectively (Table 5.2). It was clear therefore that the solubility of GF in both of the diluted microemulsions was less than the solubility of GF in the SDS micelles.

Table 5.2 Solubility of powdered griseofulvin in microemulsions with and without a saturation amount of testosterone propionate at $25.0 \pm 0.1\ ^{\circ}C$.

Sample*	Concentration (w/v%) of griseofulvin (mean ± SD, n = 9)				
	6 h	24 h	48 h	72 h	96 h
S20B14/5/0.76	0.16 ± 0.02	0.17 ± 0.01	0.17 ± 0.00	0.16 ± 0.00	0.17 ± 0.00
S20B14/5-TP/0.76	0.17 ± 0.00	0.16 ± 0.00	0.17 ± 0.00	0.16 ± 0.00	0.17 ± 0.01
S20C08/5 /0.76	0.23 ± 0.01	0.24 ± 0.00	0.23 ± 0.00	0.24 ± 0.00	0.24 ± 0.01
S20C08/5-TP/0.76	0.20 ± 0.01	0.19 ± 0.00	0.19 ± 0.00	0.19 ± 0.00	0.18 ± 0.01

*The solubility of griseofulvin was determined in supernatant after centrifugation of 0.76 mL of microemulsions namely S20B14/5, S20B14/5-TP, S20C08/5 and S20C08/5-TP, and 0.24 mL of H_2O, with and without a saturation amount of griseofulvin (GF).

This result was surprising because it was expected that the solubility of GF in the EB containing SDS microemulsions would be greater than the solubility of GF in the EC-containing SDS microemulsions, because the measured solubility of GF in EB was almost three times that obtained in EC. Even despite the fact that the final concentration of EC was less than the final concentration of EB at the same concentration of surfactant, the solubility of GF in the EC-containing SDS-stabilised microemulsions was more than was achieved in those containing EB. Furthermore, the solubilisation obtained in both microemulsions was less than that achieved in the SDS micelles. This result for GF is consistent with the solubility determined for TP in SDS-stabilised microemulsions.

Similarly Hsieh (2010) observed that, despite the fact that TP was more soluble in EB than EC, the solubility of TP in microemulsions stabilised by either the zwitterionic surfactant, dimethyldodecylamminopropylsulphate (DDAPS), the cationic surfactant, dodecyltrimethyl- ammonium bromide (DTAB), or the anionic surfactant, SDS was greater in the EC-containing microemulsions than those containing EB. In his study, Hsieh (2010) proposed that the reversal of the expected TP solubility in the microemulsions was a result of the difference way in which the two oils are incorporated. It is likely that the reversal in predicted GF solubility is also a consequence of the different sites of incorporation of the two oils into the microemulsions.

In the present study, it is proposed that the reason why GF was solubilised to a greater extent in SDS micelles than in SDS-stabilised microemulsion containing EB is that GF prefers to sit in the surfactant head group and/or surfactant interfacial region and that EB disrupts the packing in this region and thereby replaces the GF molecules. As can be seen in Table 5.2, there was no significant difference between solubility of powdered GF in the EB containing SDS-stabilised microemulsions with and without a presence of a saturation amount of TP at any of the time points tested ($p > 0.05$). In contrast, however the solubility of powdered GF in the EC-containing SDS stabilised microemulsions with a saturation amount of TP (i.e. S20C08/5/0.76) was significantly lower than those without containing TP at all time points ($p < 0.05$).

Table 5.3 shows the apparent solubility of TP in S20B14/5-TP/0.76 and S20C08/5-TP/0.76 microemulsions, without and with the presence of a saturation of GF. Note that

the concentration of surfactant and oil in the microemulsions in Table 5.3 are the same as those in Table 5.2 and that, furthermore the solubility of TP was approximately constant between 6 and 96 h ($p > 0.05$). Significantly, the solubility of TP in the SDS-stabilised microemulsions containing either EB or EC in a presence of saturation of GF was less than those in an absence of a saturation of GF, particularly in the EC-containing microemulsions ($p < 0.05$).

Table 5.3 Solubility of testosterone propionate in microemulsions, with and without a saturation amount of griseofulvin, at $25.0 \pm 0.1\ ^{\circ}$C.

Sample*	Concentration (w/v%) of testosterone propionate (mean ± SD, n = 9)				
	6 h	24 h	48 h	72 h	96 h
S20B14/5-TP/0.76 without GF	0.50 ± 0.00	0.50 ± 0.02	0.50 ± 0.00	0.50 ± 0.02	0.49 ± 0.01
S20B14/5-TP/0.76 with GF	0.45 ± 0.01	0.45 ± 0.01	0.45 ± 0.00	0.45 ± 0.01	0.47 ± 0.01
S20C08/5-TP/0.76 without GF	0.71 ± 0.00	0.71 ± 0.00	0.71 ± 0.00	0.71 ± 0.00	0.71 ± 0.00
S20C08/5-TP/0.76 with GF	0.60 ± 0.01	0.60 ± 0.02	0.61 ± 0.01	0.58 ± 0.01	0.58 ± 0.02

*The solubility of testosterone propionate (TP) was determined in supernatant after centrifugation of 0.76 mL of microemulsion (i.e. S20B14/5-TP or S20C08/5-TP) and 0.24 mL of H_2O, with and without a saturation amount of griseofulvin (GF).

As a consequence of these results it is likely that GF and TP are solubilised in the same place in the SDS-stabilised microemulsions particularly in the microemulsions containing EC. Indeed the solubility of GF in EC-containing SDS-stabilised microemulsions in the presence of TP was less than in the corresponding TP-free microemulsions. This observation may be a consequence of the replacement in the EC-containing SDS-stabilised microemulsions of some TP molecules by some GF molecules. In order to substantiate this hypothesis, advanced techniques such as SANS,

are required to fully understand the behaviour of the two drugs in SDS-stabilised microemulsions.

5.3 Solubility of griseofulvin and testosterone propionate in microemulsion of a nanosuspomicroemulsions

Fortunately it was possible to use centrifugation to separate the microemulsions from the GF-NPs due to their differences in particle size and density: the GF-NPs are both larger and denser. As a consequence the GF-NPs are sedimented upon centrifugation, while the supernatant is comprised of the microemulsions. In order to understand behaviour of the two drugs after mixing the microemulsions with the GF-NS, the solubility of GF and TP were determined in the supernatant of the NSME after centrifugation.

Figure 5.3 shows the solubility of GF in the supernatant of the S20B14/5, S20B14/5-TP, S20C08/5 and S20C08/5-TP microemulsions after centrifugation of the NSME with respect to their time of preparation. The solubility of GF in supernatant of water was 0.006 w/v% which then increased to 0.17 and 0.24 w/v% after 30 minutes mixing with the S20B14/5 and S20C08/5 microemulsions, respectively and remained approximately constant over the 96 h incubation finishing at 0.16 and 0.25 w/v%, respectively. As recorded previously the solubility of GF in the S10B14/5 microemulsion supernatant remained approximately constant ($p > 0.05$), regardless of the absence or presence of a saturation amount of TP. In contrast, the solubility of GF in the supernatant containing SDS microemulsion composed of EC (i.e. S20C08/5-TP microemulsions) was significantly less than in the supernatant of the S20C08/5 microemulsions ($p < 0.05$). Encouragingly, these results are consistent with the results of the solubility study of powdered GF and TP-containing, SDS-stabilised microemulsions. As mentioned before, it is possible to explain the results on the basis that GF and TP are solubilised in the same location in the microemulsions.
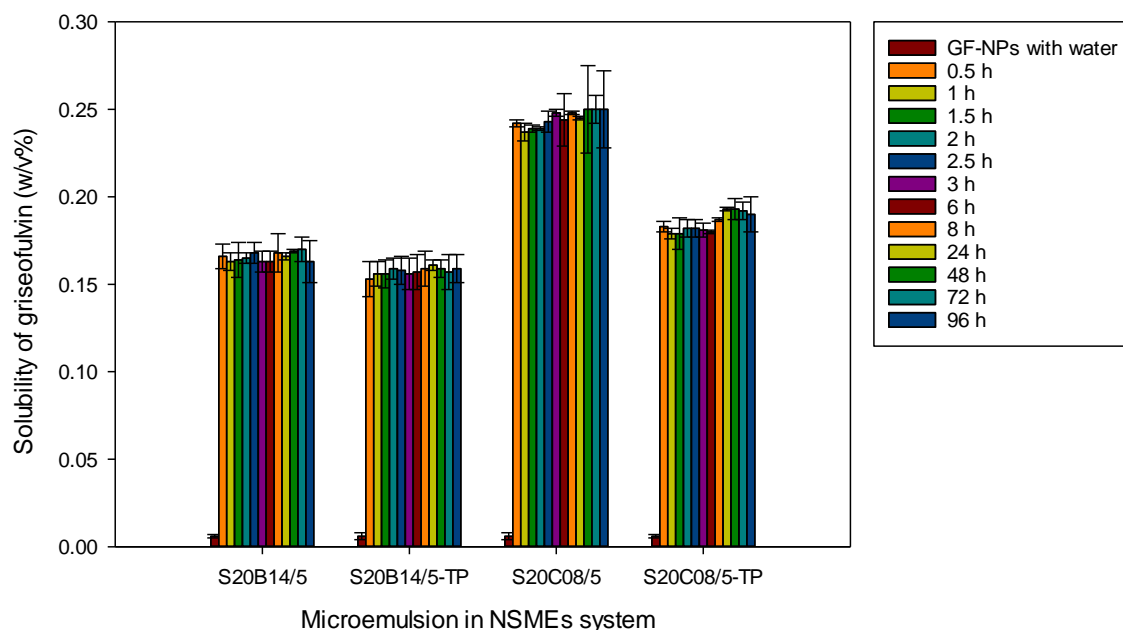
Figure 5.3 Solubility of griseofulvin in the microemulsion-containing supernatant after centrifugation of the NSMEs with time after preparation at $25.0 \pm 0.1\ ^{\circ}$C (mean $\pm$ SD, n = 9).

In contrast, Figure 5.4 shows the solubility of TP in the supernatant containing the S20B14/5-TP or S20C08/5-TP microemulsions, either with time after mixing with the GF-NPs or immediately after separation from the GF-NPs. Initially, the solubility of TP in S20B14/5-TP and S20C08/5-TP microemulsions before mixing with the GF-NPs was at 0.50 and 0.71 w/v%, respectively. However, after mixing with the GF-NPs, the solubility of TP in the S20B14/5-TP and S20C08/5-TP microemulsion-containing supernatant decreased within 30 minutes to 0.46 and 0.61 w/v%, respectively and thereafter remained approximately constant for 96 h (longer time points were not tested).
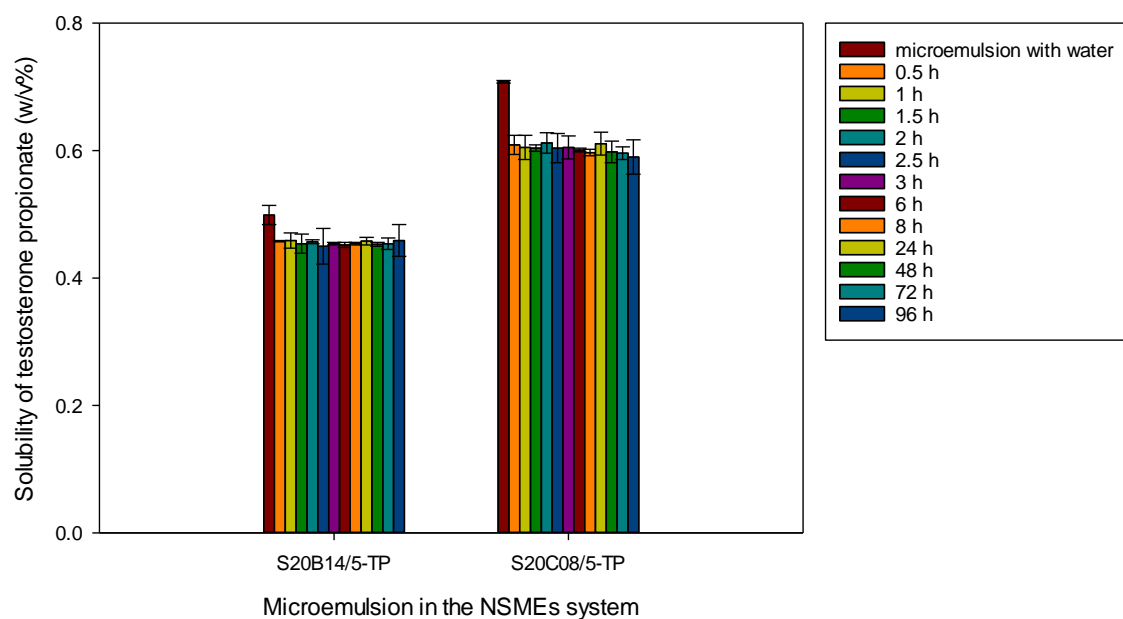
Figure 5.4 Solubility of testosterone propionate in the microemulsion-containing supernatant after centrifugation of the NSMEs with time after preparation at 25.0 ± 0.1 °C (mean $\pm$ SD, n = 9).

These results are consistent with the solubility of TP in the diluted microemulsions (i.e. S20B14/5/0.76 and S20C08/5/0.76) in a presence of a saturation amount of powdered GF, in that the solubility of TP in the microemulsion-containing supernatant after centrifugation of the NSME decreased compared to the solubility of TP in the diluted microemulsions (i.e. S20B14/5/0.76 and S20C08/5/0.76) prior to their mixing to the GF-NPs. This observation supports the hypothesis that GF and TP are preferentially solubilised in the same location in the microemulsions, especially in the EC-containing SDS-stabilised microemulsions.

5.4 Characterization of griseofulvin nanoparticles in the nanosuspomicroemulsions by photon correlation spectroscopy

Visual observation of the NSMEs showed that, when left to stand about an hour in a standard size vial, the microemulsions separated from the nanosuspension. Reassuringly, however, the microemulsions and nanoparticles readily dispersed or re-formed after gentle shaking. It is likely that the rapid separation of the NSME was a consequence of the differences in particle size distribution and density of the

microemulsion and nanoparticles. As a result, of the size and density differences, the top layer of the separated NSME was thought to be a microemulsion, while the bottom layer was considered to be comprised of the GF-NPs. Centrifugation speeded up this separation as did storing the NSME in the large surface to volume 'banjo cells' using for small angle neutron scattering. When using centrifugation to separate microemulsions from the GF-NPs, it was significant that there were no droplets of oil on the surface of the supernatant, suggesting that the microemulsion had remained intact and were not destabilised from contact with the GF-NPs (Santos et al., 2013). Indeed, in no case, any of the microemulsions exhibit any instability when or after being placed in the contact with the GF-NPs.

It was not possible to determine the apparent droplet size of the SDS-stabilised microemulsions *in situ* in the NSMEs using PCS due to their small particle size, so as a consequence SANS was used to characterize their morphology instead. As a consequence, only the variation over time of the particle size of the GF-NPs after mixing with the microemulsions was determined using PCS and compared with their apparent hydrodynamic size prior to mixing.

Assuming the microemulsion and the GF-NPs remained intact upon mixing then the NSMEs will contain two populations of particles, one in the size range of ~ 10 nm arising from the microemulsions and the second larger sized particles, in the range of ~ 350 nm belonging to the GF-NPs. Figure 5.5 shows the apparent hydrodynamic size of the GF-NPs before mixing with the microemulsions and their apparent hydrodynamic size over time when in the form of a NSMEs after mixing with microemulsions, both with and without a saturation amount of TP. As can be seen in Figure 5.5 there was slight increase in the apparent hydrodynamic size of the GF-NPs from 342.3 nm prior to mixing with the microemulsions to 362.4, 370.7, 379.0 and 368.7 nm when in the form of NSMEs namely as NSS20B14/5, NSS20B14/5-TP, NSS20C08/5 and NSS20C08/5-TP, respectively. However, as can be seen in Figure 5.5, the GF-NPs in a form of all NSMEs showed no increase in apparent hydrodynamic size from 5 minutes to 96 h (longer time courses were not tested). This stability could be due to the fact that the stabiliser for both the nanosuspension and the microemulsions were SDS. As a consequence, the use of SDS as stabiliser for both particles would eliminate the

stabiliser displacement events described by Tadros (1990) which would be expected to result in the destabilisation of the system.
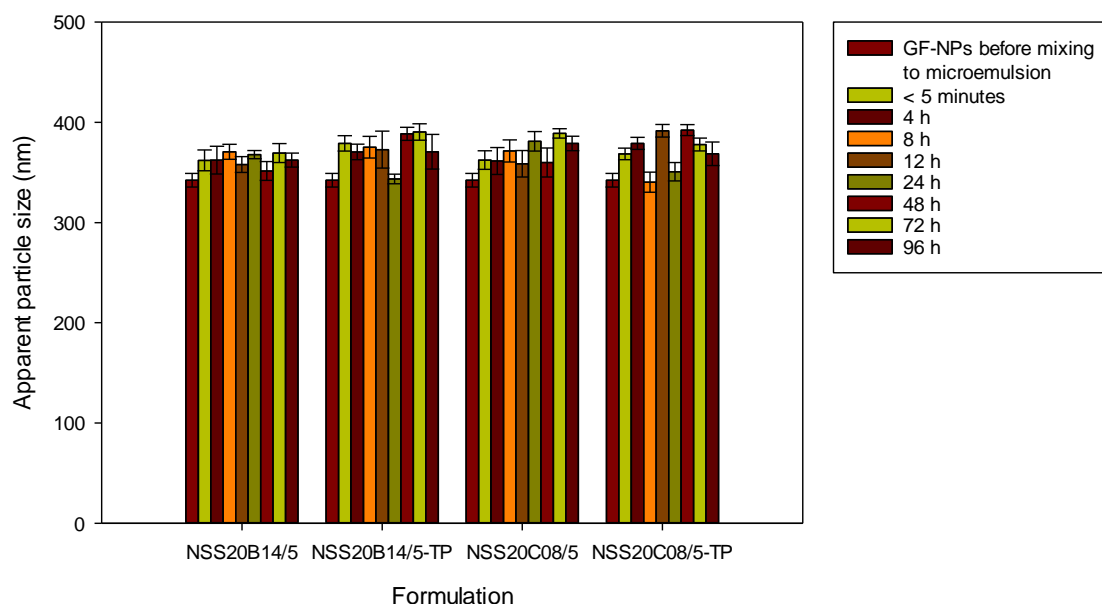
Figure 5.5 Apparent hydrodynamic size of griseofulvin nanoparticles with preparation time when mixed with microemulsions in the form of a NSME at $25.0 \pm 0.1\ ^{o}$C (mean $\pm$ SD, n = 9).

All NSMEs were centrifuged to separate then in their constituents parts in order to determine the apparent particle size of the GF-NPs after being removed from contact with the microemulsion. Figure 5.6 shows the apparent particle size of the GF-NPs prior to mixing with the microemulsions and GF-NPs after separation from microemulsions. The apparent hydrodynamic size of the GF-NPs before mixing to microemulsions was 342.3 nm, while the apparent hydrodynamic size of the GF-NPs after separation from the microemulsions, S20B14/5, S20B14/5-TP, S20C08/5 and S20C08/5-TP, was 478.1, 539.7, 658.7 and 728.0 nm, respectively, after only 5 minutes incubation. Interestingly at the measured hydrodynamic size of the GF-NPs decreased to 459.7, 522.0, 582.9 and 678.9 nm after mixing with the microemulsions S20B14/5, S20B14/5-TP, S20C08/5 and S20C08/5-TP, respectively after mixing for 96 h (longer time courses were not tested). As can be seen in Figure 5.6, the apparent hydrodynamic size of the GF-NPs that had been in contact with the ethyl caprylate microemulsions, S20C08/5 and S20C08/5-TP, were bigger than the GF-NPs that had been in contact with the ethyl

butyrate microemulsions, S20B14/5 and S20B14/5-TP. This result contradicts the results shown in Figure 5.5 and may suggest that after the GF-NPs had been in contact with and separated from the S20C08/5 and S20C08/5-TP microemulsions were more difficult to re-disperse than when the GF-NPs had been in contacted and separated from the S20B14/5 and S20B14/5-TP microemulsions. Despite this difference, the apparent hydrodynamic size of the GF-NPs after separation from all types of microemulsions, regardless of the incubation time, were significantly larger than the apparent hydrodynamic size of the GF-NPs measured in the form of a NSME. While the GF-NPs after contact with the EC-containing microemulsions appear to be more difficult to re-disperse, this observation may be partly a consequence of the method of nanoparticle re-dispersal which involved the use of a small microspatula. This suggests that it would be far better to measure the particle size of both the nanoparticles and the microemulsions *in situ* and as a consequence SANS studies were explored.
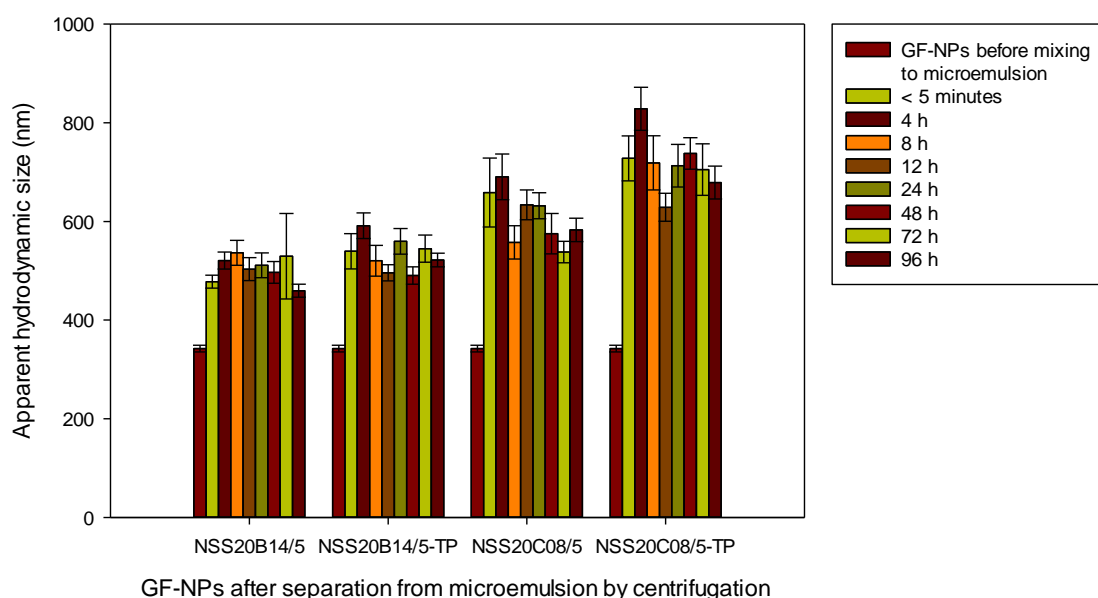
Figure 5.6 Apparent hydrodynamic size of griseofulvin nanoparticles after separation from microemulsions with time the griseofulvin nanoparticles were in the form of a NSME at 25.0 ± 0.1 °C (mean ± SD, n = 9).

5.5 Determination of the hydration value of microemulsions

Viscosity measurement was performed in order to understand the shape of microemulsion droplet as aggregates shape and /or a number of surfactant aggregates. As we established a measured value of intrinsic viscosity of 2.5 mL/g means that the particle is an unsolvated sphere as predicted by Einstein's equation. Figure 5.7 and 5.8 present a function of relative viscosity (η_{rel}), expressed as In η_{rel}/c and specific viscosity (η_{sp}), expressed as η_{sp} /c of SDS micellar solutions and the SDS-stabilised microemulsions containing either EB or EC, both in an absence and a presence of a saturation of TP, as a function of SDS concentration, corrected for the cmc of SDS in 0.2M NaCl. As shown in Figure 5.7 and 5.8, the values of both η_{rel} and η_{sp} of SDS micellar solutions and microemulsions increase linearly with an increase in surfactant concentration.
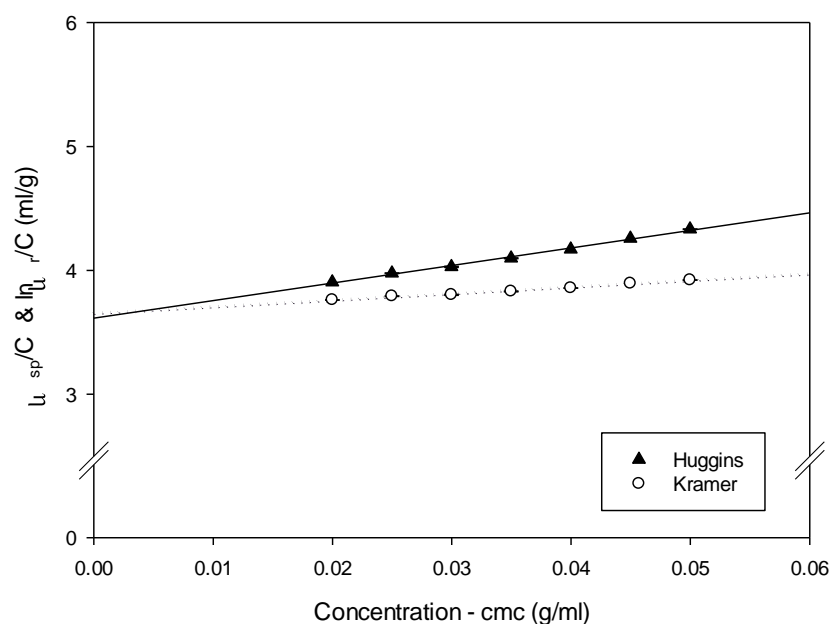
Figure 5.7 Variation in the intrinsic viscosity of sodium dodecyl sulphate (SDS) micellar solutions as a function of concentration at 25.0 ± 0.1 °C (mean ± SD, n = 9).
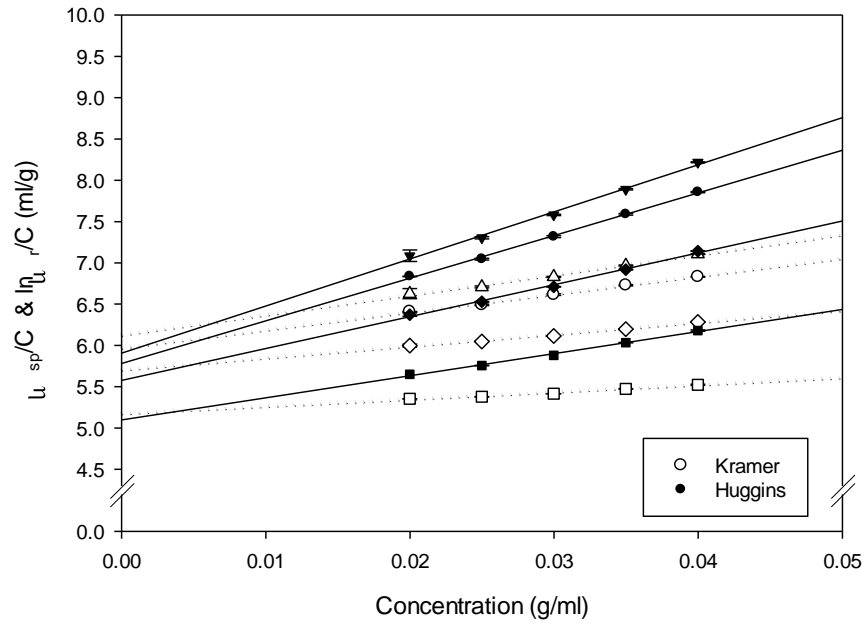
Figure 5.8 Variation in the intrinsic viscosity of sodium dodecyl sulphate stabilised microemulsions containing with either ethyl butyrate and ethyl caprylate without and with a presence of a saturation of testosterone propionate at 25.0 ± 0.1 °C. (○:S20B14/5, ∆:S20B14/5-TP, □:S20C08/5, ◊:S20C08/5-TP) (mean ± SD, n = 9).

Table 5.4 lists the intrinsic viscosity of the SDS micelles and the EB or EC containing SDS-stabilised microemulsions, with or without a saturation amount of TP, calculated as the mean of the intercept values of the Huggins and Kramers plots. As can be seen, the intrinsic viscosity of the SDS micelles was much less than the intrinsic viscosity of the various SDS microemulsions. It is clear that the presence of EB and EC in the SDS-stabilised microemulsions causes an increase in the viscosity of the SDS aggregates and suggests that the presence of the oils causes either a change in the shape of the aggregates and/or a change in hydration. In addition, the values of both η_{rel} and η_{sp} increase in the microemulsions containing a saturation amount of TP.

Table 5.4 The intrinsic viscosity of sodium dodecyl sulphate (SDS) micelles and SDS-stabilised microemulsions containing either ethyl butyrate or ethyl caprylate, without and with a presence of a saturation of testosterone propionate at 25.0 ± 0.1 ºC.

Sample	Intrinsic viscosity (mL/g) (mean ± SD, n = 9)
SDS micelle	3.64 ± 0.03
S20B14/5	5.87 ± 0.03
S20B14/5-TP	6.01 ± 0.05
S20C08/5	5.13 ± 0.05
S20C08/5-TP	5.64 ± 0.09

Because it is not possible to determine whether the increase in the intrinsic viscosity is due to a change in shape and/or an increase in aggregation number of the SDS microemulsions, complementary SANS experiments were performed. By using information on the shape of the micelles and microemulsions determined from the SANS studies, it was possible to use the viscosity measurements to calculate the hydration value and therefore determine a percent hydration of the micelle and the microemulsion shell to help the fitting of the SANS data. The partial specific volume of the SDS micelles and the microemulsions (which is needed to interpret the viscosity data) was calculated by equation:

$$\rho = \rho_0 + (1 - \tilde{\upsilon}\rho_0)C$$

where ρ is the density of the micellar solution or microemulsion at a given concentration (C), ρ_0 is density of aqueous solvent and $\tilde{\upsilon}$ is partial specific volume of the micelle or microemulsion. The density of micelles and microemulsions are shown in Appendix B.

The hydration value, expressed as g of solvent divided by g of solute, was calculated by using the intrinsic viscosity and the partial specific volume as shown:

$$[\eta] = \nu[\tilde{\upsilon} + W_1\tilde{\upsilon}_1^0]$$

where v is the shape factor and $\tilde{\upsilon}_1^0$ is the partial specific volume of aqueous solvent. The shape factor can be determined from knowledge of the axial ratio of the micelle or microemulsion (as determined by SANS) by applying Harding's shape factor (Table 5.5).

Table 5.5 Conversion of shape factor (v) to the axial ratio (a/b) values assuming a prolate ellipsoid of revolution (Harding et al., 1995).

a/b	shape factor (v)
1	2.5000
1.1	2.5068
1.2	2.5252
1.3	2.5529
1.4	2.5882
1.5	2.6298
1.6	2.6769
1.7	2.7286
1.8	2.7846
1.9	2.8444
2	2.9076
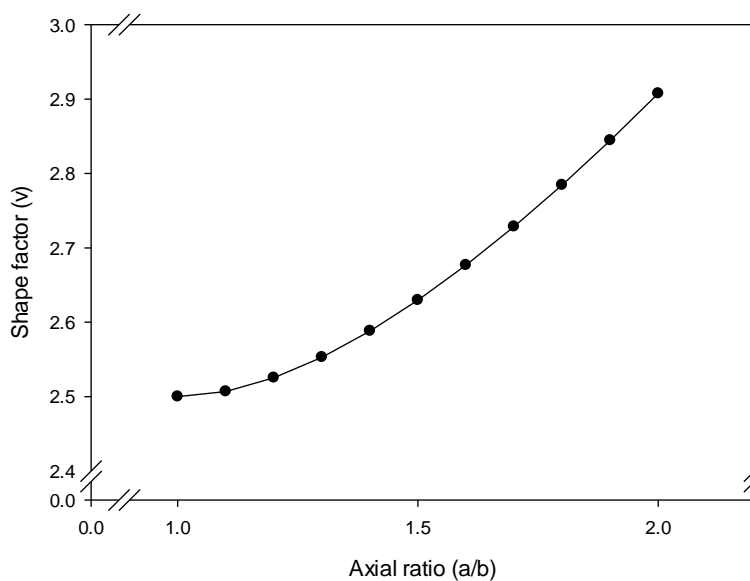
Figure 5.9 Shape factor (v) as a function of the prolate ellipsoidal axial ratio fitted by a quadratic polynomial equation.

The percent of solvent in the shell can be calculated using the following equation:

$$\%solvent\ in\ shell = \frac{(no.molecule_{H_2O} \times mol\ vol_{H_2O})}{(no.molecule_{H_2O} \times mol\ vol_{H_2O}) + (mol\ vol_{surfactant}\ of\ 1\ molecule)} \times 100$$

where *mol vol* is molecular volume ($\mathring{A}^3$).

The number of molecules of H_2O per molecule of surfactant can then be calculated using the following equation:

$$no.molecule_{(H_2O)}\ per\ 1\ molecule\ of\ surfactant\ = \frac{\left(\frac{W_1}{MW_{H_2O}}\right)}{\left(\frac{1}{MW_{surfactant}}\right)}$$

where *MW* is the molecular weight (g mol^{-1}).

Finally the percent of solvent per surfactant head group can be calculated by the following equation:

$$\%solvent/\text{headgroup} = \frac{(no.molecule_{H_2O} \times mol\ vol_{H_2O})}{(no.molecule_{H_2O} \times mol\ vol_{H_2O}) + (mol\ vol_{\text{headgroup}}\ of\ 1\ molecule)} \times 100$$

In the case of SDS, the head group is SO_4Na which has a molecular volume of 60.5 $\mathring{A}^3$ (Vass et al., 1989).

Alternatively, the level of hydration can be predicted from fitting the SANS data. From the SANS studies, the shape of all the microemulsions examined was prolate ellipsoid (see SANS section 5.6.1). The axial ratio determined from analysis of the SANS data for the following microemulsions, S20B14/5, S20B14/5-TP, S20C08/5 and S20C08/5-TP, was 1.4, 1.7, 1.5 and 1.6, respectively, while the hydration value and a percent solvation of the shell at 25 ℃ calculated using the droplet axial ratio are given in Table 5.6. The hydration value of the SDS microemulsions obtained from the SANS measurements was in the range 1.1-1.3 mL/g, while the % solvent in the shell was 55-61 % and the solvent per surfactant head group of surfactant was ~ 90%. It is clear from Table 5.6 that the values obtained for the hydration and the percent solvent in the shell for microemulsions containing either EB or EC in the presence of a saturation amount of TP was slightly higher than the values obtained for microemulsions in the absence of TP.

Table 5.6 Summary of the intrinsic viscosity and hydration value of microemulsions containing either ethyl butyrate or ethyl caprylate, with and without the presence of a saturation amount of testosterone propionate, at 25.0 ± 0.1 ℃ calculated by using the shape of the microemulsion obtained from SANS measurements.

Sample	intrinsic viscosity	partial specific volume	hydration	no molecule of water/SDS	% solvent in shell	% solvent/ head group
S20B14/5	5.87	0.919	1.34	21.4	60.8	91.4
S20B14/5-TP	6.01	0.901	1.32	21.2	60.5	91.3
S20C08/5	5.13	0.896	1.06	17.0	55.2	89.4
S20C08/5-TP	5.64	0.881	1.24	19.9	59.1	90.8

5.6 Characterization of microemulsions and nanoparticles in the nanosuspomicroemulsions by small angle neutron scattering

5.6.1 Small angle neutron scattering of microemulsions before mixing with the griseofulvin nanoparticles

Small angle neutron scattering (SANS) studies were used to determine the microstructure of the SDS-stabilised microemulsions in dilute aqueous solution. In order to understand whether the presence of oil and TP had any effect on the morphology of the microemulsion droplets, including their size and shape, SANS experiments on the microemulsions, were performed using 43.25 v/v% of D_2O in H_2O as solvent. This solvent was selected because it was the solvent that is required when the GF-NPs are present in order to make the NPs 'invisible' to neutrons. Of particular interest in this study, is whether it was possible to study the SDS-stabilised microemulsions *in situ* in the presence of the GF-NPs in order to gain an understanding of effect of the GF-NPs on the stability of the microemulsion droplets.

To establish the most suitable model with which to analyse the SANS data obtained for the microemulsion stabilised by the anionic surfactant SDS, preliminary analysis were performed, using two hypotheses, using the SANS data obtained for the S20B14/5 microemulsions. The first hypothesis assumed that the core of the microemulsion consisted only of oil, while the shell contained the whole surfactant molecule plus any associated counter-ions and any solvent in shell. The second hypothesis assumed that

the core consisted of all oil molecules together with the surfactant tails, while the shell was composed of the surfactant head groups along with any associated counter-ions and the water of hydration. The SANS data for the S20B14/5 microemulsions dispersed in 43.25 v/v% D_2O in H_2O were fitted using an ellipsoidal model together with the Haytor-Penfold structure factor to account for inter particulate interactions. Regardless of the hypothesis assumed, the SLD and volume fraction of microemulsion droplets and the percent solvent in the shell were constrained while the radius of core (R_{core}), shell thickness (δ), the axial radius of core, radius of Hayter-Penfold structure factor (R_{H-P}) and the total charge of the aggregate (Z) were all varied in order to obtain the best fit to the experimental SANS data.

Table 5.7 gives a comparison of the parameters used to obtained the best fit to the SANS data for the S20B14/5 microemulsion using the two hypotheses outlined above. The calculated percent solvent in shell of the S20B14/5 microemulsions obtained from the viscosity experiments (Table 5.6), was used to fit the SANS data obtained for S20B14/5. When the first hypothesis was explored, the percent solvent in shell was ~ 60 v/v%, while when the second hypothesis was used, the percent solvent in the shell was ~ 90 v/v%. However, the best fit to the SANS data obtained for S20B14/5 microemulsion with the second hypothesis were obtained using a solvent in shell of 87 v/v% as opposed to 90 v/v%. Reassuringly, the value of the fitted parameters obtained in the present study were in line with those reported by Griffiths et al. (2005), who reported that the length of SDS head group was 3.5 Å, while the length of the extended tail was 16.8 Å, values determined from SANS experiments on SDS micelles at an SDS concentration of 50 mM.

Table 5.7 Comparison of the parameters used to obtained the best fit to the SANS data for the S20B14/5 microemulsion using two different hypotheses.

Sample	R_{core} (Å)	core axial ratio (x)	δ (Å)	R_{H-P} (Å)	Z	$1/k$	SSE	major radius (Å)	minor radius (Å)	axial ratio (X)
1st hypothesis	12.3	1.7	7.6	24.5	20.6	0.040	145	28.1	19.9	1.4
2nd hypothesis	18.0	1.5	3.5	24.6	20.7	0.040	115	30.8	21.5	1.4

1st hypothesis - core of the microemulsion consisted only of oil while the shell contained the whole surfactant molecule plus any associated counter-ions and any solvent in shell
2nd hypothesis - core consisted of all oil molecules together with the surfactant tails while the shell was composed of the surfactant head groups along with any associated counter-ions and the water of hydration.
Note that estimated uncertainly for the R_{core}, x, R_{H-P}, Z and 1/k were ± 0.2, ± 0.1, ± 0.1, ± 1.0, ± 0.002 respectively.

In addition, Figures 5.10 and 5.11 show the best fit to the SANS data obtained for S20B14/5 microemulsion with hypothesis one (Figure 5.10) where the core of the microemulsion consisted only of oil, while the shell contained the whole surfactant molecule plus any associated counter-ions and any solvent in shell and hypothesis two (Figure 5.11) where core consisted of all oil molecules together with the surfactant tails, while the shell was composed of the surfactant head groups along with any associated counter-ions and water of hydration. As can be seen, the SANS data obtained for S20B14/5 were fitted slightly better in the Q range of between 0.1 and 0.4 Å^{-1} when using the second hypothesis as opposed to the hypothesis one.
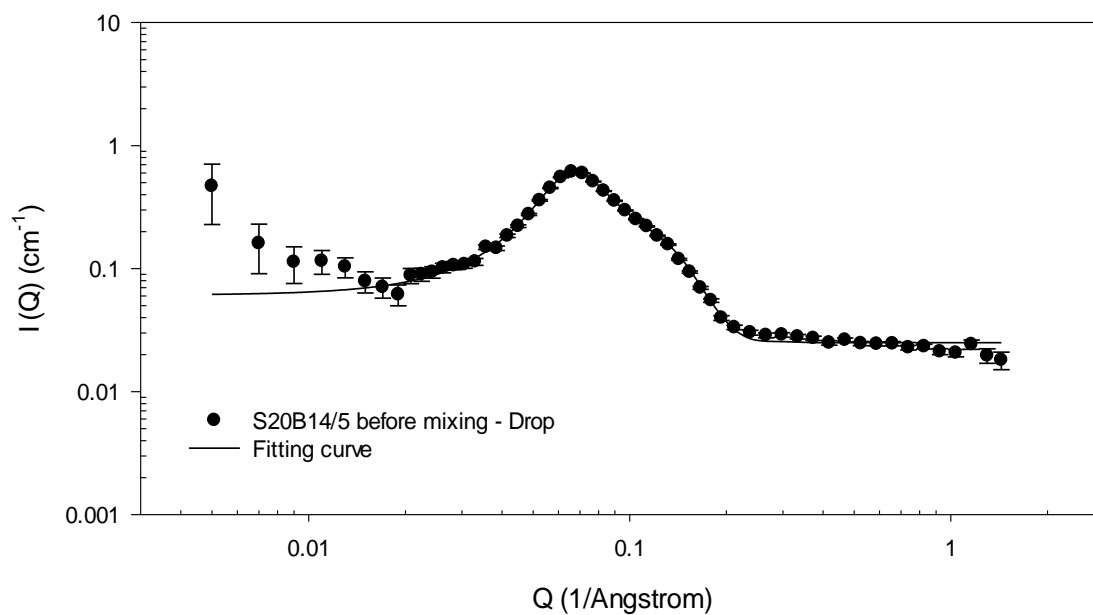
Figure 5.10 SANS data and best fit to the S20B14/5 microemulsion assumed that the core of the microemulsion consisted only of oil, while the shell contained the whole surfactant molecule plus any associated counter-ions and any solvent in shell. Measurement carried out on SANS2D at 25.0 ± 0.1 °C.
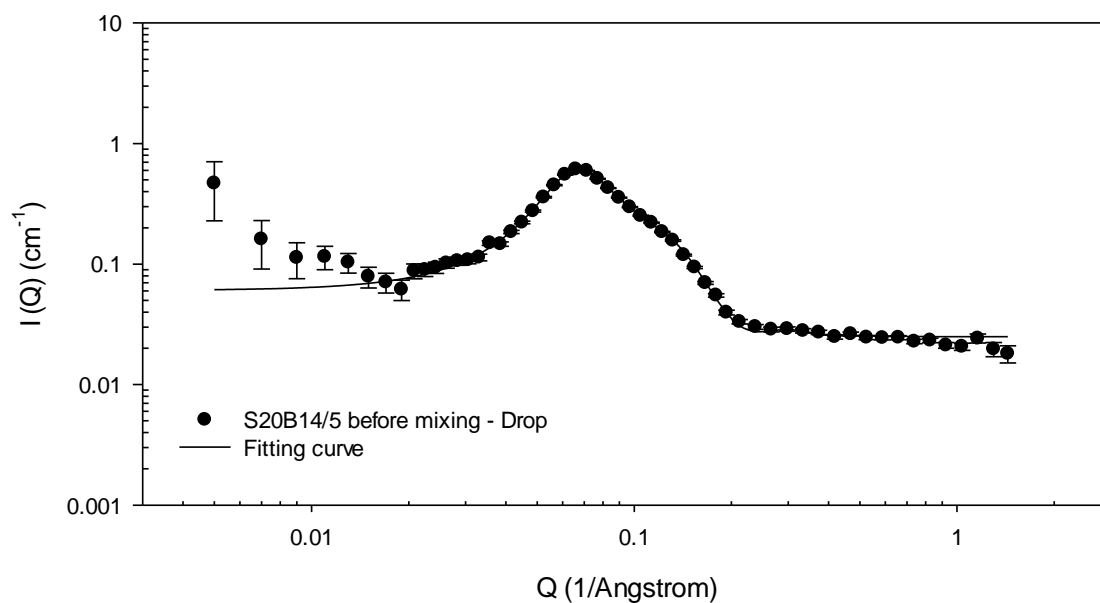
Figure 5.11 SANS data and best fit to the S20B14/5 microemulsion core consisted of all oil molecules together with the surfactant tails, while the shell was composed of the surfactant head groups along with any associated counter-ions and the water of hydration. Measurement carried out on SANS2D at 25.0 ± 0.1 °C.

As a consequence of this preliminary analysis, the second hypothesis in which the core consisted of all oil molecules together with the surfactant tails, while the shell was composed of the surfactant head groups along with any associated counter-ions and water of hydration was used to fit all the remaining microemulsion SANS data, namely S20B14/5-TP, S20C08/5 and S20C08/5-TP.

Table 5.8 summarises the parameters used to obtain the fit to the SANS data obtained for SDS-stabilised microemulsions containing either EB or EC, with and without the presence of a saturation amount of TP, using an ellipsoidal model together with the Hayter-Penfold structure factor to account for the charged nature of the microemulsion droplets. For the SDS-stabilised microemulsion containing EB, as can be seen, there was only a relatively small increase in the value of R_{core} in the presence of a saturation amount of TP. Furthermore, Figure 5.12 shows the SANS data and best fits for drop contrast of both the S20B14/5 and S20B14/5-TP microemulsion. As can be seen there is only a small difference in the SANS data between the two samples. As a consequence of the slight increase in the size of the core, there was a slight increase of the major radius of the whole microemulsion drop, from 30.8 to 35.4 Å, and an increase in the axial ratio of the microemulsion drop from 1.4 to 1.7, although the charge on the microemulsion drop in the presence of TP did not change. Similarly, a previous study by Hsieh (2010) found that the major radius and the drop axial ratio of 3 w/v% SDS microemulsions containing 2.25 w/v% of EB and 0.48 w/v% of TP were larger than the corresponding microemulsions without the presence of TP.

Table 5.8 Summary of the fits of the drop contrast of microemulsions containing 4 w/w% of sodium dodecyl sulphate and either 2.8 w/w% of ethyl butyrate or 1.6 w/w% of ethyl caprylate with and without the presence of a saturation amount of testosterone propionate. Measurement carried out on SANS2D at 25.0 ± 0.1 ℃.

Sample	R_{core} (Å)	core axial ratio (x)	δ (Å)	$R_{H\text{-}P}$ (Å)	Z	1/k	SSE	major radius (Å)	minor radius (Å)	axial ratio (X)
S20B14/5	18.0	1.5	3.5	24.6	20.7	0.040	115	30.8	21.5	1.4
S20B14/5-TP	17.9	1.8	3.6	24.8	21.4	0.040	96	35.4	21.5	1.7
S20C08/5	23.3	1.5	3.5	28.8	27.0	0.034	184	39.5	26.8	1.5
S20C08/5-TP	24.6	1.7	3.5	29.1	31.4	0.035	295	44.2	28.1	1.6

Note that estimated uncertainty for the R_{core}, x, $R_{H\text{-}P}$, Z and 1/k were ± 0.2, ± 0.1, ± 0.1, ± 1.0, ± 0.002 respectively.
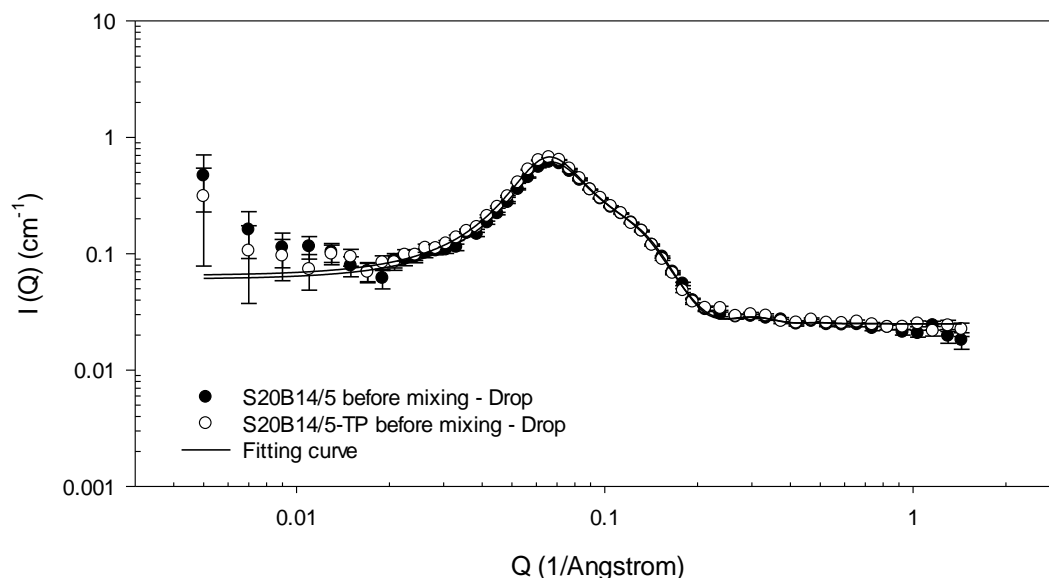
Figure 5.12 SANS data and best fit for the drop contrast of S20B14/5 and S20B14/5-TP microemulsions. Measurements carried out on SANS2D at 25.0 ± 0.1 °C.

Similarly, for the SDS-stabilised microemulsions containing EC there was a slight increase in the value of R_{core} in the presence of a saturation amount of TP as well as a slight increase in the major and minor radii of the whole microemulsion drop from 39.5 to 44.2 Å and from 26.8 to 28.1 Å, respectively. As a consequence the axial ratio of the microemulsion drop increased from 1.5 to 1.6. In contrast to the EB-containing microemulsions, the charge on the EC-containing microemulsion slightly changed, suggesting that the presence of TP might have some effect in the head group region of the microemulsion droplets. As can be seen in Figure 5.13, there is slightly stronger interparticle repulsion, which occurs in the Q range of between 0.05 and 0.06 Å^{-1}, present in the EC than the EB-containing microemulsions. Note that, however, in order to establish the most reasonable fitting of SANS data of S20C08/5 microemulsion, the percent solvent in the shell of this microemulsion was fitted at 78 v/v%, using a head group length for SDS at 3.5 Å (Griffiths et al., 2005), even though the viscosity experiment (Table 5.6) indicated that the percent solvent in SDS shell of the EC-containing microemulsions was ~ 90 v/v%.
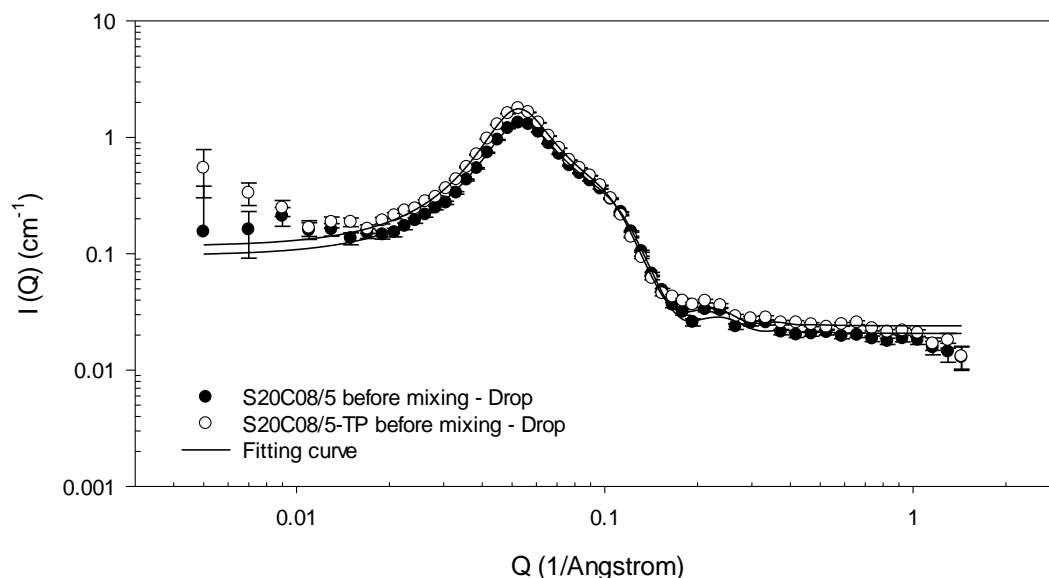
Figure 5.13 SANS data and best fit for the drop contrast of S20C08/5 and S20C08/5-TP microemulsions. Measurements carried out on SANS2D at 25.0 ± 0.1 ℃.

Comparing the EB- and EC-containing SDS-stabilised microemulsions containing TP, it is clear that the microemulsions containing EC were larger in size. Although the SDS-stabilised microemulsions containing EC in the absence of a saturation amount of TP were more asymmetric than those containing EB, it appears that the EC-containing SDS microemulsions become less asymmetric in the presence of TP. This observation may the result of EC forming a central core in the SDS-stabilised microemulsion drop, whereas it is probable that EB does not form a central core and as a consequence the EC-containing microemulsions have a greater capacity for dissolving TP than the microemulsions containing EB. Figures 5.14 and 5.15 show schematics representation of the molecular architecture of SDS-stabilised microemulsions containing EB and EC, respectively.
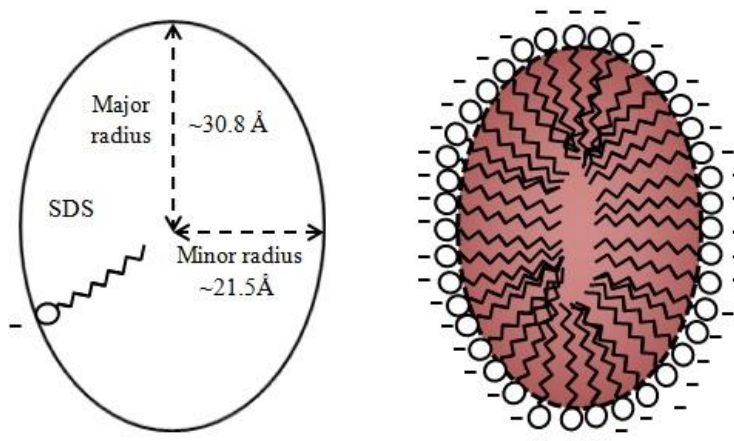
Figure 5.14 Schematic representation of the shape and molecular architecture of sodium dodecyl sulphate stabilised microemulsion droplets containing ethyl butyrate.
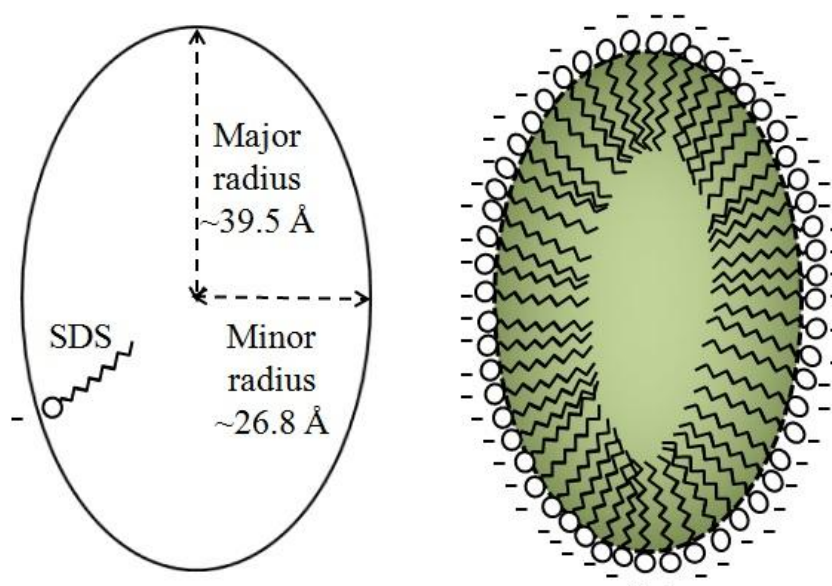
Figure 5.15 Schematic representation of the shape and molecular architecture of sodium dodecyl sulphate microemulsion droplets containing ethyl caprylate.

5.6.2 Small angle neutron scattering data of microemulsions in the presence of griseofulvin nanoparticles

The SANS profiles and the best fit to drop contrast for each microemulsion prior to mixing with the GF-NPs, microemulsion in contacting with the GF-NPs and microemulsion after separation, by centrifugation, from the GF-NPs after 24 h contact were determined to examine the stability of microemulsions when in the form of a NSME and whether or not the size and/or shape of microemulsions was altered. Note that the physical appearance of the supernatant of the NSME after centrifugation, namely the microemulsion showed no separation, for example no drops of oil on the top of the supernatant, regardless of its composition, whether it contained EB or EC, or TP or no TP.

Table 5.9 and 5.10 summarise the parameters used to obtain the best fit for the drop contrast of the EB-containing SDS microemulsions, with and without the presence of a saturation amount of TP, using a core-shell ellipsoidal model together with the Hayter-Penfold structure factor to account for the charged nature of the SDS-coated particles. As can be seen the best fit parameters, including the major radius, minor radius and the drop axial ratio of the SDS microemulsions containing EB regardless of the presence of TP, were largely unaltered when the GF-NPs were present and were only slightly smaller after separation from the GF-NPs by centrifugation. As can be seen from Figures 5.16 and 5.17, the SANS data and the best fits for the drop contrast for the S20B14/5 and S20B14/5-TP microemulsions before mixing with the GF-NPs were very similar to the corresponding microemulsions after their separation from the GF-NPs after 24 h contact by centrifugation.

Table 5.9 Summary of the parameters used for the best fit to the drop contrast of microemulsions containing 4 w/w% of sodium dodecyl sulphate and 2.8 w/w% of ethyl butyrate prior to mixing to griseofulvin nanoparticles, after contacting to griseofulvin nanoparticles for differing periods of time and also after separation from griseofulvin nanoparticles by centrifugation after 24 h contact.

Sample	R_{core} (Å)	core axial ratio (x)	δ (Å)	R_{H-P} (Å)	Z	$1/k$	SSE	major radius (Å)	minor radius (Å)	axial ratio (X)
ME before mixing	18.0	1.5	3.5	24.6	20.7	0.040	115	30.8	21.5	1.4
ME at t=0	17.7	1.5	3.5	24.2	20.4	0.041	303	30.4	21.2	1.4
ME at t=4	17.8	1.5	3.5	24.2	20.3	0.040	164	30.2	21.3	1.4
ME at t=8	17.8	1.5	3.5	24.2	20.5	0.040	214	30.4	21.3	1.4
ME at t=24	17.7	1.5	3.5	24.1	20.5	0.040	222	30.7	21.1	1.5
ME after separation	17.0	1.5	3.4	24.2	20.2	0.041	102	29.1	20.4	1.4

Note that estimated uncertainly for the R_{core}, x, R_{H-P}, Z and 1/k were ± 0.2, ± 0.1, ± 0.1, ± 1.0, ± 0.002 respectively.

**Table 5.10** Summary of the parameters used for the best fit to the drop contrast of microemulsions containing 4 w/w% of sodium dodecyl sulphate and 2.8 w/w% of ethyl butyrate in the presence of a saturation amount of testosterone propionate prior to mixing to griseofulvin nanoparticles, after contacting to griseofulvin nanoparticles for differing periods of time and also after separation from griseofulvin nanoparticles by centrifugation after 24 h contact.

Sample	R_{core} (Å)	core axial ratio (x)	δ (Å)	R_{H-P} (Å)	Z	$1/k$	SSE	major radius (Å)	minor radius (Å)	axial ratio (X)
ME before mixing	17.9	1.8	3.6	24.8	21.4	0.040	96	35.4	21.5	1.6
ME at t=0	18.3	1.7	3.7	24.6	21.7	0.040	251	35.3	22.0	1.6
ME at t=4	18.2	1.7	3.7	24.6	21.7	0.040	113	35.2	21.9	1.6
ME at t=8	18.2	1.7	3.7	24.6	21.8	0.040	130	35.2	21.9	1.6
ME at t=24	18.1	1.7	3.7	24.6	21.7	0.040	180	35.1	21.8	1.6
ME after separation	17.3	1.8	3.5	24.4	20.9	0.040	107	33.8	20.9	1.6

Note that estimated uncertainly for the R_{core}, x, R_{H-P}, Z and 1/k = ± 0.2, ± 0.1, ± 0.1, ± 1.0, ± 0.002 respectively.

Figure 5.16 SANS data and best fit for the drop contrast of S20B14/5 microemulsions before mixing with the griseofulvin nanoparticles and after separation from the griseofulvin nanoparticles by centrifugation at 24 h. Measurements carried out on SANS2D at 25.0 ± 0.1 ℃.
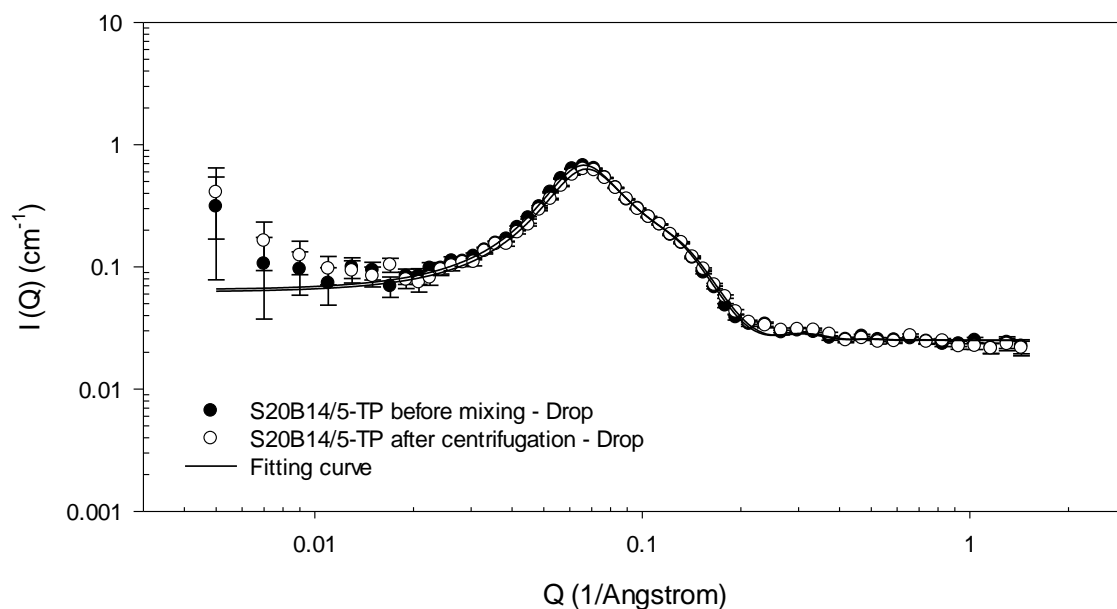
Figure 5.17 SANS data and best fit for the drop contrast of S20B14/5-TP microemulsions before mixing with the griseofulvin nanoparticles and after separation from the griseofulvin nanoparticles by centrifugation at 24 h. Measurements carried out on SANS2D at 25.0 ± 0.1 ℃.

Table 5.11 and 5.12 summarise the parameters used to obtain the best fit to the drop contrast of SDS microemulsions containing EC, with and without the presence of a saturation amount of TP, using a core-shell ellipsoidal model together with the Hayter-Penfold structure factor to account for the charged nature of the particles. As can be seen, the parameters used for the best fit, including the major radius and minor radius of the SDS microemulsions containing EC, with and without a saturation amount of TP, after separation from the GF-NPs by centrifugation, slightly decreased from those used to fit the corresponding microemulsions prior to mixing with the GF-NPs. Figure 5.18 and 5.19 shows the SANS data and the best fit to the drop contrast of the S20C08/5 and S20C08/5-TP microemulsions before mixing with the GF-NPs and the same microemulsions after their separation from the GF-NPs by centrifugation at 24 h. As can be seen from Figures 5.18 and 5.19, the SANS data and best fits to the S20C08/5 and S20C08/5-TP microemulsions after separation from the GF-NPs by centrifugation at 24 h were slightly different to those obtained from the corresponding microemulsions prior to mixing with the GF-NPs.

Interestingly, the size and the shape of the microemulsions, regardless of whether they contained EB or EC or TP, remained constant in the presence of GF-NPs for at least 24 h contact time (longer time courses were not tested).

Table 5.11 Summary of the parameters used for the best fit to the drop contrast of microemulsions containing 4 w/w% of sodium dodecyl sulphate and 1.6 w/w% of ethyl caprylate prior to mixing to griseofulvin nanoparticles, after contacting to griseofulvin nanoparticles for differing periods of time and also after separation from griseofulvin nanoparticles by centrifugation after 24 h contact.

Sample	R_{core} (Å)	core axial ratio (x)	δ (Å)	R_{H-P} (Å)	Z	$1/k$	SSE	major radius (Å)	minor radius (Å)	axial ratio (X)
ME before mixing	23.3	1.5	3.5	28.8	27.0	0.034	184	39.5	26.8	1.5
ME at t=0	23.2	1.6	3.5	28.3	27.2	0.035	727	39.5	26.7	1.5
ME at t=4	23.1	1.5	3.5	28.5	27.5	0.034	56	38.9	26.5	1.5
ME at t=8	22.9	1.6	3.5	28.2	28.0	0.035	364	39.1	26.4	1.5
ME at t=24	22.8	1.6	3.4	28.2	27.2	0.034	297	38.7	26.2	1.5
ME after separation	21.6	1.5	3.6	27.4	26.5	0.034	211	36.9	25.2	1.5

Note that estimated uncertainly for the R_{core}, x, R_{H-P}, Z and $1/k$ were ± 0.2, ± 0.1, ± 0.1, ± 1.0, ± 0.002 respectively.

Table 5.12 Summary of the parameters used for the best fit to the drop contrast of microemulsions containing 4 w/w% of sodium dodecyl sulphate and 1.6 w/w% of ethyl caprylate in the presence of a saturation amount of testosterone propionate prior to mixing to griseofulvin nanoparticles, after contacting to griseofulvin nanoparticles for differing periods of time and also after separation from griseofulvin nanoparticles by centrifugation after 24 h contact.

Sample	R_{core} (Å)	core axial ratio (x)	δ (Å)	R_{H-P} (Å)	Z	$1/k$	SSE	major radius (Å)	minor radius (Å)	axial ratio (X)
ME before mixing	24.6	1.7	3.5	29.1	31.4	0.036	295	44.2	28.1	1.6
ME at t=0	24.4	1.6	3.5	28.6	30.7	0.035	874	43.5	27.9	1.6
ME at t=4	24.3	1.6	3.5	28.6	31.8	0.037	257	43.3	27.8	1.6
ME at t=8	24.2	1.6	3.5	28.6	31.9	0.037	183	43.1	27.7	1.6
ME at t=24	24.2	1.6	3.5	28.6	31.8	0.037	236	43.2	27.7	1.6
ME after separation	22.5	1.6	3.5	27.7	30.4	0.037	284	40.3	26.0	1.6

Note that estimated uncertainly for the R_{core}, x, R_{H-P}, Z and $1/k$ were ± 0.2, ± 0.1, ± 0.1, ± 1.0, ± 0.002 respectively.
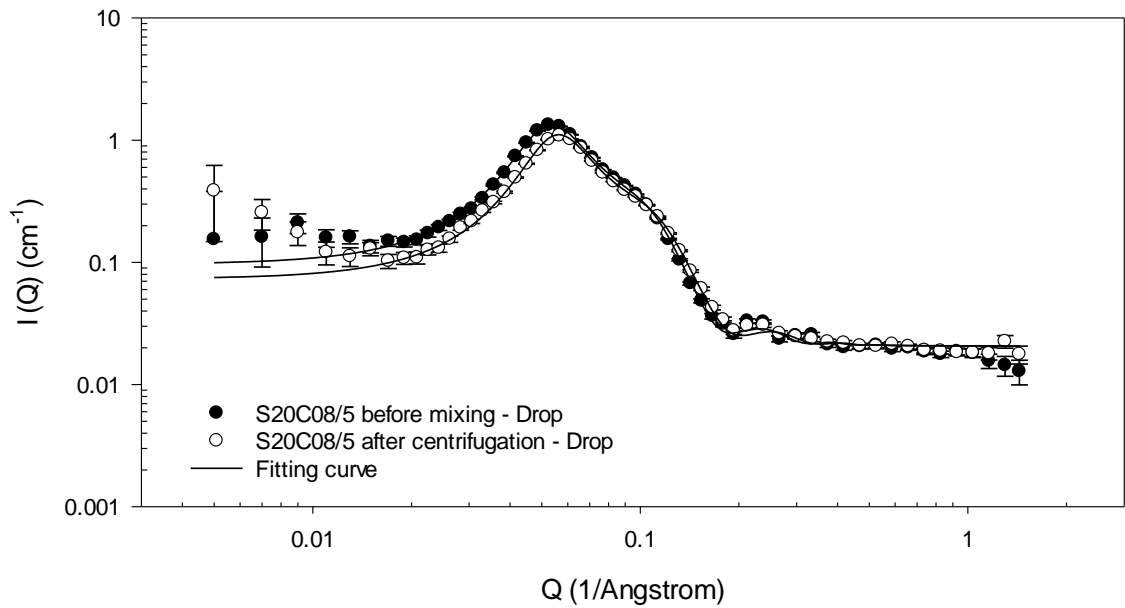
Figure 5.18 SANS data and best fit for the drop contrast of S20C08/5 microemulsions before mixing with the griseofulvin nanoparticles and after separation from the griseofulvin nanoparticles by centrifugation at 24 h. Measurements carried out on SANS2D at 25.0 ± 0.1 ℃.
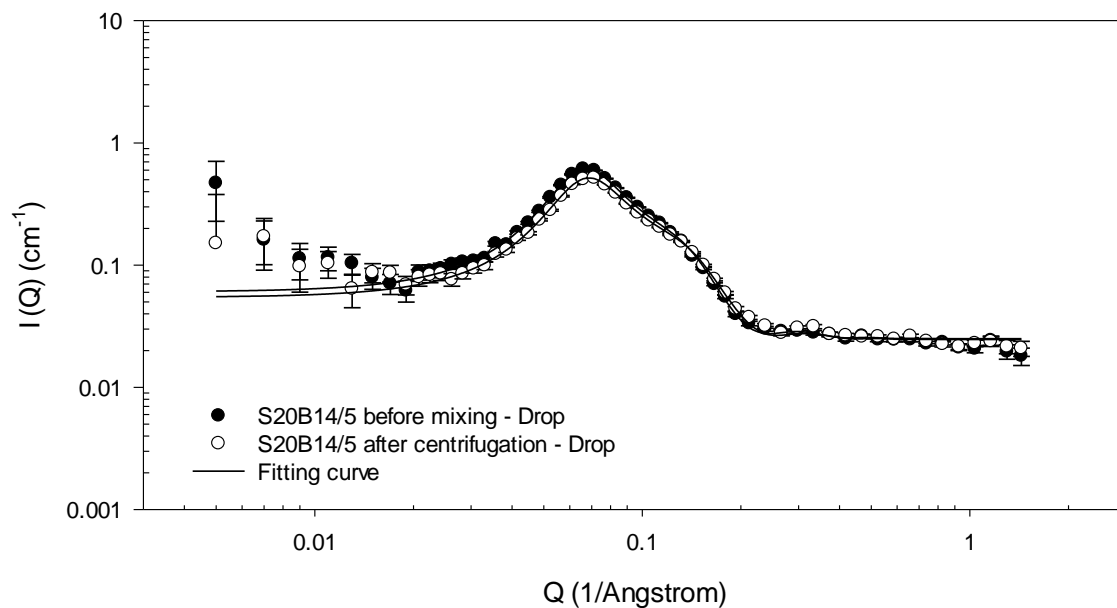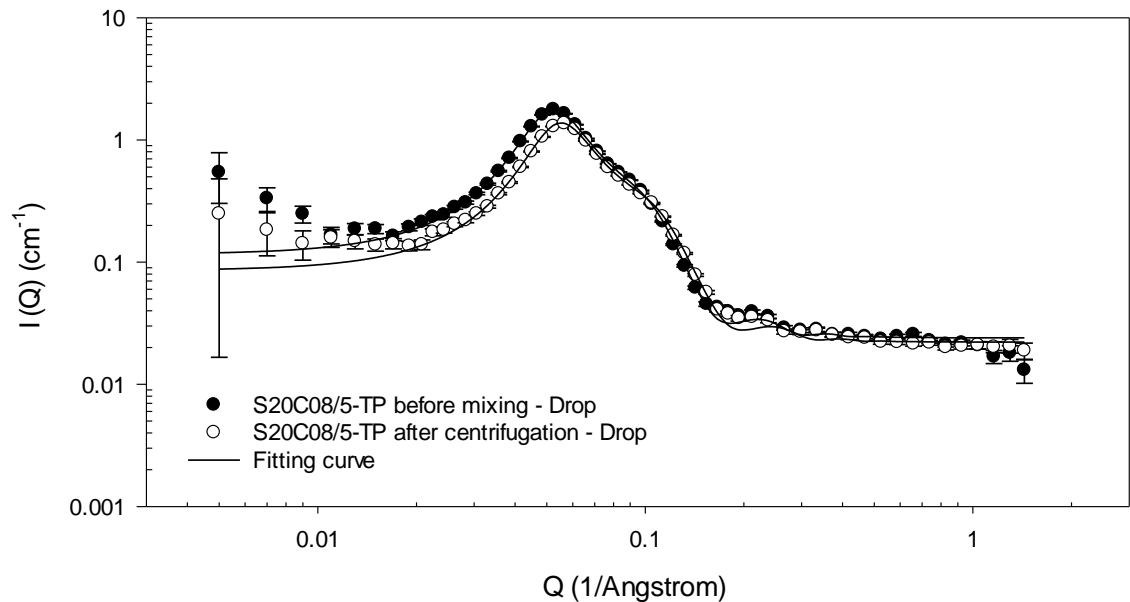

Figure 5.19 SANS data and best fit for the drop contrast of S20C08/5-TP microemulsions before mixing with the griseofulvin nanoparticles and after separation from the griseofulvin nanoparticles by centrifugation at 24 h. Measurements carried out on SANS2D at 25.0 ± 0.1 ℃.

In comparison to the NSMEs consisting of GF-NPs and EB-containing SDS-stabilised microemulsions, with a saturation amount of TP, the size of the SDS-stabilised microemulsions containing EC in the presence of TP after separation from the GF-NPs by centrifugation after 24 h contacting slightly decreased when compared to the microemulsions before mixing to the GF-NPs. This result, which was far less noticeable in the case of the EB-containing microemulsions, may be a consequence of the fact that EC forms a central core in the SDS microemulsion leads to a greater level of TP solubilisation. These results suggest the movement of some TP molecules from the microemulsion to the GF nanoparticles where they displace GF molecules in nanoparticle as a consequence of TP and GF being solubilised at the same location in the microemulsion. In agreement with this hypothesis, the solubility of GF and TP in the supernatant comprised of EC-containing microemulsions after separation from the GF-NPs had changed to a greater extent than was seen with the EB-containing microemulsions, as shown in Figures 5.3 and 5.4.

In summary, the size and shape of SDS-stabilised microemulsions containing either EB or EC in the absence of TP after 24 h contact with the GF-NPs, were unchanged compared to their parent microemulsions. In contrast, the corresponding microemulsions in the presence of TP did slightly alter after contact with the GF-NPs. Indeed in comparison to the SDS-stabilised microemulsions containing EC in the presence of TP, the corresponding EB-containing SDS-stabilised microemulsions incorporating TP may be more advantageous in terms of delivering poorly water-soluble drug as their size and shape after separation from the GF-NPs by centrifugation did not change much. In addition, the solubility of TP in EB-containing microemulsions after separation from the GF-NPs by centrifugation was comparable to its solubility in the corresponding microemulsions prior to their mixing with GF-NPs.

5.6.3 Small angle neutron scattering of griseofulvin nanoparticles in the presence of a microemulsion

In this study, contrast matching was used to make the various SDS-stabilised microemulsions 'invisible' to neutrons, thereby allowing the stability of the GF-NPs,

when in the form of a NSMEs for 24 h and the GF-NPs after their separation from the microemulsions after 24 h contact, to be established.

Figures 5.20 and 5.21 show the SANS profiles of the GF-NPs before mixing with either the S20B14/5 or S20B14/5-TP microemulsions, the GF-NPs when in the form of NSMEs over time and the GF-NPs after their separation from the EB-containing microemulsions, by centrifugation, after 24 h contact. Figures 5.22 and 5.23 show the SANS profiles of the GF-NPs prior to their mixing with either the S20C08/5 or S20C08/5-TP microemulsions, the GF-NPs when in the form of NSMEs over time and the GF-NPs after their separation from the EC-containing microemulsions, by centrifugation after 24 h contact.

Figure 5.20 SANS profiles of griseofulvin nanoparticles prior to their mixing with S20B14/5 microemulsions, the griseofulvin nanoparticles when in the form of NSMEs over 24 h and griseofulvin nanoparticles after their separation from the S20B14/5 microemulsion by centrifugation after 24 contact. Measurements carried out on SANS2D at 25.0 ± 0.1 °C.

Figure 5.21 SANS profiles of griseofulvin nanoparticles prior to their mixing with S20B14/5-TP microemulsions, the griseofulvin nanoparticles when in the form of NSMEs over 24 h and griseofulvin nanoparticles after their separation from the S20B14/5-TP microemulsion by centrifugation after 24 contact. Measurements carried out on SANS2D at 25.0 ± 0.1 ℃.

Figure 5.22 SANS profiles of griseofulvin nanoparticles prior to their mixing with S20C08/5 microemulsions, the griseofulvin nanoparticles when in the form of NSMEs over 24 h and griseofulvin nanoparticles after their separation from the S20C08/5 microemulsion by centrifugation after 24 contact. Measurements carried out on SANS2D at 25.0 ± 0.1 ℃.

Figure 5.23 SANS profiles of griseofulvin nanoparticles prior to their mixing with S20C08/5-TP microemulsions, the griseofulvin nanoparticles when in the form of NSMEs over 24 h and griseofulvin nanoparticles after their separation from the S20C08/5-TP microemulsion by centrifugation after 24 contact. Measurements carried out on SANS2D at 25.0 ± 0.1 ℃.

As stated in Chapter 4, it was not possible to successfully fit the SANS data obtained for GF-NPs prior to their mixing with the microemulsions. It was, however, possible to compare the slope of the SANS data obtained for the GF-NPs to see if the NPs had remained stable. Indeed, the slope of all the GF-NPs during remained constant over the Q range of 0.03 and 0.4 Å^{-1}, suggesting that no matter what the state of the GF-NPs was, they remained stable when in contact with the microemulsions. Furthermore, blowing up the SANS data (Figures 5.24-5.27) to more closely examine it, supported the comment that the slope of the SANS data for the GF-NPs remained constant. The main difference observed was the height of the slope, suggesting a 'loss' of NPs. This difference was particularly noticeable with the GF-NPs after their separation from the microemulsions, a process which required centrifugation of the GF-NPs, their dilution and re-suspension. Consequently, this difference may be a result of the 'sedimentation' and/or the incomplete 're-suspension' of a portion of the GF-NPs. Note that the SANS profiles obtained for the GF-NPs when in contact with the various microemulsions (i.e. S20B14/5, S20B14/5-TP, S20C08/5 and S20C08/5-TP) was much more variable. To confirm that the slope of the SANS data remained unchanged, the SANS data of the GF-NPs after their separation from the microemulsions were multiplied by factors to get

them to the same 'height'. In order to obtain the same 'height' the SANS data of the GF-NPs after separation from the various microemulsions (i.e. S20B14/5, S20B14/5-TP, S20C08/5 and S20C08/5-TP) were multiplied with 1.4, 1.7, 2.0 and 2.2 respectively. The results of this manipulation of the SANS data are shown in Figures 5.24 – 5.27. As can be clearly seen, the slopes obtained after manipulation of the SANS data were identical to the SANS slope obtained for the GF-NPS prior to their mixing with the microemulsions, suggesting that some GF-NPs were 'lost' during their separation from the microemulsions and re-suspension. Note that the GF-NPs were indeed slightly difficult to re-suspending after centrifugation. As the neutron scattering intensity is influenced by the volume of scattering particles, it is possible that the apparent decrease in scattering intensity of the GF-NPs after their separation from the microemulsions was due to a loss of some NPs leading to a decrease in the volume of the GF-NPs.
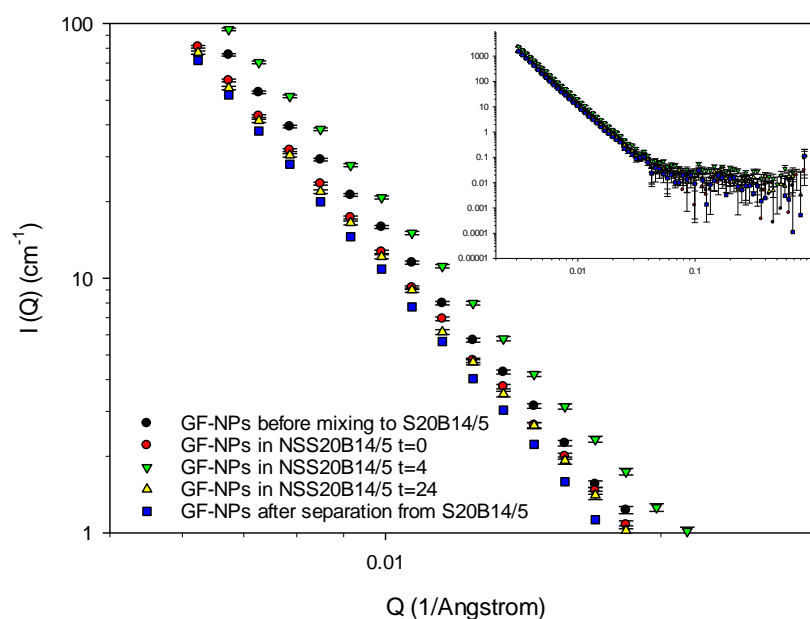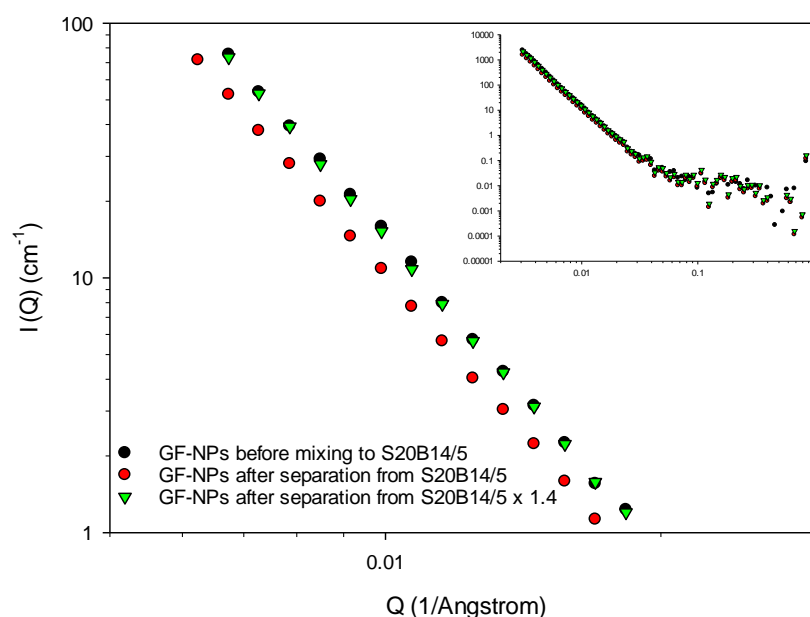

Figure 5.24 SANS profiles of griseofulvin nanoparticles prior to their mixing with the S20B14/5 microemulsions, the griseofulvin nanoparticles after their separation from the S20B14/5 microemulsions and the griseofulvin nanoparticles after their separation from the S20B14/5 microemulsions multiplied by 1.4.
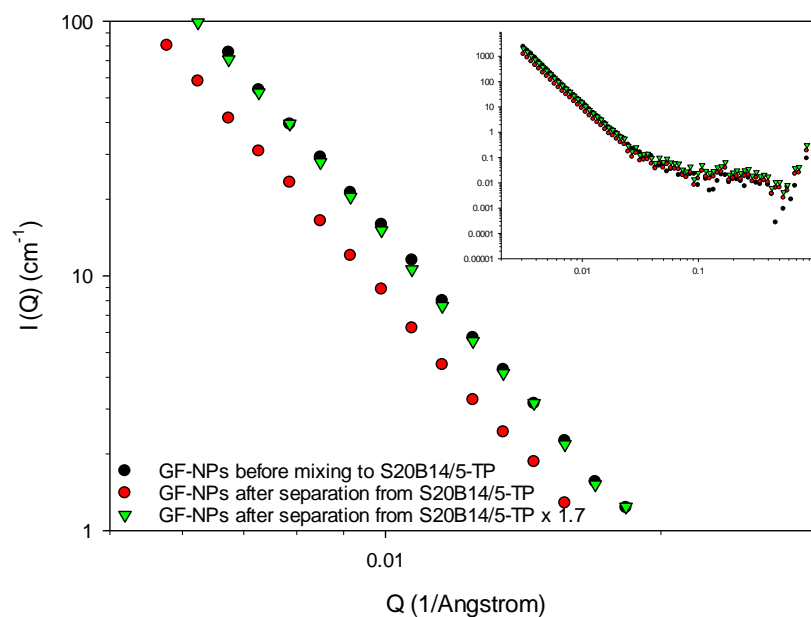
Figure 5.25 SANS profiles of griseofulvin nanoparticles prior to their mixing with the S20B14/5-TP microemulsions, the griseofulvin nanoparticles after their separation from the S20B14/5-TP microemulsions and the griseofulvin nanoparticles after their separation from the S20B14/5-TP microemulsions multiplied by 1.7.
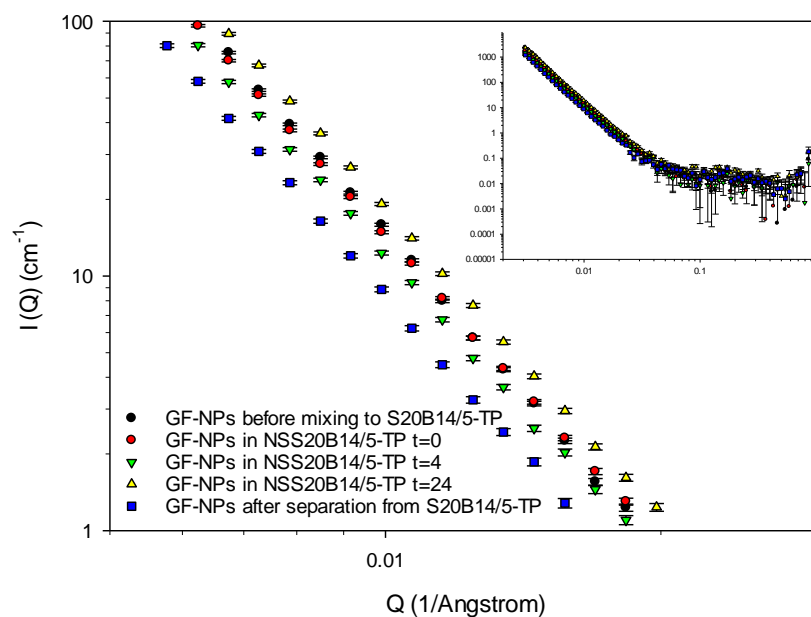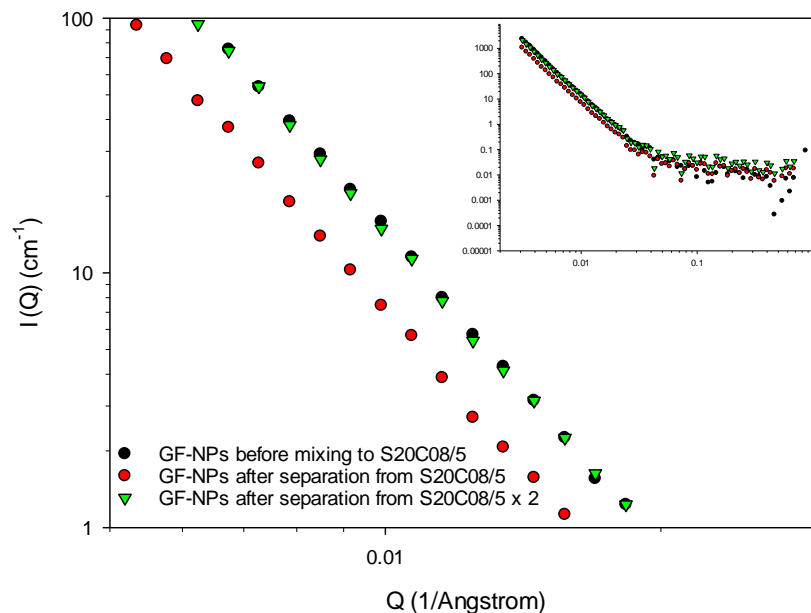

Figure 5.26 SANS profiles of griseofulvin nanoparticles prior to their mixing with the S20C08/5 microemulsions, the griseofulvin nanoparticles after their separation from the S20C08/5 microemulsions and the griseofulvin nanoparticles after their separation from the S20C08/5 microemulsions multiplied by 2.0.
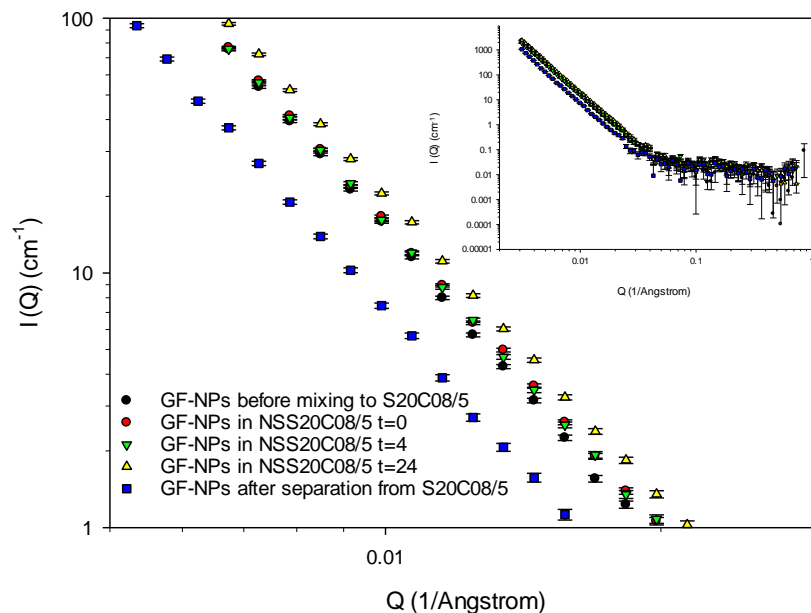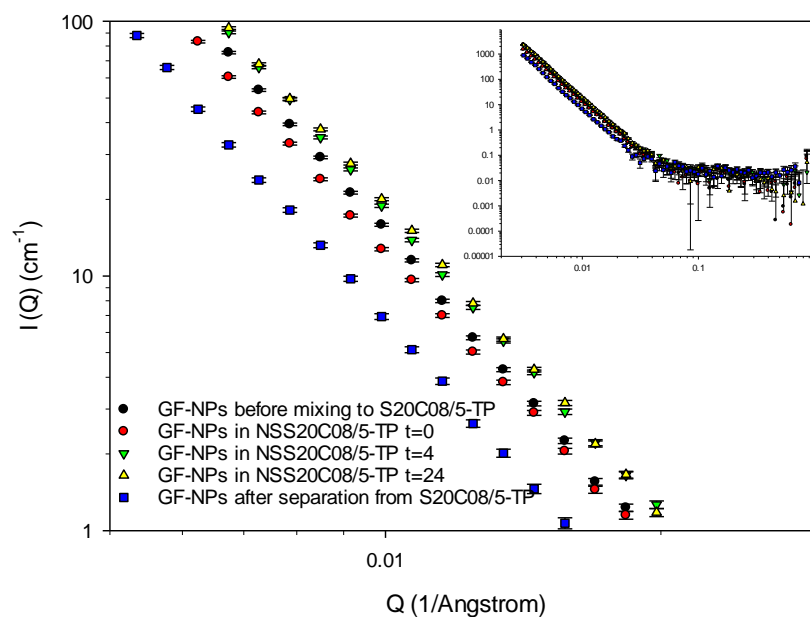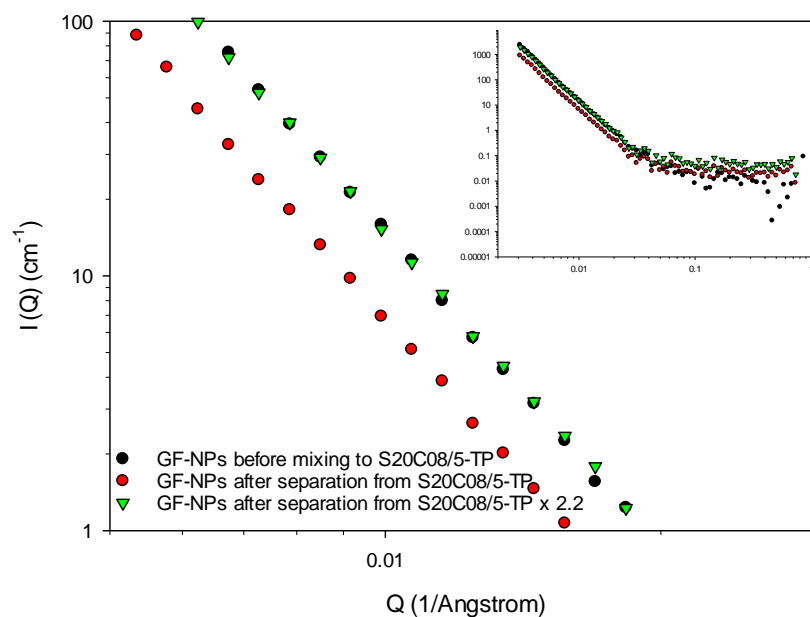
Figure 5.27 SANS profiles of griseofulvin nanoparticles prior to their mixing with the S20C08/5-TP microemulsions, the griseofulvin nanoparticles after their separation from the S20C08/5-TP microemulsions and the griseofulvin nanoparticles after their separation from the S20C08/5-TP microemulsions multiplied by 2.2.

A comparison of the SANS profiles obtained for the GF-NPs after their separation from the S20B14/5 microemulsions in both the presence and absence of a saturation amount of TP and the SANS profiles of the GF-NPs after their separation from S20C08/5 again both in the absence and presence of a saturation amount of TP by centrifugation showed that they were much less in intensity than the GF-NPs prior to their mixing with the microemulsions, suggesting that, regardless of both the absence and presence of TP, the SDS-stabilised microemulsions containing EC were harder to re-suspended the GF-NPs after contact with these microemulsions. In good agreement with the results of the PCS measurements of the particle size of the GF-NPs after their separation from microemulsions, the GF-NPs that had been in contact with the EC-containing SDS microemulsions, both with and without a saturation amount of TP increased in size to a greater extent than those GF-NPs that had been in contact with the EB-containing microemulsions, both with and without a saturation amount of TP. As a consequence, it might be concluded that the GF-NPs after their separation from the microemulsions, especially the EC-containing SDS microemulsions were much more difficult to re-disperse. It would be interesting; however, if other advanced techniques such as scanning electron microscope were used to further substantiate these observations.

Chapter 6 Conclusion and future prospects

6.1 Conclusion

Oil-in-water nanoemulsions, oil-in-water microemulsions and nanosuspensions are excellent candidates as drug delivery systems because of their many advantages, for example, their ability to protect drug, their ability to increase the bioavailability of hydrophobic drugs, their high drug solubilisation capacity, their long shelf life, and their ease of preparation and administration. Alongside this, combining drug therapies into one single, preparation has become a popular approach for the treatment of chronic diseases such as AIDS, diabetes and cardiovascular disease. As a consequence, the considerable benefits of oil-in-water nanoemulsions, oil-in-water microemulsions and nanosuspensions, have led us to the concept of combining two of these formulations into a single preparation for the delivery of two poorly-water soluble drugs for the personalisation of the medicine in respect to dosing. By combining two products in this way, it should be possible to reduce production costs, simplify disease management and improve patient compliance, amongst other things. The ultimate goal of this thesis, therefore, was proof of concept of the preparation of such novel combination formulations with a view to their intended use in personalised medicine.

This thesis reports the results of the formation of the novel combination formulations, termed either a nanosusponanoemulsion (NSNE) when the system is composed of an oil-in-water nanoemulsion and containing the model drug testosterone propionate (TP) and a nanosuspension of griseofulvin nanoparticles (GF-NPs) or a nanosuspomicroemulsion (NSME), when the formulation was comprised of an oil-in-water microemulsion containing the model drug testosterone propionate (TP) and a nanosuspension of griseofulvin nanoparticles (GF-NPs). In order to better understand the formation of these novel combination formulations, the physico-chemical behaviour of the component oil-in-water nanoemulsions, oil-in-water microemulsions and nanosuspension prior to their mixing was determined. The physico-chemical properties of either an oil-in-water nanoemulsion or an oil-in-water microemulsion and

nanosuspension in the form of a NSNE or NSME were determined. This characterization was performed using a wide variety of physico-chemical techniques, including phase behaviour, UV spectroscopy, phase inversion temperature, viscosity and dynamic light scattering. In addition, small angle neutron scattering in combination with contrast matching was extensively used to study the detailed molecular architecture of either the oil-in-water nanoemulsions or the oil-in-water microemulsions alone and in combination with a nanosuspension in the form of a NSNE and NSME.

The apparent solubility of the poorly water-soluble, low dose drug, testosterone propionate (TP), can be improved by its solubilisation within oil-in-water nanoemulsions composed of the nonionic surfactant as Brij 97 and containing the oil, glyceryl trioctanoate (TON) and in oil-in-water microemulsions composed of the anionic surfactant, sodium dodecyl sulphate (SDS), and containing one of the ethyl ester oils, namely ethyl butyrate (EB) or ethyl caprylate (EC). Indeed, many factors including the nature of the surfactant, the structure and molecular volume of oil have an influence on the drugs solubilisation capacity. Nanoparticles containing the poorly-water soluble, high dose drug, namely griseofulvin (GF) could be produced by wet bead milling using an anionic surfactant, here SDS. The optimum amount of SDS required for stable GF nanoparticle production was established to be 1.5 wt%.

Light scattering was used to study Brij 97-stabilised nanoemulsions, with and without a saturation amount of TP. (Note that SDS-stabilised microemulsions are practically very difficult to study using light scattering due to their very small size and highly charged nature.) The light scattering measurements indicated that the particle size of the Brij 97-stabilised nanoemulsions increased with increasing oil concentration and in the presence of a saturation amount of TP. In terms of nanoemulsions stability, Brij 97-stabilised nanoemulsion containing 0.3 wt% of TON was found to be more stable than those containing 0.5 wt% TON due to a growth in size of the latter nanoemulsions over time, most probably due to Ostwald ripening.

After mixing either Brij 97-stabilised nanoemulsions or SDS-stabilised microemulsions with the GF-NPs, the solubility of TP in the case of Brij 97-stabilised nanoemulsion containing the low concentration of TON before and after mixing with the GF-NPs was about the same suggesting that TP and GF might be incorporated in different sites in Brij 97-stabilised nanoemulsion containing low amounts of TON. While the solubility

of TP in SDS-stabilised microemulsions containing either EB or EC after mixing with the GF-NPs was less than the solubility of TP in the same microemulsions prior to their mixing with the GF-NPs, suggesting that TP and GF might be incorporated in the same site in SDS-stabilised microemulsions.

In addition, the particle size of the GF-NPs when in the form of either a NSNE or NSME was determined by PCS, although light scattering has a major limitation when measuring particle size in turbid samples. In addition, assessing the particle sizes of the NSNEs and NSMEs using light scattering is complicated due to the presence in these novel combination formulations of two populations of particle size. As a consequence, small angle neutron scattering (SANS) was used to determine the particle size of the Brij 97-stabilised nanoemulsions, the SDS-stabilised microemulsions and the GF-NPs *in situ* in the form of a NSNE or a NSME using contrast matching.

Both the shape and size of either Brij 97-stabilised nanoemulsions or SDS-stabilised microemulsions when in the form a NSNE or a NSME using contrast matching were determined by SANS. The results showed that the shape of Brij 97-stabilised nanoemulsions were oblate ellipsoid while the shape of SDS-stabilised microemulsions were prolate ellipsoid. Furthermore, the droplet size of the Brij 97-stabilised nanoemulsions increased in size as the concentration of the oil was increased and in the presence of a saturation amount of TP. The droplet size of the SDS-stabilised microemulsions containing either EB or EC was larger in a presence of a saturation amount of TP. In addition, the SANS experiments showed that the apparent drop size of the Brij 97-stabilised nanoemulsion containing the low amount of TON did not change after separation from the GF-NPs for 24 h compared to their size prior to mixing with the GF-NPs. In contrast, however, the size of the SDS-stabilised microemulsions containing EC after separation from the GF-NPs for 24 h, slightly decreased when compared to their size prior to mixing with the GF-NPs. This size decrease was far less noticeable in the case of the EB-containing microemulsions. Moreover, the size of the GF-NPs after separation from either the Brij 97-stabilised nanoemulsion containing the low amount of TON or the SDS-stabilised microemulsions containing either EB or EC did not change, even though the scattering intensity of the GF-NPs fluctuated due to the difficulty of re-suspending the GF-NPs. It can be concluded, however, that the GF-NPs that had been in contact with the Brij 97-stabilised nanoemulsion containing a low

amount of TON were re-suspended easier than those that had been in the presence of SDS-stabilised microemulsions containing either EB or EC.

In conclusion, the studies detailed in the present thesis confirm the proof of principle of the novel combination formulations (i.e. the NSNE and the NSME). Overall, based on a consideration of particle size, particle size stability and drug solubilisation capacity of the novel system, the NSNE comprising an oil-in-water nanoemulsion comprising of 2.4 wt% of Brij 97 and 0.3 wt% of TON when mixed with the GF-NPs stabilised by 1.5 wt% SDS were the most promising combination formulation. This combination formulation might be useful for the delivery of two poorly water-soluble drugs in one preparation suitable for use in personalised medicine.

6.2 Future prospects

In addition to the novel combination formulations developed in the present study, a short study using a second high dose drug, namely indomethacin (IND), and low dose drug, namely testosterone propionate (TP), was performed. This novel combination formulation was composed of indomethacin nanoparticles (IND-NPs) stabilised by 1.5 wt% of the nonionic polymer namely polyvinylpyrrolidone 30 (PVP 30) and an oil-in-water nanoemulsion stabilised by the nonionic surfactant, Brij 97, and glyceryl trioctanoate (TON) as oil and incorporating the poorly-water soluble drug, TP. Observations from this preliminary study showed that the particle size of the IND-NPs as determined by PCS when in the form of a combination formulation was the same as prior to their mixing with the nanoemulsion. This result might be a consequence of the fact that both stabilisers used were both nonionic molecules. In contrast, however, the particle size of the nanoemulsion after contact with the IND-NPs was increased compared to its size prior to mixing with the IND-NPs. Interestingly in terms of drug solubilisation, the solubility of TP in the nanoemulsions after contact with the IND-NPs remained constant compared to the solubility of TP in the nanoemulsions prior to their mixing with the IND-NPs. Again this observation might be a consequence of the fact that both stabilisers are nonionic molecules, either a surfactant or a polymer coupled with differences in the location of IND and TP in nanoemulsion droplets. These results

also support the importance of carefully formulating these novel combination formulations.

Based on the results reported in the thesis a series of preliminary guidelines can be drawn up to successfully formulate the novel combination formulations:

a) the amount of drug incorporated in the nanoemulsion/microemulsion formulations should be more than the minimum required for a patient,

b) the stabiliser used for nanoemulsion production should not be as same as that used to stabilise the nanoparticle,

c) the stabiliser used for nanoparticle formation should not be used to prepare either the nanoemulsions or the microemulsions,

d) both of the poorly-water soluble drugs should not be solubilised in the same location in the nanoemulsion or microemulsion and

e) the greater the water insolubility of the drug, the more appropriate it is to be incorporated in the novel combination formulation.

The goal of personalised medicine is the right drug for the right person at the right time in order to avoid drug adverse reactions, to eliminate invalid therapy, to improve efficiency of treatments, and thereby achieving optimal health outcomes. In order to exploit the benefits of personalised medicine, different dose combinations will be required for different patients. The novel combination formulations present in the present thesis aims to do just that. It would be of benefit if the two parent preparations (i.e. a nanoemulsion/microemulsion and a nanosuspension) could be in the form of an anhydrous preparation, which could be reconstituted upon the addition of water. Freeze-drying is one means of preparing anhydrous pre-concentrate forms of both the nanoemulsion/microemulsions and nanosuspension. The advantages of this would be the ability to reconstitute the original liquid systems after storage in a dry form which would reduce the cost of transportation and allow a longer shelf life. Consequently, a preparation of anhydrous forms of these two formulations (i.e. a nanoemulsion/microemulsion and a nanosuspension) would be of interest in further studies.

Furthermore, additional possible studies could usually focus on:

a) gaining an understanding of the interactions between stabilisers from the different component formulations.

b) varying the ratio of the amount of the oil-in-water nanoemulsion or the oil-in-water microemulsion and the nanosuspension to optimize the formulation for use in personalised medicine.

c) examining a range of poorly water-soluble drugs that could be incorporated within either the oil-in-water nanoemulsion or the nanosuspension in order to understand the influence of the drugs on the stability of the novel combination systems. Table 6.1 shows examples of combinations of high dose drug and low dose drug on the market to treat patients with diabetes type II, HIV and hypertension using oral administration. The most interesting combination to study would be the combination of verapamil and trandolapril as their solubility in water in Table 6.1 are the lowest in the table at 0.00394 and 0.0207 mg/mL, respectively.

Table 6.1 Examples of high dose drug and low dose drug combinations for oral administration in the market

Disease	Brand name	Combination of drugs	dosage
Diabetes type II	Kazano	alogliptin /metformin	12.5 mg/500 mg
			12.5 mg/1000 mg
	Invokamet	canagliflozin/metformin	50 mg/500 mg
	Janumet	sitagliptin/metformin	50 mg/500 mg
HIV	Eviplera	rilpivirine/emtricitabine/ tenofovir disoproxil	25 mg/200 mg/ 245 mg
Hypertensive	Aldoril	methyldopa/ hydrochlorothiazide	250 mg/15 mg,
			250 mg/25 mg,
			500 mg/30 mg,
			500 mg/50 mg
	Tarka	verapamil/trandolapril	180 mg/2 mg,
			240 mg/1 mg,
			240 mg/2 mg

An understanding of these properties should enable us to more successfully formulate the combination formulations containing two poorly water-soluble drugs for use in personalised medicine.

References

Ali M.S., Alam M.S., Alam N., Siddiqui M.R. (2014). Preparation, Characterization and Stability Study of Dutasteride Loaded Nanoemulsion for Treatment of Benign Prostatic Hypertrophy. Iranian Journal of Pharmaceutical Research 13: 1125-1140.

Allen D.T., Saaka Y., Lawrence M.J., Lorenz C.D. (2014). Atomistic description of the solubilisation of testosterone propionate in a sodium dodecyl sulfate micelle. J Phys Chem B 118(46): 13192-13201.

Anton N., Benoit J.-P., Saulnier P. (2008). Design and production of nanoparticles formulated from nano-emulsion templates—A review. Journal of Controlled Release 128(3): 185-199.

Araújo F.A., Kelmann R.G., Araújo B.V., Finatto R.B., Teixeira H.F., Koester L.S. (2011). Development and characterization of parenteral nanoemulsions containing thalidomide. European Journal of Pharmaceutical Sciences 42(3): 238-245.

Arleth L., Pedersen J.S. (2001). Droplet polydispersity and shape fluctuations in AOT [bis (2-ethylhexyl) sulfosuccinate sodium salt] microemulsions studied by contrast variation small-angle neutron scattering. Physical Review E 63(6): 061406.

Arunkumar N., Deecaraman M., Rani C. (2009). Nanosuspension technology and its applications in drug delivery. Asian journal of pharmaceutics 3(3): 168.

Ashcroft N.W., Lekner J. (1966). Structure and Resistivity of Liquid Metals. Physical Review 145(1): 83-90.

Aveyard R., Binks B.P., Fletcher P.D.I. (1989). Interfacial tensions and aggregate structure in pentaethylene glycol monododecyl ether/oil/water microemulsion systems. Langmuir 5(5): 1210-1217.

Aveyard R., Lawless T.A. (1986). Interfacial tension minima in oil-water-surfactant systems. Systems containing pure non-ionic surfactants, alkanes and inorganic salts. Journal of the Chemical Society, Faraday Transactions 1: Physical Chemistry in Condensed Phases 82(9): 2951-2963.

References

Basa S., Muniyappan T., Karatgi P., Prabhu R., Pillai R. (2008). Production and In Vitro Characterization of Solid Dosage form Incorporating Drug Nanoparticles. Drug Development and Industrial Pharmacy 34(11): 1209-1218.

Bergenholtz J., Romagnoli A.A., Wagner N.J. (1995). Viscosity, Microstructure, and Interparticle Potential of AOT/H2O/n-Decane Inverse Microemulsions. Langmuir 11(5): 1559-1570.

Bergström M., Pedersen J.S. (1999). Structure of pure SDS and DTAB micelles in brine determined by small-angle neutron scattering (SANS). Physical Chemistry Chemical Physics 1(18): 4437-4446.

Berr S.S., Coleman M.J., Jones R.R.M., Johnson J.S. (1986). Small-angle neutron scattering study of the structural effects of substitution of tetramethylammonium for sodium as the counterion in dodecyl sulfate micelles. The Journal of Physical Chemistry 90(24): 6492-6499.

Berr S.S., Jones R.R. (1989). Small-angle neutron scattering from aqueous solutions of sodium perfluorooctanoate above the critical micelle concentration. The Journal of Physical Chemistry 93(6): 2555-2558.

Bivas-Benita M., Oudshoorn M., Romeijn S., van Meijgaarden K., Koerten H., van der Meulen H., et al. (2004). Cationic submicron emulsions for pulmonary DNA immunization. Journal of Controlled Release 100(1): 145-155.

Bohdanecky M. (1983). New method for estimating the parameters of the wormlike chain model from the intrinsic viscosity of stiff-chain polymers. Macromolecules 16(9): 1483-1492.

Brown J.C., Pusey P., Dietz R. (1975). Photon correlation study of polydisperse samples of polystyrene in cyclohexane. The journal of chemical physics 62(3): 1136-1144.

Capek I. (2004). Degradation of kinetically-stable o/w emulsions. Adv Colloid Interface Sci 107(2–3): 125-155.

References

Caponetti E., Chillura-Martino D., Pedone L. (2004). Partitioning of macrocyclic compounds in a cationic and an anionic micellar solution: A small-angle neutron scattering study. Langmuir 20(10): 3854-3862.

Carlota O.R.-Y., Adalberto P.-J., Leoberto C.T. (2005). Micellar solubilization of drugs. Jounal of Pharm Pharmaceut Sci 2(8): 147-163.

Chen H., Khemtong C., Yang X., Chang X., Gao J. (2011). Nanonization strategies for poorly water-soluble drugs. Drug discovery today 16(7): 354-360.

Chen S.J., Evans D.F., Ninham B.W., Mitchell D.J., Blum F.D., Pickup S. (1986). Curvature as a determinant of microstructure and microemulsions. The Journal of Physical Chemistry 90(5): 842-847.

Chen Y., Liu J., Yang X., Zhao X., Xu H. (2005). Oleanolic acid nanosuspensions: preparation, in-vitro characterization and enhanced hepatoprotective effect. Journal of Pharmacy and Pharmacology 57(2): 259-264.

Chingunpituk J. (2011). Nanosuspension technology for drug delivery. Walailak Journal of Science and Technology (WJST) 4(2): 139-153.

Clogston J.D., Patri A.K. (2011). Zeta potential measurement. Characterization of nanoparticles intended for drug delivery: 63-70.

Cooper E.R. (2010). Nanoparticles: A personal experience for formulating poorly water soluble drugs. Journal of Controlled Release 141(3): 300-302.

Corti M., Minero C., Degiorgio V. (1984). Cloud point transition in nonionic micellar solutions. The Journal of Physical Chemistry 88(2): 309-317.

Das S., Suresh P.K. (2011). Nanosuspension: a new vehicle for the improvement of the delivery of drugs to the ocular surface. Application to amphotericin B. Nanomedicine: Nanotechnology, Biology and Medicine 7(2): 242-247.

Date A.A., Patravale V.B. (2004). Current strategies for engineering drug nanoparticles. Current Opinion in Colloid & Interface Science 9(3-4): 222-235.

References

Debye P., Bueche A.M. (1948). Intrinsic Viscosity, Diffusion, and Sedimentation Rate of Polymers in Solution. The Journal of Chemical Physics 16(6): 573-579.

Delgado Á.V., González-Caballero F., Hunter R., Koopal L., Lyklema J. (2007). Measurement and interpretation of electrokinetic phenomena. Journal of colloid and interface science 309(2): 194-224.

Deminiere B., Colin A., Calderon F.L., Bibette J. (1998). Chapter 8 Lifetime and Destruction of Concentrated Emulsions Undergoing Coalescence. In: (ed)^(eds). Modern Aspects of Emulsion Science, edn: The Royal Society of Chemistry. p^pp 261-291.

Devi S., Pokhriyal N.K. (2003). Microemulsion-Based Viscosity Index Improvers. In: Mittal KL, Shah DO (ed)^(eds). Adsorption and aggregation of surfactants in solution, edn, Vol. 109. New York: Marcel Dekker, Inc. p^pp 431-451.

Djekic L., Primorac M. (2008). The influence of cosurfactants and oils on the formation of pharmaceutical microemulsions based on PEG-8 caprylic/capric glycerides. International Journal of Pharmaceutics 352(1–2): 231-239.

El-Badry M., Fetih G., Fathy M. (2009). Improvement of solubility and dissolution rate of indomethacin by solid dispersions in Gelucire 50/13 and PEG4000. Saudi Pharmaceutical Journal 17(3): 217-225.

Elworthy P.H., Macfarlane C.B. (1965). The physical chemistry of some non-ionic detergents*. Journal of Pharmacy and Pharmacology 17(2): 65-82.

Engels T., Förster T., Von Rybinski W. (1995). The influence of coemulsifier type on the stability of oil-in-water emulsions. Colloids and Surfaces A: Physicochemical and Engineering Aspects 99(2): 141-149.

Engelskirchen S., Elsner N., Sottmann T., Strey R. (2007). Triacylglycerol microemulsions stabilized by alkyl ethoxylate surfactants—A basic study: Phase behavior, interfacial tension and microstructure. Journal of Colloid and Interface Science 312(1): 114-121.

References

Ericsson C.A., Söderman O., Garamus V.M., Bergström M., Ulvenlund S. (2004). Effects of Temperature, Salt, and Deuterium Oxide on the Self-Aggregation of Alkylglycosides in Dilute Solution. 1. n-Nonyl-β-d-glucoside. Langmuir 20(4): 1401-1408.

Ericsson C.A., Söderman O., Garamus V.M., Bergström M., Ulvenlund S. (2005). Effects of Temperature, Salt, and Deuterium Oxide on the Self-Aggregation of Alkylglycosides in Dilute Solution. 2. n-Tetradecyl-β-d-maltoside. Langmuir 21(4): 1507-1515.

Fernandez P., André V., Rieger J., Kühnle A. (2004). Nano-emulsion formation by emulsion phase inversion. Colloids and Surfaces A: Physicochemical and Engineering Aspects 251(1–3): 53-58.

Florence A.T., Arunothayanun P., Kiri S., Bernard M.-S., Uchegbu I.F. (1999). Some Rheological Properties of Nonionic Surfactant Vesicles and the Determination of Surface Hydration. The Journal of Physical Chemistry B 103(11): 1995-2000.

Florence A.T., Attwood D. (1998). *Physicochemical Principles of Pharmcy*. 3 edn. PALGRAVE: New York.

Forgiarini A., Esquena J., González C., Solans C. (2001a). Formation and stability of nano-emulsions in mixed nonionic surfactant systems. In: (ed)^(eds). Trends in colloid and interface science XV, edn: Springer. p^pp 184-189.

Forgiarini A., Esquena J., González C., Solans C. (2001b). Formation of Nano-emulsions by Low-Energy Emulsification Methods at Constant Temperature. Langmuir 17(7): 2076-2083.

Forster T.H., Schambil F., Tesmann H. (1990). Emulsification by the phase inversion temperature method: the role of self-bodying agents and the influence of oil polarity. International Journal of Cosmetic Science 12(5): 217-227.

Freire J.M., Domingues M.M., Matos J., Melo M.N., Veiga A.S., Santos N.C., et al. (2011). Using zeta-potential measurements to quantify peptide partition to lipid membranes. European Biophysics Journal 40(4): 481-487.

References

Gaikwad S.G., Pandit A.B. (2008). Ultrasound emulsification: effect of ultrasonic and physicochemical properties on dispersed phase volume and droplet size. Ultrasonics sonochemistry 15(4): 554-563.

Gao L., Liu G., Ma J., Wang X., Zhou L., Li X., et al. (2013). Application of drug nanocrystal technologies on oral drug delivery of poorly soluble drugs. Pharmaceutical research 30(2): 307-324.

García de la Torre J., del Rio Echenique G., Ortega A. (2007). Improved Calculation of Rotational Diffusion and Intrinsic Viscosity of Bead Models for Macromolecules and Nanoparticles. The Journal of Physical Chemistry B 111(5): 955-961.

Ghadimi A., Saidur R., Metselaar H.S.C. (2011). A review of nanofluid stability properties and characterization in stationary conditions. International Journal of Heat and Mass Transfer 54(17-18): 4051-4068.

Ghosh P.K., Majithiya R.J., Umrethia M.L., Murthy R.S. (2006). Design and development of microemulsion drug delivery system of acyclovir for improvement of oral bioavailability. Aaps Pharmscitech 7(3): E172-E177.

Glenn K., Bommel A., Bhattacharya S.C., Palepu R.M. (2005). Self aggregation of binary mixtures of sodium dodecyl sulfate and polyoxyethylene alkyl ethers in aqueous solution. Colloid and Polymer Science 283(8): 845-853.

Goodwin D.J. Polymer-stabilised drug nanoparticles. Ph.d. Thesis, University of London, 2006.

Griffiths P.C., Paul A., Khayat Z., Heenan R.K., Ranganathan R., Grillo I. (2005). A small-angle neutron scattering study of biologically relevant mixed surfactant micelles comprising 1,2-diheptanoyl-sn-phosphatidylcholine and sodium dodecyl sulfate or dodecyltrimethylammonium bromide. Soft Matter 1(2): 152.

Han J., Zhang X., Zhou Y., Ning Y., Wu J., Liang S., et al. (2012). Fabrication of CdTe nanoparticles-based superparticles for an improved detection of Cu 2+ and Ag+. Journal of Materials Chemistry 22(6): 2679-2686.

References

Harding S.E., Colfen H. (1995). Inversion Formulas for Ellipsoid of Revolution Macromolecular Shape Functions. Analytical Biochemistry 228(1): 131-142.

Hayter J., Penfold J. (1983). Determination of micelle structure and charge by neutron small-angle scattering. Colloid and Polymer Science 261(12): 1022-1030.

Hoffmann H., Ebert G. (1988). Surfactants, Micelles and Fascinating Phenomena. Angewandte Chemie International Edition in English 27(7): 902-912.

Hsieh C.-M. Investigations of pharmaceutical oil-in-water (O/W) microemulsions as drug delivery systems. Ph.d. Thesis, University of London, 2010.

Hu J., Johnston K.P., Williams III R.O. (2004). Nanoparticle engineering processes for enhancing the dissolution rates of poorly water soluble drugs. Drug development and industrial pharmacy 30(3): 233-245.

Huang Q., Yu H., Ru Q. (2010). Bioavailability and Delivery of Nutraceuticals Using Nanotechnology. Journal of Food Science 75(1): R50-R57.

Izquierdo P., Esquena J., Tadros T.F., Dederen C., Garcia M.J., Azemar N., et al. (2002). Formation and Stability of Nano-Emulsions Prepared Using the Phase Inversion Temperature Method. Langmuir 18(1): 26-30.

Izquierdo P., Esquena J., Tadros T.F., Dederen J.C., Feng J., Garcia-Celma M.J., et al. (2004). Phase Behavior and Nano-emulsion Formation by the Phase Inversion Temperature Method. Langmuir 20(16): 6594-6598.

Izquierdo P., Feng J., Esquena J., Tadros T.F., Dederen J.C., Garcia M.J., et al. (2005). The influence of surfactant mixing ratio on nano-emulsion formation by the pit method. Journal of colloid and interface science 285(1): 388-394.

Jacobs C., Müller R.H. (2002). Production and characterization of a budesonide nanosuspension for pulmonary administration. Pharmaceutical research 19(2): 189-194.

Jia L. (2005). Nanoparticle Formulation Increases Oral Bioavailability of Poorly Soluble Drugs: Approaches Experimental Evidences and Theory. Current nanoscience 1(3): 237-243.

References

Junyaprasert V.B., Morakul B. (2015). Nanocrystals for enhancement of oral bioavailability of poorly water-soluble drugs. Asian Journal of Pharmaceutical Sciences 10(1): 13-23.

Kabalnov A. (2001). Ostwald Ripening and Related Phenomena. Journal of Dispersion Science and Technology 22(1): 1-12.

Kapoor Y., Chauhan A. (2008). Ophthalmic delivery of Cyclosporine A from Brij-97 microemulsion and surfactant-laden p-HEMA hydrogels. International Journal of Pharmaceutics 361(1–2): 222-229.

Kassem M., Rahman A.A., Ghorab M., Ahmed M., Khalil R. (2007). Nanosuspension as an ophthalmic delivery system for certain glucocorticoid drugs. International journal of pharmaceutics 340(1): 126-133.

Kawabata Y., Wada K., Nakatani M., Yamada S., Onoue S. (2011). Formulation design for poorly water-soluble drugs based on biopharmaceutics classification system: basic approaches and practical applications. Int J Pharm 420(1): 1-10.

Keck C.M., Muller R.H. (2006). Drug nanocrystals of poorly soluble drugs produced by high pressure homogenisation. Eur J Pharm Biopharm 62(1): 3-16.

Kentish S., Wooster T., Ashokkumar M., Balachandran S., Mawson R., Simons L. (2008). The use of ultrasonics for nanoemulsion preparation. Innovative Food Science & Emerging Technologies 9(2): 170-175.

Khadka P., Ro J., Kim H., Kim I., Kim J.T., Kim H., et al. (2014). Pharmaceutical particle technologies: An approach to improve drug solubility, dissolution and bioavailability. Asian Journal of Pharmaceutical Sciences 9(6): 304-316.

Kim Y.I., Kim K.S., Park S.J., Park J.H., Woo J.S. (2013). Fixed dose combination formulation comprising losartan, amlodipine and hydrochlorothiazide: Google Patents.

King S.M. (1999). Small angle neutron scattering Vol. 171: John Wiley & Sons New York.

References

Ko C.J., Ko Y.J., Kim D.M., Park H.J. (2003). Solution properties and PGSE-NMR self-diffusion study of C18:1E10/oil/water system. Colloids and Surfaces A: Physicochemical and Engineering Aspects 216(1–3): 55-63.

Krishna A.K., Flanagan D.R. (1989). Micellar solubilization of a new antimalarial drug, β-arteether. Journal of Pharmaceutical Sciences 78(7): 574-576.

Ktistis G., Niopas I. (1998). A Study on the In-vitro Percutaneous Absorption of Propranolol from Disperse Systems. Journal of Pharmacy and Pharmacology 50(4): 413-418.

Kumar M., Pathak K., Misra A. (2009). Formulation and characterization of nanoemulsion-based drug delivery system of risperidone. Drug development and industrial pharmacy 35(4): 387-395.

Kuo C.-H., Chiang T.-F., Chen L.-J., Huang M.H. (2004). Synthesis of Highly Faceted Pentagonal- and Hexagonal-Shaped Gold Nanoparticles with Controlled Sizes by Sodium Dodecyl Sulfate. Langmuir 20(18): 7820-7824.

Kwade A. (1999). Wet comminution in stirred media mills - research and its practical application. Powder Technology 105: 14-20.

Lee K., Ye Y., Carr J., Karem K., D'souza M. (2011). Formulation, pharmacokinetics and biodistribution of Ofloxacin-loaded albumin microparticles and nanoparticles. Journal of microencapsulation 28(5): 363-369.

Leuner C., Dressman J. (2000). Improving drug solubility for oral delivery using solid dispersions. European Journal of Pharmaceutics and Biopharmaceutics 50(1): 47-60.

Leyden J K.K., Levy SF. (2001). The combination formulation of clindamycin 1% plus benzoyl peroxide 5% versus 3 different formulations of topical clindamycin alone in the reduction of Propionibacterium acnes. An in vivo comparative study. Am J Clin Dermatol. 2: 263-266.

Lim J.K., Majetich S.A., Tilton R.D. (2009). Stabilization of superparamagnetic iron oxide core− gold shell nanoparticles in high ionic strength media. Langmuir 25(23): 13384-13393.

References

Lipinski C.A., Lombardo F., Dominy B.W., Feeney P.J. (2001). Experimental and computational approaches to estimate solubility and permeability in drug discovery and development settings. Adv Drug Deliv Rev 64, Supplement: 4-17.

López Martínez M.C., Díaz Baños F.G., Ortega Retuerta A., García de la Torre J. (2003). Multiple Linear Least-Squares Fits with a Common Intercept: Determination of the Intrinsic Viscosity of Macromolecules in Solution. Journal of Chemical Education 80(9): 1036.

Lou H., Zhang X., Gao L., Feng F., Wang J., Wei X., et al. (2009). In vitro and in vivo antitumor activity of oridonin nanosuspension. International journal of pharmaceutics 379(1): 181-186.

Luckey M. (2014). Membrane structural biology with biochemical and biophysical foundations. edn. Cambridge university press: the United States of America.

Maestro A., Solè I., González C., Solans C., Gutiérrez J.M. (2008). Influence of the phase behavior on the properties of ionic nanoemulsions prepared by the phase inversion composition method. Journal of colloid and interface science 327(2): 433-439.

Malcolmson C., Lawrence M.J. (1995). Three-component non-ionic oil-in-water microemulsions using polyoxyethylene ether surfactants. Colloids and Surfaces B: Biointerfaces 4(2): 97-109.

Malcolmson C., Satra C., Kantaria S., Sidhu A., Jayne Lawrence M. (1998). Effect of Oil on the Level of Solubilization of Testosterone Propionate into Nonionic Oil-in-Water Microemulsions. Journal of Pharmaceutical Sciences 87(1): 109-116.

Malcolmson C.A. The physicochemical properties of nonionic oil-in-water microemulsions. Ph.d. Thesis, University of London, 1993.

Martis V., Nikitenko S., Sen S., Sankar G., van Beek W., Filinchuk Y., et al. (2011). Effects of X-rays on Crystal Nucleation in Lithium Disilicate. Crystal Growth & Design 11(7): 2858-2865.

MarzAn L.L., Samseth J., Quintela M.L. (1993). Structure of concentrated nonionic surfactant microemulsions studied by small angle neutron scattering. Le Journal de Physique IV 3(C8): C8-165-C168-168.

Mason T.G., Wilking J., Meleson K., Chang C., Graves S. (2006). Nanoemulsions: formation, structure, and physical properties. Journal of Physics: Condensed Matter 18(41): R635.

Masuelli M.A. (2013). Dextrans in Aqueous Solution. Experimental Review on Intrinsic Viscosity Measurements and Temperature Effect. Journal of Polymer and Biopolymer Physics Chemistry 1(1): 13-21.

Mathis G., Leempoel P., Ravey J.C., Selve C., Delpuech J.J. (1984). A novel class of nonionic microemulsions: fluorocarbons in aqueous solutions of fluorinated poly(oxyethylene) surfactants. Journal of the American Chemical Society 106(21): 6162-6171.

McClements D.J. (2012). Nanoemulsions versus microemulsions: terminology, differences, and similarities. Soft matter 8(6): 1719-1729.

Merisko-Liversidge E., Liversidge G.G., Cooper E.R. (2003). Nanosizing: a formulation approach for poorly-water-soluble compounds. European Journal of Pharmaceutical Sciences 18(2): 113-120.

Merisko-Liversidge E.M., Liversidge G.G. (2008). Drug Nanoparticles: Formulating Poorly Water-Soluble Compounds. Toxicologic Pathology 36(1): 43-48.

Mistry A., Stolnik S., Illum L. (2009). Nanoparticles for direct nose-to-brain delivery of drugs. International Journal of Pharmaceutics 379(1): 146-157.

Mohanraj V., Chen Y. (2006). Nanoparticles–a review. Trop J Pharm Res 5(1): 561-573.

Monduzzi M., Caboi F., Larché F., Olsson U. (1997). DDAB MicroemulsionsDependence on the Oil Chain Length. Langmuir 13(8): 2184-2190.

References

Morales D., Gutiérrez J.M., García-Celma M.J., Solans Y.C. (2003). A Study of the Relation between Bicontinuous Microemulsions and Oil/Water Nano-emulsion Formation. Langmuir 19(18): 7196-7200.

MOULIK, S. P. & PAUL, B. K. 1998. Structure, dynamics and transport properties of microemulsions. Advances in Colloid and Interface Science, 78, 99-195.

Mueller E.A., Kovarik J.M., van Bree J.B., Tetzloff W., Grevel J., Kutz K. (1994). Improved dose linearity of cyclosporine pharmacokinetics from a microemulsion formulation. Pharmaceutical research 11(2): 301-304.

Muller R.H., Becker R., Kruss B., Peters K. (1999). Pharmaceutical nanosuspensions for medicament administration as systems with increased saturation solubility and rate of solution: Google Patents.

Müller R.H., Jacobs C., Kayser O. (2001). Nanosuspensions as particulate drug formulations in therapy: Rationale for development and what we can expect for the future. Advanced Drug Delivery Reviews 47(1): 3-19.

Müller R.H., Jacobs C. (2002). Buparvaquone mucoadhesive nanosuspension: preparation, optimisation and long-term stability. International Journal of Pharmaceutics 237(1–2): 151-161.

Nagao M., Okabe S., Shibayama M. (2005). Small-angle neutron-scattering study on a structure of microemulsion mixed with polymer networks. J Chem Phys 123(14): 144909.

Nagarajan R., Shah K.M., Hammond S. (1982). Viscometric detection of sphere to cylinder transition and polydispersity in aqueous micellar solutions. Colloids and Surfaces 4(2): 147-162.

Nagarwal R.C., Kant S., Singh P., Maiti P., Pandit J. (2009). Polymeric nanoparticulate system: a potential approach for ocular drug delivery. Journal of Controlled Release 136(1): 2-13.

Narang A.S., Delmarre D., Gao D. (2007). Stable drug encapsulation in micelles and microemulsions. Int J Pharm 345(1-2): 9-25.

References

Ortega A., García de la Torre J. (2007). Equivalent Radii and Ratios of Radii from Solution Properties as Indicators of Macromolecular Conformation, Shape, and Flexibility. Biomacromolecules 8(8): 2464-2475.

Ozeki S., Ikeda S. (1980). The viscosity behavior of aqueous NaCl solutions of dodecyldimethylammonium chloride and the flexibility of its rod-like micelle. Journal of Colloid and Interface Science 77(1): 219-231.

Pamies R., Cifre J.G.H., Martínez M.d.C.L., de la Torre J.G. (2008). Determination of intrinsic viscosities of macromolecules and nanoparticles. Comparison of single-point and dilution procedures. Colloid and Polymer Science 286(11): 1223-1231.

Panmai S., Prud'homme R.K., Peiffer D.G. (1999). Rheology of hydrophobically modified polymers with spherical and rod-like surfactant micelles. Colloids and Surfaces A: Physicochemical and Engineering Aspects 147(1–2): 3-15.

Pedersen J.S. (1997). Analysis of small-angle scattering data from colloids and polymer solutions: modeling and least-squares fitting. Advances in Colloid and Interface Science 70: 171-210.

Penott-Chang E.K., Gouveia L., Fernández I.J., Müller A.J., Díaz-Barrios A., Sáez A.E. (2007). Rheology of aqueous solutions of hydrophobically modified polyacrylamides and surfactants. Colloids and Surfaces A: Physicochemical and Engineering Aspects 295(1–3): 99-106.

Pouton C.W. (2006). Formulation of poorly water-soluble drugs for oral administration: physicochemical and physiological issues and the lipid formulation classification system. Eur J Pharm Sci 29(3-4): 278-287.

Preu H., Zradba A., Rast S., Kunz W., Hardy E.H., Zeidler M.D. (1999). Small angle neutron scattering of D 2 O–Brij 35 and D 2 O–alcohol–Brij 35 solutions and their modelling using the Percus–Yevick integral equation. Physical Chemistry Chemical Physics 1(14): 3321-3329.

Rabinow B.E. (2004). Nanosuspensions in drug delivery. Nat Rev Drug Discov 3(9): 785-796.

References

Rao J., McClements D.J. (2011). Formation of flavor oil microemulsions, nanoemulsions and emulsions: influence of composition and preparation method. Journal of agricultural and food chemistry 59(9): 5026-5035.

Rao J., McClements D.J. (2012). Lemon oil solubilization in mixed surfactant solutions: Rationalizing microemulsion & nanoemulsion formation. Food Hydrocolloids 26(1): 268-276.

Rao J., McClements D.J. (2010). Stabilization of Phase Inversion Temperature Nanoemulsions by Surfactant Displacement. Journal of Agricultural and Food Chemistry 58(11): 7059-7066.

Rautio J., Kumpulainen H., Heimbach T., Oliyai R., Oh D., Jarvinen T., et al. (2008). Prodrugs: design and clinical applications. Nat Rev Drug Discov 7(3): 255-270.

Rübe A., Hause G., Mäder K., Kohlbrecher J. (2005). Core-shell structure of Miglyol/poly(d,l-lactide)/Poloxamer nanocapsules studied by small-angle neutron scattering. Journal of Controlled Release 107(2): 244-252.

Ruiz C.C., Aguiar J. (2000). Interaction, Stability, and Microenvironmental Properties of Mixed Micelles of Triton X100 and n-Alkyltrimethylammonium Bromides: Influence of Alkyl Chain Length. Langmuir 16(21): 7946-7953.

Runkana V., Somasundaran P., Kapur P. (2006). A population balance model for flocculation of colloidal suspensions by polymer bridging. Chemical Engineering Science 61(1): 182-191.

Santos J., Trujillo L.A., Calero N., Alfaro M.C., Muñoz J. (2013). Physical Characterization of a Commercial Suspoemulsion as a Reference for the Development of Suspoemulsions. Chemical Engineering & Technology 36(11): 1883-1890.

Schultz S., Wagner G., Urban K., Ulrich J. (2004). High-pressure homogenization as a process for emulsion formation. Chemical Engineering & Technology 27(4): 361-368.

Seebergh J.E., Berg J.C. (1994). Depletion flocculation of aqueous, electrosterically-stabilized latex dispersions. Langmuir 10(2): 454-463.

Serajuddin A.T.M. (1999). Solid dispersion of poorly water-soluble drugs: Early promises, subsequent problems, and recent breakthroughs. Journal of Pharmaceutical Sciences 88(10): 1058-1066.

Shafiq S., Shakeel F., Talegaonkar S., Ahmad F.J., Khar R.K., Ali M. (2007). Development and bioavailability assessment of ramipril nanoemulsion formulation. European Journal of Pharmaceutics and Biopharmaceutics 66(2): 227-243.

Shi J. (2002). Steric Stabilization.

Shinoda K., Arai H. (1964). The Correlation between Phase Inversion Temperature In Emulsion and Cloud Point in Solution of Nonionic Emulsifier. The Journal of Physical Chemistry 68(12): 3485-3490.

Solans C., Izquierdo P., Nolla J., Azemar N., Garcia-Celma M.J. (2005). Nano-emulsions. Current Opinion in Colloid & Interface Science 10(3–4): 102-110.

Somasundaran P., Fu E., Xu Q. (1992). Coadsorption of anionic and nonionic surfactant mixtures at the alumina-water interface. Langmuir 8(4): 1065-1069.

Stanley H.B., Banerjee D., van Breemen L., Ciston J., Liebscher C.H., Martis V., et al. (2014). X-ray irradiation induced reduction and nanoclustering of lead in borosilicate glass. CrystEngComm 16(39): 9331-9339.

Solè I., Solans C., Maestro A., González C., Gutiérrez J. (2012). Study of nano-emulsion formation by dilution of microemulsions. Journal of colloid and interface science 376(1): 133-139.

Tadros T., Izquierdo P., Esquena J., Solans C. (2004). Formation and stability of nano-emulsions. Adv Colloid Interface Sci 108–109: 303-318.

Tadros T.F. (1990). Disperse systems in pesticidal formulations. Advances in Colloid and Interface Science 32(2): 205-234.

Taylor P. (1998). Ostwald ripening in emulsions. Advances in Colloid and Interface Science 75(2): 107-163.

References

Thiagarajan P. (2011). Nanoemulsions for drug delivery through different routes. Research in Biotechnology 2(3).

Thurn T., Couderc S., Sidhu J., Bloor D.M., Penfold J., Holzwarth J.F., et al. (2002). Study of Mixed Micelles and Interaction Parameters for ABA Triblock Copolymers of the Type EOm−POn−EOm and Ionic Surfactants: Equilibrium and Structure. Langmuir 18(24): 9267-9275.

Tirop L.J. Polymer-surfactant stanilised drug nanoparticles. Ph.d. Thesis, University of London, 2012.

Tong K., Zhao C., Sun D. (2016). Formation of nanoemulsion with long chain oil by W/O microemulsion dilution method. Colloids and Surfaces A: Physicochemical and Engineering Aspects 497: 101-108.

Torchilin V.P. (2001). Structure and design of polymeric surfactant-based drug delivery systems. Journal of Controlled Release 73(2–3): 137-172.

Trotta M. (1999). Influence of phase transformation on indomethacin release from microemulsions. Journal of Controlled Release 60(2–3): 399-405.

Tscharnuter W. (2006). Photon Correlation Spectroscopy in Particle Sizing. Encyclopedia of Analytical Chemistry. , 15 September 2016 edn.

Valenta C., Schultz K. (2004). Influence of carrageenan on the rheology and skin permeation of microemulsion formulations. Journal of Controlled Release 95(2): 257-265.

Van Eerdenbrugh B., Van den Mooter G., Augustijns P. (2008). Top-down production of drug nanocrystals: Nanosuspension stabilization, miniaturization and transformation into solid products. International Journal of Pharmaceutics 364(1): 64-75.

Vasconcelos T., Sarmento B., Costa P. (2007). Solid dispersions as strategy to improve oral bioavailability of poor water soluble drugs. Drug Discov Today 12(23-24): 1068-1075.

Vass S., Torok T., Jakli G., Berecz E. (1989). Sodium alkyl sulfate apparent molar volumes in normal and heavy water: connection with micellar structure. The Journal of Physical Chemistry 93(17): 6553-6559.

Verma S., Kumar S., Gokhale R., Burgess D.J. (2011). Physical stability of nanosuspensions: Investigation of the role of stabilizers on Ostwald ripening. International Journal of Pharmaceutics 406(1–2): 145-152.

Wang H., Li Q., Reyes S., Zhang J., Xie L., Melendez V., et al. (2013). Formulation and particle size reduction improve bioavailability of poorly water-soluble compounds with antimalarial activity. Malar Res Treat 2013: 769234.

Wang L., Mutch K.J., Eastoe J., Heenan R.K., Dong J. (2008). Nanoemulsions Prepared by a Two-Step Low-Energy Process. Langmuir 24(12): 6092-6099.

Warisnoicharoen W. Pharmaceutical nonionic oil-in-water microemulsions. Ph.d. Thesis, University of London, 1998.

Warisnoicharoen W., Lansley A., Lawrence M.J. (2000a). Light-scattering investigations on dilute nonionic oil-in-water microemulsions. AAPS PharmSci 2(2): 16-26.

Warisnoicharoen W., Lansley A.B., Lawrence M.J. (2000b). Nonionic oil-in-water microemulsions: the effect of oil type on phase behaviour. International Journal of Pharmaceutics 198(1): 7-27.

Wasutrasawat P. Formation and physicochemical properties of nonionic oil-in-water nanoemulsions containing liquid and solid triglyceride. Ph.d. Thesis, Chulalongkorn University, 2011.

Whiddon C., Söderman O. (2001). Unusually Large Deuterium Isotope Effects in the Phase Diagram of a Mixed Alkylglucoside Surfactant/Water System. Langmuir 17(6): 1803-1806.

Williams RL C.T., Blume CD. (1984). Clinical experience with a new combination formulation of triamterene and hydrochlorothiazide (Maxzide) in patients with mild to moderate hypertension. Am J Med 77: 62-66.

References

Wooster T.J., Golding M., Sanguansri P. (2008). Impact of Oil Type on Nanoemulsion Formation and Ostwald Ripening Stability. Langmuir 24(22): 12758-12765.

Xu Q., Vasudevan T.V., Somasundaran P. (1991). Adsorption of anionic—nonionic and cationic—nonionic surfactant mixtures on kaolinite. Journal of Colloid and Interface Science 142(2): 528-534.

Xu R. (2008). Progress in nanoparticles characterization: Sizing and zeta potential measurement. Particuology 6(2): 112-115.

Yadollahi R., Vasilev K., Simovic S. (2015). Nanosuspension technologies for delivery of poorly soluble drugs. Journal of Nanomaterials 2015.

Yang L., Alexandridis P., Steytler D.C., Kositza M.J., Holzwarth J.F. (2000). Small-Angle Neutron Scattering Investigation of the Temperature-Dependent Aggregation Behavior of the Block Copolymer Pluronic L64 in Aqueous Solution. Langmuir 16(23): 8555-8561.

Yarnell A. (2012). Nanoparticles Boost Drug Solubility. Chemical & Engineering News Archive 90(4): 30-31.

Yeap S.P., Ahmad A.L., Ooi B.S., Lim J. (2012). Electrosteric Stabilization and Its Role in Cooperative Magnetophoresis of Colloidal Magnetic Nanoparticles. Langmuir 28(42): 14878-14891.

Zemb T., Charpin P. (1985). Micellar structure from comparison of X-ray and neutron small-angle scattering. Journal de Physique 46(2): 249-256.

Zhang R., Somasundaran P. (2006). Advances in adsorption of surfactants and their mixtures at solid/solution interfaces. Advances in Colloid and Interface Science 123–126: 213-229.

Appendix A Supplementary UV/VIS spectroscopy results

Calibration curve of griseofulvin in isopropanol by UV/Vis spectroscopy

Figure A1 and A2 showed the absorbance when scanning to find out the maximum wavelength at vary concentration of griseofulvin in isopropanol which were 2, 4, 6, 8, 10, 12 and 14 µg/ml. As the result, griseofulvin presented λ_{max} at 292 nm However, the absorbance when scanning to find out the maximum wavelength at vary concentration of testosterone propionate in isopropanol which were 5, 10, 15, 20, 25 and 30 µg/ml as shown in Figure A3 and A4. As the result, testosterone propionate presented λ_{max} at 240 nm. So that the wavelength at 292 and 240 nm will be chosen to measure the solubility of griseofulvin and testosterone propionate, respectively.
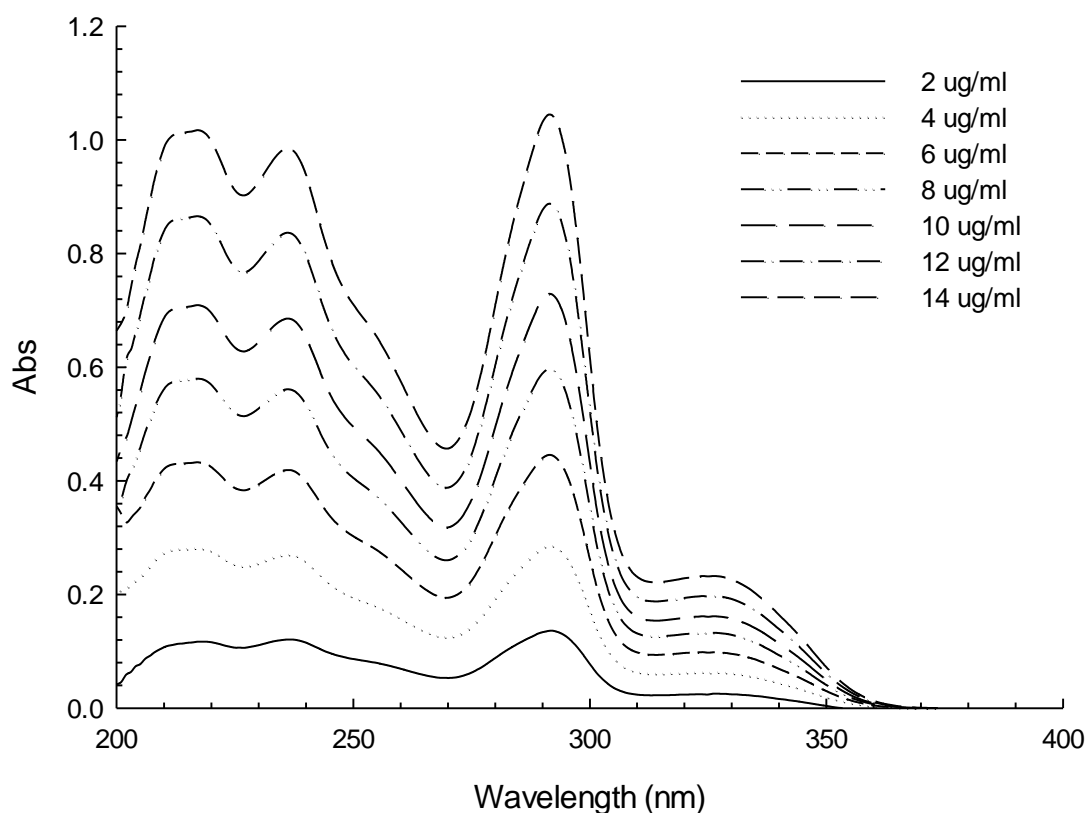

Figure A1 UV/Vis spectra of varying griseofulvin concentrations in isopropanol.
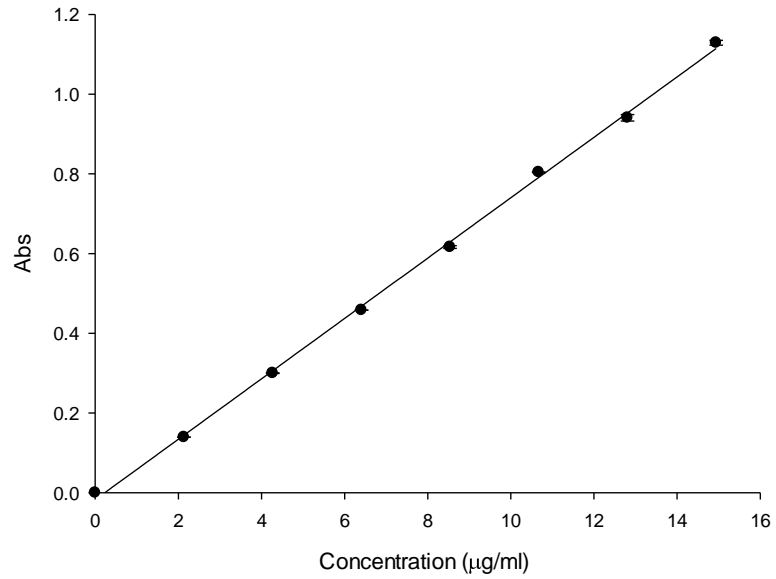
Figure A2 The absorbance of griseofulvin concentration in isopropanol at 2, 4, 6, 8, 10, 12 and 14 µg/ml at the wavelength 292 nm (mean ± SD, n=9), error bars within size of symbol.
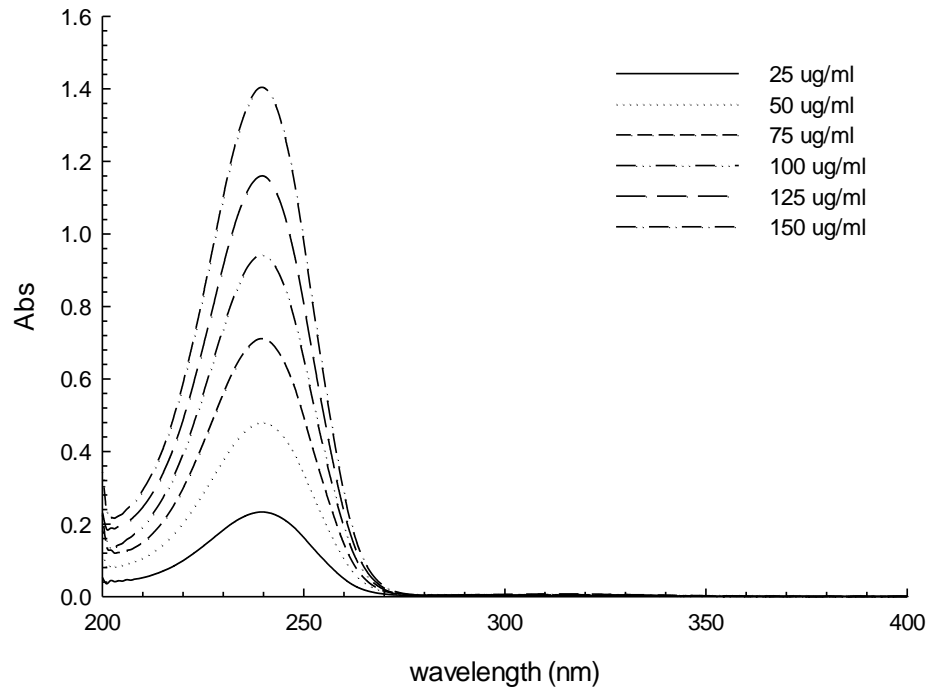

Figure A3 UV/Vis spectra of varying testosterone propionate concentrations in isopropanol.
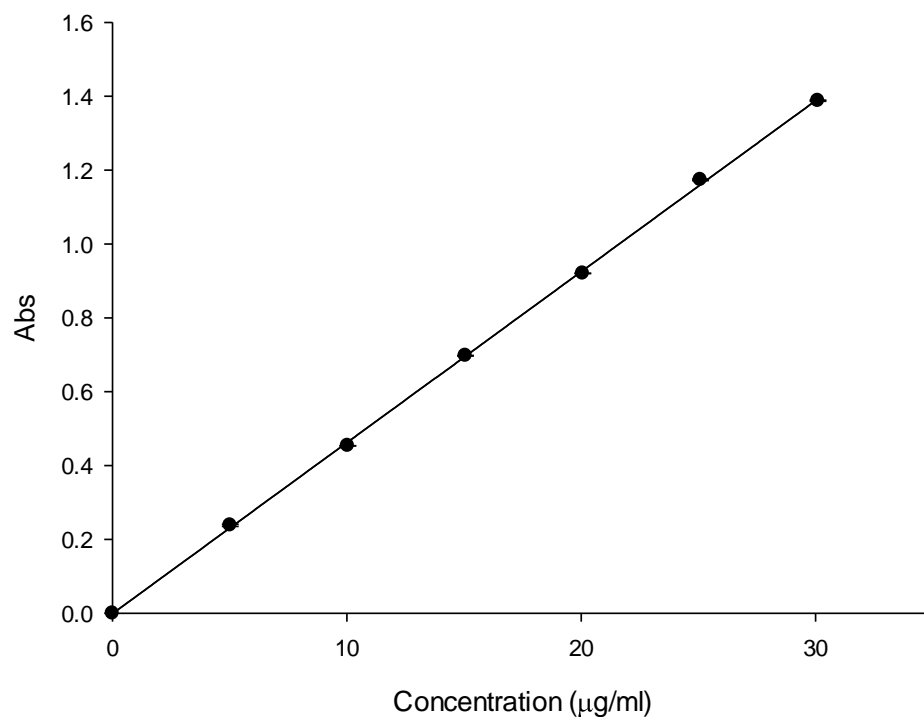
Figure A4 The absorbance of testosterone propionate concentration in isopropanol at 5, 10, 15, 20, 25 and 30 µg/ml at the wavelength 240 nm (mean ± SD, n=9), error bars within size of symbol.

Appendix B Supplementary density measurements

Table B1 Density values and partial specific volumes of micellar, nanoemulsion and microemulsion solutions at 25 ℃. (mean ± SD, n =9)

Sample	Density (g/cm^3)	Partial specific volume (cm^{-3}/g^{-1})
Brij 97	0.9980 ± 0.0012	0.969
B24T3/10	0.9986 ± 0.0015	0.936
B24T3/10-TP	0.9990 ± 0.0018	0.919
B24T5/10	0.9989 ± 0.0013	0.924
B24T5/10-TP	0.9991 ± 0.0016	0.924
SDS	1.0021 ± 0.0002	0.832
S20B14/5	1.0003 ± 0.0009	0.919
S20B14/5-TP	1.0010 ± 0.0003	0.901
S20C08/5	1.0006 ± 0.0005	0.896
S20C08/5-TP	1.0018 ± 0.0004	0.881